Dynamics of Tissue-Resident Regulatory T Cell Populations

Dynamics of Tissue-Resident Regulatory T Cell Populations

A dissertation presented

By

Dmitriy Pavlovich Kolodin

To

The Division of Medical Sciences

in partial fulfillment of the requirements

for the degree of

Doctor of Philosophy

in the subject of

Immunology

Harvard University

Cambridge, Massachusetts

April 2014

Dissertation Advisors: Dr. Diane Mathis & Dr. Christophe Benoist

Dmitriy Pavlovich Kolodin

Dynamics of Tissue-Resident Regulatory T Cell Populations

Abstract

In recent years, there has been a worldwide increase in obesity, which parallels a rise in pathologies, including type 2 diabetes, collectively termed the metabolic syndrome. Chronic, low-grade inflammation has been implicated as a major link between these diseases. Recent work showed the presence of a unique subset of $CD4^+Foxp3^+$ regulatory T cells residing in visceral adipose tissue (VAT T_{reg}) with PPAR-γ being the key transcription factor responsible for their phenotype and function in controlling adipose tissue inflammation and, thereby, insulin sensitivity. VAT T_{regs} inversely correlated with insulin resistance. In contrast, there was a dramatic age-associated increase in frequency of VAT T_{regs} in lean animals, correlating with continued insulin sensitivity, despite significant increases in body and adipose tissue weights. This increase in T_{reg} frequencies was not observed in other lymphoid and non-lymphoid tissues, including the subcutaneous fat depot. We characterized this unique age-associated increase in VAT T_{regs} through the use of adoptive transfer models, in vivo labeling and tracking systems, parabiosis, and analysis of the T cell receptor (TCR) repertoire used by VAT T_{regs}. Our findings indicate that the progressive increase in VAT T_{regs} is not due to conversion of conventional $CD4^+$ T cells nor to substantial

infiltration of T_{regs} from the circulation and secondary lymphoid organs. However, by analyzing the TCR repertoire on a single-cell level we uncovered a striking oligo-clonal expansion of VAT T_{regs}, suggesting their accumulation results from *in situ* proliferation. We further showed that this accumulation is dependent on major histocompatibility complex (MHC) class II, but not on CD1d. Finally, we showed that IL-33 was able to induce proliferation of VAT T_{regs}. In parallel, we extended our analysis of TCR repertoire to the T_{reg} population residing in skeletal muscle. In acute and chronic models of muscle injury, muscle-resident T_{regs} underwent a substantial clonal expansion, with a particular clone being detected in multiple individuals. Taken together these studies highlight the importance of proliferation as a mechanism of T_{reg} accumulation in tissues in response to acute and chronic inflammation.

Acknowledgements

During my graduate studies I was very fortunate to have met a number of great people who were instrumental in helping me along the way.

I would like to sincerely thank my thesis advisors, Dr. Diane Mathis and Dr. Christophe Benoist. They have provided me with invaluable guidance and mentorship along the way, allowing me to grow as a scientist and a person. I want to thank you for having the patience and faith in me and for constantly challenging me to reach higher.

I would like to acknowledge and thank my undergraduate advisors Dr. Duane Sears and Dr. Daniel Morse, who gave me a start in scientific research. Through your close mentorship I developed a passion for science, which ultimately led to me to pursue a doctoral degree in immunology.

I would also like to express my gratitude to all of the CBDM lab members, past and present, with whom I've had the distinct pleasure of working. You've provided a very friendly and collegial atmosphere for me in the lab and were there to share together the successes and disappointments of research.

I would especially like to thank Angela Morton, Jenny Shu, Dalia Burzyn, and Fabien Depis for insightful discussions, collaborations, and assistance with various experimental protocols; and Kimie Hattori, Natasha Asinovski, Adriana Ortiz-Lopez, Katherine Rothamel and Kristen Leatherbee for your outstanding technical help and experimental support.

Thank you to the Joslin Diabetes Research Center Flow Cytometry Core and especially Joyce LaVecchio and Girijesh Buruzula for all of the help with single-cell sorting.

I would like to thank all of my collaborators, past and present across various labs and institutions. It was a real pleasure to have worked with such wonderful people.

I would like to acknowledge and thank all of the members of my dissertation advisory committee, Dr. Arlene Sharpe, Dr. Florian Winau, Dr. Harald von Boehmer, and Dr. Steven Shoelson for all of your helpful advice and guidance with this project.

I would also like to acknowledge all of the close friendships that I've gained in graduate school. In particular, I want to thank Jonathan Sitrin, Daniel Dwyer, Marshall Thomas, Peter Sage, Matthew Woodruff, and Nicolas Chevrier for being great friends and making sure that I also have fun outside of lab.

Last but certainly not least I would like to especially thank my parents, Pavel and Lyudmila, my brother Nikolai, and Kara Holtzclaw for being there every step of the way. You have provided me with an unbelievable amount of love and support in the tough times and shared my happiness of successes during my time in graduate school.

"Science, my lad, is made up of mistakes, but they are mistakes which it is useful to make, because they lead little by little to the truth."

– Jules Verne, *Journey to the Center of the Earth*

Table of Contents

Chapter 1: Introduction

Regulatory T cells (T_{reg} cells), defined by their expression of the forkhead-winged helix transcription factor, Foxp3, are one of the main guardians of the immune system. A large body of literature described the origin, stability, and function of T_{reg} cells in maintaining immune homeostasis and implicated this cell subset in control of autoimmunity, allergic reactions, and inflammation, as well as responses to pathogens and commensals. More recently, T_{reg} cells have also been shown to play key roles in various non-immune contexts, including helping to maintain insulin sensitivity and potentiating muscle regeneration after injury.

1.1: Regulatory T cell biology:

1.1.1: Early work and identification of Foxp3

The concept of immunologic tolerance has long been proposed, however the dominant cell types and mechanisms remained elusive. In 1995, a seminal paper by Sakaguchi *et al.* described a subset of $CD4^+$ T cells that expressed high levels of the high affinity interleukin 2 receptor-α (IL-2Rα) chain, CD25, on their cell surface and were able to suppress autoimmune inflammation elicited by lymphopenic complementation and neonatal thymectomy (Sakaguchi et al., 1995). While the $CD25^+$ T cell population was enriched in T_{reg} cells, it also contained recently activated naïve T cells, so it was important to have a more accurate cell marker in order to identify the molecular mechanisms involved in T_{reg} differentiation and function. Studies on human

patients with a fatal immunodysregulation polyendocrinopathy and enteropathy, X-linked (IPEX) syndrome, as well as *scurfy* mutant mice, pathologic conditions characterized by uncontrolled lymphoproliferation and multiorgan autoimmunity, have led to the identification of Foxp3 as the characteristic marker of T_{regs} involved in their differentiation, maintenance, and functions (Brunkow et al., 2001; Chatila et al., 2000; Bennett et al., 2001; Wildin et al., 2001). The notion that T_{reg} cells play a dominant role in maintaining immune homeostasis was further substantiated by observations that the transfer of adult Foxp3$^+$ T_{reg} cells, wild-type (WT) bone marrow, or the expression of a transgene-encoded WT *Foxp3* allele could rescue *scurfy* mutant mice (Khattri et al., 2003; Fontenot et al., 2003).

1.1.2: Differentiation of T_{reg} cells

T_{regs} can differentiate in the thymus (tT_{regs}) or as a result of conversion of conventional CD4$^+$ T (T_{conv}) cells into T_{regs} in the periphery (pT_{regs}). Although the function and numerical contributions of the pT_{reg} pool remain a topic of debate, they have been definitively shown to contribute significantly to oral tolerance, colonization by intestinal commensal microbiota, and fetal-maternal tolerance. Mice with a deletion of the conserved noncoding sequence 1 (CNS1) enhancer region in the *Foxp3* locus, necessary for differentiation of pT_{regs}, displayed an altered composition of the commensal microbiota, as well as increased inflammation in the gastrointestinal tract and lung airways (Josefowicz et al., 2012b). In addition, CNS1-mutant mice in allogeneic, but not syngeneic, pregnancies had decreased frequencies of T_{regs} and

increased inflammation in deciduas, which led to increased resorption of embryos (Samstein et al., 2012b).

A much larger body of literature, however, has focused on T_{reg} cell differentiation in the thymus. Proper differentiation of tT_{reg} cells is dependent, in part, on T cell receptor (TCR) signaling, costimulation, and cytokine signaling. Thymic differentiation of T_{reg} cells with a specific transgene-encoded TCR required the expression of the cognate ligand (Kawahata et al., 2002; Apostolou et al., 2002; Jordan et al., 2001). Additionally, effector T cells transduced with TCRs isolated from T_{regs}, but not from naive T cells, were able to proliferate and cause autoimmune inflammation in lymphopenic recipients (Hsieh et al., 2004), highlighting a degree of self-specificity among T_{reg} cells. However, TCR repertoire analyses revealed that TCR sequences between T_{regs} and T_{convs} were similarly broad and only partially overlapping (Hsieh et al., 2006; Wong et al., 2007; Feuerer et al., 2009), suggesting a broad range of specificities among T_{regs}. Additionally, mice carrying transgene-encoded TCRs derived from T_{reg} cells supported the differentiation of very few $Foxp3^+$ tT_{regs}, a phenomenon that could be overcome by drastically reducing the frequency of precursors expressing the transgene-encoded TCR, which resulted in an increased frequency of differentiating tT_{regs} (Leung et al., 2009; Bautista et al., 2009; Dipaolo and Shevach, 2009). These findings suggested the presence of a selecting "niche" for tT_{regs} with severe intraclonal precursor competition, limiting the number of T_{regs} expressing TCRs of identical specificities and allowing for generation of a broad T_{reg} TCR repertoire. Furthermore, by analyzing a panel of TCRs with a wide range of reactivity to ovalbumin (OVA), the

authors showed that TCR affinity for OVA correlated with increased niche size for T_{reg} differentiation in the rat insulin promoter (RIP)-mOVA self-antigen tolerance model (Lee et al., 2012). Consistent with the idea of increased TCR signaling, differentiating tT_{regs} expressed elevated levels of CD5, programmed cell death protein 1 (PD-1), cytotoxic T lymphocyte antigen-4 (CTLA-4), glucocorticoid-induced tumor necrosis factor receptor (GITR), and OX40 (Fontenot et al., 2005b). It is likely that signals from TCR:self-petide interaction lead to a balance between negative selection and tT_{reg} differentiation when receiving additional signals. Indeed, likely due to increased TCR signaling, differentiating T_{regs} required TGF-β (Ouyang et al., 2010a) and common γ-chain cytokine signaling (Tai et al., 2013; Burchill et al., 2007; Fontenot et al., 2005a) leading to signal transducer and activator of transcription (Stat)5 activation in order to overcome Bcl-2-regulated apoptosis (Ouyang et al., 2010a). Conversely activation of PI3K-Akt pathway diminished tT_{reg} differentiation (Patton et al., 2006; Haxhinasto et al., 2008) primarily due to decreased translocation to the nucleus and decreased binding of the promoter and CNS2 of the *Foxp3* locus by Foxo1 and Foxo3 (Ouyang et al., 2010b; Kerdiles et al., 2010).

Consistent with the idea of TCR-mediated differentiation, major histocompatibility complex (MHC) class II molecules are required for tT_{reg} differentiation (Fontenot et al., 2005b). Furthermore, decreased expression of MHC class II specifically on medullary thymic epithelial cells enhanced tT_{reg} cell differentiation and decreased clonal deletion in TCR transgenic mice expressing the cognate ligand in the thymus (Hinterberger et al., 2010). Finally, a TCR sequence that

was enriched in multiple independent mice (MJ23) has been recently isolated from prostate tumor-infiltrating T_{regs} (Malchow et al., 2013). In MJ23 TCR-transgenic mice, T_{regs} localized exclusively to the prostate and draining lymph nodes even in the absence of the tumors, highlighting that their localization to the prostate was independent of inflammation. In addition, differentiation of MJ23 TCR-transgenic tT_{regs} was dependent on expression of autoimmune regulator (AIRE) and provided the first example of tissue-resident T_{regs} differentiating in the thymus in response to self-antigen.

Beyond TCR signaling, tT_{reg} differentiation also required CD28 costimulation (Salomon et al., 2000; Tai et al., 2005), leading to induction of Foxp3 through activation of NF-κB and binding of c-Rel to noncoding sequence elements in the *Foxp3* gene (Isomura et al., 2009; Long et al., 2009; Zheng et al., 2010). Foxp3, while absolutely critical for proper T_{reg} function and maintenance, alone did not account for the entire T_{reg} phenotype. Some canonical T_{reg} genes, such as *IL2ra, Ctla4*, and *Icos* were still upregulated in differentiating tT_{regs} of mice where green fluorescent protein was inserted into the *Foxp3* locus rendering the endogenous Foxp3 protein nonfunctional (Gavin et al., 2007; Lin et al., 2007). Additionally, transduction studies have determined that Foxp3 accounted for the induction of ~10-11% of the canonical T_{reg} signature, while the rest of the signature required the expression of other transcription factors such as GATA-1, Helios, IRF4, Eos, Lef1, and others (Hill et al., 2007; Fu et al., 2012). In addition, a variety of epigenetic modifications important for T_{reg} differentiation, maintenance, stability, and function have also been described (Samstein et al., 2012a; Zheng et al., 2010).

1.1.3: T_{reg} cell control of inflammation

Foxp3 plays an important role in differentiation and maintenance of the T_{reg} cell phenotype. Conditional knockouts of Foxp3 in T cells, using a Cre recombinase to delete floxed *Foxp3* alleles, led to the recapitulation of the fatal multiorgan autoimmune disease seen in *scurfy* mutant mice, including massive lymphoproliferation, diabetes, enteropathy, thyroiditis, and exfoliative dermatitis (Fontenot et al., 2003). In addition, depletion of $Foxp3^+$ T_{reg} cells in adult mice expressing the diphtheria toxin receptor under the control of Foxp3 promoter/enhancer elements ($Foxp3^{DTR}$) showed that T_{reg} cells are required for immunologic homeostasis throughout life (Kim et al., 2007).

Multiple molecular mechanisms of T_{reg} cell-mediated suppression have since been shown to be important in different inflammatory contexts (Josefowicz et al., 2012a). T_{regs} can secrete anti-inflammatory cytokines, such as interleukin-10 (IL-10) (Rubtsov et al., 2008), transforming growth factor-β (TGF-β) (Li et al., 2007), and interleukin-35 (IL-35) (Collison et al., 2007). Additionally, T_{regs} mediate suppression via expression of a panel of cell surface molecules: CD25 deprives effector T cells and NK cells of IL-2 and inhibits their proliferation (Sitrin et al., 2013; Pandiyan et al., 2007) and CTLA-4 modulates the activation state of antigen presenting cells, inhibiting their ability to activate effector T cells (Wing et al., 2008; Friedline et al., 2009).

Inflammatory responses are heterogeneous in their nature, composed of different combinations of effector cells and polarization states; therefore, broadly-functioning molecular mechanisms are unlikely to account for the heterogeneity and specificity of

T_{reg}-mediated suppression of inflammation and control of immune homeostasis. Instead, T_{regs} coopt portions of molecular programs expressed by the effectors that are being suppressed, thereby allowing T_{regs} to be recruited to and retained at the site of inflammation, and to initiate proper suppression mechanisms. Indeed it was shown that transcription factors, key in differentiation of various T helper subsets were upregulated in T_{regs} and loss of these transcription factors led to uncontrolled inflammatory responses. T_{regs} express T-bet (Koch et al., 2009), IRF4 (Zheng et al., 2009), STAT3 (Chaudhry et al., 2009), and BCL6 (Chung et al., 2011; Linterman et al., 2011) to control Th1, Th2, Th17, and Tfh responses, respectively.

Given the potent role of T_{regs} in controlling a plethora of inflammatory responses, it was logical to evaluate their role in contexts that have not been historically associated with inflammation.

1.2: Inflammation in obesity and insulin resistance

1.2.1: Molecular mediators of adipose tissue inflammation

Over the past several decades, there has been a world-wide increase in obesity, in parallel with an impressive rise in a cluster of abnormalities termed the "metabolic syndrome", including type-2 diabetes (TD2). According to the latest estimates from the Centers for Disease Control, over 25 million people in the United States suffer from diabetes, which is associated with tremendous societal and economic burdens (Center for Disease Control and Prevention, 2011). There is by now a large body of evidence that implicates obesity in provoking chronic, low-grade inflammation, which, in turn, promotes metabolic dysregulation and systemic insulin resistance (Shoelson et al., 2006; Hotamisligil, 2006). It turns out that the function of adipose tissue is not limited to the storage of excess triglycerides, but that it is also an active endocrine organ playing multiple roles in orchestrating system-wide metabolism. A seminal insight into the pro-inflammatory potential of adipose tissue in response to obesity came from Hotamisligil *et al.*, who demonstrated increased levels of tumor necrosis factor-α (TNF-α) mRNA in adipocytes in visceral adipose tissue (epididymal, omental, etc.), but not subcutaneous fat, of obese versus lean mice (Hotamisligil et al., 1993). Since then, an increasing number of adipocyte-derived mediators, collectively called adipokines, have been described. These molecules, which can increase or decrease in response to extended caloric excess, have multiple effects on a variety of cell populations, both locally in adipose tissue and systemically (Ouchi et al., 2011). They include, but are not limited to, interleukin-1β (IL-1β) (Jager et al., 2007), IL-6 (Rotter et al., 2003), serum

amyloid A3 (SAA3) (Han et al., 2007), and macrophage chemoattractant protein-1 (MCP-1) (Kamei et al., 2006). Obesity, by triggering endoplasmic reticulum (ER) stress (Ozcan et al., 2004), hypoxia (Halberg et al., 2009), and oxidative stress (Minamino et al., 2009), results in adipocyte dysfunction, dysregulated expression of adipokines, and inappropriate inflammatory responses (Shoelson et al., 2006; Hotamisligil, 2006). There are changes in the cellular composition of adipose tissue, including adjustments in the numbers, phenotypes, and localization of multiple immune cell subsets. There are also systemic metabolic alterations through a complex signaling network that affects insulin signaling in the liver, kidney, and skeletal muscle. Activation of NF-κB (Yuan et al., 2001) and the JUN N-terminal kinase family of serine/threonine protein kinases (Hirosumi et al., 2002) leads to phosphorylation and inactivation of the insulin receptor substrate family, which collectively results in tissues becoming unresponsive to insulin signaling (Elchebly et al., 1999; Ozcan et al., 2004; Feinstein et al., 1993). (Figure 1.1)

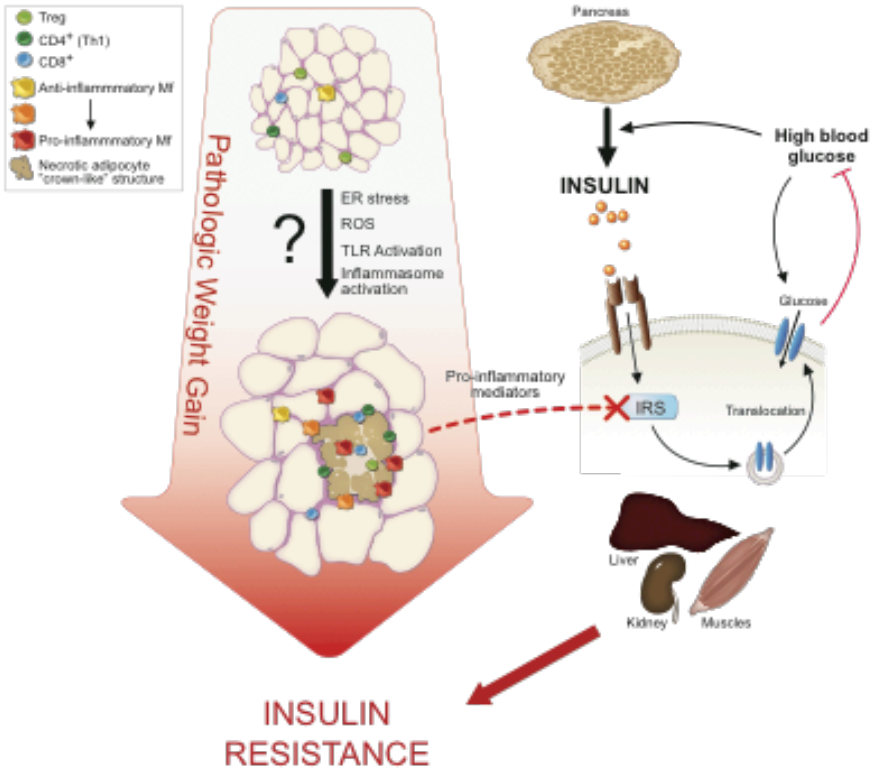

Figure 1.1: Obesity results in systemic, chronic, low-grade inflammation and insulin resistance. Excess weight gain leads to necrotic and apoptotic death of adipocytes, thereby activating various inflammatory responses such TLR and inflammasome activation, release of reactive oxygen species (ROS), and endoplasmic reticulum (ER) stress. In response to these inflammatory stimuli, adipocytes and infiltrating leukocytes release a variety of pro-inflammatory mediators that act locally in adipose tissue and distally in liver, muscle, and kidneys to inactivate insulin receptor substrates (IRS), leading to insulin resistance and persistent high blood glucose. Taken from (Cipolletta et al., 2011) *Copyright 2011 Elsevier Ltd.*

1.2.2: Innate immune system in obesity

A number of studies have implicated subsets of innate immune system cells, such as neutrophils, type 2 innate lymphoid cells (ILC2), mast cells, and macrophages in obesity-induced pathology. In mouse model of obesity, neutrophils infiltrate adipose tissue within the first three weeks of high fat diet (HFD), revealing their possible role in early phases of adipose tissue inflammation (Talukdar et al., 2012; Elgazar-Carmon et al., 2008). Neutrophils have been shown, given appropriate inflammatory cues, to expel extracellular traps, termed NETs, which consist primarily of extruded chromatin and serine proteases. These NETs possess direct antimicrobial activity and also act to amplify the immune response through recruitment of additional circulating immune cells. Genetic ablation of neutrophil elastase alleviated inflammation and improved metabolic indices, while injection of recombinant elastase led to development of glucose intolerance even in mice on a normal chow (NC) diet.

To date, the largest body of evidence implicates subsets of macrophages/ monocytes as major effectors in obesity-induced pathology. Accumulations of large numbers of macrophages around dead adipocytes, forming "crown-like structures," have been observed in visceral fat tissue of obese mice and humans (Cinti et al., 2005; Weisberg et al., 2003). Under normal chow conditions, adipose tissue presents an anti-inflammatory environment, where resident macrophages display a phenotype similar to the anti-inflammatory or alternatively-activated "M2" state, producing factors such as interleukin-10 (IL-10) and transforming growth factor-β (TGF-β) (Mosser and Edwards, 2008; Odegaard et al., 2007; Fujisaka et al., 2009; Kamei et al., 2006; Lumeng et al.,

2007a; Lumeng et al., 2007b). In contrast, in obese adipose tissue, resident and infiltrating macrophages appear to be in the pro-inflammatory or classically activated "M1" state, synthesizing numerous inflammatory factors, including TNF-α, IL-6, matrix metalloproteinases, and peroxisome proliferator activated receptor-γ (PPAR-γ), (Lumeng et al., 2007a; Lumeng et al., 2007b; Weisberg et al., 2003; Kamei et al., 2006; Fujisaka et al., 2009). In addition, adipose-tissue macrophages can also modulate the functions of infiltrating $CD4^+$ T cells to polarize toward a pro-inflammatory Th1 phenotype (Moraes-Vieira et al., 2014).

It is important to note, however, that, while adipose tissue macrophages have been historically subdivided into M1 and M2 subsets (Lumeng et al., 2007a; Lumeng et al., 2007b), and this is an attractively simple dichotomy, recent studies have challenged this binary classification, instead arguing in favor of a spectral classification (Mosser and Edwards, 2008; Shaul et al., 2010; Herrero et al., 2010). A recent study demonstrated the importance of the NLRP3 (nucleotide-binding domain leucine-rich repeat containing family, pyrin domain containing 3) inflammasome in activation of adipose-tissue macrophages and subsequent development of insulin resistance (Vandanmagsar et al., 2011). The inflammasome is a key player in sensing various "danger" stimuli, leading to secretion of IL-1β and initiation of a pro-inflammatory immune response (reviewed in Schroder and Tschopp, 2010). Previous studies have demonstrated that cholesterol or similar crystals cause Nlrp3 inflammasome activation in macrophages found in atherosclerotic lesions (Duewell et al., 2010; Rajamaki et al., 2010). By analogy, one might speculate that HFD leads to formation of cholesterol

crystals activate the Nlrp3 inflammasome, in particular in adipose tissue macrophages, resulting in a pro-inflammatory activation state and ultimately resulting in systemic inflammation and insulin resistance. Additionally, activation of adipose tissue macrophages has been shown to result from recognition of free fatty acids by Toll-like receptors (TLR) 2 and 4 in mice on HFD (Nguyen et al., 2007).

Since insulin sensitivity closely correlates with the presence of anti-inflammatory, M2-like macrophages, several studies have focused on particular populations of anti-inflammatory innate immune cells residing in VAT of lean mice. One such immune cell subset is eosinophils, known to circulate in an immature state and enter tissues following their maturation. In lean VAT, eosinophils produced high levels of IL-4, key cytokine for the differentiation and survival of anti-inflammatory, M2-like macrophages; additionally, eosinophil numbers inversely correlated with adipocity (Wu et al., 2011). Mice with reduced eosinophil numbers due to a genetic deficiency (*Gata1*$^{-/-}$ mutants) had increased adipocity, decreased glucose tolerance and worsened insulin resistance; however, *IL-5* transgenic mice that have increased eosinophil levels, showed markedly improved metabolic indices that correlated with an increase in M2-like macrophages. ILC2s are a major source of IL-5 and IL-13 in lean VAT and their number decrease with HFD treatment (Molofsky et al., 2013). IL-33-mediated increase of ILC2s led to increases in eosinophils and anti-inflammatory macrophages in VAT.

Mast cells potentiate obesity-associated inflammation (Liu et al., 2009). Mast cell numbers are increased in adipose tissue of obese mice and humans compared with

lean controls. Additionally, mice with a genetic mast cell deficiency and mice treated with a mast cell stabilizing drug displayed significantly reduced body weight and VAT mass during HFD treatment due to decreased adipose tissue and muscle angiogenesis and increased apoptosis. It is important to point out that the primary effect of mast cell stabilization was on obesity-induced weight gain that secondarily altered insulin sensitivity. Finally, using genetic knockouts, the authors showed that IL-6 and IFN-γ produced by mast cells were the key cytokines for attenuating weight gain.

1.2.3: Adaptive immune system in obesity

Even though the contributions of the innate immune system have been the central focus of many obesity-related studies, recently a growing interest in the adaptive immune system has emerged.

The role of B cells in insulin resistance remains poorly understood, as conflicting reports regarding their pro- or anti-inflammatory effects have emerged in the literature. IL-10-producing B cells, termed B_{regs}, are abundant in lean adipose tissue, but declined in various models of obesity, including *Lep*$^{ob/ob}$ mice and HFD feeding (Nishimura et al., 2013). B-cell specific deletion of *IL-10* resulted in increased adipose tissue inflammation during HFD treatment and a decline in metabolic indices, which could be reversed via transfer of WT B_{regs}, arguing for an anti-inflammatory role for B cells. However, other studies found that B cells were part of the pro-inflammatory infiltrate in the VAT during HFD feeding (Duffaut et al., 2009; Winer et al., 2011; DeFuria et al., 2013). B cell-deficient mice had decreased VAT inflammation and improved insulin sensitivity on HFD; reintroduction of B cells from mice on HFD, but not NC, led to an increase in inflammation and worsening of insulin sensitivity (Winer et al., 2011; DeFuria et al., 2013). Interestingly, decreased insulin sensitivity in HFD mice could be recapitulated by transferring the serum IgGs alone from mice on HFD, but not NC, into B cell-null recipients (Winer et al., 2011). A possible reconciliation of these seemingly contradictory results is that lean VAT contains primarily anti-inflammatory B_{reg} cells that are replaced in obesity by pro-inflammatory B cells,

mirroring the balance and dynamics of regulatory and effector T cell subsets in lean and obese adipose tissues (discussed below).

Effector and regulatory T cells have been the focal point in characterizing roles of the adaptive immune system in type-2 diabetes. It is not surprising that T cells have been implicated given their crucial roles in various other inflammatory diseases. Initial studies showed an increased frequency of $CD3^+$ T cells in obese human patients and mice (Kintscher et al., 2008). Both $CD4^+$ and $CD8^+$ T cells have been identified as key players in adipose tissue inflammation.

In response to HFD feeding, $CD8^+$ T cells infiltrated obese adipose tissue prior to the increase in macrophages (Nishimura et al., 2009). Depletion of $CD8^+$ T cells via antibody treatment or genetic knockout resulted in decreased macrophage infiltration into adipose tissue and improved insulin sensitivity. Additionally, $CD8^+$ T cell depletion resulted in decreased production of key pro-inflammatory mediators such as TNFα, IL-1, IL-6, RANTES, and MCP-1. Several *in vitro* experiments suggested that $CD8^+$ T cells isolated from obese adipose tissue had a highly activated phenotype and produced large quantities of pro-inflammatory mediators known to function in macrophage recruitment and activation (Nishimura et al., 2009; Yang et al., 2010). The frequency of $CD44^+$ $CD62L^-$ effector memory $CD8^+$ T cells was significantly higher while $CD44^-$ $CD62L^+$ $CD8^+$ T cell frequency was decreased in obese compared with lean adipose tissue, consistent with the model of an activated phenotype of $CD8^+$ T cells in obese fat (Yang et al., 2010). In addition, studies in mice deficient for the costimulatory protein, CD40, found increased adipose tissue inflammation and a corresponding increase in

insulin resistance, which was characterized by increased infiltration of $CD8^+$ T cells and macrophages in VAT (Wolf et al., 2014; Yi et al., 2014). Transfer of $CD8^+$ T cells from CD40-KO, but not WT, mice into recombination-activating genes (RAG)-null recipients led to increased inflammation and insulin resistance (Yi et al., 2014). Conversely, antibody-mediated depletion of $CD8^+$ T cells was able to ameliorate inflammation and insulin resistance in CD40-KO mice. Findings from these studies suggest that obese adipose tissue leads to activation of $CD8^+$ T cells, which, in turn, leads to recruitment and differentiation of activated macrophages to adipose tissue via pro-inflammatory mediators. However, the dominant role of $CD8^+$ T cells in VAT inflammation was challenged by the finding that mice enriched in $CD8^+$ T cells due to genetic deletion of MHC class II, thereby lacking in $CD4^+$ T cells and T_{regs}, were protected from obesity-induced insulin resistance (Deng et al., 2013).

More attention has been given to the $CD4^+$ T cell subset due to their ability to promote inflammation and recruit macrophages. Currently, the role of $CD4^+$ T cells in adipose tissue inflammation remains unclear with multiple conflicting reports. In recent years, several studies characterized the pro-inflammatory properties of effector $CD4^+$ T cells in VAT. These studies found a significant increase in $CD4^+$ T cells residing in adipose tissue of obese human patients and mice (Yang et al., 2010; Winer et al., 2009). VAT $CD4^+$ T cells were enriched for $CD44^+$ $CD62L^-$ effector memory T cells, suggesting their increasingly activated phenotype compared with $CD4^+$ T cells isolated from lean adipose tissue (Yang et al., 2010). TCR analysis revealed a repertoire bias among T cells isolated from obese adipose tissue compared with lean adipose tissue,

suggestive of antigen driven T cell activation and expansion and/or infiltration (Yang et al., 2010; Winer et al., 2009; Feuerer et al., 2009). Closer analysis of adipose tissue-resident effector $CD4^+$ T cells revealed that HFD feeding induced a Th1 T cell phenotype, (Strissel et al., 2010; Winer et al., 2009) characterized by production of IFNγ. A proposed model suggests that during development of obesity there is a phenotypic activation of T cells from a Th2 state to a pro-inflammatory and pathogenic Th1 state (Winer et al., 2009) leading to secretion of IFNγ and an increase in M1 macrophages. Indeed, there is a decrease of $Gata3^+$ $CD4^+$ T cells in adipose tissue of obese mice compared with lean controls; however the conclusion that these cells are Th2 cells is unsubstantiated. Additionally, isolated VAT $CD4^+$ T cells produced higher levels of IFNγ isolated from obese mice than from lean mice. Increase in IFNγ expression levels led to accumulation of M1 macrophages in obese fat and elevated expression of TNFα, RANTES, and MCP-1 (Rocha et al., 2008). Finally, inflamed adipose tissue further propagates Th1 T cell polarization through the production of leptin, which can act on T cells directly and indirectly to promote increased proliferation and cytokine production, specifically IL-2 and IFN-γ (Lord et al., 1998).

In contrast to the aforementioned pro-inflammatory role of VAT $CD4^+$ T cells, one study proposed a protective role for effector $CD4^+$ T cells in ameliorating obesity-associated insulin resistance (Winer et al., 2009). In this study, $CD4^+$ T cells were adoptively transferred into RAG-null mice leading to decreased body weight, fat pad mass, and improved insulin sensitivity. The authors attributed improved metabolic parameters observed after the transfer of total $CD4^+$ T cells to the protective role of Th2

$CD4^+$ T cells. An alternative interpretation of these results is that the improvement of metabolic parameters is due to lower body weight in the recipient mice and insulin sensitizing effect of T_{reg} cells, which were not excluded from the transferred population. Under lymphopenic conditions in RAG-null recipients, $CD4^+$ T cells can become activated and differentiate into Th2 cells, as suggested by the authors, but these T cells also differentiate into Th1 and Th17 subsets (Goldrath et al., 2004). Furthermore, a recent paper showed that VAT T_{reg} cells are the dominant $Gata3^+$ population among VAT $CD4^+$ T cells (Cipolletta et al., 2012); therefore the loss of $Gata3^+$ $CD4^+$ T cells following HFD treatment could be actually due to loss of T_{reg} cells in abdominal adipose tissue and cannot be equated to loss of Th2 cells. Taken together the data presented in this paper should be re-examined, and the insulin-sensitizing effects demonstrated in this study could be attributed in some cases to weight loss and in other cases to the protective effect of transferred T_{reg} cells.

Traditionally, activation of effector $CD4^+$ T cells proceeds via recognition of peptide antigens presented by MHC class II molecules on the surface of antigen-presenting cells, such as dendritic cells and macrophages, in combination with engagement of costimulatory molecules and polarization by cytokines. In adipose tissue, macrophages express high levels of MHC class II and costimulatory molecules, CD80 and CD86, all of which are further upregulated in response to HFD (Morris et al., 2013). VAT macrophages were able to stimulate proliferation of antigen-specific $CD4^+$ T cells when cultured together. Adipose tissue macrophages can become activated by high levels of retinol binding protein 4 (RBP4) through a JNK-dependent pathway

leading to polarization of $CD4^+$ T cells toward the pro-inflammatory Th1 state (Moraes-Vieira et al., 2014). Additionally, two studies have also attributed the expression of MHC class II molecules and subsequent activation of $CD4^+$ T cells to adipocytes themselves (Deng et al., 2013; Meijer et al., 2011). It is an attractive idea that upon encountering stress adipocytes themselves are able to modulate effector T cells without the need for macrophage intermediates, especially since leptin, produced by adipocytes, can promote polarization of T cells towards the Th1 state (Lord et al., 1998). However, these studies did not definitively address the possibility of macrophage contamination in the adipocyte isolations and *in vitro* adipocyte differentiation (Charriere et al., 2003), which could offer an alternative interpretation of the data.

In contrast to the pro-inflammatory effector T cells, $CD4^+$ $Foxp3^+$ T_{regs} reside in visceral adipose tissue (VAT T_{regs}) and are important regulators of VAT inflammation and insulin resistance (Feuerer et al., 2009; Cipolletta et al., 2012; Ilan et al., 2010; Eller et al., 2011; Deiuliis et al., 2011). Gene expression profiling of VAT T_{regs} revealed that they expressed ~60% of the canonical T_{reg} signature, which included the hallmark transcripts encoding Foxp3, CD25, CTLA-4, GITR, OX40, and IKAROS family zinc finger 2 (Ikzf2). Decreases in VAT T_{regs} in obesity during HFD treatment correlated with increased macrophage and monocyte numbers in VAT. Experimental manipulations of the total T_{reg} pool led to "guilt-by-association" dissection of VAT T_{reg} functions. Systemic depletion of T_{regs} using $Foxp3^{DTR}$ quickly led to increases in VAT inflammation and impairment of insulin receptor signaling in adipose tissue, liver, and muscle. Conversely, *in vivo* T_{reg} expansion using IL-2/anti-IL-2 cytokine-antibody

complexes led to improved glucose tolerance and insulin receptor signaling. Systemic depletion and expansion of T_{regs}, did not allow for specific interrogation of VAT T_{reg} function in controlling adipose tissue inflammation and insulin sensitivity. However, gene expression profiling revealed that PPARγ is highly expressed specifically in VAT $Foxp3^+$ T_{regs} (Feuerer et al., 2009; Cipolletta et al., 2012) and is able to interact with Foxp3 (Cipolletta et al., 2012), which allowed for the specific interrogation of VAT T_{regs}. PPARγ stimulation by the thiazolidinedione drug pioglitazone (Pio) increased T_{reg} cell numbers in VAT, but not in spleen, of obese mice on HFD, leading to improved insulin sensitivity. Finally, mice carrying a T_{reg}-specific deletion of *Pparg* (T_{reg}-*Pparg* mut mice), showed a drastic loss of VAT T_{regs}, leading to a reduction insulin sensitizing effects of Pio. The absolute requirement of PPARγ expression in VAT T_{regs} for proper control of adipose tissue inflammation and maintenance of insulin sensitivity can be thought of as an extension of the idea (discussed earlier) that T_{reg} cells express key transcription factors of the inflammatory cells that are being suppressed.

Taken together these studies point to a complex interaction between various immune cell types that are modulated in response to changes in adipose tissue homeostasis. To generalize, the overall immune cell milieu shifts from an anti-inflammatory composition (high levels of T_{regs}, B_{regs}, eosinophils, ILC2s, and M2-like macrophages) in lean VAT to a pro-inflammatory one (increased levels of $CD8^+$ T cells, Th1 cells, mast cells, neutrophils, M1-like macrophages) in obese VAT. (Figure 1.2).

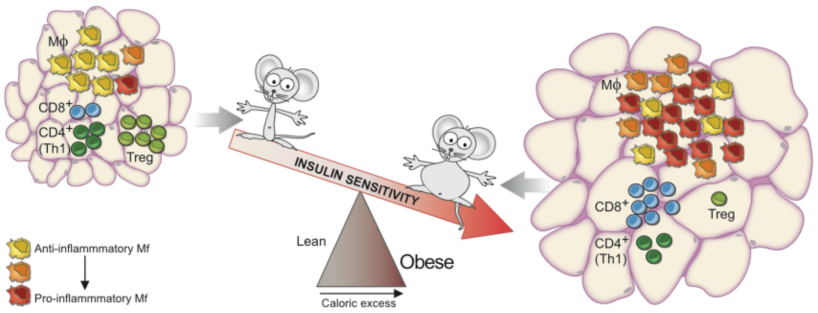

Figure 1.2: **Cellular and metabolic alterations in adipose tissue during obesity**. In lean mice, the abdominal adipose tissue hosts anti-inflammatory macrophages, as well as an elevated fraction of T_{regs}. In obese mice, by contrast, there is a switch in cellular equilibrium: more CD8+ than Th1 CD4+ T cells, fewer regulatory T cells and a preponderance of pro-inflammatory macrophages. These effector cells promote inflammation and exacerbate adipose tissue dysfunction through the production of inflammatory cytokines. Taken from (Cipolletta et al., 2011) *Copyright 2011 Elsevier Ltd.*

Therefore, given the importance of T_{regs} in suppression of a variety of inflammatory responses and in promoting immune homeostasis, their presence in adipose tissue is critical for protection from adipose tissue inflammation and insulin resistance. Interestingly, VAT T_{regs} accumulate with age in lean mice to frequencies >50% of the VAT-resident $CD4^+$ T cells, which is a much larger fraction than the ~10-20% found in lymphoid and non-lymphoid tissues, including the subcutaneous adipose depots. This degree of expansion of T_{regs} was quite striking and warranted a closer examination.

Chapter 2: Accumulation of Foxp3$^+$ regulatory T cells in lean visceral adipose tissue results from MHC class II-dependent clonal proliferation and long-term persistence.

Introduction

VAT T_{regs} accumulate with age in lean mice despite significant increases in body and adipose tissue weights. The age-associated accumulation of VAT T_{regs} is intriguing because changes specifically in visceral, but not subcutaneous, fat depots have been implicated in insulin resistance. Furthermore, T_{reg}-*Pparg* mut mice had a decrease in numbers of T_{reg} cells exclusively in VAT even in the absence of HFD challenge, highlighting the requirement of PPARγ for VAT T_{reg} recruitment, retention, and/or survival. We wanted to more carefully characterize the dynamics and the mechanism of VAT T_{reg} accumulation in lean adipose tissue. A deeper understanding of the underlying VAT T_{reg} cell biology could provide insights into what causes the loss of VAT T_{regs} during HFD diet and leads to the over-exuberant inflammatory response in VAT.

The majority of T_{regs} differentiate in the thymus as a subset of the total CD4SP population (tT_{regs}). However, a small fraction can differentiate in the periphery from mature T_{conv} cells under a variety of conditions pT_{regs} (reviewed extensively in (Josefowicz et al., 2012a) and (Bilate and Lafaille, 2012)), and were shown to play key roles in controlling inflammation in variety of tissues such as lung, gut, and decidua (Josefowicz et al., 2012b; Samstein et al., 2012b).

In addition, studies using T_{regs} carrying transgene-encoded TCRs showed that T_{regs} proliferated in tissues to control the inflammatory response in an antigen-dependent manner (Rosenblum et al., 2011; Malchow et al., 2013; Seneschal et al., 2012). Similarly, the TCR repertoire of VAT T_{reg} cells from lean mice was distinct from that of VAT T_{convs}, as well as that of T_{reg} and T_{conv} cells isolated from secondary lymphoid tissues, which suggested a degree of antigenic imprinting (Feuerer et al., 2009). Furthermore, there were several examples of VAT T_{reg} cells with the same protein sequence and different nucleotide sequences in the CDR3 region, the region most responsible for interaction with peptide-MHC complexes.

Finally, T_{regs} can also migrate to sites of inflammation in order to suppress the immune response via a process that is governed by the specific combinations of chemotactic molecules and their receptors. Previous studies showed that monocytes and macrophages could be recruited to VAT by chemokine- and receptor-mediated fashion, for example via recognition of MCP-1 produced in VAT by CCR2 on monocytes and macrophages (Kanda et al., 2006; Weisberg et al., 2006). VAT T_{regs} expressed high levels of several chemokine receptors, including CCR2, which correlated with PPARγ expression (Cipolletta et al., 2012). Additionally, a number of other transcripts that were under- and over-expressed in VAT T_{regs} were molecules involved in leukocyte migration and extravasation.

Therefore, we hypothesized that the accumulation of T_{regs} in lean VAT could result from local conversion of T_{conv} cells into pT_{regs}, *in situ* proliferation of resident T_{reg}

cells, recruitment of T_{regs} from the lymphoid organs and circulation, or some combination of the aforementioned mechanisms.

Materials and Methods:

Mice

C57BL/6 mice were purchased from Jackson Laboratories. Foxp3^{DTR}, Foxp3^{iGFP}, and Kaede.B6 mice were obtained from A. Rudensky, V. Kuchroo, and O. Kanagawa, respectively. Male mice of specified ages were used for all of the studies. All mice were bred in our specific pathogen-free facilities at Harvard Medical School. Experiments were conducted under protocols approved by Harvard Medical School's Institutional Animal Care and Use Committee.

Cell isolation

Epididymal fat pads and spleens were excised, cut into small pieces, and digested for 20 minutes with 1.5 mg/ml of collagenase type II (Sigma) in PBS supplemented with 1% fetal calf serum. Cell suspensions were then filtered through a 40-micron sieve, and the SVF fraction was collected after centrifugation at 450g for 10 min.

Flow cytometry

For T-cell analysis, cells were stained with varying combinations of anti-CD45 (clone 30-F11), -CD45.1 (A20), -CD45.2 (104), -CD3 (145-2C11), -CD4 (GK1.5), -CD8 (5H10), and -CD25 (PC61) antibodies (Biolegend), anti-Nrp1 (R&D) and -ST2 (RMST2-2) (eBiosciences); and were fixed, permeabilized and intracellularly stained for Foxp3 (FJK-16s), Ki67, BrdU (Bu20A), Helios, and GATA3 (TWAJ) according to

the manufacturer's instructions (eBiosciences); when using Foxp3^{iGFP} mice endogenous GFP expression was used. Cells were analyzed using an LSRII instrument (BD Bioscience) and FlowJo software.

Kaede.B6 photoconversion

Mice were anesthetized with ketamine/xylazine in combination (10 mg/kg/2 mg/kg ip). The fur attached to the skin covering the CLNs was removed using depilatory cream, applied for 2 mins. Mice were placed on their backs with an aluminum foil blanket covering all but the depilated area, and violet light (Electra Pro Series 405 nm Violet Handheld Laser, Laserglow Technologies) was shone onto the exposed area for a period of 3.5 mins, the pre-established time for effective but innocuous photoconversion at this anatomical site. In order to manipulate the size of the light field (beam diameter: 3.5 mm) so that both CLNs could be exposed, we attached a lens to the laser to de-focus the beam, and the source of the de-focused light beam was positioned 28cm above the mouse.

Thymectomy

Mice were anesthetized with ketamine/xylazine in combination (10 mg/kg/2 mg/kg ip). The fur attached to the skin covering the CLNs was removed using depilatory cream, applied for 2 mins. An incision was made cutting the first 3 ribs and thymus was excised using forceps. Skin was closed and secured with 2-3 clips.

Parabiosis surgery

Mice were anesthetized with 2.5% avertin (15 μl per g of body weight). Mice were shaved along opposite lateral flanks. Skin was wiped with alcohol prep pads and further cleaned with Betadine solution and 70% isopropyl alcohol. Mirrored incisions were made on lateral aspects of both mice, and ventral and dorsal skin flaps were approximated by staples to conjoin the mice. Additional sutures were placed through the olecranon and knee joints to secure the legs. In some cases, thymectomies (described above) were performed just prior to parabiosis surgery.

Intrathymic injections

Mice were anesthetized with ketamine/xylazine in combination and given an intrathymic injection of 10 μl of a 5 mg/ml solution of sulfo-NHS-LC biotin (Pierce Chemical Co.) per lobe. 24 hours later thymus, epididymal fat pads and spleen were isolated, processed for staining (described above) and stained with streptavidin-conjugated PE and other markers for analysis by flow cytometry.

Transfers

5 x 10^6 $CD4^+Foxp3^-$ T_{conv} cells or 1 x 10^6 $CD4^+Foxp3^+$ T_{reg} cells were sorted from pooled spleens and LN of CD45.1 $Foxp3^{iGFP}$ mice and transferred i.v. into 20-week old CD45.2 $Foxp3^{iGFP}$ recipient mice. Recipient mice were sacrificed 4 weeks after transfer and LN, spleen, and epididymal fat pads were isolated and analyzed by flow cytometry.

BrdU incorporation

5-bromo-2'-deoxyuridine powder (Sigma) was added to the drinking water (0.8 mg/mL) and protected from light. BrdU in water was changed every 2 days for 5 weeks.

Single-cell sorting, RT-PCR and TCR sequence analysis

$CD4^+Foxp3^+$ and $CD4^+Foxp3^-$ T cells from VAT and LN of 25-30-week old $Foxp3^{iGFP}$ mice were first sorted in bulk before resorting as individual cells on MoFlo (Beckman Coulter) into wells of 96-well PCR plates containing the reverse transcriptase reaction mix and cDNA was prepared as described by (Wong et al., 2007). Extreme caution was taken to minimize PCR and cross-contamination between wells. Preparation of reverse transcriptase reaction mix, cDNA synthesis, and first round of PCR was performed in a different building from second round PCR and final PCR product isolation. At least 2 columns of every plate were left blank for negative controls to monitor for contamination. Experiments showing evidence of PCR contamination were discarded. Resulting cDNA (1.5 μl) from each cell was split to perform multiplex nested PCR reactions to amplify the corresponding CDR3α and CDR3β transcripts using the protocol and CDR3β primers published in (Baker et al., 2002). Primers used to amplify CDR3α were designed based on nucleotide sequences of the TCRα families from the IMGT database (http://www.imgt.org; (Brochet et al., 2008)). Aliquots of the PCR products were visualized on a 1.5% agarose gel. Samples containing PCR product for both TCRα and TCRβ chains were cleaned up using ExoSAP-IT For PCR Clean-Up (Affymetrix) per manufacturers protocol and were subjected to automated sequencing

(Dana-Farber/Harvard Cancer Center High-Throughput Sequencing Core). Raw sequencing files were filtered for sequence quality, processed in automated fashion, and parsed using IMGT/V-QUEST (Brochet et al., 2008). Only sequences that produced functional in-frame rearrangements of both TCRα and TCRβ chains were used for analysis.

EdU labeling

For quantification of *in vivo* T cell proliferation, 1mg EdU was injected iv, and 4hrs later cells were processed for detection by the Click-iT EdU kit following manufacturer's protocol (Molecular Probes).

Diptheria toxin administration for *in vivo* T_{reg} depletion

$Foxp3^{DTR+}$ mice and $Foxp3^{DTR-}$ control littermates were injected ip with DT (Sigma), at 10 ng/g body weight, for 2 consecutive days.

IL-33 administration

Mice were injected ip with recombinant IL-33 (Biolegend), at 2 μg per injection every 3 days for 1 week prior to analysis.

Statistical analyses

Data were routinely presented as means ± S.D., significance assessed by the Student's t test or ANOVA using Prism 5 (GraphPad Software). A P value of <0.05 was deemed statistically significant. * $p<0.05$, ** $p<0.01$, *** $p<0.001$

Results

None of the pT_{reg} hallmarks observed among VAT T_{regs}

Currently there are no accepted markers to definitely distinguish tT_{regs} and pT_{regs}; however, low or negative expression of Ikzf2 (Helios) (Thornton et al., 2010; Verhagen and Wraith, 2010; Akimova et al., 2011) and of Neuropilin-1 (Nrp1) (Yadav et al., 2012; Weiss et al., 2012) are characteristic of pT_{regs}. We looked at expression of Nrp1 and Helios among T_{regs} from the spleen, subcutaneous lymph nodes (LN), and VAT of 15- (early phase of accumulation) and 25- (peak of accumulation) week old mice. VAT had significantly lower levels of $Helios^-$ T_{regs} (Figure 2.1A) and similar frequencies of $Nrp1^-$ T_{regs} (Figure 2.1B) compared with T_{regs} residing in the spleen and lymph nodes.

To directly address whether $Foxp3^-CD4^+$ T_{conv} cells could turn on Foxp3 expression in adipose tissue to become pT_{regs}, we performed a transfer experiment. We sorted $Foxp3^-$ T_{convs} from a reporter mouse line, where an internal ribosomal entry site followed by a gene encoding green fluorescent protein (GFP) were inserted downstream of the internal stop codon of the *Foxp3* gene ($Foxp3^{iGFP}$). Sorted CD45.1 $Foxp3^-$ T_{conv} cells were transferred into lean congenic CD45.2 recipients. Four weeks after transfer, we consistently saw a very small population (~0.04% of total $Foxp3^+$ T_{regs}; ~787 cells/spleen and ~52 cells/LN) of donor $Foxp3^+$ pT_{regs} in spleen and LN, but we did not detect converted pT_{regs} among T_{regs} in VAT in any of the recipient mice from multiple independent transfer experiments (Figure 2.1C).

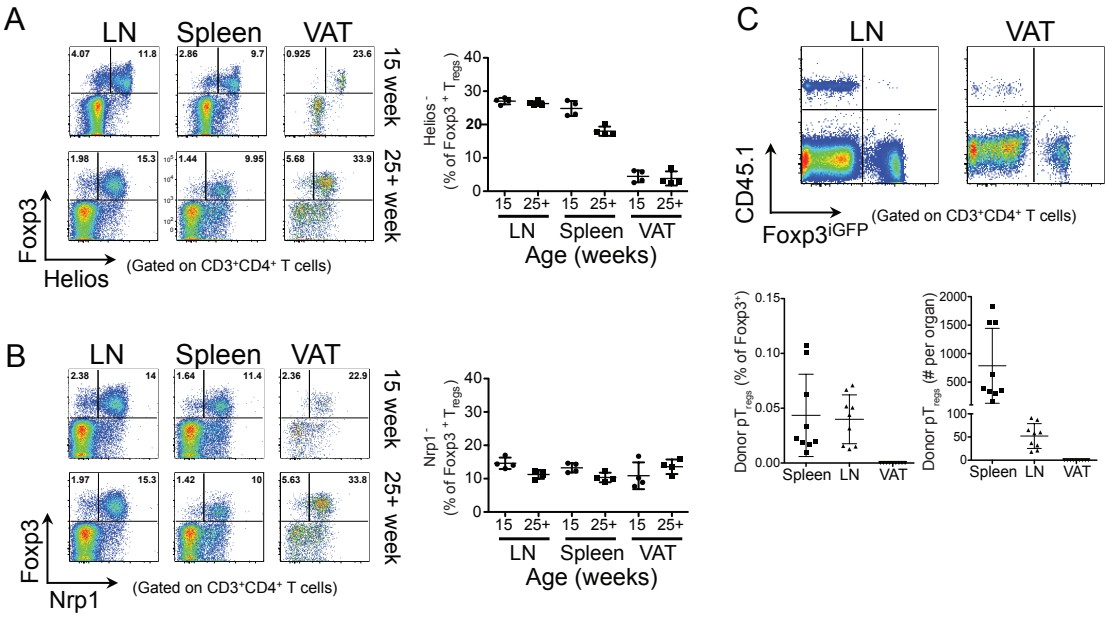

Figure 2.1: No hallmarks of pT_{regs} observed among VAT T_{regs}.
(A, B) Representative flow cytometry plots of Helios (**A, left**) and Nrp1 (**B, left**) expression among $CD4^+$ $Foxp3^+$ T_{regs} isolated from LN, spleen, and VAT of 15 and >25 week old mice. Quantification of frequency of $Helios^-$ (**A, right**) and $Nrp1^-$ (**B, right**) cells as a percentage of total T_{regs}. n = 4 for each age; pooled data from 2 independent experiments.
(C) $Foxp3^-$ T_{conv} cells from spleens and LN of CD45.1 $Foxp3^{iGFP}$ mice were transferred i.v. into CD45.2 $Foxp3^{iGFP}$ recipient mice. Representative flow cytometry plots from LN and VAT of recipient mice (top) and quantification of donor pT_{regs} as a percentage of total $Foxp3^+$ T_{regs} (bottom left) and as total number of cells recovered per organ (bottom right). n = 9; pooled data from 3 independent experiments.
All plots show means and standard deviations.

To further evaluate the contribution of pT_{regs} to the total VAT T_{reg} population, we used gene expression profiles from various pT_{reg} populations that have been previously generated in our lab and were used to define unbiased gene expression "signatures" for those pT_{reg} subsets (Feuerer et al., 2010). We chose to generate signatures of pT_{regs} from two models of *in vivo* conversion and from *in vitro* induced T_{regs} (iT_{regs}). In the first *in vivo* model, $Foxp3^+$ cells were generated by low dose administration of antigen, delivered to dendritic cells (DCs) by recombinant anti-DEC-205 antibodies fused to the influenza hemagglutinin (HA) peptide (Kretschmer et al., 2005) (referred to as "DEC205 pT_{regs}"). In the second model, conversion of naïve $CD4^+$ T_{convs} was achieved by transferring them into RAG-null mice, where the lymphopenic environment resulted in expression of Foxp3 in 5-10% of transferred cells (Haribhai et al., 2009) (referred to as "RAG-transfer pT_{regs}"). Finally, we also used iT_{regs}, which were generated from T_{conv} cells that were activated *in vitro* in the presence of IL-2 and TGFβ (Chen et al., 2003) (referred to as "TGFβ iT_{reg}").

We used the fold-change/fold-change (FC/FC) plots to compare gene expression profiles from pT_{reg} and T_{conv} cells from the same experiments (on the x-axis) versus *ex vivo* LN T_{reg} and T_{conv} cells (on the y-axis). This allowed us to exclude genes from the signatures that were differentially expressed due to experimental manipulations for generation of pT_{regs} (Figure 2.2A). We did not observe enrichment of any of the pT_{reg} signatures in VAT versus LN T_{reg} cells (Figure 2.2B). Taken together these data argue that generation of pT_{regs} from mature T_{conv} cells accounts for very few, if any, VAT T_{reg}

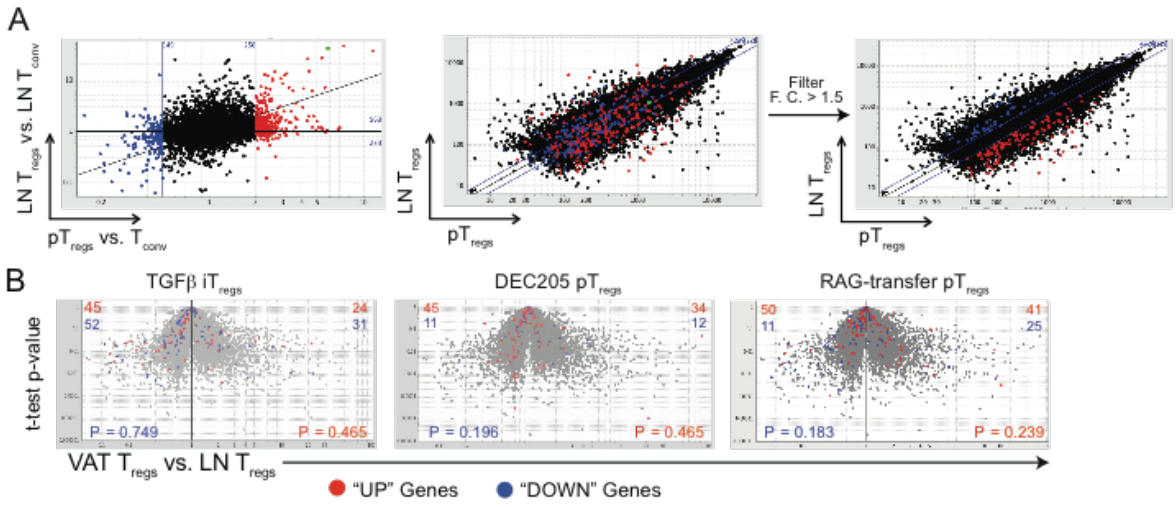

Figure 2.2: Generation of pT_{reg} signatures and analysis of VAT T_{regs} for enrichment of pT_{reg} signatures

(A) Schematic representation of the strategy used to generate pT_{reg} signatures Left: FC/FC plots comparing vis-à-vis gene expression profiles from pT_{regs} versus corresponding T_{convs} (x-axis) and *ex vivo* isolated LN T_{regs} versus T_{convs} (y-axis). Differentially expressed genes (> 2 fold) up-regulated (red) or down-regulated (blue) in were selected. Middle: genes highlighted (from left panel) on a plot comparing normalized expression values of LN T_{regs} and pT_{regs}. Right: genes that were > 1.5 fold up- or down-regulated represented the pT_{reg} signature.

(B) Volcano plots comparing VAT versus LN T_{regs} isolated from 30-week old mice (in triplicate). Indicated signatures were overlaid on each plot. *P* values were generated using chi-squared test.

cells and therefore is not the primary mechanism underlying accumulation of T_{regs} in lean VAT.

Minimal recruitment and retention of T_{regs} from lymphoid organs and circulation in VAT

Kaede transgenic (Kaede.B6) mice (Tomura et al., 2008) express a photoconvertible fluorescent protein, Kaede, in all cells under the control of *β-actin* promoter/enhance elements. Upon transcutaneous exposure to violet light, Kaede irreversibly changes in color from green to red, thereby "photo-tagging" (Kaede-Red) the cells present at the site of photoconversion in a minimally perturbant way, and allows for tracking of Kaede-Red cells in peripheral tissues using flow cytometry. We tracked the migration of T_{regs} from the cervical LN (CLN) to the VAT and the other peripheral LNs 24, 48, and 72 hours following photoconversion (Figure 2.3A). Consistent with previous findings from our laboratory (data not shown), T_{regs} were slower than T_{convs} in their egress from the LN (Figure 2.3B); however, the majority of Kaede-Red T_{regs} had egressed from the CLN by 24 hours after photoconversion. We then looked for Kaede-Red T_{regs} in two compartments: the inguinal/auxillary LNs (iLN/aLN) and the VAT. The iLN/aLN reflected the circulating T_{reg} pool among the secondary lymphoid organs, which served as a benchmark against which to measure the migration of T_{reg} to VAT. Kaede-Red T_{regs} preferentially recirculated to other lymphoid organs, as evidenced by a 2-3-fold higher frequency of Kaede-Red T_{regs} in the iLN/aLN

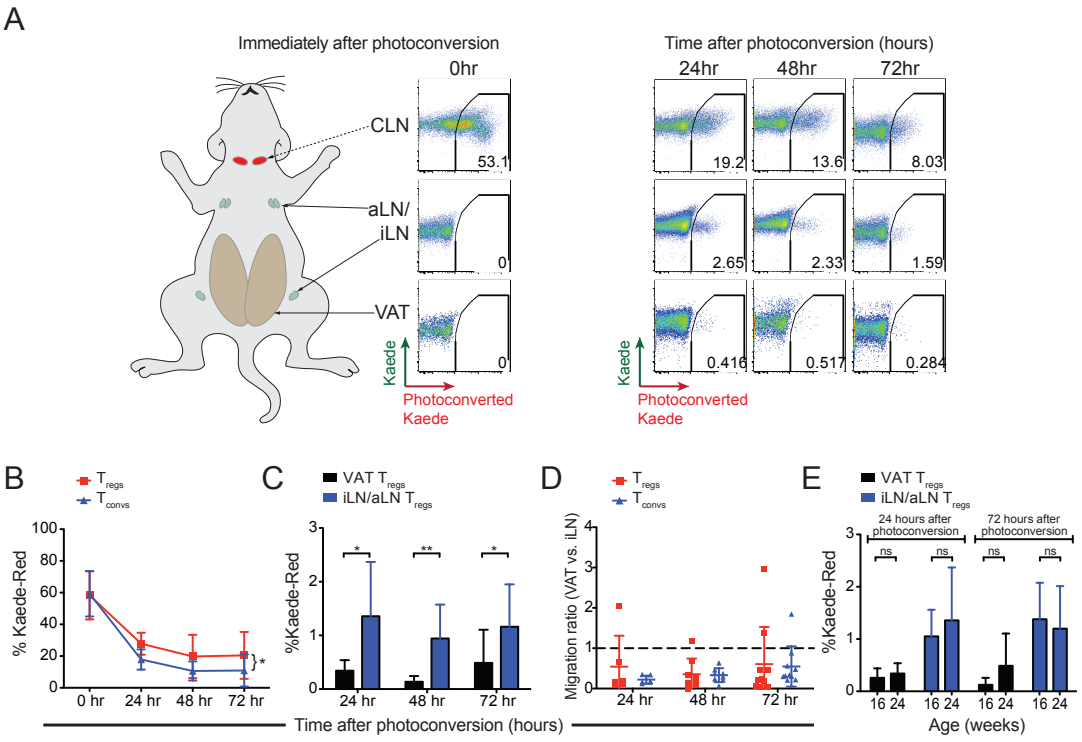

Figure 2.3: Steady-state migration of LN T_{regs} to VAT and other LN.
(A) Experimental setup and representative flow cytometry plots of $CD4^+$ T cells isolated from CLN, aLN/iLN, and VAT immediately after (0 hr) and 24, 48, and 72 hours after photoconversion.
(B) Frequency of Kaede-Red^+ T_{regs} and T_{convs} immediately after photoconversion (0hr) and after egress at 24, 48, and 72 hours after photoconversion.
(C) Frequency of Kaede-Red^+ cells as a percentage of total T_{regs} in VAT and iLN/aLN at indicated time points after photoconversion.
(D) Migration of T_{regs} and T_{convs} to VAT as a ratio of analogous populations migrating to iLN/aLN at indicated time points after photoconversion.
(E) Frequency of Kaede-Red^+ cells as a percentage of total T_{regs} in VAT and iLN/aLN 24 and 72 hours after photoconversion in 16- and 24- week old mice.
All data are n= 6-10 from 2-3 independent experiments. All plots show means and standard deviations.
* $p<0.05$, ** $p<0.01$

compared with the VAT (Figure 2.3C). It is important to point out that a small fraction of T_{regs} was indeed able to migrate from the CLN to the VAT at steady-state. Additionally, there were no changes in frequencies of Kaede-Red T_{regs} in the iLN/aLN or the VAT throughout the 72-hour experimental window (Figure 2.3C). To further assess the selective migration of Kaede-Red T_{regs} to the VAT, we quantified the frequency of Kaede-Red T_{regs} and T_{convs} in the VAT compared with analogous populations in the iLN/aLN (migration ratio). On average, Kaede-Red T_{regs} migrated preferentially to the iLN/aLN (migration ration < 1); however, in some individual animals Kaede-Red T_{reg} migration to the VAT was preferred (migration ratio > 1) (Figure 2.3D). We did not observe any differences in preferential migration between T_{regs} and T_{convs} to the VAT compared with iLN/aLN (Figure 2.3D). Finally, we looked at the effect of age on T_{reg} migration to the VAT by comparing mice at 16 and 24 weeks of age. Again, we did not observe any significant effects of age in migration of Kaede-Red T_{regs} to the iLN/aLN and the VAT in the two age groups (Figure 2.3E).

The Kaede.B6 model allowed us to study the T_{reg} migration at steady state; however, longer term studies were technically challenging, due to turnover or dilution of the photoconverted Kaede protein. We hypothesized that the small fraction that is able to migrate from the LN to the VAT might be able to accumulate given enough time and account for a larger fraction of the total VAT T_{reg} pool. To supplement our Kaede.B6 studies with longer term migration experiments, we transferred $Foxp3^{+}$ T_{regs} sorted from LN and spleens of CD45.1 $Foxp3^{iGFP}$ mice into lean, congenic CD45.2 $Foxp3^{iGFP}$ recipients. After 4 weeks, T_{regs} in the spleen and LN contained a small

fraction of transferred T_{regs}; however, this fraction was significantly lower and virtually unditectable in the VAT (Figure 2.4A). These findings were in line with the observations made with Kaede.B6 mice, suggesting that T_{regs} from LN and spleen preferentially migrate back to lymphoid organs and do not accumulate to a large fraction of VAT T_{regs}.

We wanted to investigate the effects of continuous T_{reg} migration on the total VAT T_{reg} pool over an extended period of time. For these studies, we conjoined CD45.1 mice with CD45.2 partners by parabiosis for 4 to 6 weeks, which allowed cells to circulate between the two animals and reach an equilibrium. We found that the T_{regs} in the spleen had equilibrated between the partners (chimerism of 39.8±4.2% after 4 weeks and 42.9±8.3% after 6 weeks), but the level of chimerism was significantly lower among VAT T_{regs} (chimerism of 17.2±5.8% after 4 weeks and 23.9±5.8% after 6 weeks) (Figure 2.4B), signifying that the majority of the VAT T_{reg} pool was composed of non-circulating cells. Furthermore, there were no significant differences in chimerism among T_{regs}, in either the spleen or the VAT, among pairs of mice that were conjoined for 4 or 6 weeks (Figure 2.4B), which suggested that the observed differences in chimerism between VAT and spleen T_{regs} were stable overtime.

In summary, short- and longterm migration studies argue that although a few T_{regs} can migrate from spleen and LN to VAT at steady-state, those cells account for only a small fraction of the total VAT T_{reg} pool and are not able to account for the total VAT T_{reg} accumulation over time.

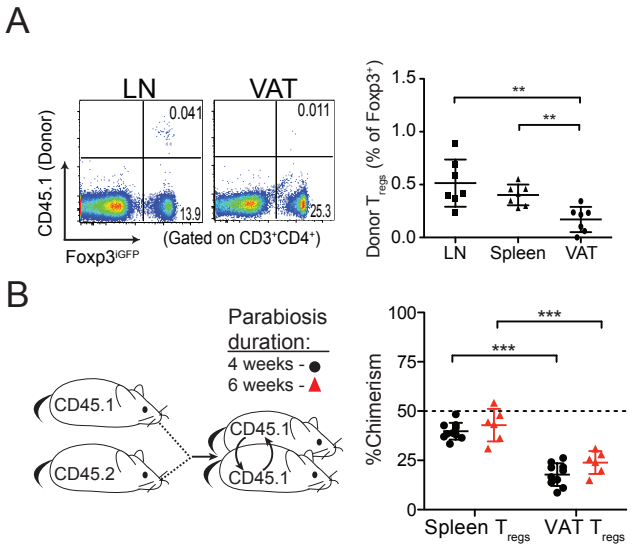

Figure 2.4: Circulating T_{regs} do not accumulate in VAT over time
(A) $CD4^+Foxp3^+$ T_{reg} cells were sorted from spleens and LN of CD45.1 $Foxp3^{iGFP}$ mice and transferred i.v. into CD45.2 $Foxp3^{iGFP}$ recipient mice. Representative flow cytometry plots of $CD4^+$ T cells from LN and VAT of recipient mice (left); quantification of donor T_{regs} expressed as a percentage of total $Foxp3^+$ T_{regs} (right). n = 7; pooled data from 3 independent experiments
(B) Schematic representation of parabiosis experiments: CD45.1 and CD45.2 mice were joined together for 4 or 6 weeks (left). Chimerism of T_{regs} in spleen and VAT (right). Chimerism = % donor / (% donor + % host). n = 6-8 for each length of parabiosis; pooled data from 2 independent experiments.
All plots show means and standard deviations. ** $p<0.01$, *** $p<0.001$

VAT T_{regs} have similar proliferative capacity, but lower turnover compared with splenic T_{regs}

Recruitment of circulating T_{regs} and conversion of T_{convs} into pT_{regs} were minor contributors to the accumulating VAT T_{reg} pool. We therefore hypothesized that *in situ* proliferation of T_{regs} in the VAT may be the dominant mechanism. Accumulation of a cell population in a given location could be a result of increased rate of proliferation or, conversely, decreased turnover rate. We first tested whether VAT T_{regs} have a higher proliferative capacity compared with splenic T_{regs}. EdU (5-ethynyl-20-deoxyuridine), incorporated by cells in S phase, was detected in similar fractions of T_{regs} in VAT and spleen after 4 hours of labeling, regardless of age (Figure 2.5A). Consistent with data from EdU-labeling experiments, we detected Ki67, which is expressed in all stages of the cell cycle except for the resting, G_0, phase, in comparable fractions among T_{regs} from VAT and spleen (Figure 2.5B). Taken together, these data suggested that VAT T_{regs} did not possess an increased proliferative rate that would account for their ability to accumulate.

Since VAT and spleen T_{regs} had similar proliferation rates, we measured their turnover using long-term bromodeoxyuridine (BrdU) incorporation followed by a BrdU-free chase. Mice were given BrdU in their drinking water for 5 weeks, starting at 15 weeks of age, to stably label the pool of dividing cells. There were no differences in the rate or extent of BrdU incorporation between VAT and splenic T_{regs}, paralleling our findings using EdU and Ki67 (Figure 2.5C left panel). After 5 weeks, BrdU was

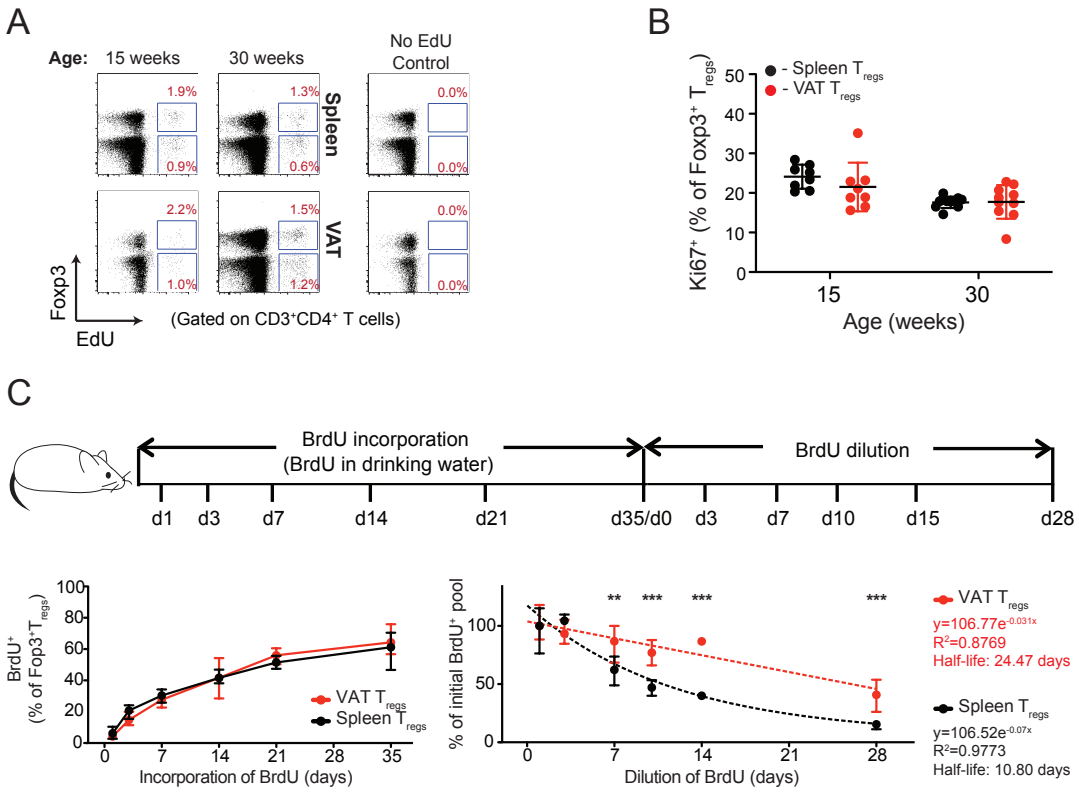

Figure 2.5: VAT T_{regs} have similar proliferative capacity, but lower turnover compared with splenic T_{regs}

(A) EdU uptake by T cells in spleen and VAT of 15- and 30-week old mice. Representative flow cytometry plots; frequencies indicate %EdU^+ among T_{regs} (top) or T_{convs} (bottom).

(B) Quantification of Ki67 expression by T cells in spleen and VAT of 15- and 30-week old mice as a percentage of $Foxp3^+$ T_{regs}.

(C) BrdU incorporation and chase experiment: schematic representation of experimental protocol (top). Quantification of $BrdU^+$ as a percentage of $Foxp3^+$ T_{regs} in spleen and VAT of mice analyzed on indicated days (bottom left). Quantification of remaining $BrdU^+$ $Foxp3^+$ T_{regs} in spleen and VAT of mice analyzed on indicated days as a percentage of the starting $BrdU^+$ $Foxp3^+$ T_{reg} pool on day 0 of chase (bottom right). Exponential decay line was fitted to each data set; equation, R^2 value, and half-life are presented (bottom right)

All data are n= 5-10 from 2-3 independent experiments. All plots show means and standard deviations.
** $p<0.01$, *** $p<0.001$

removed from the drinking water, which allowed us to measure the loss of $BrdU^+$ T_{regs} from VAT due to egress, cell death, or both. We found that VAT T_{regs} persisted significantly longer than spleen T_{regs}, evidenced by a higher fraction of the initial $BrdU^+$ T_{reg} pool remaining in VAT compared with the spleen (Figure 2.5C right panel). The calculated half-life for VAT T_{regs} was 24.5 days compared with half-life of 10.8 days for spleen T_{regs} and a half-life of 16.5 days for VAT T_{convs}, which would account for the increase in VAT T_{reg} frequency over time. Taken together our findings indicate that although T_{regs} proliferate at the same rate in the VAT and the spleen, VAT T_{regs} have a much slower rate of turnover, thereby allowing them to accumulate over time.

VAT T_{regs} are clonally expanded and display a unique TCR repertoire

We analyzed the complementarity-determining region (CDR) 3 of the TCRα and TCRβ chains on a single-cell level in order to assess the clonality of the T_{reg} populations in VAT and LN of 25-30 week old mice (Figure 2.6). This analysis allowed us to determine the contribution of the progeny originating from a single precursor to the overall VAT T_{reg} population and also to look for similarities in TCR repertoires between T_{regs} in the VAT and LN.

Consistent with the idea of a proliferation-driven accumulation, we found a striking degree of clonal expansion among VAT T_{regs}, with as much as ~77% of all TCR sequences among VAT T_{regs} of an individual mouse derived from clonally expanded populations, with individual clones accounting for up to ~30% of the total repertoire

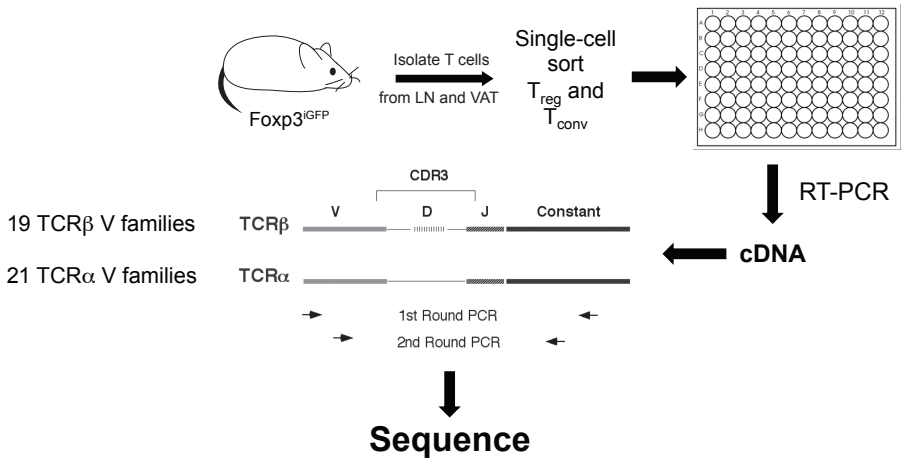

Figure 2.6: Schematic representation of single-cell TCR sequencing protocol
Individual T_{reg} or T_{conv} cells from VAT and LN were sorted into 96-well plates containing master mix for cDNA synthesis using TCRα and β constant region primers; cDNA was split in half and two rounds of nested multiplex PCR were used to separately amplify the TCRα and TCRβ CDR3 regions. Final PCR product was submitted for sequencing.

(Figure 2.7A). This observation was in stark contrast to VAT T_{convs} and LN T_{regs} (Figure 2.7B-D), where we found very few sequences that repeated more than one time. Furthermore, we did not find a single instance of sequence overlap between VAT T_{regs} and T_{convs}, consistent with previously reported sequencing results using mice with a genetically restricted TCR repertoire (Feuerer et al., 2009). Additionally, we did not find any sequences that were shared between LN and VAT T_{regs} highlighting the unique nature of the TCR repertoire among VAT T_{regs}. The total frequency of clonally expanded VAT T_{regs} directly correlated with the total frequency of VAT T_{regs} among VAT $CD4^+$ T cells (Figure 2.7E). Finally we did not detect any bias in the lengths of CDR3 loops (Figure 2.7F) nor the N-region length (data not shown) among the TCRs from clonally expanded VAT T_{regs} or total VAT T_{regs} compared with TCRs from LN T_{regs}, arguing that VAT T_{reg} differentiation occurred postnatally when terminal deoxynucleotidyl transferase (TdT) expression in the thymus was upregulated (Bogue et al., 1992).

In summary, the VAT T_{reg} TCR repertoire is restricted, with a few clones expressing particular TCRs being able to proliferate and expand to account for as much as 30% of all TCRs among VAT T_{regs}. In addition, the absence of shared TCR sequences between VAT T_{regs} and VAT T_{convs} as well as LN T_{regs}, highlights the distinctive nature of the VAT T_{reg} TCR repertoire.

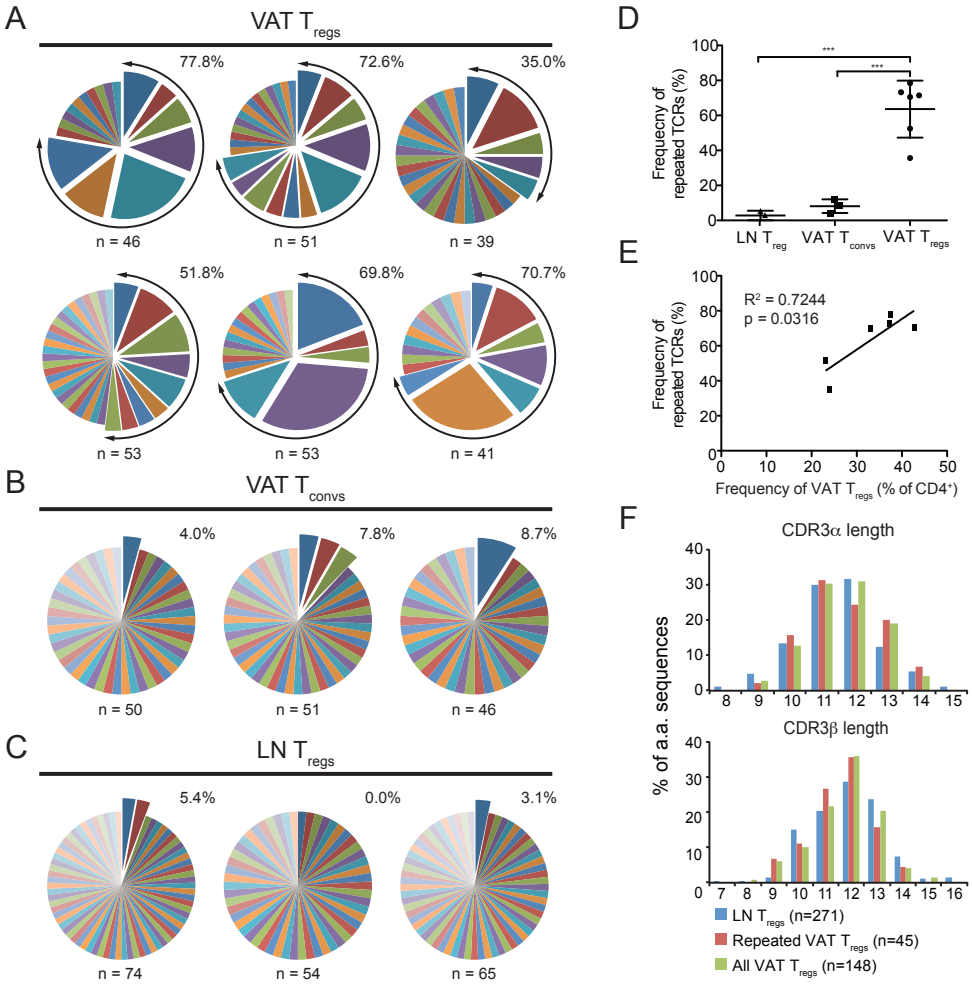

Figure 2.7: VAT T_{regs} are clonally expanded and display a unique TCR repertoire

(A - C) TCR CDR3α and CDR3β sequences for individual cells. **(A)** VAT T_{regs}, **(B)** VAT T_{convs}, and **(C)** LN T_{regs}. Each pie chart represents a single mouse. n, number of analyzed sequences per mouse. Total frequency of expanded clones shown at the top right.

(D) Quantification of clonal TCR frequencies among the examined T cell subsets. Mean and standard deviation are plotted. Sequences obtained from n = 3-6 individual mice

(E) Correlation between frequency of $Foxp3^+$ T_{regs} (% of $CD4^+$ T cells) and total frequency of repeated TCRs in each individual. R^2 value and p value generated using linear regression.

(F) Length of CDR3α and β amino-acid sequences in indicated populations. n, numbers of unique sequences in each indicated population.

Minimal contribution of adult thymus to Gata3$^+$ VAT T_{reg} pool

The extent of clonality that was present among VAT T_{regs} suggested that a "seeding" population of T_{regs} might infiltrate the VAT shortly after birth and proliferate *in situ* over a long period of time. This led us to hypothesize that thymic differentiation of T_{regs} in adult mice would not be required for VAT T_{reg} accumulation. We performed thymectomy (Thx) experiments in mice at 3, 6, and 13.5 weeks of age, just prior to VAT T_{reg} accumulation, and let the mice age until the peak of expansion at 25 weeks of age. Consistent with the idea that VAT T_{reg} accumulation occurs primarily due to proliferation, we did not see any differences in VAT T_{reg} expansion in mice Thx at 13.5 weeks of age (Figure 2.8A-C). Interestingly, Thx as early as 3 weeks of age also did not abrogate the expansion of VAT T_{regs} (Figure 2.8A-C).

PPARγ is required for VAT T_{reg} accumulation and for the ability of these cells to control adipose tissue inflammation. Previous studies demonstrated that Gata3 expression correlated with PPARγ expression in VAT T_{regs}, and treatment with a PPARγ antagonist led to a specific loss of Gata3$^+$ VAT T_{regs} (Cipolletta et al., 2012). There is currently no reliable way to detect expression of PPARγ by flow cytometry, so for the following studies we decided to use Gata3 as a surrogate marker for the expression of PPARγ. We wanted to confirm that the T_{regs} that accumulated in the VAT after Thx were bona fide VAT T_{regs}. Indeed we did not see any differences in frequency of Gata3$^+$ T_{regs} in the VAT of Thx animals compared with sham controls (Figure 2.8D).

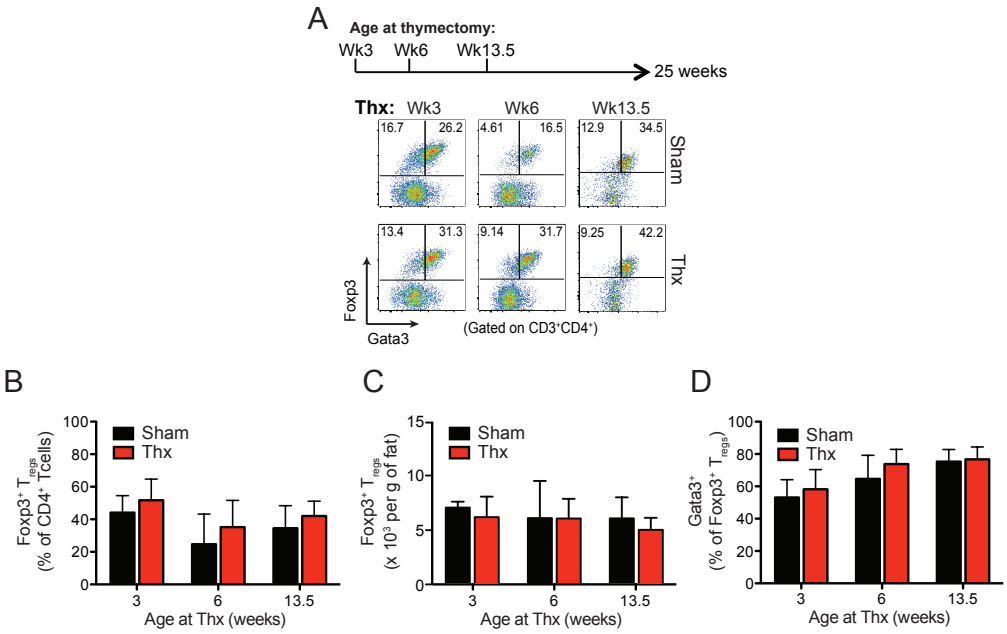

Figure 2.8: Minimal contribution of adult thymus to Gata3$^+$ VAT T_{reg} pool

(A) Schematic representation of thymectomy (Thx) experiments (top) and representative flow cytometry plots from VAT and spleens of Thx and sham surgery mice analyzed at 25 weeks of age (bottom).
(B - D) Quantification of (**B**) frequency of Foxp3$^+$ (% of CD4$^+$ T cells), (**C**) total numbers of Foxp3$^+$ T_{regs} (# per gram of adipose tissue), and (**D**) frequency of Gata3$^+$ (% of Foxp3$^+$ T_{regs}) in VAT described in (A). All data are n= 5-10 from 2-3 independent experiments. All plots show means and standard deviations.

Experiments with Thx mice showed that VAT T_{regs} can expand in the absence of an adult thymus, but it did not allow for the dissection of the contribution of the thymus to the total VAT T_{reg} pool throughout the expansion phase. To address this question we conjoined Thx mice with sham surgery (Sham) partners at 13.5 weeks of age for 4 weeks (Figure 2.9A). Since there was only one thymus in each parabiotic pair, the differences in chimerism among T_{reg} populations between the two partners would reflect the contribution of tT_{regs} that differentiated during the course of the experiment. Consistent with our hypothesis, the Thx partner had significantly higher level of chimerism among T_{regs} in the spleen (44.9±4.3% in Thx vs 33.2±3.2% in Sham) (Figure 2.9B), suggesting that the decreased chimerism in Sham partner reflected the lack of contribution of recent thymic emigrants (RTEs) to the splenic T_{reg} pool. Similarly we observed a significant decrease in overall chimerism among VAT T_{regs} (18.1±9.4% in Thx vs 8.1±4.9% in Sham) (Figure 2.9C), suggesting a significant infiltration of RTE T_{regs} into VAT. However, a closer analysis of the chimerisms among $Gata3^+$ and $Gata3^-$ VAT T_{reg} subsets revealed that there was a significant increase in chimerism among $Gata3^-$ VAT T_{regs} (Figure 2.9D); however, among $Gata3^+$ T_{regs} we did not detect a significant increase in chimerism, although a trend indicating a differential was evident (Figure 2.9E). These data suggest that VAT T_{regs} are composed of two population: a dynamic $Gata3^-$ T_{reg} population composed in part of cells coming from the thymus and circulation, and a more stable $Gata3^+$ T_{reg} population that is probably composed of bona fide VAT T_{regs}.

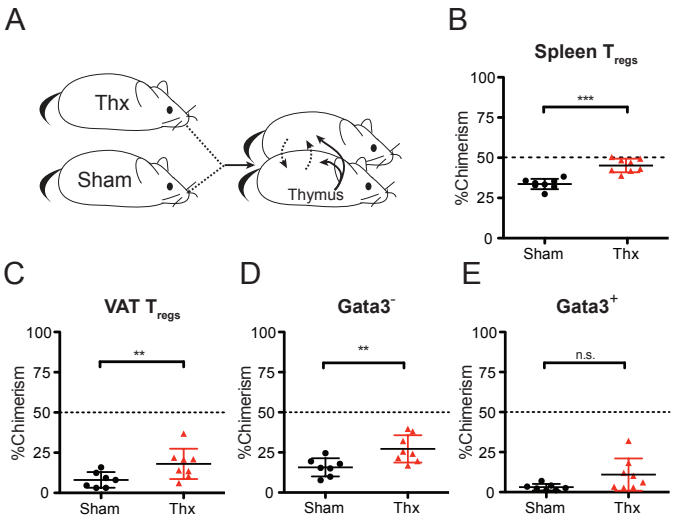

Figure 2.9: Adult thymus contributes to dynamic Gata3$^-$ VAT T$_{reg}$ pool
(A) Schematic representation of parabiosis pairs: thymectomy or sham surgeries were performed on CD45.1 and CD45.2 mice just prior to parabiosis; pairs were conjoined for 4 weeks before analysis.
(B) Quantification of chimerism among T$_{regs}$ from the spleen.
(C-E) Quantification of chimerism among (**C**) total VAT T$_{regs}$, (**D**) Gata3$^-$ VAT T$_{regs}$, and (**E**) Gata3$^+$ VAT T$_{regs}$.
All data are n= 8 parabiosis pairs from 2 independent experiments. All plots show means and standard deviations. ** p<0.01, *** p<0.001

These findings indicate that the bona fide VAT T_{reg} population, identified by the expression of Gata3, is seeded in the VAT at an early age and remains minimally infiltrated by circulating T_{regs} and RTE T_{reg} cells.

Ability of adult thymus to repopulate VAT T_{reg} compartment is age-dependent

One explanation for the minimal contribution of RTEs to the Gata3^{+} VAT T_{reg} pool in adult mice is that the "VAT T_{reg} niche" (a hypothetical combination of availability of presented-antigen, prosurvival factors, co-stimulatory molecules, etc.) is already completely occupied by resident T_{regs}, thereby preventing RTEs from being able to be retained or to survive in the VAT. Therefore, we wanted to directly test the ability of adult RTEs to seed the VAT at different ages by transiently depleting the VAT T_{reg} "niche". We treated Foxp3^{DTR} mice of varying ages with 2 daily injections of diphtheria toxin (Dtx) to punctually ablate T_{regs} systemically for a very brief period of time, in order to avoid development of autoimmune pathology. The mice were allowed to age until 25 weeks of age, at which point we assessed the accumulation of VAT T_{regs} (Figure 2.10A). Foxp3^{DTR} mice treated with Dtx at 16 days or 3-5 weeks of age had the same frequency of total T_{regs} (Figure 2.10B) and Gata3^{+} T_{regs} (Figure 2.10C) as Dtx-treated WT controls. However, Foxp3^{DTR} mice treated with Dtx at 13.5 weeks of age failed to accumulate VAT T_{regs} and had a significant decrease in the frequency of Gata3^{+} VAT T_{regs}, suggesting that neither tT_{regs} from an adult thymus or the converted pTregs contained the potential precursor pool capable of repopulating VAT T_{reg}.

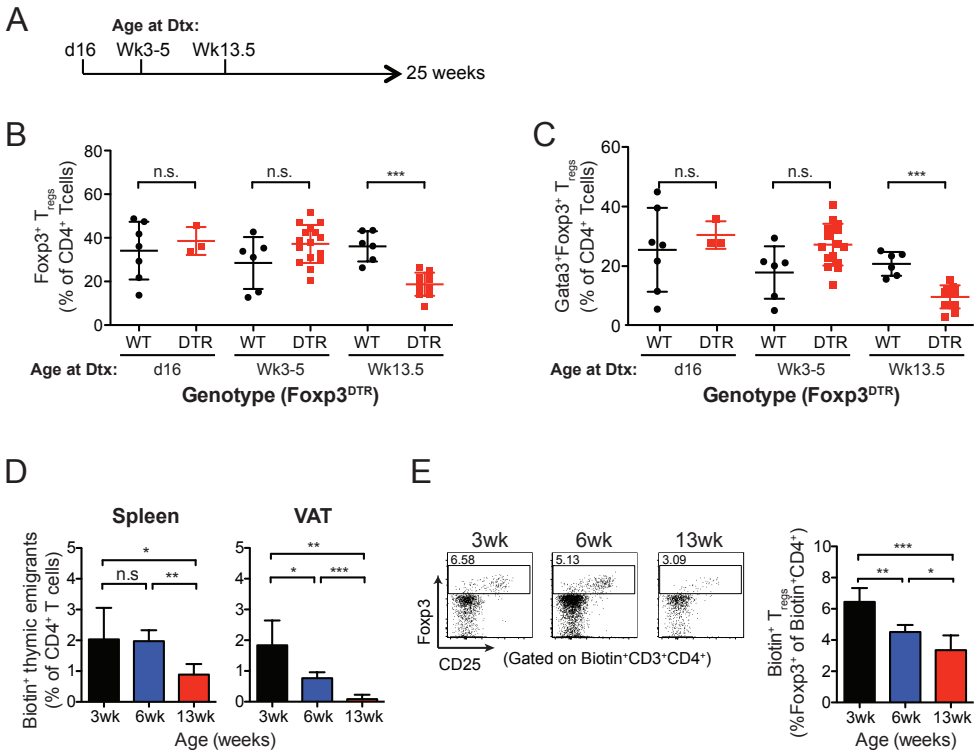

Figure 2.10: Ability of adult thymus to repopulate VAT T_{reg} compartment is age-dependent
(A-C) T_{reg} ablation in Foxp3^{DTR} mice via Dtx injection (**A**) Schematic representation of Dtx injection experiments. Quantification of (**B**) Foxp3$^+$ VAT T_{regs} (% of CD4$^+$ T cells) and (**C**) Gata3$^+$ T_{regs} (% of CD4$^+$ T cells) from Foxp3^{DTR} and WT littermates injected with Dtx at indicated ages. n = 3-16 mice for each age and genotype; data are pooled from multiple independent experiments.
(D-E) Tracking recent thymic emigrants (RTEs) following intrathymic injections with biotin.
(**D**) Quantification of Biotin$^+$ RTEs (% of CD4$^+$ T cells) in spleen (left) and VAT (right) in mice of indicated ages. (**E**) Representative flow cytometry plots of Foxp3 expression among RTEs (left) and quantification of percentage of Foxp3$^+$ cells among RTEs (right). n = 5 mice of each age; data are pooled from 2 independent experiments.
All plots show means and standard deviations. * $p<0.05$; ** $p<0.01$; *** $p<0.001$

A possible explanation for the inability of adult Foxp3^{DTR} mice to accumulate VAT T_{regs} following Dtx was that it was simply a reflection of the decreased thymic output in adult mice (Palmer, 2013), thereby decreasing the chances of differentiating a T_{reg} cell capable of repopulating the VAT. To test this directly, we performed intrathymic injections of a biotinylating agent in mice 3, 6, and 13 weeks of age, which allowed us to track RTEs in the periphery. Examination of the spleen and VAT revealed a progressive decline in RTEs in both tissues with age (Figure 2.10D). The decrease in RTEs infiltrating the VAT was particularly striking in 13-week old mice, which paralleled their inability to reconstitute the VAT T_{reg} compartment following Dtx. Furthermore, there was an age-associated decline in the frequency of Foxp3^{+} T_{regs} among RTEs in the spleen (Figure 2.10E) (Note inadequate numbers precluded a comparison with analogous populations from VAT).

In conclusion, RTE T_{regs} were able to seed the VAT when the VAT T_{reg} "niche" was perturbed in an age-dependent manner. This age-dependence was a result of decreased frequency of RTEs and a more striking decrease in frequency of Foxp3^{+} T_{regs} among the RTEs.

VAT T_{reg} accumulation requires MHC class II, but not CD1d

The striking clonanlity observed among VAT T_{regs} suggested that their proliferation might have been antigen-driven. We investigated the type of antigen presentation that was required for expansion of VAT T_{regs}. CD1d is a non-classical

MHC-like antigen presentation molecule that is able to present lipid antigens. Given the high abundance of lipids in the VAT and the ability of VAT T_{regs} to take up lipid (Cipolletta et al., 2012), we postulated that antigen-presentation on CD1d may be driving VAT T_{reg} expansion. Consistent with previously published results (Lynch et al., 2012), *CD1d*$^{-/-}$ mice had similar levels of VAT T_{reg} accumulation compared with WT mice (Figure 2.11A). Furthermore, we did not see any changes in expression of Gata3 among VAT T_{regs} in *CD1d*$^{-/-}$ and WT mice, confirming that antigen presentation by CD1d is not required for expansion of bona fide VAT T_{regs}.

Next we investigated the role of antigens presented by MHC class II molecules in driving expansion of VAT T_{regs}. MHC class II molecules play key roles in T_{reg} differentiation and maintenance; however, non-classical Foxp3^{+} cells have been reported in mice deficient in MHC class II (Bienvenu et al., 2005). MHC class II-null (*H2A*$^{-/-}$) mice had lower frequencies and numbers of Foxp3^{+} T cells compared with WT mice (Figure 2.11B). Furthermore, the few Foxp3^{+} T cells recovered from the VAT of *H2A*$^{-/-}$ mice expressed drastically lower levels of Gata3, suggesting that they were different from true VAT T_{regs}. Finally, we wanted to identify cells that express MHC class II molecules in VAT. Flow cytometric analysis revealed that MHC class II molecules restricted to the hematopoietic lineage evidenced by the expression of CD45 (99.1±0.35% CD45^{+} among I-A/I-E^{+} cells) (Figure 2.11C). Among I-A/I-E^{+} CD45^{+}, the majority of the cells were CD11b^{+} mononuclear cells that also co-expressed F4/80, therefore they were likely to be macrophages.

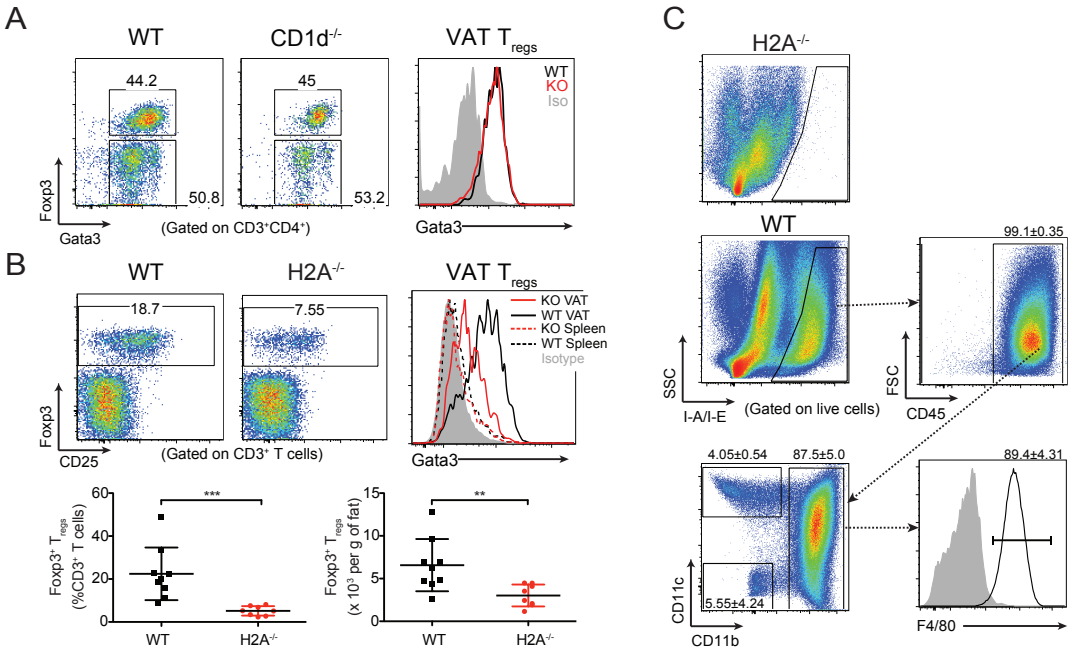

Figure 2.11: VAT T_{reg} accumulation requires MHC class II, but not CD1d

(A) Representative flow cytometry plots of VAT T_{regs} frequency (% of $CD4^+$ T cells) in WT (left) and *CD1d*$^{-/-}$ (middle) mice. (Right) Gata3 expression among VAT T_{regs}. Data representative of n = 3 for each genotype.

(B) Representative flow cytometry plots of VAT T_{regs} frequency (% of $CD3^+$ T cells) in WT (top left) and *H2A*$^{-/-}$ (top middle) mice. (Top right) Gata3 expression among $Foxp3^+$ T_{regs} from VAT and spleens of WT and KO animals. Quantification of frequency of $Foxp3^+$ T_{regs} (% of $CD3^+$ T cells) (bottom left) and number of $Foxp3^+$ T_{regs} (bottom right). n = 8 for each genotype; data pooled from 2 independent experiments. Plots show means and standard deviations. ** $p<0.01$; *** $p<0.001$

(C) Identification of MHC class II expressing population in VAT. Means and standard deviations in different gates are indicated. Flow cytometry plots are representative of n = 5 mice from 2 independent experiments.

In summary, VAT T_{reg} expansion requires the expression of MHC class II molecules and the dominant population that expresses MHC class II in VAT are the $CD45^+CD11b^+F4/80^+$ mononuclear phagocytes that are likely to be macrophages.

VAT T_{regs} express increasing amounts ST2 with age and *in vivo* administration of IL-33 elicits a potent expansion of VAT T_{reg}

ST2 (encoded by *Il1rl1*) is a receptor for the "alarmin" IL-33 (Schmitz et al., 2005). Previous results showed that *Il1rl1* was part of the *Pparg* co-cluster (Cipolletta et al., 2012), a collection of genes that positively correlated with *Pparg* expression. In one study, *in vivo* administration of IL-33 in obese mice led to amelioration of inflammation and improvement in insulin sensitivity (Miller et al., 2010). The authors attributed the insulin sensitizing effects of IL-33 to the polarization of macrophages towards M2-like phenotype and to an increase in Th2 cells; however, the study did not explore the potential effect of IL-33 on VAT T_{regs}. IL-33 was shown to be expressed in adipose tissue (Wood et al., 2009; Zeyda et al., 2013) and given the role of IL-33 as an "alarmin" (Schmitz et al., 2005; Pei et al., 2014), we hypothesized that T_{regs} might accumulate in VAT in response to IL-33.

First, we analyzed the expression of ST2 on T_{regs} from VAT and spleen at different ages. In the spleen, the population of $ST2^+$ T_{regs} was barely detectable and remained stable with age (Figure 2.12A); however, there was a dramatic increase of $ST2^+$ T_{regs} in the VAT (~90% of VAT T_{regs} were $ST2^+$ by 30 weeks of age), which

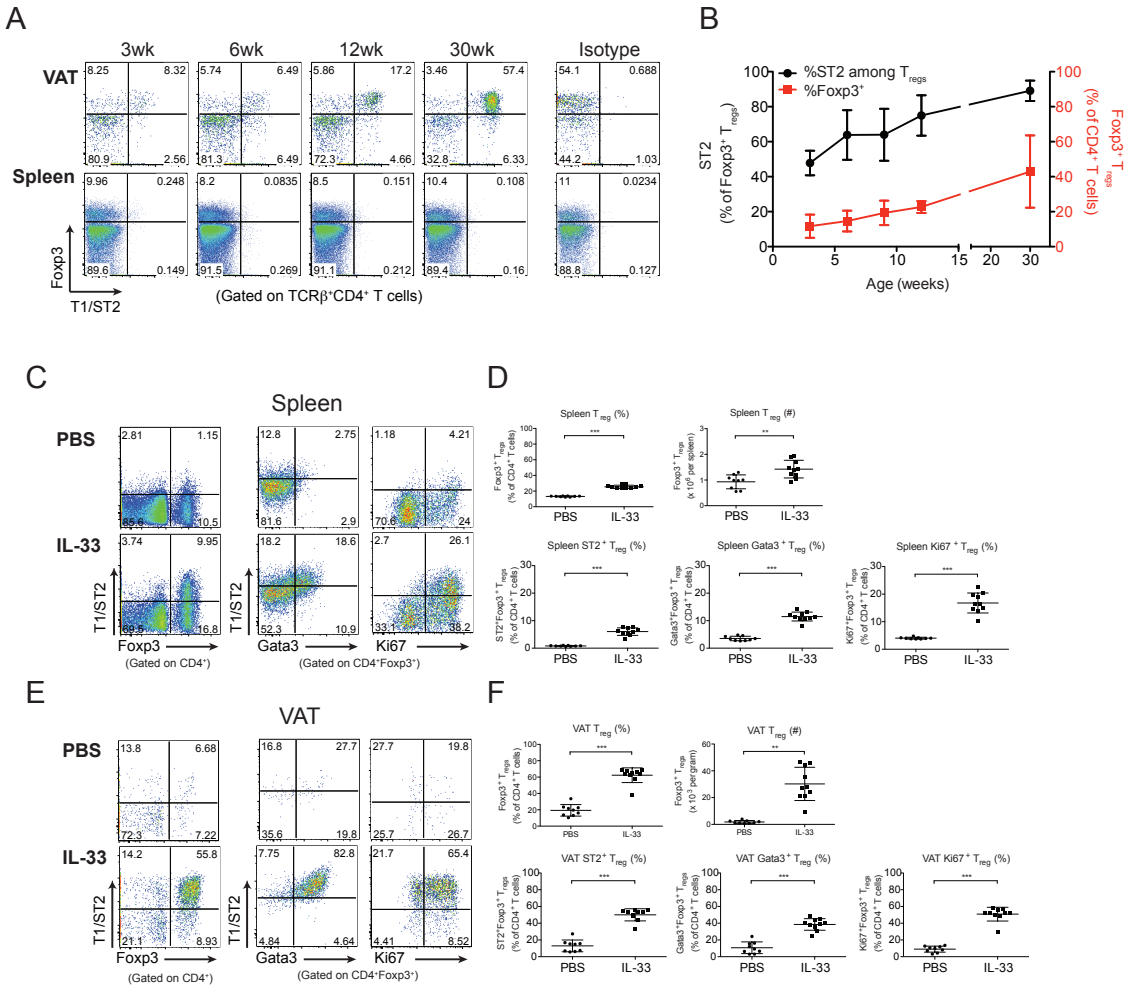

Figure 2.12: VAT T_{regs} express increasing amounts ST2 with age and *in vivo* administration of IL-33 elicits a potent expansion of VAT T_{regs}

(A) Representative flow cytometry plots of ST2 expression in T_{regs} from VAT and spleen analyzed at indicated ages.

(B) Quantification of data from (A): frequency of $Foxp3^+$ T_{regs} (% of $CD4^+$ T cells) (red) and frequency of $ST2^+$ T_{regs} (% of $Foxp3^+$ T_{regs}) (black) in different ages. n = 4-9 for each age; data are pooled from 3 independent experiments.

(C-F) 8-week old mice were treated with 2 injections of IL-33 or PBS every 3 days for 1 week prior to analysis. Representative flow cytometry plots from spleens (**C**) and VAT (**E**) of ST2, Gata3, and Ki67 expression by T_{regs}. Quantification of T_{reg} frequencies, absolute numbers, and ST2, Gata3, and Ki67 expressing populations in spleens (**D**) and VAT (**F**)**.** n = 10 mice per group; data pooled from 2 independent experiments.

All plots show means and standard deviations. ** p<0.01; *** p<0.001

directly correlated with accumulation of VAT T_{regs} (Figure 2.12A and B). Next we directly tested the effect of IL-33 on VAT T_{regs} through administration of recombinant IL-33 *in vivo* in 8-week old mice when frequency of VAT T_{regs} was still very low (on average < 15% of $CD4^+$ T cells). Even in the spleen, we saw a modest but significant increase in T_{reg} frequency and total numbers in IL-33-injected animals compared with PBS-injected controls (Figure 2.12C). This increase was most likely a result of proliferation as we observed a significant increase in the frequency of $Ki67^+$ T_{regs}. Interestingly, IL-33 administration led to a marked increase in Gata3 expression in splenic T_{regs}. The effect of IL-33 was even more pronounced in the VAT. VAT T_{reg} frequency increase 3-fold and the absolute numbers of VAT T_{regs} increased 15-fold (Figure 2.12D), which paralleled an increase in $Ki67^+$ fraction. There was a marked increase in the frequencies of $ST2^+$ $Gata3^+$ T_{regs} suggesting that the population of VAT T_{regs} responding to IL-33 treatment was phenotypically similar, at least by those two markers, to the population of bona fide VAT T_{regs} that expands clonally with age.

In summary, there is an age-associated increase in ST2 expression on VAT T_{regs}. IL-33 is produced in adipose tissue, and *in vivo* administration of exogenous IL-33 could drastically expand VAT T_{regs} through proliferation.

Discussion

There is increased appreciation for the role of T_{reg} cells in regulating homeostasis far beyond the scope of the traditional immune responses. The striking loss of VAT T_{regs} in obesity coupled with experimental and genetic manipulations of this population demonstrated their pivotal role in controlling adipose-tissue inflammation and maintaining insulin sensitivity (Feuerer et al., 2009; Cipolletta et al., 2012). The observation that VAT T_{regs} accumulated with age in lean mice to frequencies > 50% of the VAT-resident $CD4^+$ T cells, prompted us to try to get a deeper understanding of the mechanisms at play during this accumulation of VAT T_{regs}. A more profound knowledge of the dynamics of this important population of T_{regs} could help explain why lean mice remained insulin sensitive despite significant increases in total body and adipose tissue weights. We showed that VAT T_{reg} accumulation was not due to induction of Foxp3 expression in $CD4^+$ T_{conv} cells. We also observed minimal recruitment and migration of T_{regs} to VAT from circulation. Instead, VAT T_{regs} accumulated almost exclusively via proliferation and long-term persistence in VAT. The analysis of the TCR repertoire of VAT T_{regs} revealed a striking degree of clonal expansion and the extent of clonality correlated with the total frequency of VAT T_{regs}. Limiting the contribution of newly differentiated T_{regs} via thymectomy or, conversely, the deletion of T_{regs} at various ages revealed that up to a certain age newly differentiated tT_{regs} were capable of accumulation in the VAT. This potential of newly differentiated tT_{regs} for retention and expansion in VAT was decreased, in parallel, with the decrease

in total tT_{reg} output from the thymus. Expression of MHC class II molecules, on either macrophages or adipocytes themselves, was required for VAT T_{reg} expansion. Finally, VAT T_{regs} progressively increased with age in their expression of ST2, the receptor for IL-33, and *in vivo* administration of IL-33 was able to dramatically increase the numbers and frequencies of T_{regs} in VAT that were phenotypically similar to bona fide VAT T_{regs}.

It is highly unlikely that VAT T_{reg} accumulation represented a conversion of T_{convs} to pT_{regs} since essentially all VAT T_{regs} expressed high levels of Helios and Nrp1, considered to be markers of T_{regs} that differentiated in the thymus. In addition, we did not find enrichment of more comprehensive "gene signatures" of pT_{regs} in gene expression profiles from VAT T_{regs}. Transfer of sorted T_{conv} cells into lean recipients led to conversion of donor T_{convs} into pT_{regs} in spleens and LNs of recipient mice, albeit at a very low frequency; however, donor pT_{reg} were not detected among VAT T_{regs}, inconsistent with the high frequencies of conversion that we would have needed to detect in order to be considered as the dominant mechanism of VAT T_{reg} accumulation. Finally, analysis of TCR sequences from mice with genetically restricted repertoires (Feuerer et al., 2009) and from WT mice in our studies showed distinctly unique TCR repertoires in VAT T_{regs} and T_{convs}, arguing against conversion. However, a more definitive experiment to rule out conversion as a mechanism for VAT T_{reg} accumulation would be to analyze the accumulation of VAT T_{regs} in CNS1-mutant mice that are unable to generate pT_{regs}.

Similarly accumulation of VAT T_{regs} was not a result of recruitment of T_{regs} from the periphery. Kaede.B6 studies suggested that T_{regs} preferentially recirculate between lymphoid compartments, which was confirmed by parabiosis and transfer experiments. Even though we saw small fractions of T_{regs} migrating into the VAT in all of our experimental models, they represented only a minor fraction of the VAT T_{reg} compartment. Parabiosis experiments demonstrated that the chimerism of VAT T_{regs} was significantly lower than the chimerism of splenic T_{regs}. More importantly, there were no significant differences in chimerism of VAT T_{regs} comparing pairs conjoined for 4 or 6 weeks. These findings were inconsistent with the idea of continuous recruitment of circulating T_{regs} to VAT, which would have predicted an increase in chimerism over time.

Recruitment of T_{regs} from the peripheral lymphoid organs and circulation seemed like an attractive hypothesis given studies that showed recruitment of monocytes, neutrophils, and macrophages to VAT. However, those studies focused primarily on inflamed adipose tissue in the context of obesity, situations that correlated with the loss, and not accumulation, of VAT T_{regs}. Interestingly, the few T_{regs} recovered from obese VAT started to become more phenotypically similar to T_{regs} found in spleen and LN (unpublished observations), suggesting the possibility that in the uncontrolled inflammatory response in obese VAT there may actually be increased recruitment of circulating T_{regs}. On the contrary, we found that in lean VAT recruited T_{regs} constituted a minority of the total VAT T_{reg} compartment. Furthermore, when we divided the total VAT T_{reg} pool based on the expression of Gata3 in our studies combining Thx and

parabiosis, we showed that the majority of migrating T_{regs} did not express Gata3. This finding is particularly interesting, since Gata3 expression correlated with expression of PPARγ, and $Gata3^{+}$ VAT T_{regs} were preferentially lost after administration of a PPARγ antagonist and in T_{reg}-*Pparg* mut mice (Cipolletta et al., 2012). Taken together, these observations suggest that the bona fide VAT T_{reg} population that possesses the majority of the insulin sensitizing properties is not composed of recruited T_{regs}.

Instead, VAT T_{regs} accumulate due to local proliferation and retention *in situ*. VAT T_{regs}, in contrast to muscle T_{regs} (Burzyn et al., 2013), did not have an impressive proliferative burst, but rather proliferated at the same basal rate as splenic T_{regs}. However, BrdU-labeling experiments revealed that VAT T_{regs} were able to persist for a longer period of time as evidenced by their longer half-life compared with both VAT T_{convs} and spleen T_{regs}. Since there is minimal recruitment of T_{regs} to the VAT, this finding also suggests that there is no sizeable egress of T_{regs} from the VAT; however this point requires a more direct examination. Additional studies are needed to characterize the nature of the signals that allowed for enhanced survival of VAT T_{regs}. The analysis of the VAT T_{reg} TCR sequences confirmed and expanded upon the previous finding (Feuerer et al., 2009) that there was antigenic pressure driving the selection and expansion of a particular repertoire of TCR sequences. We found an unexpected and striking degree of clonal restriction among TCRs isolated from VAT T_{regs}. All in all, our findings suggest that there is an initial "seeding" of the VAT, where < 10 T_{reg} cells infiltrate the VAT, are retained therein, and are able to proliferate with age to a point where > ~70% of all VAT T_{regs} express one of those TCRs.

The origin of VAT T_{regs} remains unclear. Thymectomy experiments revealed that already by 3 weeks of age the VAT contained T_{regs} expressing the "correct" TCR to achieve the same levels of accumulation as seen in WT mice, which suggested that the adult thymus is dispensable for VAT T_{reg} accumulation. These findings paralleled with the observations that when a thymectomized partner was joined to a euthymic mouse there were significant differences in chimerism of $Gata3^-$ VAT T_{regs}, which we believe to be coming from the circulation. Although there was a slight, non-significant trend toward increased chimerism among the $Gata3^+$ population of VAT T_{regs}, these differences could be attributed to technical challenges arising from the analysis performed on exceedingly small numbers of donor T_{regs} that infiltrate the VAT, evidenced by the low chimerism of VAT T_{regs}. Taken together, these findings suggest that true VAT T_{regs} infiltrate the tissue very early and that the adult thymus has very minimal impact on VAT T_{reg} expansion.

Several immune cell subsets such as B1 cells, γδ T cell subsets, and tissue-resident macrophages have been shown to develop from fetal precursors, so it is possible that VAT T_{regs} have a similar ontogeny. However, several lines of evidence suggest that VAT T_{regs} differentiate postnatally. First, committed adipocyte precursor cells do not appear until postnatal day 4 and VAT does not become visible until postnatal day 7 (Rosen and Spiegelman, 2014); therefore the initial infiltration by T_{regs} probably occurs sometime between days 7 and 21 (the earliest age of thymectomies in our studies). Second, we did not detect a bias towards a shorter CDR3 lengths in the TCRs isolated from VAT $T_{regs,}$ suggesting that their TCR rearrangement occurred when

ample levels of TdT were expressed in the thymus, which functions in addition of nucleotides to generate extra diversity of CDR3 (Bogue et al., 1992). Finally, depletion of T_{regs} in $Foxp3^{DTR}$ mice did not abrogate VAT T_{reg} accumulation when performed at 16 days or 3-4 weeks of age, suggesting that the T_{regs} that differentiated after Dtx treatment contained appropriate VAT T_{reg} precursors. However, Dtx administration into $Foxp3^{DTR}$ mice at 13.5 weeks of age diminished VAT T_{reg} accumulation, which could be explained by the decrease in total thymic output in mice of that age, and a decreased frequency of $Foxp3^{+}$ T_{regs} among RTEs. In summary, there is a window in the first couple of weeks after birth when T_{regs} differentiate in the thymus, are able to infiltrate the VAT, and are able to proliferate with age. Future studies are needed to more carefully characterize the timing and molecular cues required for this initial seeding event, as well as to characterize the phenotype of T_{regs} that initially infiltrate the VAT. Several tools would need to be developed for these studies, in particular generation of transgenic mice encoding a TCR isolated from a clonally expanded VAT T_{reg} and a fluorescent *Pparg* reporter to determine the precise timing of PPARγ expression.

Consistent with the idea that the TCR is instructive in proliferation and expansion of VAT T_{regs}, we found that MHC class II molecules were required for VAT T_{reg} accumulation. We identified macrophages as the dominant population in the VAT that expressed MHC class II molecules, so the simplest interpretation is that macrophages might be presenting antigen to T_{regs}. Indeed, several previous reports indicated that VAT-resident macrophages were able to stimulate $CD4^{+}$ T cells *in vitro* and polarize $CD4^{+}$ T cells toward a Th1 phenotype *in vivo* (Morris et al., 2013; Moraes-

Vieira et al., 2014). These findings demonstrated that VAT-resident macrophages are capable of efficient antigen presentation and T cell stimulation. Furthermore, the localization of macrophages around dying adipocytes, forming crown-like structures, raises the possibility that the components of dying adipocytes engulfed by macrophages may be the source of antigen for the VAT T_{regs} and T_{convs}. This proposition is especially intriguing, since there is very little adipocyte death in lean fat; however, upon challenge with HFD, adipocyte death increases and initially is paralleled by an increase in IL-10 producing macrophages (Strissel et al., 2007). We can extrapolate these observations to suggest that lean adipose tissue in aged animals is similar to that of mice in the first few weeks of HFD, where low levels of adipocyte death are controlled by M2-like macrophages that produce a lot of IL-10 and might also activate VAT T_{regs}. Therefore, it would be interesting to correlate adipocyte death with VAT T_{reg} accumulation. In addition to macrophages, two reports claimed that adipocytes themselves were able to express MHC class II molecules and were able stimulate $CD4^+$ T cells in co-culture experiments (Meijer et al., 2011; Deng et al., 2013). Imaging experiments would be needed to confirm the interaction between the TCR on VAT T_{regs} and the MHC class II molecules expressed on either macrophages or adipocytes. It would be interesting to further dissect the role of MHC class II presentation by the two cell types through the use of conditional knockout mice, using *Adiponectin-Cre* or *LysM-Cre* to specifically eliminate expression of MHC class II molecules on adipocytes or macrophages, respectively, in order to determine which cell type is required by VAT T_{regs} for proper antigen presentation and for accumulation in VAT.

Several of the aforementioned lines of evidence suggested that TCR:MHC class II interactions are required for the accumulation of VAT T_{regs}, but the nature of the antigen remains unknown. We showed that antigen presentation on CD1d is dispensable, so it is likely that the antigen being recognized is not a lipid. However, several lines of evidence support the hypothesis that VAT T_{regs} may recognize adipose tissue-specific self-antigens. First, T_{regs} bearing the MJ23 TCR (specific for a prostate antigen) only infiltrated the prostate, the tissue of origin for the cloned TCR, and not any other tissues (Malchow et al., 2013). Second, in mice expressing an OVA-specific transgene-encoded TCR in combination with a second transgene, which allowed for inducible skin-restricted expression of OVA, there was a high frequency of T_{regs} that accumulated in the skin upon expression of OVA in order to attenuate inflammation driven by T_{conv} cells expressing the same transgene-encoded TCR. Extrapolating from these findings, it is likely that VAT T_{regs} are retained exclusively in the VAT, and recognize adipose-tissue specific antigens, quite possibly the same antigens that are being encountered by T_{convs} in the VAT.

In addition to TCR-mediated signaling, it is likely that VAT T_{regs} require other survival and proliferations signals for their expansion. Previous studies showed that PPARγ was required for VAT T_{reg} accumulation. Furthermore treatment of mice with a pharmacological agonist of PPARγ allowed for survival and expansion of T_{regs} even in obese VAT. We found that ST2, the receptor for IL-33, was upregulated in VAT T_{regs} with age and its expression correlated with expression of PPARγ. IL-33, an IL-1 family member, is an "alarmin" that is released into the extracellular space as an endogenous

danger signal for neighboring cells (Miller, 2011; Pei et al., 2014). Previous studies showed that IL-33 administration improved insulin sensitivity, although the exact mechanism was not clear (Molofsky et al., 2013; Miller et al., 2010). Both studies saw an increase in M2-macrophages and increased IL-10 production; however, one study suggested that the effect of IL-33 was on ILC2s, leading to eosinophil recruitment and polarization of macrophages (Molofsky et al., 2013), while the other report claimed that IL-33 promoted accumulation and activation of Th2 cells (Miller et al., 2010). We showed that administration of IL-33 also had a very profound effect on proliferation of VAT T_{regs}. The expanded population of VAT T_{regs} expressed high levels of Gata3 and Klrg1 (data not shown), markers that were lost in T_{reg}-*Pparg* mut mice; suggesting that IL-33 was acting on bona fide fat T_{reg} cells. Further studies will be needed to determine whether the effect of IL-33 on VAT T_{reg} cells is direct, due to their own expression of ST2 or if it acts indirectly through another cell subset. IL-33 was reported to be expressed in human adipose tissue (Wood et al., 2009; Zeyda et al., 2013); therefore, since IL-33 is an alarmin we can speculate that as a result of adipocyte death in VAT of aging mice, the active form of IL-33 is released by adipocytes and can induce T_{regs} to proliferate in order to control the associated inflammation.

In conclusion, our studies suggest that VAT T_{regs} differentiate in the thymus and infiltrate adipose tissue early after birth (probably postnatal day 7-21). Once inside the adipose tissue, they undergo clonal proliferation in response to antigen presented by MHC class II molecules by resident macrophages or adipocytes themselves. We speculate that the antigen is likely an adipose-tissue-restricted protein, potentially

derived from distressed or dying adipocytes that are picked up by macrophages. As a result of adipocyte death, the active form of IL-33 is released and is sensed by ST2 on T_{regs}, which, in combination with the TCR signal, results in clonal expansion and long-term survival of VAT T_{regs}.

Chapter 3: Clonal expansion of T_{regs} during skeletal muscle regeneration after acute and chronic injuries.

Note: The contents of this chapter have been previously published (Burzyn et al., 2013).

Introduction

There is a substantial accumulation of $Foxp3^+CD4^+$ T cells in skeletal muscle undergoing repair after acute injury. Skeletal muscle regeneration follows an orchestrated course of events that are driven largely by satellite cells, a pool of quiescent precursors closely associated with muscle fibers (Tabebordbar et al., 2013). In response to injury, these cells become activated, proliferate, differentiate, migrate, and fuse to form new myofibers. This series of events is controlled by the sequential activation and repression of specific transcription factors – for example Pax7, MyoD, myogenin (MyoG), and MEF2 (Rudnicki et al., 2008). With muscular dystrophies, in which chronic myofiber loss occurs due to genetic defects, the satellite cell pool is called on repeatedly, so it can exhaust or lose function over time, dampening the repair process (Tabebordbar et al., 2013). Additionally, regeneration of skeletal muscle is accompanied by a series of coordinated inflammatory events (Tidball and Villalta, 2010). Initially, circulating monocytes, neutrophils, and other myeloid mononuclear cells infiltrate the injured tissue. Within days, the pro-inflammatory state of the myeloid infiltrate switches to an anti-inflammatory phenotype, a shift that is critical for proper

muscle repair. Pro-inflammatory, or M1-type, macrophages function to clear apoptotic or necrotic cells and derivative debris. In contrast, the anti-inflammatory, or M2-type, macrophages have various pro-regenerative functions, such as matrix remodeling and promotion of angiogenesis. Ablation or impaired recruitment of monocytes and macrophages severely compromises muscle repair.

Given the importance of VAT T_{regs} in promoting adipose tissue homeostasis and insulin sensitivity, where a proper balance between pro- and anti-inflammatory macrophages is necessary, we investigated the role of T_{regs} in muscle regeneration. A unique population of $CD4^{+}Foxp3^{+}$ T_{reg} cells accumulates in skeletal muscle shortly after acute injury (Figure 3.1) (Burzyn et al., 2013). This population is a phenotypically and functionally distinct population of T_{reg} cells that rapidly accumulates in acutely injured skeletal muscle of mice, and correlates with the timing when invading myeloid-lineage cells switches from a pro-inflammatory to a pro-regenerative state. Consistent with acute muscle injury, a T_{reg} population with similar phenotype accumulated in muscles of genetically dystrophic mice. Punctual depletion of T_{reg} cells during the repair process prolonged the pro-inflammatory infiltrate and impaired muscle regeneration, while treatments that expanded or decreased T_{regs} enhanced or diminished muscle regeneration, respectively. Finally, muscle T_{reg} cells expressed the growth factor Amphiregulin (Areg), which acted directly on muscle satellite cells *in vitro* and improved muscle regeneration *in vivo*.

The accumulation of T_{regs} at the site of injury, which correlated with increased inflammation and infiltration of macrophages, was quite similar to the accumulation of

T_{regs} in VAT. This observation led us to ponder whether TCR-mediated clonal expansion was driving the accumulation of T_{regs} in skeletal muscle following acute injury and in muscles of dystrophic mice.

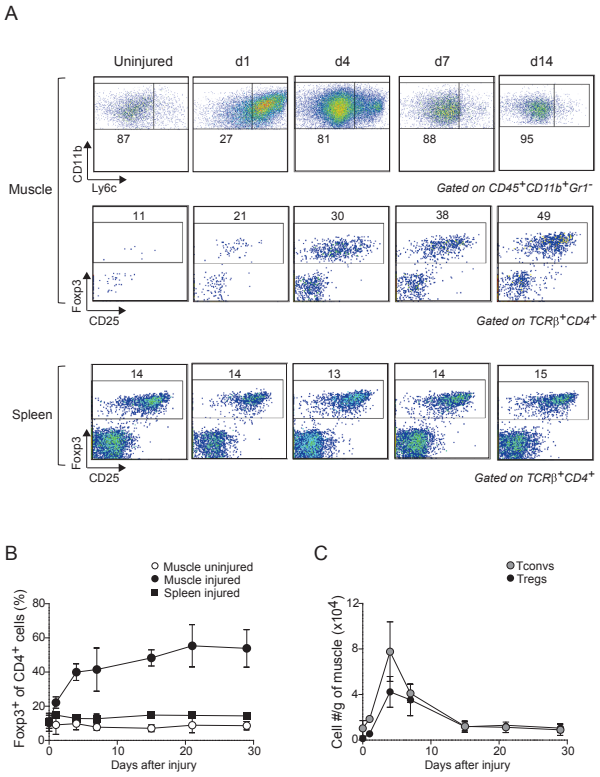

Figure 3.1: Treg accumulation at the site of injury. **(A-C)** Cytofluorometric analyses of hind-limb muscle infiltrates after Ctx injury. **(A)** Top: Ly6c expression by $CD11b^{+}$ cells. Middle and bottom: $Foxp3^{+}$ by $CD4^{+}$ cells. Numbers depict % $Ly6c^{low}$ (top) or % $Foxp3^{+}$ (middle and bottom) of gated cells. Representative of 3 independent experiments. **(B, C)** Summary data on fraction and number of cells. Mean ± s.d. ($n \geq 4$). Data in this figure were generated by Dr. Dalia Burzyn. Taken from (Burzyn et al., 2011) *Copyright 2013 Elsevier Ltd.*

Additional Materials and Methods

Mice

C57BL/10ScSn-Dmd^{mdx} mice were purchased from Jackson Laboratories. All mice were bred in our specific pathogen-free facilities at Harvard Medical School. Experiments were conducted under protocols approved by Harvard Medical School's Institutional Animal Care and Use Committee.

Skeletal muscle injury

Anesthetized mice were injected intramuscularly with 0.03 ml/muscle of Naja mossambica mossambica cardiotoxin (0.03 mg/ml) (Sigma) in one or more hindlimb muscles

Isolation of leukocytes from muscle

TA, gastrocnemius and quadriceps muscles were excised after perfusing the mice with PBS. Muscles were cut in small pieces and digested for 30 minutes with collagenase II (2 mg/ml, Invitrogen) and DNAse I (150 mg/ml, Sigma). The digested product was filtered through a 70mm mesh using a plunger to disrupt undigested tissue and washed with DMEM supplemented with serum. To separate the leukocyte fraction, the cells were resuspended in 40% Percoll, overlayed on 80% Percoll and spun for 25 minutes. The interphase containing leukocytes was recovered, washed and stained for single-cell sorting for TCR sequencing.

Results

T_{reg} cells in injured muscle are clonally expanded and display a unique repertoire of TCRs.

The rapid accumulation of T_{reg} cells at the injury site (Figure 3.1) could reflect their influx, proliferation or some combination of the two. Assessing expression of the cell-cycle marker, Ki67, and incorporation of the nucleotide analog, 5-ethynyl-2'-deoxyuridine (EdU), by muscle $CD4^+$ T cells four days after injury, i.e. at the peak of both T_{reg} and T_{conv} accumulation we showed that both T_{regs} and T_{convs} in skeletal muscle were actively proliferating. The level of proliferation by muscle $CD4^+$ T cells was much higher than that of their splenic counterparts (Burzyn et al., 2013).

To assess clonality of the T_{reg} population expanding in acutely injured skeletal muscle, we studied TCR repertoires by sequencing the complementarity-determining region (CDR)3 of both the TCR-α and -β chains of individually sorted cells. Already at day 2 after injury, and continuing out at least until day 8, a substantial proportion (20-40%) of muscle T_{reg} cells was clonally expanded (Figures 3.2A, 3.2B). This sequence profile contrasted starkly with that of splenic T_{reg} cells, for which there was not one repeat sequence in the 672 sampled. As expected from the Ki67 and EdU stainings (Burzyn et al., 2013), we also found clonal expansion of muscle T_{conv} cells (Figure 3.2B). However, there was not a single example of TCR-sequence sharing between muscle T_{reg} and T_{conv} cells.

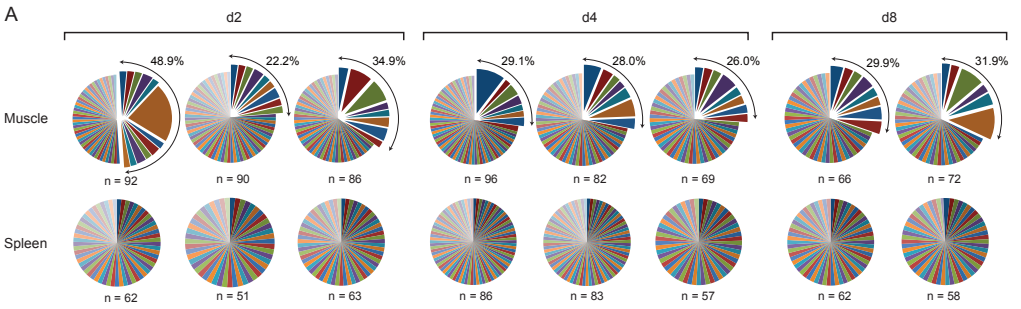

C

Mouse ID	Vα	Jα	CDR3α	Vβ	D	Jβ	CDR3β	Count (#)	Frequency of sequence (%)
d4 Mouse #1	TRAV9D-4*03	TRAJ39*01	CAVSNNAGAKLTF	TRBV13-2*01	None	TRBJ2-7*01	CASGDEQYF	10	10.42
d4 Mouse #2	TRAV9D-4*03	TRAJ39*01	CAVSNNAGAKLTF	TRBV13-2*01	None	TRBJ2-7*01	CASGDEQYF	5	6.10
d4 Mouse #3	TRAV9D-4*03	TRAJ39*01	CAVSNNAGAKLTF	TRBV13-2*01	None	TRBJ2-7*01	CASGDEQYF	2	2.90
d4 Mouse #4	TRAV9D-4*03	TRAJ39*01	CAVSNNAGAKLTF	TRBV13-2*01	None	TRBJ2-7*01	CASGDEQYF	1	1.27
d4 Mouse #5	TRAV9D-4*03	TRAJ39*01	C**VL**SNNAGAKLTF	TRBV13-2*01	None	TRBJ2-7*01	CASGDEQYF	8	8.89
d4 Mouse #6	TRAV9D-4*03	TRAJ39*01	CAVSNNAGAKLTF	TRBV13-2*01	None	TRBJ2-7*01	CASGDEQYF	1	0.84
d4 Mouse #7	TRAV9D-4*04	TRAJ39*01	CAVSNNAGAKLTF	TRBV13-2*01	None	TRBJ2-7*01	CASGDEQYF	4	2.88
d4 Mouse #8	TRAV9D-4*04	TRAJ39*01	CAVSNNAGAKLTF	TRBV13-2*01	None	TRBJ2-7*01	CASGDEQYF	4	3.42
d2 Mouse #1	TRAV9D-4*03	TRAJ39*01	CAVSNNAGAKLTF	TRBV13-2*01	None	TRBJ2-7*01	CASGDEQYF	2	2.17
d2 Mouse #2	TRAV9D-4*03	TRAJ39*01	CAVSNNAGAKLTF	TRBV13-2*01	None	TRBJ2-7*01	CASGDEQYF	1	1.11
d2 Mouse #3	TRAV9D-4*03	TRAJ39*01	C**VL**SNNAGAKLTF	TRBV13-2*01	None	TRBJ2-7*01	CASGDEQYF	1	1.16

Figure 3.2: Clonal expansion of the Treg population at the injury site. (A) TCR CDR3-α and CDR3-β sequences for individual cells. Each pie chart represents a single mouse. n: number of analyzed sequences per mouse. Total frequency of expanded clones shown at the top right. **(B)** Summary of clonal TCR frequencies over time. Open circles correspond to mice analyzed later in independent experiments for Figure 3.4. **(C)** Identical paired CDR3-α and β sequences found in multiple individuals in independent experiments. Two CDR3α sequences from independent mice bear two conserved substitutions. Taken from (Burzyn et al., 2013) *Copyright 2013 Elsevier Ltd.*

In the muscle T_{reg} datasets, there was a striking case of a repeatedly detected TCR: identical paired CDR3 α and β (and corresponding nucleotide) sequences picked up in multiple mice in completely independent experiments (Figure 3.2C). (Note that extensive precautions were taken to avoid contamination in this highly sensitive assay, and each sequencing plate was rigorously monitored). Interestingly, there were a few T_{reg} cells (from multiple individuals) that had the same TCR-β chain paired with an α chain whose CDR3 was modified only conservatively (AV→VL). These repeat sequences were found in mice 2 or 4, but not 8, days post-injury. They never showed up in the bulk spleen T_{reg} or muscle T_{conv} cell pools. These data document an early expansion of T_{reg} (and T_{conv}) cells in injured skeletal muscle within days after acute injury. To detect such expansions in mice with an unrestricted TCR repertoire is unexpected and quite striking. The muscle T_{reg} microexpansions render this population's TCR repertoire distinct from that of other T_{reg} populations.

Similar clonal expansions of T_{reg} population are found in the damaged muscles of mouse models of muscular dystrophy.

In muscular dystrophies, chronic destruction of muscle fibers is accompanied by an inflammatory response and, in general, a permanent infiltrate. Mdx mice carry a nonsense mutation in the *Dmd* gene (encoding Dystrophin), which is analogous to those found in DMD patients. In the mouse model, as in the human disease, the most affected sites are the diaphragm and hind-limb muscles (Grounds et al., 2008). We previously

showed that the fraction of T_{reg} cells in the muscles of mdx mice was significantly elevated vis-à-vis the frequency in corresponding muscles of wild-type mice in multiple ages; however, such an increase was not observed in the spleen.

Given the extent of clonal expansion in muscle T_{regs} following acute injury, we reasoned that similar microexpansions may be present in the muscles of mdx mice. The T_{reg} populations of mdx muscle exhibited clonal expansions, with an even greater fraction of the population derived from expanded clones (48.3% in mdx vs. 31.2% in Ctx-injured mice) and an even larger average clone size (4.68% in mdx vs. 3.68% in Ctx-injured mice) than found for Ctx-injured muscles of wild-type mice (compare Figures 3.2A and 3.3).

TCR sequences are shared between Areg$^+$ splenic T_{reg} and muscle infiltrating T_{reg} cells.

We showed that muscle T_{regs} expressed high levels of mRNA and protein encoding Areg, a protein that belongs to the epithelial growth factor (EGF) family and signals through the EGF receptor (EGFR) system (Shoyab et al., 1989). EGFR is expressed by a variety of cells, including muscle satellite cells and a myoblast cell line, in which it appears to have anti-apoptotic/survival functions (Golding et al., 2007; Horikawa et al., 1999). We showed that Areg augmented colony formation of muscle satellite cells *in vitro* and improved muscle regeneration following *in vivo*

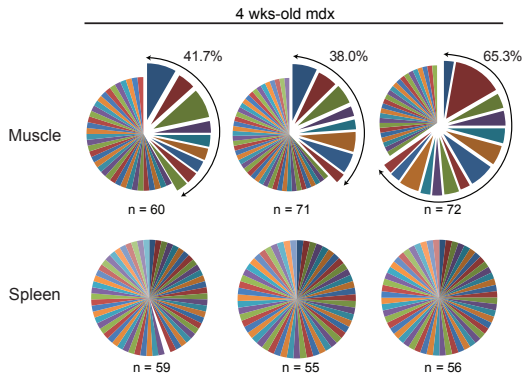

Figure 3.3: Clonal expansion of T_{reg} cells in muscles of dystrophic mice. T_{reg} clonal expansion in mdx muscle and spleens. TCR CDR3-α and CDR3-β sequences for individual cells. Each pie chart represents a single mouse. n: number of analyzed sequences per mouse. Total frequency of expanded clones shown at the top right. Taken from (Burzyn et al., 2011) *Copyright 2013 Elsevier Ltd.*

administration. In contrast to the high frequency Areg-expressing T_{reg} cells infiltrating the muscle, only a small fraction of spleen T_{regs} expressed Areg.

Since Areg was expressed by a small fraction of splenic T_{reg} cells in addition to a considerable proportion of muscle T_{regs}, we wondered whether the two $Areg^+$ populations might somehow be related. The TCR repertoires of splenic $Areg^+$ T_{reg} and muscle $Areg^+$ and $Areg^-$ T_{reg} cells shed interesting light on this issue (Figure 3.4). First, as opposed to the lack of clonality characteristic of bulk, unfractioned, splenic T_{reg} cells (Figure 3.2A), ~5% of the splenic $Areg^+$ subset was clonally expanded (Figure 3.4A). Second, a small population of splenic $Areg^+$ Treg cells appeared to include a muscle Treg constituent. There was some degree of overlap between the CDR3-α and -β sequences of splenic $Areg^+$ T_{reg} cells and those of muscle T_{regs} (Figure 3.4B). However the sharing of TCR sequences was independent of their expression of Areg. Third, the muscle $Areg^+$ and $Areg^-$ subsets showed no difference in their extent of clonal expansion (Figure 3.4C). Finally, although we again detected the oft-repeated TCR sequence described in Figure 3.2, there was no bias in its representation among the muscle $Areg^+$ and $Areg^-$ subsets.

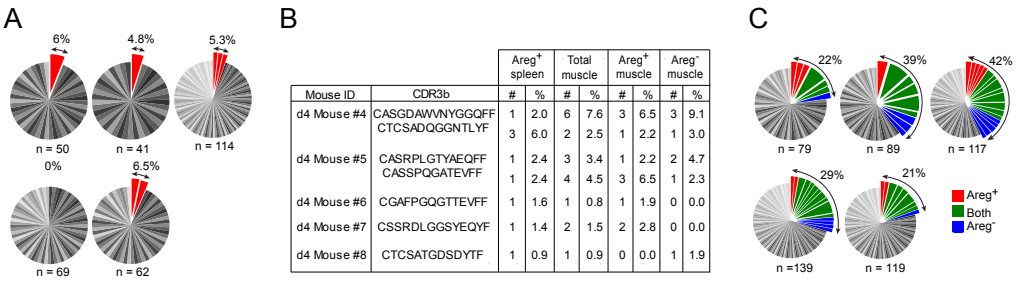

		Areg+ spleen		Total muscle		Areg+ muscle		Areg- muscle	
Mouse ID	CDR3b	#	%	#	%	#	%	#	%
d4 Mouse #4	CASGDAWVNYGGQFF	1	2.0	6	7.6	3	6.5	3	9.1
	CTCSADQGGNTLYF	3	6.0	2	2.5	1	2.2	1	3.0
d4 Mouse #5	CASRPLGTYAEQFF	1	2.4	3	3.4	1	2.2	2	4.7
	CASSPQGATEVFF	1	2.4	4	4.5	3	6.5	1	2.3
d4 Mouse #6	CGAFPGQGTTEVFF	1	1.6	1	0.8	1	1.9	0	0.0
d4 Mouse #7	CSSRDLGGSYEQYF	1	1.4	2	1.5	2	2.8	0	0.0
d4 Mouse #8	CTCSATGDSDYTF	1	0.9	1	0.9	0	0.0	1	1.9

Figure 3.4: Sharing of TCR sequences between Areg$^+$ splenic T_{reg} cells and muscle infiltrating T_{reg} cells. (A) TCR CDR3-α and -β sequences for individual Areg$^+$ splenic T_{reg} cells. Each pie chart represents a single mouse. n: number of analyzed sequences per mouse. Total frequency of expanded clones shown at the top right. **(B)** Identical paired CDR3-α (not shown) and -β sequences found in splenic Areg$^+$ and muscle Areg$^+$ and Areg$^-$ T_{reg} cells from the same individual in independent experiments. #: number of times the sequence was found. %: frequency of Tregs expressing the same sequence. **(C)** As in **A**, for muscle T_{reg} cells. Clones represented in Areg$^+$, Areg$^-$ or both subsets of muscle T_{regs} were labeled in red, blue and green, respectively. Taken from (Burzyn et al., 2011) *Copyright 2013 Elsevier Ltd.*

Discussion

T_{reg} cells began to accumulate in injured muscle within days after an injury. The fact that none of their TCRs was shared with muscle T_{conv} cells, suggests that this enrichment is unlikely to be due to a conversion of the T_{conv} to the pT_{reg} phenotype. Rather, the elevated levels of muscle T_{regs} appear to reflect population expansion: they were proliferating in the muscle, substantially more so than in the spleen, and constituted a number of clonally expanded micropopulations.

In addition, the TCR repertoires of injured-muscle and lymphoid-organ T_{reg} cells were clearly distinct. As expected, sampling of individual spleen T_{regs} never yielded the same TCR-α or -β chain sequence more than once, reflecting the huge diversity of the T cell repertoire. In contrast, there were striking clonal expansions in the muscle T_{reg} population, and one TCR-α and -β chain pair was found over and over again in different individuals despite extreme caution being utilized to avoid contamination. Interestingly, the small subset of $Areg^{+}$ splenic T_{regs} did share TCR sequences with muscle T_{reg} cells, whether Areg-positive or -negative. But it is not clear at present whether the splenic population seeds or arises from the T_{reg} population accumulating in injured muscle. These findings raise the possibility that a muscle antigen might be involved in recruiting T_{reg} cells to the site of injury and/or retaining them therein.

VAT T_{reg} cells share many of the particularities of injured-muscle T_{regs}: their enrichment, unusual transcriptome, and clonally expanded TCR repertoire ((Feuerer et al., 2009) and data from Chapter 2). However, none of the TCR sequences were shared

between VAT and muscle T_{regs}, hinting at the possibility that the expansion is driven by a different set of tissues-specific antigens in the two tissues. Indeed, this would be consistent with the observation that T_{regs} bearing the MJ23 TCR only infiltrated the prostate, the tissue of origin for the cloned TCR, and not any other tissues (Malchow et al., 2013). Furthermore, the fact that the same, or very closely related, sequence was consistently found across multiple individual mice during muscle injury suggests the presence of strong antigenic pressure. Indeed, it would be very interesting to see if the oft-repeated TCR sequence would be able to lead to efficient T_{reg} cell differentiation, depend on AIRE expression, and restrict T_{regs} to skeletal muscle, as was the case for MJ23.

Chapter 4: General Discussion

In recent years, more attention has been paid to the role of T_{regs} in controlling non-immune functions, such as improving insulin sensitivity and potentiating muscle regeneration after injury. Striking effects on pathologies, achieved through various experimental manipulations of these populations, make them attractive targets for therapies. However, simply measuring accumulation or loss of these T_{reg} populations does not paint the whole picture of complexity that is involved in the dynamics of tissue-resident T_{regs}. A deeper understanding of the mechanisms that underlie the dynamics of these populations could provide new insights into the functions of these cells.

In the case of VAT T_{regs}, we were considering three different mechanisms of expansion (recruitment, conversion, and proliferation), but were surprised to find that essentially only proliferation seemed to be involved in accumulation of true fat T_{regs}. In contrast, we did not find nearly the same level of clonal expansion in muscle T_{regs}, which could mean that the accumulation of T_{regs} in the regenerating muscle may be driven by recruitment rather than expansion. Indeed, the TCR sequencing data revealed that a few clones were shared between the T_{regs} isolated from muscles and spleen of the same individual, suggesting that the two compartments may be linked. Finally, in contrast to both the VAT and muscle contexts, T_{regs} residing at barrier surfaces, especially in the gastrointestinal tract rely on conversion of T_{convs} to pT_{regs} in response to certain species of commensal microbiota. Taken together these findings provide us with

a glimpse of heterogeneity and division of labor among tissue-resident T_{regs} through the lens of the methods used for tissue-accumulation.

Our studies on VAT and muscle T_{regs} allowed us to compare and contrast the dynamics of the two populations. An interesting contrast between muscle and VAT T_{regs} is the level of clonality seen among these cells. The muscle T_{reg} population is dominated by a large number of microexpansions, while VAT T_{regs} are composed of only a few clones in each individual. This difference could reflect the length of time needed for expansion, a few days for muscle T_{regs} and months of VAT T_{regs}, allowing for selection of optimal combination of clones over time in VAT. Alternatively, the differences could be driven by the degree of inflammation in each situation. VAT is characterized by chronic low-grade inflammation that never resolves, while the inflammatory response in muscle injury is acute and prodigious. Consistent with this notion, mdx mice that suffer from a lower level of inflammation that persists for a much longer time compared with acute Ctx-injury displayed larger average clone size and a larger fraction of the total population derived from clonally expanded cells. However, an alternative explanation for the differences between mdx mice and the Ctx-injury model is that in the former the injury is driven by a single mutation and does not have nearly the level of heterogeneity of tissue damage that is present in Ctx-injury model. Yet a third interpretation is that the mechanisms of accumulation are different for muscle and fat T_{regs}. It is possible that since the inflammation is induced so rapidly and to such a large extent that a large pool of T_{regs} with a broad range of phenotypes and TCR-specificities is recruited to the site of inflammation. As the acute phase of inflammation resolves and the regenerative phase

begins, the population of T_{regs} changes over time to perform different functions. This notion would help explain why the oft-repeated TCR sequence in the muscle T_{regs} was isolated only from mice at early, but not late, time-points after injury. In contrast, the more restricted TCR usage among T_{reg} clones isolated from VAT hints that VAT T_{regs} are probably responding to a more restricted set of antigens that persist for a long time. This makes having a local pool of T_{regs} with a narrowly defined set of TCRs more effective at suppressing the low-grade inflammation in adipose tissue of aging mice.

The scope of my studies allowed us to begin making some generalizations about the relationships between the dynamics of a population and their function. However technological challenges and the difficulties of interrogating the tissue-resident T_{regs} specifically have limited our ability to perform more complex analyses to uncover the relationship between TCRs of tissue resident T_{regs} and their corresponding functions. Future studies would need to focus on relating TCR sequences expressed by T_{regs} to the preferred mechanism of accumulation and to their functions in suppressing inflammation. The emergence of technologies to profile various "omic-level" parameters in individual cells could begin to answer some of these questions and provide another level of complexity to the population dynamics and functions of tissue-resident regulatory T cells.

Several overarching questions emerge from these studies: What are the advantages and disadvantages of each of these methods of accumulation? When and how do tissue T_{regs} become specialized and begin to utilize the appropriate mode of accumulation? What factors and signals govern each of these mechanisms? Our current

understanding is just beginning to scratch the surface of the answers to these questions and future studies will undoubtedly uncover even more functions and complexities of tissue-resident regulatory T cells.

References

Akimova, T., Beier, U.H., Wang, L., Levine, M.H., and Hancock, W.W. (2011). Helios expression is a marker of T cell activation and proliferation. PLoS. ONE. *6*, e24226.

Apostolou, I., Sarukhan, A., Klein, L., and von Boehmer, H. (2002). Origin of regulatory T cells with known specificity for antigen. Nat Immunol *3*, 756-763.

Baker, F.J., Lee, M., Chien, Y.H., and Davis, M.M. (2002). Restricted islet-cell reactive T cell repertoire of early pancreatic islet infiltrates in NOD mice. Proc Natl Acad Sci U S A *99*, 9374-9379.

Bautista, J.L., Lio, C.W., Lathrop, S.K., Forbush, K., Liang, Y., Luo, J., Rudensky, A.Y., and Hsieh, C.S. (2009). Intraclonal competition limits the fate determination of regulatory T cells in the thymus. Nat. Immunol. *10*, 610-617.

Bennett, C.L., Christie, J., Ramsdell, F., Brunkow, M.E., Ferguson, P.J., Whitesell, L., Kelly, T.E., Saulsbury, F.T., Chance, P.F., and Ochs, H.D. (2001). The immune dysregulation, polyendocrinopathy, enteropathy, X-linked syndrome (IPEX) is caused by mutations of FOXP3. Nat. Genet. *27*, 20-21.

Bienvenu, B., Martin, B., Auffray, C., Cordier, C., Becourt, C., and Lucas, B. (2005). Peripheral CD8+CD25+ T lymphocytes from MHC class II-deficient mice exhibit regulatory activity. J Immunol *175*, 246-253.

Bilate, A.M. and Lafaille, J.J. (2012). Induced CD4+Foxp3+ regulatory T cells in immune tolerance. Annu. Rev. Immunol. *30*, 733-758.

Bogue, M., Gilfillan, S., Benoist, C., and Mathis, D. (1992). Regulation of N-region diversity in antigen receptors through thymocyte differentiation and thymus ontogeny. Proc. Natl. Acad. Sci. U. S. A *89*, 11011-11015.

Brochet, X., Lefranc, M.P., and Giudicelli, V. (2008). IMGT/V-QUEST: the highly customized and integrated system for IG and TR standardized V-J and V-D-J sequence analysis. Nucleic Acids Res. *36*, W503-W508.

Brunkow, M.E., Jeffery, E.W., Hjerrild, K.A., Paeper, B., Clark, L.B., Yasayko, S.A., Wilkinson, J.E., Galas, D., Ziegler, S.F., and Ramsdell, F. (2001). Disruption of a new forkhead/winged-helix protein, scurfin, results in the fatal lymphoproliferative disorder of the scurfy mouse. Nat. Genet. *27*, 68-73.

Burchill, M.A., Yang, J., Vogtenhuber, C., Blazar, B.R., and Farrar, M.A. (2007). IL-2 receptor beta-dependent STAT5 activation is required for the development of Foxp3+ regulatory T cells. J Immunol *178*, 280-290.

Burzyn, D., Kuswanto, W., Kolodin, D., Shadrach, J.L., Cerletti, M., Jang, Y., Sefik, E., Tan, T.G., Wagers, A.J., Benoist, C., and Mathis, D. (2013). A special population of regulatory T cells potentiates muscle repair. Cell *155*, 1282-1295.

Center for Disease Control and Prevention (2011). 2011 National Diabetes Fact Sheet.

Charriere, G., Cousin, B., Arnaud, E., Andre, M., Bacou, F., Penicaud, L., and Casteilla, L. (2003). Preadipocyte conversion to macrophage. Evidence of plasticity. J Biol. Chem. *278*, 9850-9855.

Chatila, T.A., Blaeser, F., Ho, N., Lederman, H.M., Voulgaropoulos, C., Helms, C., and Bowcock, A.M. (2000). JM2, encoding a fork head-related protein, is mutated in X-linked autoimmunity-allergic disregulation syndrome. J Clin Invest *106*, R75-R81.

Chaudhry, A., Rudra, D., Treuting, P., Samstein, R.M., Liang, Y., Kas, A., and Rudensky, A.Y. (2009). CD4+ regulatory T cells control TH17 responses in a Stat3-dependent manner. Science *326*, 986-991.

Chen, W., Jin, W., Hardegen, N., Lei, K.J., Li, L., Marinos, N., McGrady, G., and Wahl, S.M. (2003). Conversion of peripheral CD4+CD25- naive T cells to CD4+CD25+ regulatory T cells by TGF-beta induction of transcription factor Foxp3. J. Ex. Med. *198*, 1875-1886

Chung, Y., Tanaka, S., Chu, F., Nurieva, R.I., Martinez, G.J., Rawal, S., Wang, Y.H., Lim, H., Reynolds, J.M., Zhou, X.H., Fan, H.M., Liu, Z.M., Neelapu, S.S., and Dong, C. (2011). Follicular regulatory T cells expressing Foxp3 and Bcl-6 suppress germinal center reactions. Nat Med *17*, 983-988.

Cinti, S., Mitchell, G., Barbatelli, G., Murano, I., Ceresi, E., Faloia, E., Wang, S., Fortier, M., Greenberg, A.S., and Obin, M.S. (2005). Adipocyte death defines macrophage localization and function in adipose tissue of obese mice and humans. J Lipid. Res. *46*, 2347-2355.

Cipolletta, D., Feuerer, M., Li, A., Kamei, N., Lee, J., Shoelson, S.E., Benoist, C., and Mathis, D. (2012). PPAR-gamma is a major driver of the accumulation and phenotype of adipose tissue Treg cells. Nature *486*, 549-553.

Cipolletta, D., Kolodin, D., Benoist, C., and Mathis, D. (2011). Tissular T(regs): a unique population of adipose-tissue-resident Foxp3+CD4+ T cells that impacts organismal metabolism. Semin. Immunol. *23*, 431-437.

Collison, L.W., Workman, C.J., Kuo, T.T., Boyd, K., Wang, Y., Vignali, K.M., Cross, R., Sehy, D., Blumberg, R.S., and Vignali, D.A. (2007). The inhibitory cytokine IL-35 contributes to regulatory T-cell function. Nature *450*, 566-569.

DeFuria, J., Belkina, A.C., Jagannathan-Bogdan, M., Snyder-Cappione, J., Carr, J.D., Nersesova, Y.R., Markham, D., Strissel, K.J., Watkins, A.A., Zhu, M., Allen, J., Bouchard, J., Toraldo, G., Jasuja, R., Obin, M.S., McDonnell, M.E., Apovian, C., Denis, G.V., and Nikolajczyk, B.S. (2013). B cells promote inflammation in obesity and type 2 diabetes through regulation of T-cell function and an inflammatory cytokine profile. Proc Natl Acad Sci U S A *110*, 5133-5138.

Deiuliis, J., Shah, Z., Shah, N., Needleman, B., Mikami, D., Narula, V., Perry, K., Hazey, J., Kampfrath, T., Kollengode, M., Sun, Q., Satoskar, A.R., Lumeng, C., Moffatt-Bruce, S., and Rajagopalan, S. (2011). Visceral adipose inflammation in obesity is associated with critical alterations in tregulatory cell numbers. PLoS. ONE. *6*, e16376.

Deng, T., Lyon, C.J., Minze, L.J., Lin, J., Zou, J., Liu, J.Z., Ren, Y., Yin, Z., Hamilton, D.J., Reardon, P.R., Sherman, V., Wang, H.Y., Phillips, K.J., Webb, P., Wong, S.T., Wang, R.F., and Hsueh, W.A. (2013). Class II Major Histocompatibility Complex Plays an Essential Role in Obesity-Induced Adipose Inflammation. Cell Metab *17*, 411-422.

Dipaolo, R.J. and Shevach, E.M. (2009). CD4+ T-cell development in a mouse expressing a transgenic TCR derived from a Treg. Eur. J. Immunol. *39*, 234-240.

Duewell, P., Kono, H., Rayner, K.J., Sirois, C.M., Vladimer, G., Bauernfeind, F.G., Abela, G.S., Franchi, L., Nunez, G., Schnurr, M., Espevik, T., Lien, E., Fitzgerald, K.A., Rock, K.L., Moore, K.J., Wright, S.D., Hornung, V., and Latz, E. (2010). NLRP3 inflammasomes are required for atherogenesis and activated by cholesterol crystals. Nature *464*, 1357-1361.

Duffaut, C., Galitzky, J., Lafontan, M., and Bouloumie, A. (2009). Unexpected trafficking of immune cells within the adipose tissue during the onset of obesity. Biochem Biophys. Res. Commun. *384*, 482-485.

Elchebly, M., Payette, P., Michaliszyn, E., Cromlish, W., Collins, S., Loy, A.L., Normandin, D., Cheng, A., Himms-Hagen, J., Chan, C.C., Ramachandran, C., Gresser, M.J., Tremblay, M.L., and Kennedy, B.P. (1999). Increased insulin sensitivity and obesity resistance in mice lacking the protein tyrosine phosphatase-1B gene. Science *283*, 1544-1548.

Elgazar-Carmon, V., Rudich, A., Hadad, N., and Levy, R. (2008). Neutrophils transiently infiltrate intra-abdominal fat early in the course of high-fat feeding. J Lipid Res. *49*, 1894-1903.

Eller, K., Kirsch, A., Wolf, A.M., Sopper, S., Tagwerker, A., Stanzl, U., Wolf, D., Patsch, W., Rosenkranz, A.R., and Eller, P. (2011). Potential role of regulatory T cells

in reversing obesity-linked insulin resistance and diabetic nephropathy. Diabetes *60*, 2954-2962.

Feinstein, R., Kanety, H., Papa, M.Z., Lunenfeld, B., and Karasik, A. (1993). Tumor necrosis factor-alpha suppresses insulin-induced tyrosine phosphorylation of insulin receptor and its substrates. J Biol. Chem. *268*, 26055-26058.

Feuerer, M., Herrero, L., Cipolletta, D., Naaz, A., Wong, J., Nayer, A., Lee, J., Goldfine, A.B., Benoist, C., Shoelson, S., and Mathis, D. (2009). Lean, but not obese, fat is enriched for a unique population of regulatory T cells that affect metabolic parameters. Nat Med *15*, 930-939.

Feuerer, M., Hill, J.A., Kretschmer, K., von Boehmer, H., Mathis, D., and Benoist, C. (2010). Genomic definition of multiple ex vivo regulatory T cell subphenotypes. Proc Natl Acad Sci U S A *107*, 5919-5924.

Fontenot, J.D., Gavin, M.A., and Rudensky, A.Y. (2003). Foxp3 programs the development and function of CD4+CD25+ regulatory T cells. Nat. Immunol *4*, 330-336.

Fontenot, J.D., Rasmussen, J.P., Gavin, M.A., and Rudensky, A.Y. (2005a). A function for interleukin 2 in Foxp3-expressing regulatory T cells. Nat. Immunol *6*, 1142-1151.

Fontenot, J.D., Rasmussen, J.P., Williams, L.M., Dooley, J.L., Farr, A.G., and Rudensky, A.Y. (2005b). Regulatory T cell lineage specification by the forkhead transcription factor foxp3. Immunity *22*, 329-341.

Friedline, R.H., Brown, D.S., Nguyen, H., Kornfeld, H., Lee, J., Zhang, Y., Appleby, M., Der, S.D., Kang, J., and Chambers, C.A. (2009). CD4+ regulatory T cells require CTLA-4 for the maintenance of systemic tolerance. J Exp Med *206*, 421-434.

Fu, W., Ergun, A., Lu, T., Hill, J.A., Haxhinasto, S., Fassett, M.S., Gazit, R., Adoro, S., Glimcher, L., Chan, S., Kastner, P., Rossi, D., Collins, J.J., Mathis, D., and Benoist, C. (2012). A multiply redundant genetic switch 'locks in' the transcriptional signature of regulatory T cells. Nat Immunol. *13*, 972-980.

Fujisaka, S., Usui, I., Bukhari, A., Ikutani, M., Oya, T., Kanatani, Y., Tsuneyama, K., Nagai, Y., Takatsu, K., Urakaze, M., Kobayashi, M., and Tobe, K. (2009). Regulatory mechanisms for adipose tissue M1 and M2 macrophages in diet-induced obese mice. Diabetes *58*, 2574-2582.

Gavin, M.A., Rasmussen, J.P., Fontenot, J.D., Vasta, V., Manganiello, V.C., Beavo, J.A., and Rudensky, A.Y. (2007). Foxp3-dependent programme of regulatory T-cell differentiation. Nature. *445*, 771-775.

Golding, J.P., Calderbank, E., Partridge, T.A., and Beauchamp, J.R. (2007). Skeletal muscle stem cells express anti-apoptotic ErbB receptors during activation from quiescence. Exp. Cell Res. *313*, 341-356.

Goldrath, A.W., Luckey, C.J., Park, R., Benoist, C., and Mathis, D. (2004). The molecular program induced in T cells undergoing homeostatic proliferation. Proceedings of the National Acedemy of Sciences.

Grounds, M.D., Radley, H.G., Lynch, G.S., Nagaraju, K., and De, L.A. (2008). Towards developing standard operating procedures for pre-clinical testing in the mdx mouse model of Duchenne muscular dystrophy. Neurobiol. Dis. *31*, 1-19.

Halberg, N., Khan, T., Trujillo, M.E., Wernstedt-Asterholm, I., Attie, A.D., Sherwani, S., Wang, Z.V., Landskroner-Eiger, S., Dineen, S., Magalang, U.J., Brekken, R.A., and Scherer, P.E. (2009). Hypoxia-inducible factor 1alpha induces fibrosis and insulin resistance in white adipose tissue. Mol. Cell Biol. *29*, 4467-4483.

Han, C.Y., Subramanian, S., Chan, C.K., Omer, M., Chiba, T., Wight, T.N., and Chait, A. (2007). Adipocyte-derived serum amyloid A3 and hyaluronan play a role in monocyte recruitment and adhesion. Diabetes *56*, 2260-2273.

Haribhai, D., Lin, W., Edwards, B., Ziegelbauer, J., Salzman, N.H., Carlson, M.R., Li, S.H., Simpson, P.M., Chatila, T.A., and Williams, C.B. (2009). A central role for induced regulatory T cells in tolerance induction in experimental colitis. J. Immunol. *182*, 3461-3468.

Haxhinasto, S., Mathis, D., and Benoist, C. (2008). The AKT-mTOR axis regulates de novo differentiation of CD4+Foxp3+ cells. J Exp Med *205*, 565-574.

Herrero, L., Shapiro, H., Nayer, A., Lee, J., and Shoelson, S.E. (2010). Inflammation and adipose tissue macrophages in lipodystrophic mice. Proc Natl Acad Sci U S A *107*, 240-245.

Hill, J.A., Feuerer, M., Tash, K., Haxhinasto, S., Perez, J., Melamed, R., Mathis, D., and Benoist, C. (2007). Foxp3 transcription-factor-dependent and -independent regulation of the regulatory T cell transcriptional signature. Immunity. *27*, 786-800.

Hinterberger, M., Aichinger, M., da Costa, O.P., Voehringer, D., Hoffmann, R., and Klein, L. (2010). Autonomous role of medullary thymic epithelial cells in central CD4(+) T cell tolerance. Nat. Immunol. *11*, 512-519.

Hirosumi, J., Tuncman, G., Chang, L., Gorgun, C.Z., Uysal, K.T., Maeda, K., Karin, M., and Hotamisligil, G.S. (2002). A central role for JNK in obesity and insulin resistance. Nature. *420*, 333-336.

Horikawa, M., Higashiyama, S., Nomura, S., Kitamura, Y., Ishikawa, M., and Taniguchi, N. (1999). Upregulation of endogenous heparin-binding EGF-like growth factor and its role as a survival factor in skeletal myotubes. FEBS Lett. *459*, 100-104.

Hotamisligil, G.S. (2006). Inflammation and metabolic disorders. Nature. *444*, 860-867.

Hotamisligil, G.S., Shargill, N.S., and Spiegelman, B.M. (1993). Adipose expression of tumor necrosis factor-alpha: direct role in obesity-linked insulin resistance. Science *259*, 87-91.

Hsieh, C.S., Liang, Y., Tyznik, A.J., Self, S.G., Liggitt, D., and Rudensky, A.Y. (2004). Recognition of the peripheral self by naturally arising CD25+ CD4+ T cell receptors. Immunity *21*, 267-277.

Hsieh, C.S., Zheng, Y., Liang, Y., Fontenot, J.D., and Rudensky, A.Y. (2006). An intersection between the self-reactive regulatory and nonregulatory T cell receptor repertoires. Nat. Immunol *7*, 401-410.

Ilan, Y., Maron, R., Tukpah, A.M., Maioli, T.U., Murugaiyan, G., Yang, K., Wu, H.Y., and Weiner, H.L. (2010). Induction of regulatory T cells decreases adipose inflammation and alleviates insulin resistance in ob/ob mice. Proc Natl Acad Sci U S A *107*, 9765-9770.

Isomura, I., Palmer, S., Grumont, R.J., Bunting, K., Hoyne, G., Wilkinson, N., Banerjee, A., Proietto, A., Gugasyan, R., Wu, L., McNally, A., Steptoe, R.J., Thomas, R., Shannon, M.F., and Gerondakis, S. (2009). c-Rel is required for the development of thymic Foxp3+ CD4 regulatory T cells. J Exp Med *206*, 3001-3014.

Jager, J., Gremeaux, T., Cormont, M., Le Marchand-Brustel, Y., and Tanti, J.F. (2007). Interleukin-1beta-induced insulin resistance in adipocytes through down-regulation of insulin receptor substrate-1 expression. Endocrinology *148*, 241-251.

Jordan, M.S., Boesteanu, A., Reed, A.J., Petrone, A.L., Holenbeck, A.E., Lerman, M.A., Naji, A., and Caton, A.J. (2001). Thymic selection of CD4+CD25+ regulatory T cells induced by an agonist self-peptide. Nat. Immunol. *2*, 283-284.

Josefowicz, S.Z., Lu, L.F., and Rudensky, A.Y. (2012a). Regulatory T Cells: Mechanisms of Differentiation and Function. Annu. Rev. Immunol. *30*, 531-564.

Josefowicz, S.Z., Niec, R.E., Kim, H.Y., Treuting, P., Chinen, T., Zheng, Y., Umetsu, D.T., and Rudensky, A.Y. (2012b). Extrathymically generated regulatory T cells control mucosal TH2 inflammation. Nature *482*, 395-399.

Kamei, N., Tobe, K., Suzuki, R., Ohsugi, M., Watanabe, T., Kubota, N., Ohtsuka-Kowatari, N., Kumagai, K., Sakamoto, K., Kobayashi, M., Yamauchi, T., Ueki, K.,

Oishi, Y., Nishimura, S., Manabe, I., Hashimoto, H., Ohnishi, Y., Ogata, H., Tokuyama, K., Tsunoda, M., Ide, T., Murakami, K., Nagai, R., and Kadowaki, T. (2006). Overexpression of monocyte chemoattractant protein-1 in adipose tissues causes macrophage recruitment and insulin resistance. J Biol. Chem. *281*, 26602-26614.

Kanda, H., Tateya, S., Tamori, Y., Kotani, K., Hiasa, K., Kitazawa, R., Kitazawa, S., Miyachi, H., Maeda, S., Egashira, K., and Kasuga, M. (2006). MCP-1 contributes to macrophage infiltration into adipose tissue, insulin resistance, and hepatic steatosis in obesity. J Clin Invest *116*, 1494-1505.

Kawahata, K., Misaki, Y., Yamauchi, M., Tsunekawa, S., Setoguchi, K., Miyazaki, J., and Yamamoto, K. (2002). Generation of CD4(+)CD25(+) regulatory T cells from autoreactive T cells simultaneously with their negative selection in the thymus and from nonautoreactive T cells by endogenous TCR expression. J Immunol *168*, 4399-4405.

Kerdiles, Y.M., Stone, E.L., Beisner, D.R., McGargill, M.A., Ch'en, I.L., Stockmann, C., Katayama, C.D., and Hedrick, S.M. (2010). Foxo transcription factors control regulatory T cell development and function. Immunity. *33*, 890-904.

Khattri, R., Cox, T., Yasayko, S.A., and Ramsdell, F. (2003). An essential role for Scurfin in CD4+CD25+ T regulatory cells. Nat. Immunol *4*, 337-342.

Kim, J.M., Rasmussen, J.P., and Rudensky, A.Y. (2007). Regulatory T cells prevent catastrophic autoimmunity throughout the lifespan of mice. Nat. Immunol *8*, 191-197.

Kintscher, U., Hartge, M., Hess, K., Foryst-Ludwig, A., Clemenz, M., Wabitsch, M., Fischer-Posovszky, P., Barth, T.F., Dragun, D., Skurk, T., Hauner, H., Bluher, M., Unger, T., Wolf, A.M., Knippschild, U., Hombach, V., and Marx, N. (2008). T-lymphocyte infiltration in visceral adipose tissue: a primary event in adipose tissue inflammation and the development of obesity-mediated insulin resistance. Arterioscler. Thromb. Vasc. Biol *28*, 1304-1310.

Koch, M.A., Tucker-Heard, G., Perdue, N.R., Killebrew, J.R., Urdahl, K.B., and Campbell, D.J. (2009). The transcription factor T-bet controls regulatory T cell homeostasis and function during type 1 inflammation. Nat. Immunol. *10*, 595-602.

Kretschmer, K., Apostolou, I., Hawiger, D., Khazaie, K., Nussenzweig, M.C., and von, B.H. (2005). Inducing and expanding regulatory T cell populations by foreign antigen. Nat. Immunol. *6*, 1219-1227.

Lee, H.M., Bautista, J.L., Scott-Browne, J., Mohan, J.F., and Hsieh, C.S. (2012). A broad range of self-reactivity drives thymic regulatory T cell selection to limit responses to self. Immunity *37*, 475-486.

Leung, M.W., Shen, S., and Lafaille, J.J. (2009). TCR-dependent differentiation of thymic Foxp3+ cells is limited to small clonal sizes. J. Exp. Med. *206*, 2121-2130.

Li, M.O., Wan, Y.Y., and Flavell, R.A. (2007). T cell-produced transforming growth factor-beta1 controls T cell tolerance and regulates Th1- and Th17-cell differentiation. Immunity *26*, 579-591.

Lin, W., Haribhai, D., Relland, L.M., Truong, N., Carlson, M.R., Williams, C.B., and Chatila, T.A. (2007). Regulatory T cell development in the absence of functional Foxp3. Nat. Immunol *8*, 359-368.

Linterman, M.A., Pierson, W., Lee, S.K., Kallies, A., Kawamoto, S., Rayner, T.F., Srivastava, M., Divekar, D.P., Beaton, L., Hogan, J.J., Fagarasan, S., Liston, A., Smith, K.G., and Vinuesa, C.G. (2011). Foxp3+ follicular regulatory T cells control the germinal center response. Nat Med *17*, 975-982.

Liu, J., Divoux, A., Sun, J., Zhang, J., Clement, K., Glickman, J.N., Sukhova, G.K., Wolters, P.J., Du, J., Gorgun, C.Z., Doria, A., Libby, P., Blumberg, R.S., Kahn, B.B., Hotamisligil, G.S., and Shi, G.P. (2009). Genetic deficiency and pharmacological stabilization of mast cells reduce diet-induced obesity and diabetes in mice. Nat. Med. *15*, 940-945.

Long, M., Park, S.G., Strickland, I., Hayden, M.S., and Ghosh, S. (2009). Nuclear factor-kappaB modulates regulatory T cell development by directly regulating expression of Foxp3 transcription factor. Immunity. *31*, 921-931.

Lord, G.M., Matarese, G., Howard, J.K., Baker, R.J., Bloom, S.R., and Lechler, R.I. (1998). Leptin modulates the T-cell immune response and reverses starvation-induced immunosuppression. Nature *394*, 897-901.

Lumeng, C.N., Bodzin, J.L., and Saltiel, A.R. (2007a). Obesity induces a phenotypic switch in adipose tissue macrophage polarization. J Clin Invest *117*, 175-184.

Lumeng, C.N., Deyoung, S.M., Bodzin, J.L., and Saltiel, A.R. (2007b). Increased inflammatory properties of adipose tissue macrophages recruited during diet-induced obesity. Diabetes *56*, 16-23.

Lynch, L., Nowak, M., Varghese, B., Clark, J., Hogan, A.E., Toxavidis, V., Balk, S.P., O'Shea, D., O'Farrelly, C., and Exley, M.A. (2012). Adipose tissue invariant NKT cells protect against diet-induced obesity and metabolic disorder through regulatory cytokine production. Immunity *37*, 574-587.

Malchow, S., Leventhal, D.S., Nishi, S., Fischer, B.I., Shen, L., Paner, G.P., Amit, A.S., Kang, C., Geddes, J.E., Allison, J.P., Socci, N.D., and Savage, P.A. (2013). Aire-

dependent thymic development of tumor-associated regulatory T cells. Science *339*, 1219-1224.

Meijer, K., de, V.M., Al-Lahham, S., Bruinenberg, M., Weening, D., Dijkstra, M., Kloosterhuis, N., van der Leij, R.J., van der Want, H., Kroesen, B.J., Vonk, R., and Rezaee, F. (2011). Human primary adipocytes exhibit immune cell function: adipocytes prime inflammation independent of macrophages. PLoS. ONE. *6*, e17154.

Miller, A.M. (2011). Role of IL-33 in inflammation and disease. J Inflamm. (Lond) *8*, 22.

Miller, A.M., Asquith, D.L., Hueber, A.J., Anderson, L.A., Holmes, W.M., McKenzie, A.N., Xu, D., Sattar, N., McInnes, I.B., and Liew, F.Y. (2010). Interleukin-33 induces protective effects in adipose tissue inflammation during obesity in mice. Circ. Res. *107*, 650-658.

Minamino, T., Orimo, M., Shimizu, I., Kunieda, T., Yokoyama, M., Ito, T., Nojima, A., Nabetani, A., Oike, Y., Matsubara, H., Ishikawa, F., and Komuro, I. (2009). A crucial role for adipose tissue p53 in the regulation of insulin resistance. Nat. Med. *15*, 1082-1087.

Molofsky, A.B., Nussbaum, J.C., Liang, H.E., Van Dyken, S.J., Cheng, L.E., Mohapatra, A., Chawla, A., and Locksley, R.M. (2013). Innate lymphoid type 2 cells sustain visceral adipose tissue eosinophils and alternatively activated macrophages. J Exp. Med *210*, 535-549.

Mombaerts, P., Iacomini, J., Johnson, R.S., Herrup, K., Tonegawa, S., and Papaioannou, V.E. (1992). RAG-1-deficient mice have no mature B and T lymphocytes. Cell *68*, 869-877.

Moraes-Vieira, P.M., Yore, M.M., Dwyer, P.M., Syed, I., Aryal, P., and Kahn, B.B. (2014). RBP4 Activates Antigen-Presenting Cells, Leading to Adipose Tissue Inflammation and Systemic Insulin Resistance. Cell Metab *19*, 512-526.

Morris, D.L., Cho, K.W., Delproposto, J.L., Oatmen, K.E., Geletka, L.M., Martinez-Santibanez, G., Singer, K., and Lumeng, C.N. (2013). Adipose tissue macrophages function as antigen-presenting cells and regulate adipose tissue CD4+ T cells in mice. Diabetes *62*, 2762-2772.

Mosser, D.M. and Edwards, J.P. (2008). Exploring the full spectrum of macrophage activation. Nat. Rev. Immunol. *8*, 958-969.

Nguyen, M.T., Favelyukis, S., Nguyen, A.K., Reichart, D., Scott, P.A., Jenn, A., Liu-Bryan, R., Glass, C.K., Neels, J.G., and Olefsky, J.M. (2007). A subpopulation of macrophages infiltrates hypertrophic adipose tissue and is activated by free fatty acids

via Toll-like receptors 2 and 4 and JNK-dependent pathways. J Biol. Chem. *282*, 35279-35292.

Nishimura, S., Manabe, I., Nagasaki, M., Eto, K., Yamashita, H., Ohsugi, M., Otsu, M., Hara, K., Ueki, K., Sugiura, S., Yoshimura, K., Kadowaki, T., and Nagai, R. (2009). CD8+ effector T cells contribute to macrophage recruitment and adipose tissue inflammation in obesity. Nat Med *15*, 914-920.

Nishimura, S., Manabe, I., Takaki, S., Nagasaki, M., Otsu, M., Yamashita, H., Sugita, J., Yoshimura, K., Eto, K., Komuro, I., Kadowaki, T., and Nagai, R. (2013). Adipose Natural Regulatory B Cells Negatively Control Adipose Tissue Inflammation. Cell Metab.

Odegaard, J.I., Ricardo-Gonzalez, R.R., Goforth, M.H., Morel, C.R., Subramanian, V., Mukundan, L., Eagle, A.R., Vats, D., Brombacher, F., Ferrante, A.W., and Chawla, A. (2007). Macrophage-specific PPARgamma controls alternative activation and improves insulin resistance. Nature. *447*, 1116-1120.

Ouchi, N., Parker, J.L., Lugus, J.J., and Walsh, K. (2011). Adipokines in inflammation and metabolic disease. Nat. Rev. Immunol. *11*, 85-97.

Ouyang, W., Beckett, O., Ma, Q., and Li, M.O. (2010a). Transforming growth factor-beta signaling curbs thymic negative selection promoting regulatory T cell development. Immunity. *32*, 642-653.

Ouyang, W., Beckett, O., Ma, Q., Paik, J.H., DePinho, R.A., and Li, M.O. (2010b). Foxo proteins cooperatively control the differentiation of Foxp3+ regulatory T cells. Nat Immunol. *11*, 618-627.

Ozcan, U., Cao, Q., Yilmaz, E., Lee, A.H., Iwakoshi, N.N., Ozdelen, E., Tuncman, G., Gorgun, C., Glimcher, L.H., and Hotamisligil, G.S. (2004). Endoplasmic reticulum stress links obesity, insulin action, and type 2 diabetes. Science *306*, 457-461.

Palmer, D.B. (2013). The Effect of Age on Thymic Function. Front Immunol *4*, 316.

Pandiyan, P., Zheng, L., Ishihara, S., Reed, J., and Lenardo, M.J. (2007). CD4+CD25+Foxp3+ regulatory T cells induce cytokine deprivation-mediated apoptosis of effector CD4+ T cells. Nat Immunol. *8*, 1353-1362.

Patton, D.T., Garden, O.A., Pearce, W.P., Clough, L.E., Monk, C.R., Leung, E., Rowan, W.C., Sancho, S., Walker, L.S., Vanhaesebroeck, B., and Okkenhaug, K. (2006). Cutting edge: the phosphoinositide 3-kinase p110 delta is critical for the function of CD4+CD25+Foxp3+ regulatory T cells. J Immunol *177*, 6598-6602.

Pei, C., Barbour, M., Fairlie-Clarke, K.J., Allan, D., Mu, R., and Jiang, H.R. (2014). Emerging role of interleukin-33 in autoimmune diseases. Immunology *141*, 9-17.

Rajamaki, K., Lappalainen, J., Oorni, K., Valimaki, E., Matikainen, S., Kovanen, P.T., and Eklund, K.K. (2010). Cholesterol crystals activate the NLRP3 inflammasome in human macrophages: a novel link between cholesterol metabolism and inflammation. PLoS. ONE. *5*, e11765.

Rocha, V.Z., Folco, E.J., Sukhova, G., Shimizu, K., Gotsman, I., Vernon, A.H., and Libby, P. (2008). Interferon-gamma, a Th1 cytokine, regulates fat inflammation: a role for adaptive immunity in obesity. Circ. Res. *103*, 467-476.

Rosen, E.D., and Spiegelman, B.M. (2014). What we talk about when we talk about fat. Cell *156*, 20-44.

Rosenblum, M.D., Gratz, I.K., Paw, J.S., Lee, K., Marshak-Rothstein, A., and Abbas, A.K. (2011). Response to self antigen imprints regulatory memory in tissues. Nature *480*, 538-542.

Rotter, V., Nagaev, I., and Smith, U. (2003). Interleukin-6 (IL-6) induces insulin resistance in 3T3-L1 adipocytes and is, like IL-8 and tumor necrosis factor-alpha, overexpressed in human fat cells from insulin-resistant subjects. J Biol. Chem. *278*, 45777-45784.

Rubtsov, Y.P., Rasmussen, J.P., Chi, E.Y., Fontenot, J., Castelli, L., Ye, X., Treuting, P., Siewe, L., Roers, A., Henderson, W.R., Jr., Muller, W., and Rudensky, A.Y. (2008). Regulatory T cell-derived interleukin-10 limits inflammation at environmental interfaces. Immunity. *28*, 546-558.

Rudnicki, M.A., Le, G.F., McKinnell, I., and Kuang, S. (2008). The molecular regulation of muscle stem cell function. Cold Spring Harb. Symp. Quant. Biol. *73*, 323-331.

Sakaguchi, S., Sakaguchi, N., Asano, M., Itoh, M., and Toda, M. (1995). Immunologic self-tolerance maintained by activated T cells expressing IL-2 receptor alpha-chains (CD25). Breakdown of a single mechanism of self-tolerance causes various autoimmune diseases. J Immunol *155*, 1151-1164.

Salomon, B., Lenschow, D.J., Rhee, L., Ashourian, N., Singh, B., Sharpe, A., and Bluestone, J.A. (2000). B7/CD28 costimulation is essential for the homeostasis of the CD4+CD25+ immunoregulatory T cells that control autoimmune diabetes. Immunity *12*, 431-440.

Samstein, R.M., Arvey, A., Josefowicz, S.Z., Peng, X., Reynolds, A., Sandstrom, R., Neph, S., Sabo, P., Kim, J.M., Liao, W., Li, M.O., Leslie, C., Stamatoyannopoulos,

J.A., and Rudensky, A.Y. (2012a). Foxp3 exploits a pre-existent enhancer landscape for regulatory T cell lineage specification. Cell *151*, 153-166.

Samstein, R.M., Josefowicz, S.Z., Arvey, A., Treuting, P.M., and Rudensky, A.Y. (2012b). Extrathymic generation of regulatory T cells in placental mammals mitigates maternal-fetal conflict. Cell *150*, 29-38.

Schmitz, J., Owyang, A., Oldham, E., Song, Y., Murphy, E., McClanahan, T.K., Zurawski, G., Moshrefi, M., Qin, J., Li, X., Gorman, D.M., Bazan, J.F., and Kastelein, R.A. (2005). IL-33, an interleukin-1-like cytokine that signals via the il-1 receptor-related protein st 2 and induces t helper type 2-associated cytokines. Immunity *23*, 479-490.

Schroder, K. and Tschopp, J. (2010). The inflammasomes. Cell *140*, 821-832.

Seneschal, J., Clark, R.A., Gehad, A., Baecher-Allan, C.M., and Kupper, T.S. (2012). Human epidermal Langerhans cells maintain immune homeostasis in skin by activating skin resident regulatory T cells. Immunity *36*, 873-884.

Shaul, M.E., Bennett, G., Strissel, K.J., Greenberg, A.S., and Obin, M.S. (2010). Dynamic, M2-like remodeling phenotypes of CD11c+ adipose tissue macrophages during high-fat diet--induced obesity in mice. Diabetes *59*, 1171-1181.

Shoelson, S.E., Lee, J., and Goldfine, A.B. (2006). Inflammation and insulin resistance. J Clin Invest *116*, 1793-1801.

Shoyab, M., Plowman, G.D., McDonald, V.L., Bradley, J.G., and Todaro, G.J. (1989). Structure and function of human amphiregulin: a member of the epidermal growth factor family. Science *243*, 1074-1076.

Sitrin, J., Ring, A., Garcia, K.C., Benoist, C., and Mathis, D. (2013). Regulatory T cells control NK cells in an insulitic lesion by depriving them of IL-2. J Exp. Med *210*, 1153-1165.

Strissel, K.J., DeFuria, J., Shaul, M.E., Bennett, G., Greenberg, A.S., and Obin, M.S. (2010). T-cell recruitment and Th1 polarization in adipose tissue during diet-induced obesity in C57BL/6 mice. Obesity. (Silver. Spring) *18*, 1918-1925.

Strissel, K.J., Stancheva, Z., MIYOSHI, H., Perfield, J.W., DeFuria, J., Jick, Z., Greenberg, A.S., and Obin, M.S. (2007). Adipocyte death, adipose tissue remodeling, and obesity complications. Diabetes *56*, 2910-2918.

Tabebordbar, M., Wang, E.T., and Wagers, A.J. (2013). Skeletal muscle degenerative diseases and strategies for therapeutic muscle repair. Annu. Rev. Pathol. *8*, 441-475.

Tai, X., Cowan, M., Feigenbaum, L., and Singer, A. (2005). CD28 costimulation of developing thymocytes induces Foxp3 expression and regulatory T cell differentiation independently of interleukin 2. Nat. Immunol *6*, 152-162.

Tai, X., Erman, B., Alag, A., Mu, J., Kimura, M., Katz, G., Guinter, T., McCaughtry, T., Etzensperger, R., Feigenbaum, L., Singer, D.S., and Singer, A. (2013). Foxp3 transcription factor is proapoptotic and lethal to developing regulatory T cells unless counterbalanced by cytokine survival signals. Immunity *38*, 1116-1128.

Talukdar, S., Oh, d.Y., Bandyopadhyay, G., Li, D., Xu, J., McNelis, J., Lu, M., Li, P., Yan, Q., Zhu, Y., Ofrecio, J., Lin, M., Brenner, M.B., and Olefsky, J.M. (2012). Neutrophils mediate insulin resistance in mice fed a high-fat diet through secreted elastase. Nat Med *18*, 1407-1412.

Thornton, A.M., Korty, P.E., Tran, D.Q., Wohlfert, E.A., Murray, P.E., Belkaid, Y., and Shevach, E.M. (2010). Expression of Helios, an Ikaros transcription factor family member, differentiates thymic-derived from peripherally induced Foxp3+ T regulatory cells. J Immunol. *184*, 3433-3441.

Tidball, J.G. and Villalta, S.A. (2010). Regulatory interactions between muscle and the immune system during muscle regeneration. Am. J Physiol Regul. Integr. Comp Physiol *298*, R1173-R1187.

Tomura, M., Yoshida, N., Tanaka, J., Karasawa, S., Miwa, Y., Miyawaki, A., and Kanagawa, O. (2008). Monitoring cellular movement in vivo with photoconvertible fluorescence protein "Kaede" transgenic mice. Proc Natl Acad Sci U S A *105*, 10871-10876.

Vandanmagsar, B., Youm, Y.H., Ravussin, A., Galgani, J.E., Stadler, K., Mynatt, R.L., Ravussin, E., Stephens, J.M., and Dixit, V.D. (2011). The NLRP3 inflammasome instigates obesity-induced inflammation and insulin resistance. Nat. Med. *17*, 179-188.

Verhagen, J. and Wraith, D.C. (2010). Comment on "Expression of Helios, an Ikaros transcription factor family member, differentiates thymic-derived from peripherally induced Foxp3+ T regulatory cells". J Immunol. *185*, 7129.

Weisberg, S.P., Hunter, D., Huber, R., Lemieux, J., Slaymaker, S., Vaddi, K., Charo, I., Leibel, R.L., and Ferrante, A.W., Jr. (2006). CCR2 modulates inflammatory and metabolic effects of high-fat feeding. J Clin Invest *116*, 115-124.

Weisberg, S.P., McCann, D., Desai, M., Rosenbaum, M., Leibel, R.L., and Ferrante, A.W., Jr. (2003). Obesity is associated with macrophage accumulation in adipose tissue. J Clin Invest *112*, 1796-1808.

Weiss, J.M., Bilate, A.M., Gobert, M., Ding, Y., Curotto de Lafaille, M.A., Parkhurst, C.N., Xiong, H., Dolpady, J., Frey, A.B., Ruocco, M.G., Yang, Y., Floess, S., Huehn, J., Oh, S., Li, M.O., Niec, R.E., Rudensky, A.Y., Dustin, M.L., Littman, D.R., and Lafaille, J.J. (2012). Neuropilin 1 is expressed on thymus-derived natural regulatory T cells, but not mucosa-generated induced Foxp3+ T reg cells. J Exp. Med *209*, 1723-42, S1.

Wildin, R.S., Ramsdell, F., Peake, J., Faravelli, F., Casanova, J.L., Buist, N., Levy-Lahad, E., Mazzella, M., Goulet, O., Perroni, L., Bricarelli, F.D., Byrne, G., McEuen, M., Proll, S., Appleby, M., and Brunkow, M.E. (2001). X-linked neonatal diabetes mellitus, enteropathy and endocrinopathy syndrome is the human equivalent of mouse scurfy. Nat. Genet. *27*, 18-20.

Winer, D.A., Winer, S., Shen, L., Wadia, P.P., Yantha, J., Paltser, G., Tsui, H., Wu, P., Davidson, M.G., Alonso, M.N., Leong, H.X., Glassford, A., Caimol, M., Kenkel, J.A., Tedder, T.F., McLaughlin, T., Miklos, D.B., Dosch, H.M., and Engleman, E.G. (2011). B cells promote insulin resistance through modulation of T cells and production of pathogenic IgG antibodies. Nat. Med. *17*, 610-617.

Winer, S., Chan, Y., Paltser, G., Truong, D., Tsui, H., Bahrami, J., Dorfman, R., Wang, Y., Zielenski, J., Mastronardi, F., Maezawa, Y., Drucker, D.J., Engleman, E., Winer, D., and Dosch, H.M. (2009). Normalization of obesity-associated insulin resistance through immunotherapy. Nat Med *15*, 921-929.

Wing, K., Onishi, Y., Prieto-Martin, P., Yamaguchi, T., Miyara, M., Fehervari, Z., Nomura, T., and Sakaguchi, S. (2008). CTLA-4 control over Foxp3+ regulatory T cell function. Science *322*, 271-275.

Wolf, D., Jehle, F., Anto, M.N., Bukosza, E.N., Rivera, J., Chen, Y.C., Hoppe, N., Dufner, B., Ortiz, R.A., Colberg, C., Nieto, L., Rupprecht, B., Wiedemann, A., Schulte, L., Peikert, A., Bassler, N., Lozhkin, A., Hergeth, S.P., Stachon, P., Hilgendorf, I., Willecke, F., von Zur, M.C., von, E.D., Binder, C.J., Aichele, P., Varo, N., Febbraio, M.A., Libby, P., Bode, C., Peter, K., and Zirlik, A. (2014). Co-Inhibitory Suppression of T Cell Activation by CD40 Protects from Obesity and Adipose Tissue Inflammation in Mice. Circulation.

Wong, J., Obst, R., Correia-Neves, M., Losyev, G., Mathis, D., and Benoist, C. (2007). Adaptation of TCR repertoires to self-peptides in regulatory and nonregulatory CD4+ T cells. J Immunol *178*, 7032-7041.

Wood, I.S., Wang, B., and Trayhurn, P. (2009). IL-33, a recently identified interleukin-1 gene family member, is expressed in human adipocytes. Biochem Biophys. Res. Commun. *384*, 105-109.

Wu, D., Molofsky, A.B., Liang, H.E., Ricardo-Gonzalez, R.R., Jouihan, H.A., Bando, J.K., Chawla, A., and Locksley, R.M. (2011). Eosinophils sustain adipose alternatively activated macrophages associated with glucose homeostasis. Science *332*, 243-247.

Yadav, M., Louvet, C., Davini, D., Gardner, J.M., Martinez-Llordella, M., Bailey-Bucktrout, S., Anthony, B.A., Sverdrup, F.M., Head, R., Kuster, D.J., Ruminski, P., Weiss, D., Von, S.D., and Bluestone, J.A. (2012). Neuropilin-1 distinguishes natural and inducible regulatory T cells among regulatory T cell subsets in vivo. J Exp. Med *209*, 1713-1719.

Yang, H., Youm, Y.H., Vandanmagsar, B., Ravussin, A., Gimble, J.M., Greenway, F., Stephens, J.M., Mynatt, R.L., and Dixit, V.D. (2010). Obesity increases the production of proinflammatory mediators from adipose tissue T cells and compromises TCR repertoire diversity: implications for systemic inflammation and insulin resistance. J. Immunol. *185*, 1836-1845.

Yi, Z., Stunz, L.L., and Bishop, G.A. (2014). CD40-mediated maintenance of immune homeostasis in the adipose tissue microenvironment. Diabetes.

Yuan, M., Konstantopoulos, N., Lee, J., Hansen, L., Li, Z.W., Karin, M., and Shoelson, S.E. (2001). Reversal of obesity- and diet-induced insulin resistance with salicylates or targeted disruption of Ikkbeta. Science *293*, 1673-1677.

Zeyda, M., Wernly, B., Demyanets, S., Kaun, C., Hammerle, M., Hantusch, B., Schranz, M., Neuhofer, A., Itariu, B.K., Keck, M., Prager, G., Wojta, J., and Stulnig, T.M. (2013). Severe obesity increases adipose tissue expression of interleukin-33 and its receptor ST2, both predominantly detectable in endothelial cells of human adipose tissue. Int. J Obes. (Lond) *37*, 658-665.

Zheng, Y., Chaudhry, A., Kas, A., Deroos, P., Kim, J.M., Chu, T.T., Corcoran, L., Treuting, P., Klein, U., and Rudensky, A.Y. (2009). Regulatory T-cell suppressor program co-opts transcription factor IRF4 to control T(H)2 responses. Nature *458*, 351-356.

Zheng, Y., Josefowicz, S., Chaudhry, A., Peng, X.P., Forbush, K., and Rudensky, A.Y. (2010). Role of conserved non-coding DNA elements in the Foxp3 gene in regulatory T-cell fate. Nature *463*, 808-812.

Publications

Appendix A:

Cohen, P., Levy, J.D., Zhang, Y., Frontini, A., **Kolodin, D.**, Svensson, K.J., Lo, J.C., Zeng, X., Ye, L., Khandekar, M.J., Wu, J., Gunawardana, S.C., Banks, A.S., Camporez, J.P., Jurczak, M.J., Kajimura, S., Piston, D.W., Mathis, D., Cinti, S., Shulman, G.I., Seale, P., and Spiegelman, B.M. (2014) Ablation of PRDM16 and Beige Adipose Causes Metabolic Dysfunction and a Subcutaneous to Visceral Fat Switch. Cell. *156*, 304-316.

Appendix B:

Burzyn, D., Kuswanto, W., **Kolodin, D.**, Shadrach, J.L., Cerletti, M., Jang, Y., Sefik, E., Tan, T.G., Wagers, A.J., Benoist, C., and Mathis, D. (2013). A special population of regulatory T cells potentiates muscle repair. Cell *155*, 1282-1295.

Appendix C:

Cipolletta, D.*, **Kolodin, D.***, Benoist, C., and Mathis, D. (2011). Tissular T(regs): a unique population of adipose-tissue-resident Foxp3+CD4+ T cells that impacts organismal metabolism. Semin. Immunol. *23*, 431-437. (* these authors contributed equally)

Unpublished Manuscripts

Piesche, M., Ho, V., Kim, H., Nakazaki, Y., Nehil, M., Yaghi, N., **Kolodin, D.**, Weiser, J., Altevogt, P., Kiefel, H., Alyea, E., Antin, J., Cutler, C., Koreth, J., Canning, C., Ritz, J., Soiffer, R., and Dranoff, G. Angiogenic cytokines are antibody targets of leukemia cell vaccines early after allogeneic hematopoietic stem cell transplantation. (Manuscript submitted to Blood)

Yang, S., Fujikado, N., **Kolodin, D.**, Benoist, C., and Mathis, D. Around birth, Aire induces a Treg compartment with a distinct role in maintaining self-tolerance. (Manuscript in revision at Science).

Cell

Ablation of PRDM16 and Beige Adipose Causes Metabolic Dysfunction and a Subcutaneous to Visceral Fat Switch

Paul Cohen,[1,2] Julia D. Levy,[1] Yingying Zhang,[1] Andrea Frontini,[3] Dmitriy P. Kolodin,[4] Katrin J. Svensson,[1] James C. Lo,[1,2] Xing Zeng,[1] Li Ye,[1] Melin J. Khandekar,[1] Jun Wu,[1] Subhadra C. Gunawardana,[5] Alexander S. Banks,[1] João Paulo G. Camporez,[6] Michael J. Jurczak,[6] Shingo Kajimura,[8] David W. Piston,[5] Diane Mathis,[4] Saverio Cinti,[3] Gerald I. Shulman,[6,7] Patrick Seale,[9] and Bruce M. Spiegelman[1,*]

[1]Dana-Farber Cancer Institute and Department of Cell Biology, Harvard Medical School, Boston, MA 02215, USA
[2]Cardiovascular Division, Department of Medicine, Brigham and Women's Hospital, Boston, MA 02115, USA
[3]Department of Experimental and Clinical Medicine, Università Politecnica delle Marche, Ancona 60020, Italy
[4]Division of Immunology, Department of Microbiology and Immunobiology, Harvard Medical School, Boston, MA 02115, USA
[5]Department of Molecular Physiology and Biophysics, Vanderbilt University, Nashville, TN 37232, USA
[6]Department of Internal Medicine, Yale University School of Medicine, New Haven, CT 06519, USA
[7]Department of Cellular and Molecular Physiology and Howard Hughes Medical Institute, Yale University School of Medicine, New Haven, CT 06519, USA
[8]UCSF Diabetes Center and Department of Cell and Tissue Biology, University of California San Francisco, San Francisco, CA 94143, USA
[9]Institute for Diabetes, Obesity, and Metabolism, Perelman School of Medicine at the University of Pennsylvania, Philadelphia, PA 19104, USA
*Correspondence: bruce_spiegelman@dfci.harvard.edu
http://dx.doi.org/10.1016/j.cell.2013.12.021

SUMMARY

A clear relationship exists between visceral obesity and type 2 diabetes, whereas subcutaneous obesity is comparatively benign. Here, we show that adipocyte-specific deletion of the coregulatory protein PRDM16 caused minimal effects on classical brown fat but markedly inhibited beige adipocyte function in subcutaneous fat following cold exposure or β3-agonist treatment. These animals developed obesity on a high-fat diet, with severe insulin resistance and hepatic steatosis. They also showed altered fat distribution with markedly increased subcutaneous adiposity. Subcutaneous adipose tissue in mutant mice acquired many key properties of visceral fat, including decreased thermogenic and increased inflammatory gene expression and increased macrophage accumulation. Transplantation of subcutaneous fat into mice with diet-induced obesity showed a loss of metabolic benefit when tissues were derived from PRDM16 mutant animals. These findings indicate that PRDM16 and beige adipocytes are required for the "browning" of white fat and the healthful effects of subcutaneous adipose tissue.

INTRODUCTION

Obesity has become a global epidemic, contributing to increases in the prevalence of type 2 diabetes, hypertension, cardiovascular disease, and certain cancers. Generally, two broad categories of obesity are recognized: visceral (VISC) and subcutaneous (SubQ). The location where fat is deposited appears to have a great influence on the likelihood of an individual developing many of the sequelae of obesity (Gesta et al., 2007). Importantly, VISC adiposity is strongly associated with increased mortality, even in individuals with a normal body mass index (Pischon et al., 2008). SubQ adiposity, however, appears to be comparatively benign (Manolopoulos et al., 2010). The association between regional fat deposition and adverse health complications was first noted with pioneering clinical descriptions in the 1950s (Vague, 1956). It has also been recognized for centuries that men have a greater propensity for deposition of VISC fat, while premenopausal women have a greater tendency to accumulate fat in SubQ stores, though substantial variation exists in both sexes (Vague, 1947).

The relationship between site of adipose tissue accumulation and metabolic disease has been shown in several animal models. Transgenic mice overexpressing 11-β HSD-1 in adipose tissue develop VISC obesity along with insulin resistance, diabetes, and hyperlipidemia (Masuzaki et al., 2001). Conversely, transgenic mice overexpressing adiponectin or mitoNEET in adipose tissue develop remarkable SubQ obesity, but remain metabolically healthy (Kim et al., 2007; Kusminski et al., 2012). The functional importance of these adipose depots has been directly demonstrated in studies showing metabolic benefit by transplantation of SubQ fat or surgical removal of VISC fat (Gabriely et al., 2002; Tran et al., 2008).

These divergent metabolic effects of different adipose depots have raised interest in the unique properties of VISC and SubQ fat. VISC fat is notable for having a substantial degree of inflammation when obesity is present. Originally recognized as the secretion of TNFα and other inflammatory cytokines from fat tissue of obese animals (Hotamisligil et al., 1993), it is now known that there is a broad increase in a variety of immune cells

in obese fat (Weisberg et al., 2003; Xu et al., 2003). On the other hand, SubQ fat is notable because it can easily ''brown'' when animals are stimulated with cold, β-adrenergic agonists, or other hormone-like stimuli (Vitali et al., 2012; Wu et al., 2013). This browning includes the induction of UCP1 mRNA and protein, and expression of a gene program that gives rise to uncoupled respiration and heat production. Some stimuli, such as the genetic ablation of RALDH1, cause considerable browning of the VISC depots in mice (Kiefer et al., 2012), but this phenomenon is much less common than the browning of SubQ depots.

It is now recognized that there are at least two distinct types of brown fat cells. Classical brown adipose tissue (BAT), epitomized by the interscapular depot in rodents, arises from a *Myf5*$^+$, muscle-like cell lineage. PRDM16, a transcriptional regulatory protein, appears to control this muscle-brown fat decision between days 9–12 of gestation in mice (Lepper and Fan, 2010; Seale et al., 2008). The postnatal role of PRDM16 in classical BAT has not been studied. In contrast, the UCP1$^+$ cells that emerge in white fat depots under certain stimuli, termed beige or brite cells, do not come from a *Myf5*$^+$ lineage. However, PRDM16 also appears to be involved in the development and function of beige cells (Ohno et al., 2012; Seale et al., 2011). Hence, beige and classical brown fat cells both express PRDM16 and UCP1 but they are quite distinct cell types. Beige fat cells have now been cloned and characterized (Wu et al., 2012). Importantly, the depots of ''brown fat'' visualized in humans share more molecular properties with rodent beige fat than with classical BAT (Lidell et al., 2013; Sharp et al., 2012; Wu et al., 2012). The kite-like structure in the interscapular region of human infants, however, seems to have characteristics of rodent classical BAT, and some classical brown fat cells may be retained in adult humans (Cypess et al., 2013; Jespersen et al., 2013; Lidell et al., 2013).

Analysis of the relative physiological importance of the classical BAT versus the browning of white fat has been very difficult because many important browning agents, such as cold and β-adrenergic compounds, affect both types of brown fat cells. Similarly, while ablation of UCP1$^+$ cells or mutation of *Ucp1* illustrate the overall importance of brown fat in preventing obesity and diabetes in animals, the individual contributions of the two types of brown fat cells has been impossible to determine (Feldmann et al., 2009; Lowell et al., 1993). Agents that affect browning of white fat selectively, including transgenic expression of PRDM16, have caused metabolic benefit, suggesting that browning of white tissues could be important (Seale et al., 2011). On the other hand, it has been argued that there are insufficient beige cells to affect whole-body physiology under ambient conditions (Nedergaard and Cannon, 2013).

We have now created an adipocyte-selective mutation in the *Prdm16* gene that ablates the thermogenic program of beige fat cells, while leaving the classical BAT functionally intact. Mice lacking beige fat function develop obesity and insulin resistance when exposed to high-fat diet (HFD) and also develop hepatic steatosis. In addition, there is a striking change in the SubQ fat, which takes on many of the morphological and molecular characteristics of VISC fat. These data demonstrate that PRDM16 and beige fat cells are major regulators of systemic physiology. Moreover, PRDM16 determines some of the key functional differences between SubQ and VISC fat.

RESULTS

PRDM16 Is Enriched in SubQ Adipose Tissues and Required for Thermogenic Gene Expression

PRDM16 is involved in the development and function of classical brown and beige adipocytes. To determine how PRDM16 might be involved in the function of different adipose tissues that are considered ''white,'' we measured mRNA levels in multiple SubQ and VISC fat depots and compared these to the classical interscapular brown fat. *Prdm16* was significantly elevated in two SubQ depots (inguinal and axillary) relative to the very low levels of expression in two VISC depots (epididymal and mesenteric). As expected, the highest levels of expression were seen in interscapular BAT (Figure 1A). This depot enrichment was maintained in primary adipocytes differentiated in vitro from the inguinal SubQ or epididymal VISC stromal vascular fraction (SVF) (Figure 1B). Expression of *Ucp1*, the prototypical thermogenic gene, was also enriched across SubQ depots, consistent with the presence of beige adipocytes in these pads (Figures S1A and S1B available online). These data suggested that PRDM16 could play a role in multiple SubQ depots.

We generated a conditional *Prdm16* allele (*Prdm16*$^{lox/lox}$) by engineering loxP sites flanking exon 9, which we have shown to be required for mediating the effects of PRDM16 on thermogenic gene expression (Seale et al., 2008) (Figure S1C). We initially crossed *Prdm16*$^{lox/lox}$ mice to *Zp3-cre* mice to generate a germline deletion. As expected, these animals had craniofacial defects and died within 24 hr of birth, confirming that this mutation created a null allele of *Prdm16* (Bjork et al., 2010).

We next crossed *Prdm16*$^{lox/lox}$ and *Adiponectin-cre* mice (Eguchi et al., 2011) to generate mice with an adipocyte-specific knockout (KO) of *Prdm16* (Adipo-PRDM16 KO). This promoter expresses cre recombinase after the early developmental time point when the classical brown fat/muscle fate decision has been established (Lepper and Fan, 2010). We performed metabolic characterization of *Adiponectin-cre* mice and confirmed that the Cre recombinase is not likely to contribute to the KO phenotype (Figure S1D). Analysis of mRNA expression from multiple tissues confirmed that the deletion was specific to white and brown adipose tissues (Figure 1C). Notably, PRDM16 mRNA levels in epididymal fat trended downward in KO mice, though expression in this depot was at the margin of detection. The trend toward decreased *Prdm16* in the kidney of KO mice may reflect expression in adipose tissue surrounding this organ. Western blotting of nuclear extracts showed a marked reduction of PRDM16 protein in both classical BAT and inguinal SubQ adipose tissue from KO mice (Figure 1D). PRDM16 protein was too low to detect in the VISC depots.

PRDM16 deletion in the classical BAT resulted in a relatively normal pattern of gene expression (Figure 1E). The SubQ adipose tissue of Adipo-PRDM16 KO mice, however, showed reduced expression of a broad panel of thermogenic (*Dio2*, *Pgc1a*, and *Ucp1*), brown adipose identity (*Cidea*, *Otop1*, and *PPARa*), and mitochondrial electron transport genes (*Coxiii*, *Cox5b*, and *Cox8b*) (Figure 1F). There was no alteration in the

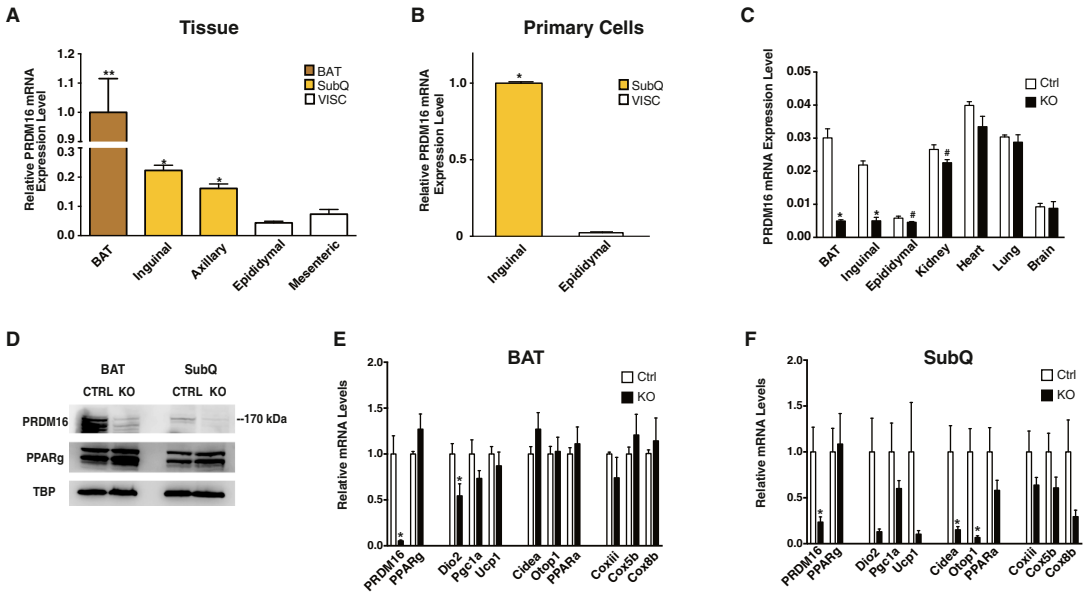

Figure 1. PRDM16 Deletion in Adipocytes Results in Altered Subcutaneous Adipose Tissue Gene Expression

(A and B) qPCR analysis of *Prdm16* mRNA from multiple adipose tissues from 8- to 10-week-old, male wild-type mice (n = 9), normalized to mRNA expression in BAT (A) or from in vitro differentiated primary adipocytes, normalized to mRNA expression in inguinal cells (n = 3) (B).

(C) qPCR analysis of *Prdm16* mRNA from multiple tissues from 6- to 8-week-old male Adipo-PRDM16 KO mice (n = 4) and controls (n = 4).

(D) PRDM16 protein in nuclear extracts from BAT or inguinal SubQ adipose tissue from Adipo-PRDM16 KO and controls. PPARγ and TBP protein are shown as controls.

(E and F) Normalized gene expression of thermogenic, brown adipose, and mitochondrial genes in BAT (E) and SubQ adipose tissue (F) from Adipo-PRDM16 KO and control mice at RT. Mice were males, 6–8 weeks old, n = 5 per group.

Data are presented as mean ± SEM. *p < 0.05. #, p = 0.053 for kidney and 0.079 for epididymal fat. See also Figure S1.

expression of *Pparg*, which is a general marker of adipose differentiation. *Ucp1* mRNA was reduced by 90% in the inguinal SubQ depot. This did not reach statistical significance (p = 0.14) due to the large variance in *Ucp1* mRNA levels in control mice. Adipo-PRDM16 KO mice also had decreased expression of a few of these genes in VISC adipose tissue, compared to controls, though the absolute expression level of these genes was very low (Figure S1E).

Since SubQ adipose tissues are particularly prone to inducing a thermogenic gene program (“browning”), we examined the effects of two potent stimuli: cold exposure and treatment with a β-adrenergic agonist. In interscapular BAT, the thermogenic program was induced similarly in both control and Adipo-PRDM16 KO animals following cold exposure or CL 316,243 (hereafter referred to as CL) treatment. There were some small but statistically significant differences in the induction of several genes with cold and CL treatment (Figures 2A and 2B). In contrast, the very robust increase in the entire panel of thermogenic gene expression seen in control inguinal adipose tissues (cold: 74-fold induction of *Ucp1*, CL: > 400-fold induction of *Ucp1*) was almost completely blocked in KO animals (Figures 2C and 2D). A similar pattern showing selective effects in SubQ adipose tissue was seen with prolonged cold exposure for 6 days (Figures S2A and S2B). *Ucp1* showed blunted induction in VISC adipose tissue of the Adipo-PRDM16 KO mice following CL treatment, though the levels of thermogenic genes were overall very low in this depot (Figure S2C).

The morphology and UCP1 content of these adipose depots was also examined in control and Adipo-PRDM16 KO mice. No differences in UCP1 were seen in the BAT between mice of either genotype, with or without cold exposure (Figure 2E). The SubQ adipose tissue from Adipo-PRDM16 KO mice, however, contained larger adipocytes and fewer small, multilocular UCP1$^+$ adipocytes (Figure 2E). Moreover, cold exposure resulted in the emergence of numerous small, multilocular UCP1$^+$ adipocytes in controls, while KO mice showed no change in appearance relative to RT (Figure 2E). Of note, Adipo-PRDM16 KO mice showed no difference in core temperature following 6 hr (Figure S2D) or 96 hr at 4°C (36.04°C ± 0.19 in KOs versus 35.78°C ± 0.26 in controls, p = 0.44). This further indicates that these mice have little apparent defect in the function of BAT since ablation of classical BAT or UCP1 is associated with severe cold intolerance (Enerbäck et al., 1997; Lowell et al., 1993).

We next asked whether these changes in the thermogenic program of SubQ adipose tissue were cell autonomous. SubQ

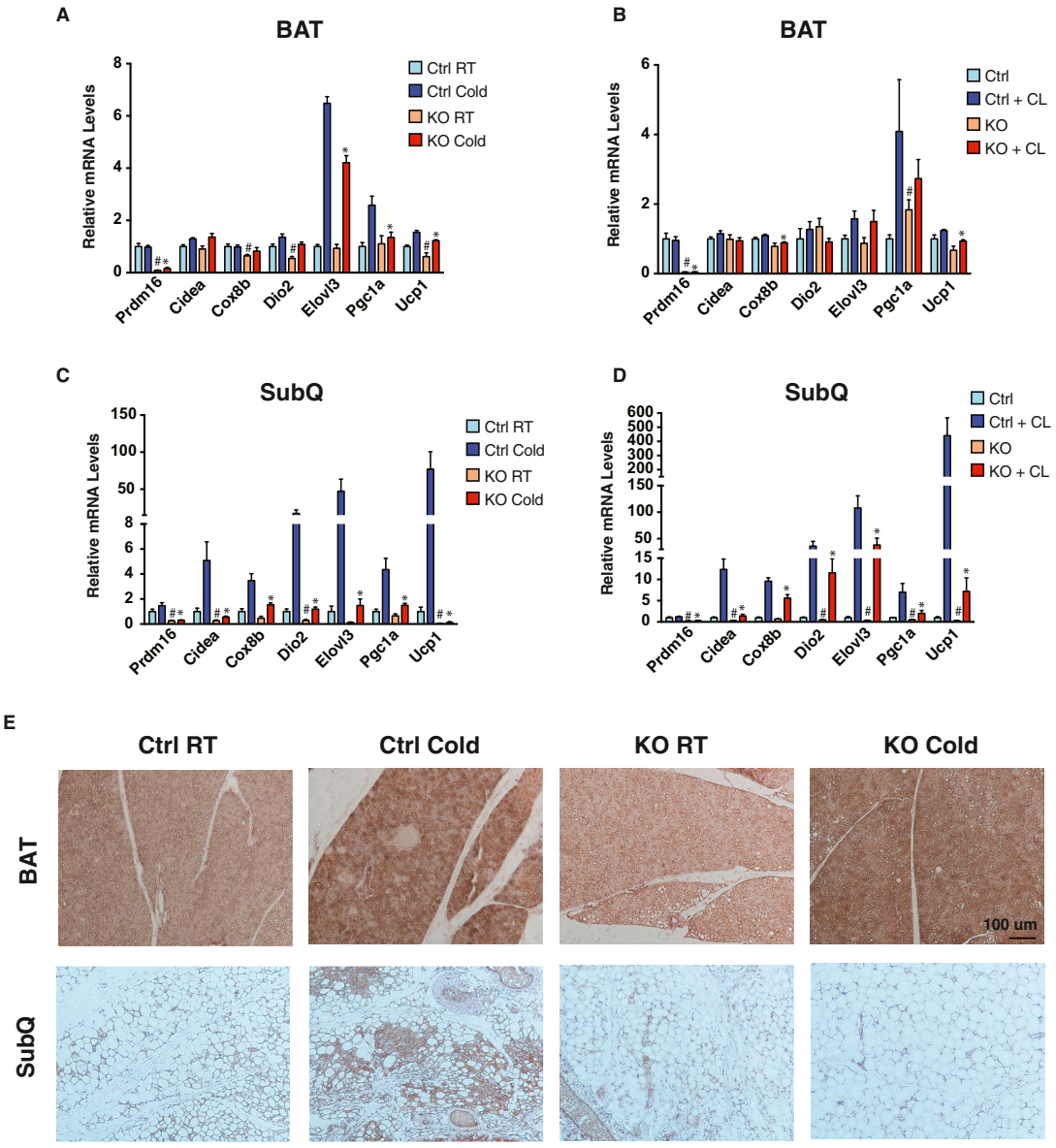

Figure 2. PRDM16 Regulates Beige Adipose Thermogenic Gene Expression

(A–D) Normalized thermogenic gene expression in BAT (A and B) and SubQ adipose tissue (C and D) from Adipo-PRDM16 KO and control mice at RT and following 48 hr at 4°C (A and C) or following five daily injections of 1 mg/kg CL (B and D). Cold exposure was done with male 6- to 8-week-old mice, n = 5–6 per group. CL treatment was done with female 6- to 8-week-old mice, n = 5–6 per group. Data are presented as mean ± SEM. *$p < 0.05$ KO versus control cold exposed or CL treated. #, $p < 0.05$ KO versus control room temperature or untreated.

(E) Representative images from UCP1 immunohistochemistry on sections of interscapular BAT or inguinal SubQ adipose tissue from Adipo-PRDM16 KO and control mice at RT or following 48 hr at 4°C. Images are shown at 10× magnification. Scale bar, 100 μm.

See also Figure S2.

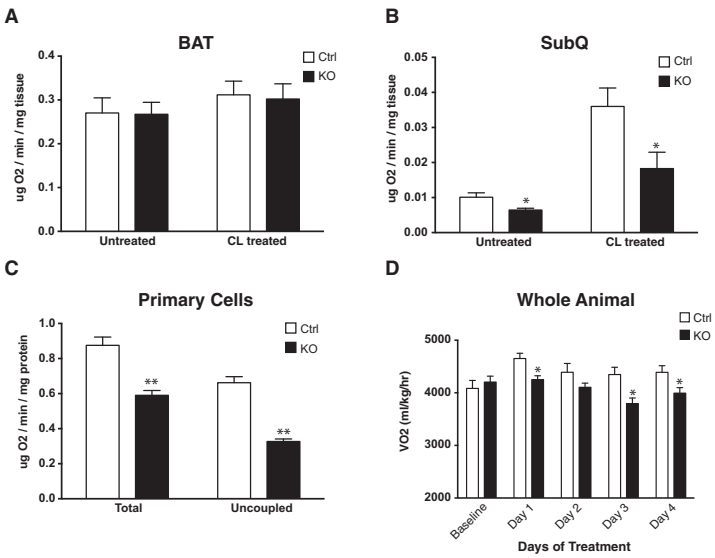

Figure 3. Altered Subcutaneous Adipose Tissue and Whole-Body O_2 Consumption in Adipo-PRDM16 KO Mice

(A and B) O_2 consumption in brown (A) and SubQ adipose tissue (B) from control and Adipo-PRDM16 KO mice. Tissues from untreated animals and animals treated with 5 daily injections of 1 mg/kg CL were analyzed. CL treatment was done with female 6- to 8-week-old mice, n = 5–6 per group.

(C) Total and uncoupled respiration in primary SubQ adipocytes from control and Adipo-PRDM16 KO mice. n = 6 per group.

(D) O_2 consumption in 8- to 10-week-old Adipo-PRDM16 KO and control male mice, n = 8 per group. Data were recorded at baseline and for 6 hr following daily injection of 0.1 mg/kg CL.

Data are presented as mean ± SEM. *p < 0.05. **p < 0.001. See also Figure S3.

adipocytes from KO mice differentiated in vitro also showed a significant reduction in the expression of most thermogenic (81% reduction in *Ucp1*), brown fat identity (97% reduction in *Cidea*), and mitochondrial genes (80% reduction in *Cox8b*), strongly suggesting a cell-autonomous role for PRDM16 in browning (Figure S2E). Cells from Adipo-PRDM16 KO mice also showed a blunted response to stimuli that induce browning, such as isoproterenol and FGF21 (Figures S2F ad S2G) (Fisher et al., 2012; Wu et al., 2013).

PRDM16 Regulates Adipose Tissue and Whole-Body Energy Expenditure

Given the preferential effect of this PRDM16 deletion on thermogenic gene expression in beige adipocytes, we assessed the physiological effect of this ablation, using O_2 consumption as a readout. SubQ and BAT pads were removed from mice and O_2 consumption was measured. These assays were performed both in untreated animals and after 5 days of CL treatment. Importantly, O_2 consumption in interscapular BAT was unchanged between KOs and controls in both basal and stimulated states (Figure 3A). In contrast, O_2 consumption in SubQ adipose tissue from Adipo-PRDM16 KO mice was significantly reduced, both at baseline (36% reduced) and following stimulation with CL (49% reduced) (Figure 3B). O_2 consumption in VISC adipose tissue was below the limit of detection in most animals. Assays in primary SubQ adipocytes showed a significant reduction in both total (33% reduced) and uncoupled (51% reduced) respiration in KO cells compared to controls (Figure 3C). Taken together, these results indicate that adipose-selective deletion of PRDM16 results in a large defect in a broad program of thermogenesis in SubQ adipose tissue, while classical BAT is relatively unaffected.

This selective ablation of beige cell thermogenic function offered a unique opportunity to study the role of these cells and the browning of white fat on whole-body physiology. When Adipo-PRDM16 KO mice were fed a chow diet, no difference was observed in food intake or activity between the mutant and control groups (Figures S3A and S3B). Adipo-PRDM16 KO mice also showed no difference in O_2 consumption but did have a significantly increased respiratory exchange ratio (RER), suggesting a decrease in utilization of fatty acid oxidation as an energy substrate (Figures S3C and S3D). We also studied these animals after injection with CL. Control animals showed a significant increase in O_2 consumption (6.5%–13.9%) following each injection. KO mice showed no increase in O_2 consumption, suggesting that ablation of beige adipocyte function can affect whole-body energy expenditure (Figure 3D).

Adipo-PRDM16 KO Mice Develop Obesity and Insulin Resistance

Animals were then subjected to a physiological challenge in the form of a high-fat, high-carbohydrate diet. Adipo-PRDM16 KO mice showed no difference in body weight from control animals on a chow diet, but demonstrated increased weight gain on a HFD (Figures 4A and 4B). Over 7 weeks at thermoneutrality, KOs on either a chow or HFD showed no difference in body weight compared to controls (Figures S4A and S4B). Of note, *Ucp1* KO mice show significant weight gain over this time period at thermoneutrality, presumably due to defects in classical brown fat function (Feldmann et al., 2009).

Body composition analysis was done after 16 weeks on HFD, when the weight curves had just started to diverge. Mutant animals had significantly increased fat mass, with no change in lean body mass (Figure 4C). These mice also showed an interesting change in the distribution of fat mass: KO animals had SubQ fat mass (inguinal depot) nearly twice that of controls, while the VISC (epididymal) and BAT masses were unchanged (Figure 4D). Metabolic analysis of mice after 2 weeks of HFD showed no significant differences in food intake, activity, O_2

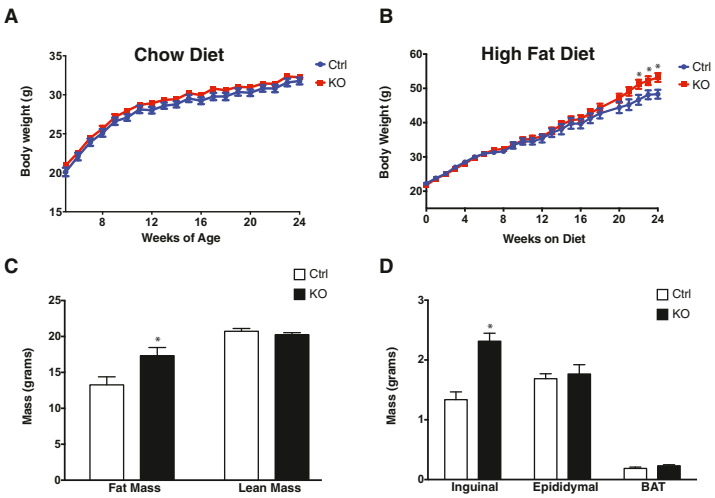

Figure 4. Obesity and Altered Fat Distribution in Adipo-PRDM16 KO Mice

(A and B) Body weights of Adipo-PRDM16 KO and control mice on standard chow (A) or HFD (B). HFD was started at 4 weeks of age. Experiments were done with male mice, n = 12–15 per group.

(C) Body composition of Adipo-PRDM16 KO and control mice following 16 weeks on HFD. n = 12 for controls and n = 19 for KOs.

(D) Weights of individual fat pads from Adipo-PRDM16 KO and control mice following 18 weeks on HFD. n = 11 per group.

Data are presented as mean ± SEM. *p < 0.05. See also Figure S4.

consumption, or RER compared to control animals (Figures S4C–S4F). O_2 consumption was also unchanged after longer periods on HFD, likely reflecting the fact that indirect calorimetry is insufficiently sensitive to detect small differences in energy expenditure, which could result in modest obesity over a prolonged period (Butler and Kozak, 2010).

SubQ adipocytes in high-fat fed Adipo-PRDM16 KO mice were markedly larger than those in control mice (Figure 5A). Quantitative assessment confirmed a 33% increase in mean adipocyte area in the SubQ depot of mutant animals to a size equivalent to adipocytes in the VISC depot (Figure 5B). KO mice had no difference in mRNA expression levels of general markers of adipose differentiation, though they did have a trend toward increased *Glut4* mRNA levels compared to controls (Figure S5A). The morphology and size of VISC epididymal adipocytes was unchanged between control and KO animals (Figure S5B). We used flow cytometry to quantitate the major myeloid and lymphoid subsets in the adipose tissue of high-fat fed mice. When compared to control animals, SubQ adipose tissue from KOs had a significant increase in the fraction and number of $CD11b^+F4/80^+$ macrophages (Figure 5C), along with increased crown-like structures (Figure 5D). These alterations were restricted to SubQ adipose tissue, as there were no differences in the representation of $CD11b^+F4/80^+$ macrophages in the VISC adipose tissue or spleen from KO animals (Figure S5C). No other immune cell subsets, including T regulatory cells, which have been shown to play a role in metabolic disease (Cipolletta et al., 2012), were altered in adipose tissue or lymphoid organs from KO mice (Figure S5D).

We next assessed glucose homeostasis in Adipo-PRDM16 KO mice. We performed hyperinsulinemic-euglycemic clamps, a sensitive method for assessing whole-body and tissue-specific insulin sensitivity. These studies were performed at a time well before the weight curves of KO animals diverged from controls (6 weeks on HFD). There was no difference in fasting plasma glucose between groups (Figure S6A). However, fasting plasma insulin levels were significantly increased (55% increased, $p < 0.05$) in Adipo-PRDM16 KO mice, suggestive of insulin resistance (Figure 6A). During the clamp, plasma glucose levels were matched between groups at approximately 120 mg/dl (Figure S6A). Adipo-PRDM16 KO mice showed significant whole-body insulin resistance as evidenced by a markedly reduced glucose infusion rate (64% of controls) and decreased whole-body glucose uptake (Figures S6B and 6B). Mutant mice also demonstrated significant hepatic insulin resistance with decreased insulin-stimulated suppression of endogenous glucose production (53% in KOs versus 95% in controls) (Figure 6C). This primary alteration in adipose tissue was also associated with hepatic steatosis in KO animals (Figure 6D). Moreover, KO animals showed a failure in insulin-mediated suppression of lipolysis (6% in KOs versus 45% in controls) (Figure 6E). Although control and Adipo-PRDM16 KO mice were dosed with the same amount of insulin, clamped insulin levels were modestly increased in the KOs ($p = 0.08$, Figure S6C), suggesting impaired insulin clearance consistent with insulin resistance. Gene expression analysis from a separate cohort of mice following 6 weeks HFD, showed marked reductions of many thermogenic genes in KO SubQ adipose tissue compared to controls. Some of these genes showed a modest, but significant, reduction in classical BAT (Figure S6D).

A bolus of ^{14}C-2-deoxyglucose was administered to determine tissue-specific rates of glucose transport. Marked reductions in glucose uptake were observed in the SubQ (79% decreased) and VISC fat (53% decreased) (Figure 6F). Interestingly, glucose uptake in the classical BAT was actually higher in Adipo-PRDM16 KO mice. Skeletal muscle glucose uptake was no different between control and KO mice. These data indicate that deletion of PRDM16 in adipocytes results in selectively dysfunctional beige adipose function with strong effects on whole-body and tissue-specific insulin sensitivity.

Adiponectin levels showed no difference between control and KO mice (Figure S6E). Moreover, PRDM16 null adipose cells do not appear to have cell-autonomous defects in insulin signaling, as levels of total and phosphorylated Akt were unchanged between control and KO primary SubQ adipocytes (Figure S6F).

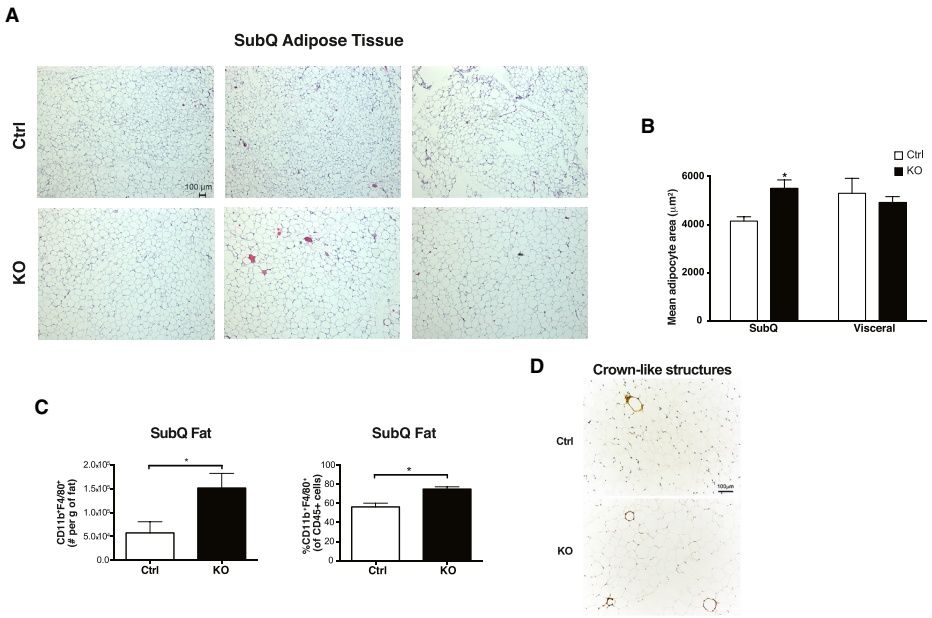

Figure 5. Increased Cell Size and Macrophage Accumulation in Subcutaneous Adipose Tissue from Adipo-PRDM16 KO Mice

(A and B) Cell size in inguinal SubQ adipose tissue from male Adipo-PRDM16 KO and control mice following 18 weeks on HFD. Representative images from hematoxylin and eosin (H&E) stained sections. Images are shown at 5× magnification. Scale bar, 100 μm. (B) Mean adipocyte area from inguinal SubQ and epididymal VISC adipose tissue. n = 3 per group.

(C) Flow cytometry quantitation of CD11b+F4/80+ macrophages in SubQ adipose tissue from Adipo-PRDM16 KO and control mice following 6 weeks on HFD.

(D) Morphological analysis for crown-like structures using Mac-2 staining from Adipo-PRDM16 KO and control mice following 6 weeks on HFD.

For (C) and (D), experiments were done with male mice 8–10 weeks old at start of HFD, n = 5–6 per group.

Data are presented as mean ± SEM. *p < 0.05. See also Figure S5.

Loss of Metabolic Benefit with Transplantation of Subcutaneous Fat from Adipo-PRDM16 KO Mice

This spectrum of phenotypes in Adipo-PRDM16 KO mice suggested that PRDM16 might be required for the healthful actions of SubQ adipose tissue. To address this, we transplanted SubQ fat pads (Gunawardana and Piston, 2012) from weanling pups of the two PRDM16 genotypes into high fat fed wild-type recipients and animals were then maintained on HFD. All recipients gained weight equally following the transplants. A glucose tolerance test was done at 6 weeks, and a highly significant difference was observed between the groups, with worse glucose tolerance in recipients of KO tissue (Figure 6G). There was no significant difference in insulin tolerance between these groups. This result has been replicated in a separate cohort of transplant recipients. The inclusion of a donor group from PRDM16 overexpressing, transgenic mice showed that glucose tolerance appears to track with PRDM16 levels in donor tissue (Figure S6G).

SubQ Adipose Tissue of Adipo-PRDM16 KO Mice Acquires a Partial VISC Adipose Phenotype

The combination of adipose and hepatic insulin resistance and the presence of larger adipocytes in KO SubQ adipose tissue with increased macrophage accumulation suggested a phenotype more typical of VISC obesity. These observations indicated that Adipo-PRDM16 KO SubQ adipose tissue might have developed some of the deleterious characteristics of VISC adipose tissue. To address this in an unbiased fashion, we used whole-genome microarrays to define depot-specific gene expression and then examined whether this molecular profile appeared "visceralized" in the SubQ adipose tissue of Adipo-PRDM16 KO animals.

Depot-enriched gene expression was studied by comparing RNA expression in adipose tissue from two SubQ depots (inguinal and axillary) to that from two VISC depots (epididymal and mesenteric). We defined a VISC gene set as containing genes with >3-fold increased expression and a p value < 0.05 between the VISC and SubQ depots. Sixty genes met these criteria. We then determined which of these genes had expression that was enriched >2-fold in fractionated adipocytes from VISC versus SubQ adipose tissue, to avoid studying differences due to other cell types. Twenty-six out of 60 genes met this requirement. We then studied the expression of these 26 visceral-selective genes in SubQ adipose tissue from control or Adipo-PRDM16 KO mice fed a HFD. 11/26 were >2-fold increased with p value < 0.05 in KOs versus controls. We then

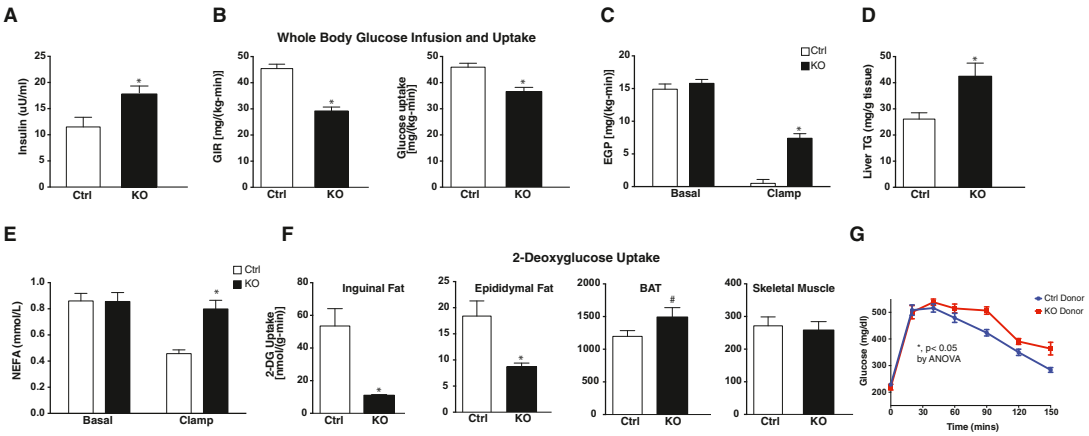

Figure 6. Insulin Resistance, Hepatic Steatosis, and Altered Glucose Uptake in Adipo-PRDM16 KO Mice

(A–E) Hyperinsulinemic-euglycemic clamp studies on Adipo-PRDM16 KO and control mice after 6 weeks on HFD.

(A) Fasting insulin levels.

(B) Glucose infusion rate and whole-body glucose uptake.

(C) Basal and insulin-stimulated endogenous glucose production.

(D) Liver triglyceride content.

(E) Basal and insulin-stimulated levels of nonesterified fatty acids.

(F) 2-deoxyglucose uptake in tissues from Adipo-PRDM16 KO and control mice.

Data are presented as mean ± SEM. *p < 0.05, # p = 0.09. Clamp studies were done with male mice, 8 weeks old at the start of HFD. n = 7–8 per group.

(G) Intraperitoneal glucose tolerance test (1.5 mg/kg) in male, high-fat-fed recipients of Adipo-PRDM16 KO or control SubQ adipose tissue. The GTT was done 6 weeks following transplantation. n = 6 per group. *p < 0.05 by ANOVA.

Data are presented as mean ± SEM. See also Figure S6.

selected 30 genes at random that were expressed in SubQ adipocytes and used these as a comparator. Only 1/30 was >2-fold increased with a p value < 0.05 in KO versus control adipose tissue.

These data are shown as a heat map with the color indicating the fold-change for each gene of this VISC fat gene expression set in SubQ adipose tissue from 11 KO mice relative to that of the control group (Figure 7A). The acquisition of a VISC-selective expression profile is highly significant (11/26 versus 1/30 genes, p = 0.0004 by chi-square). In addition this VISC profile contains a number of proinflammatory genes of known functional importance: Serum amyloid A3 (*Saa3*), Angiotensinogen (*Agt*), 12/15 lipoxygenase (*Alox15*), Osteoprotegerin (*Opgn*), and Retinaldehyde dehydrogenase 2 (*Raldh2*) (Figure 7B). The VISC-selective expression profile also includes three transcription factors (*Tcf21*, *Bnc1*, and *Wt1*) (Figure 7C). Two of these proinflammatory genes (*Agt* and Raldh2) were further increased in VISC adipose tissue from KO mice, compared to controls, though the expression of the three VISC-enriched transcription factors was unchanged (Figures S7A and S7B). Of note, more than half of these proinflammatory genes and transcription factors were significantly upregulated in PRDM16 KO SubQ fat cells differentiated in vitro (Figures S7C and S7D). This strongly suggests that the altered molecular profile in PRDM16 null adipose tissue is not simply a consequence of the metabolic dysregulation seen in these animals.

High-fat feeding also resulted in significantly decreased expression of typical thermogenic genes in SubQ adipose tissue of Adipo-PRDM16 KOs (Figure 7D), suggesting a coordinated balance between the molecular phenotype of VISC and SubQ adipose tissue. We considered whether PRDM16 might normally induce thermogenesis and repress inflammation, while a VISC-selective transcription factor might induce inflammation and repress thermogenesis. The three transcription factors identified in our VISC-enriched profile (shown above) were immediate candidates for conferring these depot-specific properties. We focused on *Wt1* because it showed cell-autonomous induction in the absence of PRDM16 (Figure S7D) and is strikingly enriched in VISC adipose tissues (Figure 7E).

We obtained *Wt1*$^{lox/lox}$ mice (Gao et al., 2006) and crossed them to *Adiponectin-cre* mice. We isolated adipose tissue SVF from *Wt1*$^{lox/lox;cre+}$ (KO) and *Wt1*$^{lox/lox;cre-}$ (control) VISC fat and differentiated them in vitro. We detected a significant reduction in the native *Wt1* transcript and a corresponding increase in a deleted transcript in KO cells compared to controls (Figure 7F). Both control and KO cells differentiated equally, with no morphological differences. There were small but significant differences in markers of adipocyte differentiation. Importantly, deletion of *Wt1* resulted in a striking induction of thermogenic genes (5.6-fold for *Cidea*, 6.1-fold for *Prdm16*, and 24.7-fold for *Ucp1*) and repression of several proinflammatory genes (46% for *Saa3* and 30% for *Agt*) compared to controls (Figure 7G). These data strongly suggest that reciprocal regulation of PRDM16 and

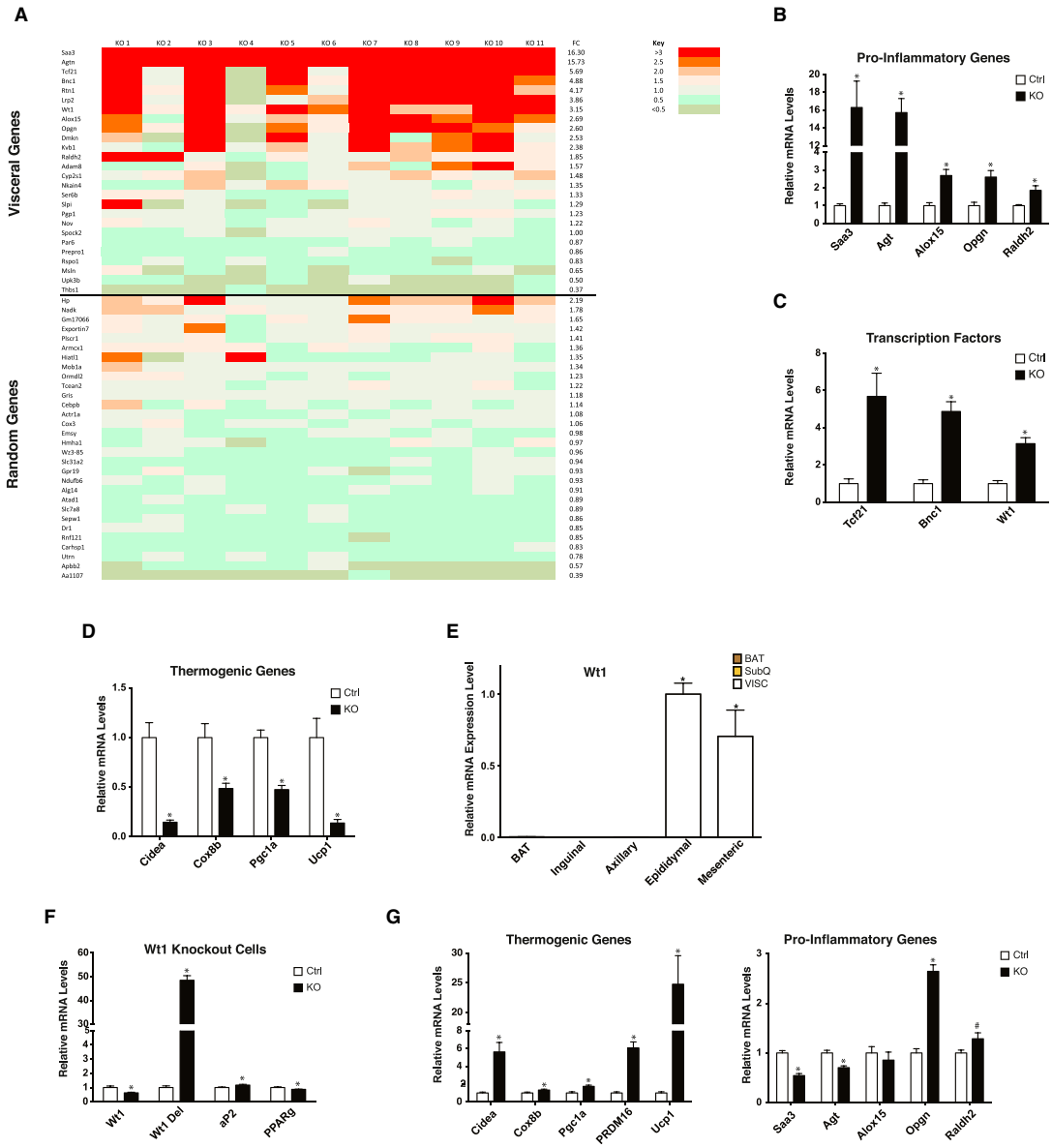

Figure 7. Induction of a Visceral Adipose Tissue Gene Expression Profile in Adipo-PRDM16 KO Subcutaneous Adipose Tissue

(A) Heat map showing relative expression of VISC-selective and randomly selected genes in SubQ adipose tissue from Adipo-PRDM16 KO mice after 18 weeks on HFD. Each row depicts an individual gene. Each column depicts the expression in a KO sample relative to the average expression in control mice. Average fold change is indicated in the column to the right. Fold change for each individual sample is color-coded according to the key.

(B and C) Normalized expression of proinflammatory genes (B) and transcription factors (C).

(D) Normalized expression of thermogenic genes.

For (A)–(D), gene expression was measured in male mice following 18 weeks HFD. n = 11 per group.

(legend continued on next page)

Wt1 is at least partly responsible for determining whether adipose expresses a SubQ or VISC gene program. Interestingly, in a differentiation time course in primary adipocytes from Adipo-PRDM16 KO mice, successive reduction in *Prdm16* mRNA levels is closely associated with progressive increases in *Wt1* mRNA levels (Figure S7E).

DISCUSSION

We have described here a mouse model with specific ablation of beige adipocyte function. Adipo-PRDM16 KO mice have significant reductions in thermogenic gene expression and O_2 consumption of white adipose tissue, both in the basal state and following stimulation with cold and the β3-adrenergic agonist CL. On the other hand, both thermogenic gene expression and O_2 consumption in classical BAT appears unaffected by PRDM16 deletion. Importantly, the direct measure of tissue-specific glucose uptake during hyperinsulinemic-euglyemic clamps indicated that there is essentially no functional deficiency in classical BAT. In fact, glucose uptake was elevated in KO BAT, suggesting this tissue might be compensating for the absence of functional beige adipose cells. This may represent a mirror image of the recent report of hyperactive beige adipose tissue in the setting of dysfunctional classical brown fat (Schulz et al., 2013). While deletion of PGC1α in adipocytes also leads to impaired thermogenic function in SubQ adipose tissue and metabolic defects (Kleiner et al., 2012; Pardo et al., 2011), the magnitude of the defect appears far greater in the Adipo-PRDM16 KO mice. *Pgc1a* expression is reduced in our KOs, consistent with PRDM16 being upstream of PGC1a (Seale et al., 2007).

The physiological relevance of beige fat has been questioned since expression of *Ucp1* mRNA and protein is at least an order of magnitude lower in these cells than in classical BAT (Nedergaard and Cannon, 2013). While mice with more beige fat cells have shown a protection from metabolic diseases (Seale et al., 2011; Vegiopoulos et al., 2010), the functional role of this cell type when present in normal amounts has not been clear. As shown here, animals deficient in competent beige adipocytes develop late-onset obesity on HFD. This is associated with increased fat mass, including a striking increase in SubQ adipose stores. While we were unable to detect differences in whole-body O_2 consumption in the basal state, KO animals showed significantly reduced energy expenditure following treatment with a β3-adrenergic agonist.

Hyperinsulinemic-euglycemic clamp studies on beige cell-deficient animals before the development of obesity showed significant insulin resistance, specifically affecting white adipose tissues and liver. Along with this, mutant animals developed hyperinsulinemia and hepatic steatosis. This model of insulin resistance is unusual in that glucose uptake in skeletal muscle seems unaffected. Beige adipocytes may have as yet undescribed actions on other tissues, with recent studies suggesting they regulate bone metabolism (Rahman et al., 2013).

This mouse model of beige fat deficiency differs in some interesting ways from mouse models with specific loss of classical BAT function. Mice with defective BAT develop obesity and insulin resistance (Feldmann et al., 2009; Hamann et al., 1996; Tseng et al., 2008). However, such animals tend to have defects in maintaining core temperature. When our KO mice were placed at 4°C, they showed no alteration in body temperature.

In the absence of PRDM16, mice developed marked enlargement of the SubQ adipose tissue. Interestingly, domestic pigs, which have abundant SubQ adipose tissue, lack functional UCP1 (Trayhurn et al., 1989). Similarly, Adipo-PRDM16 KO mice have virtually no UCP1 in their SubQ adipocytes. Histological examination of the SubQ fat from these mice demonstrated the presence of larger, unilocular cells, which become equivalent in size to VISC fat cells. KO mice also showed a virtual absence of small, multilocular $UCP1^+$ adipocytes. PRDM16-deficient animals not only lose the thermogenic program characteristic of beige adipocytes, but additionally, the SubQ adipose tissue acquires some of the deleterious characteristics of VISC fat, including the accumulation of macrophages. It is not yet clear whether acquisition of this VISC phenotype is causally related to loss of the thermogenic function of beige adipocytes or reflects a separate function of PRDM16 in adipocytes. The physiological significance of this change in depot phenotype, however, is made clear by our fat transplantation studies. Animals that received PRDM16-deficient SubQ pads had significantly worse glucose tolerance than recipients of control fat pads, recapitulating experimental animal models with increased VISC fat (Masuzaki et al., 2001).

Since reduced thermogenesis in SubQ adipose tissue of Adipo-PRDM16 KO mice is coupled to increased inflammatory gene expression and macrophage accumulation, it is not possible to disentangle the relative contribution of each of these alterations to the overall phenotype. Our data suggest that PRDM16 specifically affects the function of beige fat cells in the SubQ depots and that this is the proximal defect, occurring prior to acquisition of VISC properties upon high-fat feeding. Additionally, a recent paper showed that PRDM16 is only detected in multilocular and paucilocular cells within the omental fat of humans with pheochromocytoma (Frontini et al., 2013), consistent with its enrichment and selective expression in beige adipocytes. However, we cannot exclude possible effects from a very small amount of PRDM16 in true white adipocytes.

A comprehensive molecular analysis showed significant expression of a VISC gene signature in the SubQ fat of PRDM16 KO mice. This signature was developed based on objective criteria, using multiple depots of each type, and employing fat cell purification to avoid confounding by other cell types. These data clearly suggest that deletion of PRDM16 and ablation of beige adipocytes not only affects thermogenesis, but also results in substantial ''visceralization'' of the SubQ

(E) qPCR analysis of *Wt1* mRNA from multiple adipose tissues from 8- to 10-week-old, male wild-type mice, normalized to mRNA expression in epididymal white adipose tissue. n = 9 per group.
(F and G) Normalized expression of *Wt1* (F) and thermogenic and proinflammatory genes (G) in primary VISC $Wt1^{lox/lox;cre+}$ adipocytes. n = 6 per group.
Data are presented as mean ± SEM. *p < 0.05, #, p = 0.058. See also Figure S7.

adipose tissue. This analysis establishes with statistical significance ($p = 0.0004$) that deletion of PRDM16 results in acquisition of at least some aspects of the molecular phenotype of VISC adipose tissue. Of note, several of these VISC markers expressed in KO SubQ pads are of interest in metabolic diseases: Agt (Kalupahana et al., 2012), SAA3 (Kwon et al., 2012), Alox15 (Nunemaker et al., 2008; Sears et al., 2009), Opgn (Skopková et al., 2007), and Raldh2 (Frey and Vogel, 2011).

Three transcription factors (WT1, TCF21, and BNC1) were among the visceral signature genes induced in Adipo-PRDM16 KO SubQ adipose tissue. WT1 and TCF21 have known roles in urogenital development, and KO models of these genes have similar phenotypes (Kreidberg et al., 1993; Quaggin et al., 1999), suggesting that WT1 and TCF21 may function in the same pathway. WT1 is also a known tumor suppressor, which is mutated in Wilms' tumor (Haber et al., 1990). A role for WT1 in adipose biology has not previously been reported. Deletion of *Wt1* in primary VISC adipocytes resulted in downregulation of genes in the VISC signature and upregulation of thermogenic genes characteristic of SubQ/beige adipocytes. These data suggest an epistatic relationship between a thermogenic program regulated by PRDM16 and a VISC-specific program regulated by WT1. This appears analogous to the regulation of thermogenesis versus lipid storage by PRDM16 and TLE3 (Villanueva et al., 2013).

Thus, it is now clear that beige fat cells make an important contribution to whole-body physiology of mice. In the absence of functional beige fat, mice are prone to obesity, insulin resistance, and hepatic steatosis when challenged with HFD. In light of the presence of beige fat cells in normal adult humans (Lidell et al., 2013; Sharp et al., 2012; Wu et al., 2012), these cells are an attractive target for the treatment of obesity and type 2 diabetes. This influence of beige fat on liver metabolism is particularly interesting since there has been much more attention recently to the frequency and importance of hepatic steatosis as an important comorbidity in the metabolic syndrome (Angulo, 2002). Identification of pharmacological activators of PRDM16 targeted to beige adipocytes could hold promise as a new class of therapeutics.

EXPERIMENTAL PROCEDURES

Animals

Animal experiments were performed according to procedures approved by the Dana-Farber Cancer Institute and Yale University School of Medicine IACUC. The generation of Adipo-PRDM16 KO mice and the other mouse strains used is described in the Extended Experimental Procedures.

Molecular Studies

qPCR and western blotting were done according to standard methods. Antibodies used were PRDM16 (sheep anti-PRDM16, R&D), PPARγ (Cell Signaling), TBP (Santa Cruz), AKT and P-AKT (Cell Signaling), and Actin (Cell Signaling). Microarray hybridization and scanning were performed by the Dana-Farber Cancer Institute microarray core facility using Affymetrix Mouse Genome 430A 2.0 Gene Chip arrays. The GEO accession number for microarray data reported in this paper is GSE53307.

Histological Analysis

Tissues were fixed in 4% paraformaldehyde. Paraffin embedding and sectioning were done by the Dana-Faber/Harvard Cancer Center Research Pathology core facility. Adipocyte size was calculated as described (Vitali et al., 2012). The mean area of 200 random adipocytes (100 per section) from each animal was calculated using the Nikon LUCIA image program (version 4.61; Laboratory Imaging).

Immunohistochemistry

Immunohistochemistry was performed as previously described (Giordano et al., 2013) and as in the Extended Experimental Procedures.

Respiration

Tissue respiration was performed using a Clark electrode (Strathkelvin Instruments). Freshly isolated tissues were isolated from untreated mice or after five daily injections of 1.0 mg/kg CL (Sigma). Tissues were minced and placed in respiration buffer. For each adipose depot, readings were taken with three separate pieces of tissue of equivalent size. O_2 consumption was normalized to tissue weight. For assays on cultured cells, fully differentiated adipocytes were trypsinized and a single-cell suspension was placed in respiration buffer. Total respiration was measured and then oliogmycin was added to measure uncoupled respiration.

Flow Cytometry

Epididymal VISC and inguinal SubQ adipose tissue and spleen were excised and digested for 20 min with collagenase type II (Sigma). Cell suspensions were filtered through a 40 μm sieve, and the SVF was collected after centrifugation at 450 g for 10 min. For T cell analysis, cells were stained with anti-CD45 (clone 30-F11), -CD3 (145-2C11), -CD4 (GK1.5), -CD8 (5H10), and -CD25 (PC61) (BioLegend) and were fixed, permeabilized, and intracellularly stained for Foxp3 (FJK-16 s) and GATA3 (TWAJ) (eBiosciences). For myeloid cell analysis, cells were stained with anti-CD45, -CD3 (145-2C11), -CD11b (M1/70), -CD11c (N418), F4/80 (CI:A3-1), and anti-Ly6c (HK1.4) (BioLegend). B cells were stained with anti-CD45, and anti-CD19 (6D5) (BioLegend). Cells were analyzed using an LSRII instrument (BD Bioscience) and FlowJo software.

Metabolic Phenotyping

Metabolic phenotyping and hyperinsulinemic-euglycemic clamps were performed as described (Jurczak et al., 2012; Ye et al., 2012) and as in the Extended Experimental Procedures. All experiments were done with male mice, with the exception of the CL gene expression and tissue respiration studies. Energy expenditure was analyzed using a Comprehensive Lab Animal Monitoring System (Columbus Instruments). Fat and lean mass was measured by MRI. Cold exposure and thermoneutrality experiments were done at either 4°C or 30°C. Total adiponectin levels were measured by ELISA (Millipore).

Fat Transplant Studies

Inguinal SubQ adipose tissue was removed from 2- to 3-week-old Adipo-PRDM16 KO, littermate control mice, or aP2-PRDM16 transgenic mice (donors) and transplanted into the SubQ space of C57Bl6 mice (recipients) that had been on HFD for 6 weeks. Transplants were performed as described (Gunawardana and Piston, 2012). Glucose tolerance tests were done 6 weeks posttransplant. Animals were fasted for 4 hr and then received intraperitoneal glucose (1.5 mg/kg). Insulin tolerance tests were done 8 weeks posttransplant. Animals were fasted for 4 hr and then received intraperitoneal Humulin R insulin (1.0 U/kg, Lilly).

Cell Culture

For primary adipocytes, SVF from inguinal or epididymal fat from 5- to 6-week-old mice was prepared and differentiated for 6–8 days as described (Kajimura et al., 2009). Where indicated, cells were treated with isoproterenol 10 μM for 6 hr (Sigma) or FGF21 100 ng/ml overnight (R&D).

Statistics

The Student's t test was used for single comparisons. Two-way ANOVA with repeated-measures was used for the GTT studies. Chi-square was used to compare the VISC-selective gene set to a randomly selected set of genes. Unless specified, an asterisk (*) indicates $p < 0.05$.

ACCESSION NUMBERS

The GEO accession number for microarray data reported in this paper is GSE53307.

SUPPLEMENTAL INFORMATION

Supplemental Information includes Extended Experimental Procedures and seven figures and can be found with this article online at http://dx.doi.org/10.1016/j.cell.2013.12.021.

ACKNOWLEDGMENTS

We thank Dr. Evan Rosen (Beth Israel Deaconess Medical Center) for providing *Adiponectin-Cre* mice, Dr. Vicki Huff (MD Anderson) for providing *Wt1*$^{lox/lox}$ mice, and the Nikon Imaging Center at Harvard Medical School for use of microscopy equipment. We thank Dr. Vamsi Mootha (Massachusetts General Hospital) for guidance on data analysis and Drs. Rana Gupta, Pere Puigserver, Evan Rosen, and members of the Spiegelman lab for helpful discussions. P.C. was supported by the American Heart Association grant 11FTF7510004. D.P.K. was supported by a National Science Foundation Graduate Research Fellowship. This work was supported by NIH grants DK040936, DK045735, DK059635 (G.I.S.); NIH grant DK092541 (D.M.); and by NIH grant DK031405 and the JPB foundation (B.M.S.).

Received: August 9, 2013
Revised: October 31, 2013
Accepted: December 23, 2013
Published: January 16, 2014

REFERENCES

Angulo, P. (2002). Nonalcoholic fatty liver disease. N. Engl. J. Med. *346*, 1221–1231.

Bjork, B.C., Turbe-Doan, A., Prysak, M., Herron, B.J., and Beier, D.R. (2010). Prdm16 is required for normal palatogenesis in mice. Hum. Mol. Genet. *19*, 774–789.

Butler, A.A., and Kozak, L.P. (2010). A recurring problem with the analysis of energy expenditure in genetic models expressing lean and obese phenotypes. Diabetes *59*, 323–329.

Cipolletta, D., Feuerer, M., Li, A., Kamei, N., Lee, J., Shoelson, S.E., Benoist, C., and Mathis, D. (2012). PPAR-γ is a major driver of the accumulation and phenotype of adipose tissue Treg cells. Nature *486*, 549–553.

Cypess, A.M., White, A.P., Vernochet, C., Schulz, T.J., Xue, R., Sass, C.A., Huang, T.L., Roberts-Toler, C., Weiner, L.S., Sze, C., et al. (2013). Anatomical localization, gene expression profiling and functional characterization of adult human neck brown fat. Nat. Med. *19*, 635–639.

Eguchi, J., Wang, X., Yu, S., Kershaw, E.E., Chiu, P.C., Dushay, J., Estall, J.L., Klein, U., Maratos-Flier, E., and Rosen, E.D. (2011). Transcriptional control of adipose lipid handling by IRF4. Cell Metab. *13*, 249–259.

Enerbäck, S., Jacobsson, A., Simpson, E.M., Guerra, C., Yamashita, H., Harper, M.E., and Kozak, L.P. (1997). Mice lacking mitochondrial uncoupling protein are cold-sensitive but not obese. Nature *387*, 90–94.

Feldmann, H.M., Golozoubova, V., Cannon, B., and Nedergaard, J. (2009). UCP1 ablation induces obesity and abolishes diet-induced thermogenesis in mice exempt from thermal stress by living at thermoneutrality. Cell Metab. *9*, 203–209.

Fisher, F.M., Kleiner, S., Douris, N., Fox, E.C., Mepani, R.J., Verdeguer, F., Wu, J., Kharitonenkov, A., Flier, J.S., Maratos-Flier, E., and Spiegelman, B.M. (2012). FGF21 regulates PGC-1α and browning of white adipose tissues in adaptive thermogenesis. Genes Dev. *26*, 271–281.

Frey, S.K., and Vogel, S. (2011). Vitamin A metabolism and adipose tissue biology. Nutrients *3*, 27–39.

Frontini, A., Vitali, A., Perugini, J., Murano, I., Romiti, C., Ricquier, D., Guerrieri, M., and Cinti, S. (2013). White-to-brown transdifferentiation of omental adipocytes in patients affected by pheochromocytoma. Biochim. Biophys. Acta *1831*, 950–959.

Gabriely, I., Ma, X.H., Yang, X.M., Atzmon, G., Rajala, M.W., Berg, A.H., Scherer, P., Rossetti, L., and Barzilai, N. (2002). Removal of visceral fat prevents insulin resistance and glucose intolerance of aging: an adipokine-mediated process? Diabetes *51*, 2951–2958.

Gao, F., Maiti, S., Alam, N., Zhang, Z., Deng, J.M., Behringer, R.R., Lécureuil, C., Guillou, F., and Huff, V. (2006). The Wilms tumor gene, Wt1, is required for Sox9 expression and maintenance of tubular architecture in the developing testis. Proc. Natl. Acad. Sci. USA *103*, 11987–11992.

Gesta, S., Tseng, Y.H., and Kahn, C.R. (2007). Developmental origin of fat: tracking obesity to its source. Cell *131*, 242–256.

Giordano, A., Murano, I., Mondini, E., Perugini, J., Smorlesi, A., Severi, I., Barazzoni, R., Scherer, P.E., and Cinti, S. (2013). Obese adipocytes show ultrastructural features of stressed cells and die of pyroptosis. J. Lipid Res. *54*, 2423–2436.

Gunawardana, S.C., and Piston, D.W. (2012). Reversal of type 1 diabetes in mice by brown adipose tissue transplant. Diabetes *61*, 674–682.

Haber, D.A., Buckler, A.J., Glaser, T., Call, K.M., Pelletier, J., Sohn, R.L., Douglass, E.C., and Housman, D.E. (1990). An internal deletion within an 11p13 zinc finger gene contributes to the development of Wilms' tumor. Cell *61*, 1257–1269.

Hamann, A., Flier, J.S., and Lowell, B.B. (1996). Decreased brown fat markedly enhances susceptibility to diet-induced obesity, diabetes, and hyperlipidemia. Endocrinology *137*, 21–29.

Hotamisligil, G.S., Shargill, N.S., and Spiegelman, B.M. (1993). Adipose expression of tumor necrosis factor-alpha: direct role in obesity-linked insulin resistance. Science *259*, 87–91.

Jespersen, N.Z., Larsen, T.J., Peijs, L., Daugaard, S., Homøe, P., Loft, A., de Jong, J., Mathur, N., Cannon, B., Nedergaard, J., et al. (2013). A classical brown adipose tissue mRNA signature partly overlaps with brite in the supraclavicular region of adult humans. Cell Metab. *17*, 798–805.

Jurczak, M.J., Lee, A.H., Jornayvaz, F.R., Lee, H.Y., Birkenfeld, A.L., Guigni, B.A., Kahn, M., Samuel, V.T., Glimcher, L.H., and Shulman, G.I. (2012). Dissociation of inositol-requiring enzyme (IRE1α)-mediated c-Jun N-terminal kinase activation from hepatic insulin resistance in conditional X-box-binding protein-1 (XBP1) knock-out mice. J. Biol. Chem. *287*, 2558–2567.

Kajimura, S., Seale, P., Kubota, K., Lunsford, E., Frangioni, J.V., Gygi, S.P., and Spiegelman, B.M. (2009). Initiation of myoblast to brown fat switch by a PRDM16-C/EBP-beta transcriptional complex. Nature *460*, 1154–1158.

Kalupahana, N.S., Massiera, F., Quignard-Boulange, A., Ailhaud, G., Voy, B.H., Wasserman, D.H., and Moustaid-Moussa, N. (2012). Overproduction of angiotensinogen from adipose tissue induces adipose inflammation, glucose intolerance, and insulin resistance. Obesity (Silver Spring) *20*, 48–56.

Kiefer, F.W., Vernochet, C., O'Brien, P., Spoerl, S., Brown, J.D., Nallamshetty, S., Zeyda, M., Stulnig, T.M., Cohen, D.E., Kahn, C.R., and Plutzky, J. (2012). Retinaldehyde dehydrogenase 1 regulates a thermogenic program in white adipose tissue. Nat. Med. *18*, 918–925.

Kim, J.Y., van de Wall, E., Laplante, M., Azzara, A., Trujillo, M.E., Hofmann, S.M., Schraw, T., Durand, J.L., Li, H., Li, G., et al. (2007). Obesity-associated improvements in metabolic profile through expansion of adipose tissue. J. Clin. Invest. *117*, 2621–2637.

Kleiner, S., Mepani, R.J., Laznik, D., Ye, L., Jurczak, M.J., Jornayvaz, F.R., Estall, J.L., Chatterjee Bhowmick, D., Shulman, G.I., and Spiegelman, B.M. (2012). Development of insulin resistance in mice lacking PGC-1α in adipose tissues. Proc. Natl. Acad. Sci. USA *109*, 9635–9640.

Kreidberg, J.A., Sariola, H., Loring, J.M., Maeda, M., Pelletier, J., Housman, D., and Jaenisch, R. (1993). WT-1 is required for early kidney development. Cell *74*, 679–691.

Kusminski, C.M., Holland, W.L., Sun, K., Park, J., Spurgin, S.B., Lin, Y., Askew, G.R., Simcox, J.A., McClain, D.A., Li, C., and Scherer, P.E. (2012). MitoNEET-

driven alterations in adipocyte mitochondrial activity reveal a crucial adaptive process that preserves insulin sensitivity in obesity. Nat. Med. *18*, 1539–1549.

Kwon, E.Y., Shin, S.K., Cho, Y.Y., Jung, U.J., Kim, E., Park, T., Park, J.H., Yun, J.W., McGregor, R.A., Park, Y.B., and Choi, M.S. (2012). Time-course microarrays reveal early activation of the immune transcriptome and adipokine dysregulation leads to fibrosis in visceral adipose depots during diet-induced obesity. BMC Genomics *13*, 450.

Lepper, C., and Fan, C.M. (2010). Inducible lineage tracing of Pax7-descendant cells reveals embryonic origin of adult satellite cells. Genesis *48*, 424–436.

Lidell, M.E., Betz, M.J., Dahlqvist Leinhard, O., Heglind, M., Elander, L., Slawik, M., Mussack, T., Nilsson, D., Romu, T., Nuutila, P., et al. (2013). Evidence for two types of brown adipose tissue in humans. Nat. Med. *19*, 631–634.

Lowell, B.B., S-Susulic, V., Hamann, A., Lawitts, J.A., Himms-Hagen, J., Boyer, B.B., Kozak, L.P., and Flier, J.S. (1993). Development of obesity in transgenic mice after genetic ablation of brown adipose tissue. Nature *366*, 740–742.

Manolopoulos, K.N., Karpe, F., and Frayn, K.N. (2010). Gluteofemoral body fat as a determinant of metabolic health. Int J Obes (Lond) *34*, 949–959.

Masuzaki, H., Paterson, J., Shinyama, H., Morton, N.M., Mullins, J.J., Seckl, J.R., and Flier, J.S. (2001). A transgenic model of visceral obesity and the metabolic syndrome. Science *294*, 2166–2170.

Nedergaard, J., and Cannon, B. (2013). UCP1 mRNA does not produce heat. Biochim. Biophys. Acta *1831*, 943–949.

Nunemaker, C.S., Chen, M., Pei, H., Kimble, S.D., Keller, S.R., Carter, J.D., Yang, Z., Smith, K.M., Wu, R., Bevard, M.H., et al. (2008). 12-Lipoxygenase-knockout mice are resistant to inflammatory effects of obesity induced by Western diet. Am. J. Physiol. Endocrinol. Metab. *295*, E1065–E1075.

Ohno, H., Shinoda, K., Spiegelman, B.M., and Kajimura, S. (2012). PPARγ agonists induce a white-to-brown fat conversion through stabilization of PRDM16 protein. Cell Metab. *15*, 395–404.

Pardo, R., Enguix, N., Lasheras, J., Feliu, J.E., Kralli, A., and Villena, J.A. (2011). Rosiglitazone-induced mitochondrial biogenesis in white adipose tissue is independent of peroxisome proliferator-activated receptor γ coactivator-1α. PLoS ONE *6*, e26989.

Pischon, T., Boeing, H., Hoffmann, K., Bergmann, M., Schulze, M.B., Overvad, K., van der Schouw, Y.T., Spencer, E., Moons, K.G., Tjønneland, A., et al. (2008). General and abdominal adiposity and risk of death in Europe. N. Engl. J. Med. *359*, 2105–2120.

Quaggin, S.E., Schwartz, L., Cui, S., Igarashi, P., Deimling, J., Post, M., and Rossant, J. (1999). The basic-helix-loop-helix protein pod1 is critically important for kidney and lung organogenesis. Development *126*, 5771–5783.

Rahman, S., Lu, Y., Czernik, P.J., Rosen, C.J., Enerback, S., and Lecka-Czernik, B. (2013). Inducible brown adipose tissue, or beige fat, is anabolic for the skeleton. Endocrinology *154*, 2687–2701.

Schulz, T.J., Huang, P., Huang, T.L., Xue, R., McDougall, L.E., Townsend, K.L., Cypess, A.M., Mishina, Y., Gussoni, E., and Tseng, Y.H. (2013). Brown-fat paucity due to impaired BMP signalling induces compensatory browning of white fat. Nature *495*, 379–383.

Seale, P., Kajimura, S., Yang, W., Chin, S., Rohas, L.M., Uldry, M., Tavernier, G., Langin, D., and Spiegelman, B.M. (2007). Transcriptional control of brown fat determination by PRDM16. Cell Metab. *6*, 38–54.

Seale, P., Bjork, B., Yang, W., Kajimura, S., Chin, S., Kuang, S., Scimè, A., Devarakonda, S., Conroe, H.M., Erdjument-Bromage, H., et al. (2008). PRDM16 controls a brown fat/skeletal muscle switch. Nature *454*, 961–967.

Seale, P., Conroe, H.M., Estall, J., Kajimura, S., Frontini, A., Ishibashi, J., Cohen, P., Cinti, S., and Spiegelman, B.M. (2011). Prdm16 determines the thermogenic program of subcutaneous white adipose tissue in mice. J. Clin. Invest. *121*, 96–105.

Sears, D.D., Miles, P.D., Chapman, J., Ofrecio, J.M., Almazan, F., Thapar, D., and Miller, Y.I. (2009). 12/15-lipoxygenase is required for the early onset of high fat diet-induced adipose tissue inflammation and insulin resistance in mice. PLoS ONE *4*, e7250.

Sharp, L.Z., Shinoda, K., Ohno, H., Scheel, D.W., Tomoda, E., Ruiz, L., Hu, H., Wang, L., Pavlova, Z., Gilsanz, V., and Kajimura, S. (2012). Human BAT possesses molecular signatures that resemble beige/brite cells. PLoS ONE *7*, e49452.

Skopková, M., Penesová, A., Sell, H., Rádiková, Z., Vlcek, M., Imrich, R., Koska, J., Ukropec, J., Eckel, J., Klimes, I., and Gasperíková, D. (2007). Protein array reveals differentially expressed proteins in subcutaneous adipose tissue in obesity. Obesity (Silver Spring) *15*, 2396–2406.

Tran, T.T., Yamamoto, Y., Gesta, S., and Kahn, C.R. (2008). Beneficial effects of subcutaneous fat transplantation on metabolism. Cell Metab. *7*, 410–420.

Trayhurn, P., Temple, N.J., and Van Aerde, J. (1989). Evidence from immunoblotting studies on uncoupling protein that brown adipose tissue is not present in the domestic pig. Can. J. Physiol. Pharmacol. *67*, 1480–1485.

Tseng, Y.H., Kokkotou, E., Schulz, T.J., Huang, T.L., Winnay, J.N., Taniguchi, C.M., Tran, T.T., Suzuki, R., Espinoza, D.O., Yamamoto, Y., et al. (2008). New role of bone morphogenetic protein 7 in brown adipogenesis and energy expenditure. Nature *454*, 1000–1004.

Vague, J. (1947). La différenciation sexuelle; facteur déterminant des formes de l'obésité. Presse Med. *55*, 339–340.

Vague, J. (1956). The degree of masculine differentiation of obesities: a factor determining predisposition to diabetes, atherosclerosis, gout, and uric calculous disease. Am. J. Clin. Nutr. *4*, 20–34.

Vegiopoulos, A., Müller-Decker, K., Strzoda, D., Schmitt, I., Chichelnitskiy, E., Ostertag, A., Berriel Diaz, M., Rozman, J., Hrabe de Angelis, M., Nüsing, R.M., et al. (2010). Cyclooxygenase-2 controls energy homeostasis in mice by de novo recruitment of brown adipocytes. Science *328*, 1158–1161.

Villanueva, C.J., Vergnes, L., Wang, J., Drew, B.G., Hong, C., Tu, Y., Hu, Y., Peng, X., Xu, F., Saez, E., et al. (2013). Adipose subtype-selective recruitment of TLE3 or Prdm16 by PPARγ specifies lipid storage versus thermogenic gene programs. Cell Metab. *17*, 423–435.

Vitali, A., Murano, I., Zingaretti, M.C., Frontini, A., Ricquier, D., and Cinti, S. (2012). The adipose organ of obesity-prone C57BL/6J mice is composed of mixed white and brown adipocytes. J. Lipid Res. *53*, 619–629.

Weisberg, S.P., McCann, D., Desai, M., Rosenbaum, M., Leibel, R.L., and Ferrante, A.W., Jr. (2003). Obesity is associated with macrophage accumulation in adipose tissue. J. Clin. Invest. *112*, 1796–1808.

Wu, J., Boström, P., Sparks, L.M., Ye, L., Choi, J.H., Giang, A.H., Khandekar, M., Virtanen, K.A., Nuutila, P., Schaart, G., et al. (2012). Beige adipocytes are a distinct type of thermogenic fat cell in mouse and human. Cell *150*, 366–376.

Wu, J., Cohen, P., and Spiegelman, B.M. (2013). Adaptive thermogenesis in adipocytes: is beige the new brown? Genes Dev. *27*, 234–250.

Xu, H., Barnes, G.T., Yang, Q., Tan, G., Yang, D., Chou, C.J., Sole, J., Nichols, A., Ross, J.S., Tartaglia, L.A., and Chen, H. (2003). Chronic inflammation in fat plays a crucial role in the development of obesity-related insulin resistance. J. Clin. Invest. *112*, 1821–1830.

Ye, L., Kleiner, S., Wu, J., Sah, R., Gupta, R.K., Banks, A.S., Cohen, P., Khandekar, M.J., Boström, P., Mepani, R.J., et al. (2012). TRPV4 is a regulator of adipose oxidative metabolism, inflammation, and energy homeostasis. Cell *151*, 96–110.

Cell

EXTENDED EXPERIMENTAL PROCEDURES

Animals

To generate *PRDM16*$^{lox/lox}$ mice, BAC recombineering was used to retrieve ~16 kb of genomic sequence encompassing exon 9 of *Prdm16* from a 129Sv BAC clone (RPCIB731F20213Q from 129s7/AB2.2 BAC library) into plasmid PL253 (Adams et al., 2005; Liu et al., 2003). A floxed *PGK-Neo* cassette from PL452 was integrated ~280 bp upstream of exon 9, followed by Cre mediated excision of *PGK-Neo* in bacteria, leaving a single *LoxP* site upstream of exon 9. A cassette containing *FRT-PGK-Neo-FRT-LoxP* was integrated 300 bp downstream of Exon 9. The resulting targeting construct (PL253-Prdm16Ex9Neo) was electroporated into 129Sv ES cells (courtesy of Dr. Brad Lowell). ES clones were screened for homologous recombination by Southern blotting using probes 5′ and 3′ of the targeting area. Positive clones were injected into C57Bl6 blastocysts to derive chimeric mice. Germline transmission of the targeted allele was confirmed by Southern blotting. The *PGK-Neo* selection cassette was excised by breeding with *Rosa26-Flp* deleter mice (Jackson Laboratory). *PRDM16*$^{lox/lox}$ mice were backcrossed to C57Bl6 mice for at least 8 generations. *PRDM16*$^{lox/lox}$ mice were then crossed to either *Zp3-cre* (Jackson Laboratory) or *Adiponectin-cre* mice (provided by Dr. Evan Rosen). Wt1$^{lox/lox}$ mice were provided by Dr. Vicki Huff.

Molecular Studies

Total RNA from cultured cells or tissues was isolated using TRIzol (Invitrogen) along with QIAGEN RNeasy mini kits. For qPCR analysis, RNA was reverse transcribed using the ABI high capacity cDNA synthesis kit. cDNA was used in qPCR reactions containing SYBR-green fluorescent dye (ABI). Relative mRNA expression was determined by normalization with TBP levels using the ΔΔ Ct method. Primer sequences are available on request. For western blotting, nuclear extracts or whole cell lysates were prepared, separated by SDS-PAGE, and transferred to ImmobilonP membranes (Millipore).

Immunohistochemistry

For UCP1 immunohistochemistry, slides were deparaffinized in xylene, hydrated in 95%, 80% and 70% ethanol, and rinsed in water before heat-mediated antigen retrieval in 10 mM pH 6.0 sodium citrate buffer. Quenching of endogenous peroxidases was performed using peroxidase quenching solution (Invitrogen). Slides were blocked in 10% goat serum and incubated with rabbit polyclonal UCP1 antibody (Abcam, ab10983) at 2 μg/ml in PBS-T/1% BSA overnight at 4°C. Slides were washed in PBS-T and incubated with 1:500 donkey anti-rabbit IgG HRP-linked antibody (GE healthcare) before developing using SuperPicture 3rd Gen IHC Detection Kit (Invitrogen). Hematoxylin was used as counterstain. Crown-like structures were detected by immunohistochemistry using mouse monoclonal anti-MAC2 (Cederlane Labs) as described (Giordano et al., 2013).

Metabolic Phenotyping

Mice were maintained on standard chow or 60% HFD (Research Diets) with 12 hr light cycles. Energy expenditure was analyzed using a Comprehensive Lab Animal Monitoring System (Columbus Instruments). Mice were acclimated for at least 24 hr before measurements were taken. Hyperinsulinemic euglycemic clamps were performed as described (Jurczak et al., 2012). After an overnight fast, mice were infused for 120 min with 3-^{3}H-glucose to determine basal glucose turnover. Next, mice were given a primed/constant infusion of insulin [(3 mU/kg-min)] and 3-^{3}H-glucose (0.1 μCi/min) and variable infusion of 20% dextrose to maintain euglycemia. A bolus injection of ^{14}C-2-deoxyglucose was given during the last 50 min to assess tissue-specific glucose uptake. Plasma samples were collected by tail bleed at set time points to determine plasma glucose, tracer, insulin and fatty acid concentrations. Calculations of glucose turnover were made at steady state during the last 40 min of the clamp.

SUPPLEMENTAL REFERENCES

Adams, D.J., Quail, M.A., Cox, T., van der Weyden, L., Gorick, B.D., Su, Q., Chan, W.I., Davies, R., Bonfield, J.K., Law, F., et al. (2005). A genome-wide, end-sequenced 129Sv BAC library resource for targeting vector construction. Genomics *86*, 753–758.

Liu, P., Jenkins, N.A., and Copeland, N.G. (2003). A highly efficient recombineering-based method for generating conditional knockout mutations. Genome Res. *13*, 476–484.

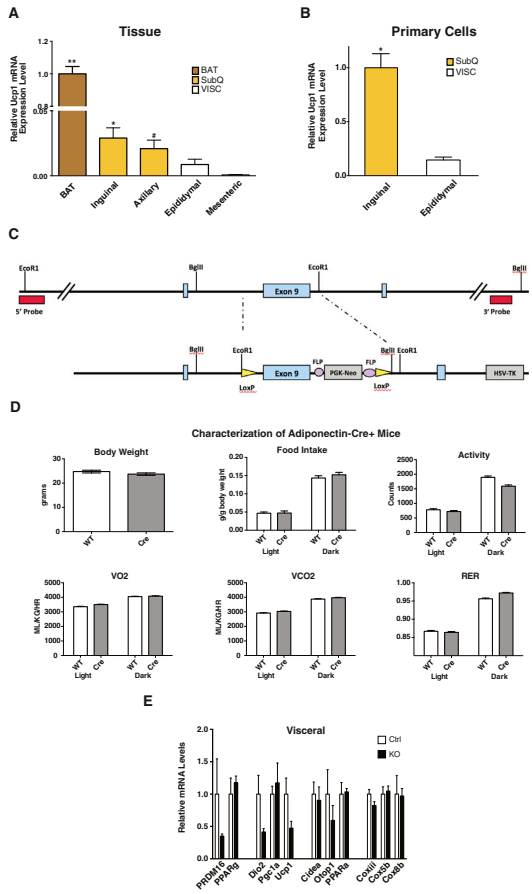

Figure S1. PRDM16 Deletion in Adipocytes Results in Altered Gene Expression, Related to Figure 1

(A and B) qPCR analysis of *Ucp1* mRNA from multiple adipose tissues from 8- to 10-week-old male wild-type mice (n = 9), normalized to mRNA expression in brown adipose tissue (A) or from in vitro differentiated primary adipocytes, normalized to mRNA expression in inguinal cells (n = 3) (B).

(C) Targeting construct for PRDM16.

(D) Metabolic characterization of male Adiponectin-Cre^{+} and wild-type control mice, n = 7 per group.

(E) Normalized gene expression of thermogenic, brown adipose, and mitochondrial genes in visceral adipose tissue (F) from Adipo-PRDM16 KO and control mice at ambient temperature. Mice were males, 6–8 weeks old, n = 5 per group.

Data are presented as mean ± SEM.

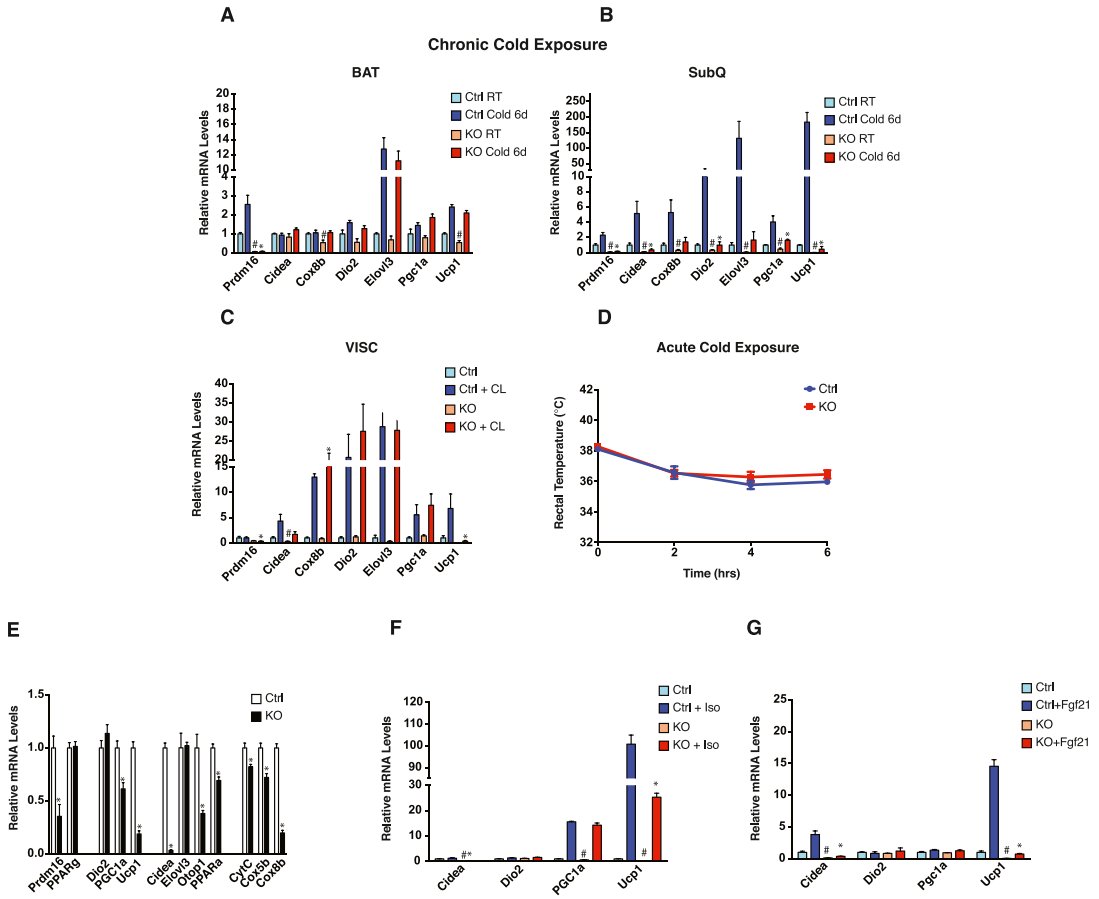

Figure S2. PRDM16 Regulates Thermogenic Gene Expression In Vivo and In Vitro, Related to Figure 2

(A and B) Normalized thermogenic gene expression in brown adipose tissue and subcutaneous adipose tissue from Adipo-PRDM16 KO and control mice either at room temperature or following 6 days at 4°C. Cold exposure was done with male 6- to 8-week-old mice, n = 4 per group.

(C) Normalized thermogenic gene expression in visceral adipose tissue from Adipo-PRDM16 KO and control mice either untreated or following five daily injections of CL 316,243 at a dose of 1 mg/kg. CL treatment was done with female 6- to 8-week-old mice, n = 5–6 per group.

Data are presented as mean ± SEM. *p < 0.05 knockout versus control cold exposed or CL 316,243 treated. #, p < 0.05 knockout versus control room temperature or untreated.

(D) Core body temperature over a time course of acute cold exposure at 4°C in control and Adipo-PRDM16 KO mice. 6-8 week old male mice were used, n = 3–4 per group.

(E) Gene expression in subcutaneous adipocytes from control and Adipo-PRDM16 KO mice, differentiated in vitro. *p < 0.05 knockout versus control.

(F and G) Subcutaneous adipocytes from control and Adipo-PRDM16 KO mice, differentiated in vitro and treated with isoproterenol (C) or FGF21 (D). #, p < 0.05 control versus knockout untreated. *p < 0.05 control versus knockout treated. n = 3 per group.

Data are presented as mean ± SEM.

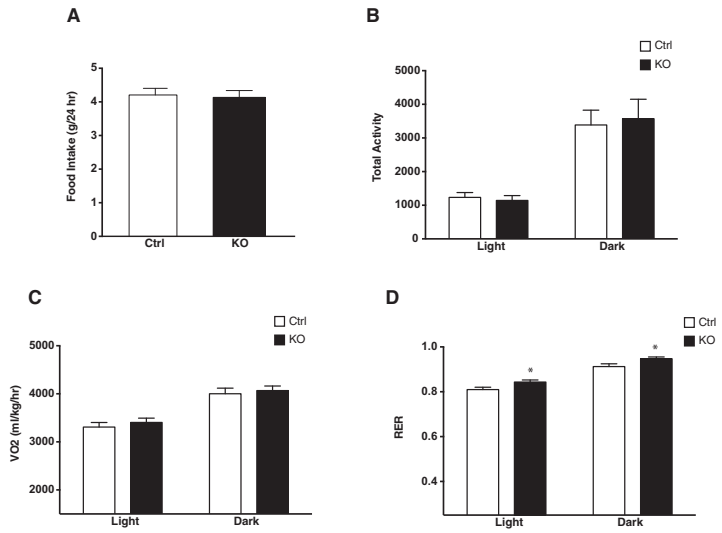

Figure S3. Metabolic Analysis in Adipo-PRDM16 KO Mice, Related to Figure 3

(A) Food intake (g/24 hr).

(B) Activity in day and night.

(C) Oxygen consumption.

(D) Respiratory exchange ratio (RER).

Data are from 10- to 12-week-old, male control and Adipo-PRDM16 KO and mice.

Data are presented as mean ± SEM. *$p < 0.05$.

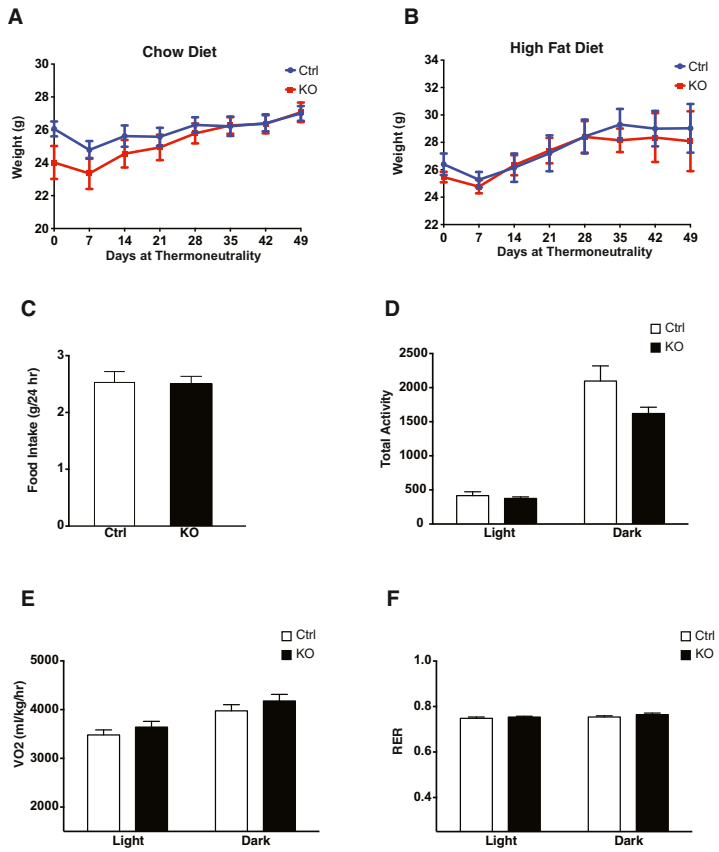

Figure S4. Metabolic Analysis in Adipo-PRDM16 KO Mice at Thermoneutrality or on HFD, Related to Figure 4

(A and B) Weight curves of control and Adipo-PRDM16 KO mice at thermoneutrality and fed either a standard chow (A) or HFD (B). Experiments were done with male mice, 6–8 weeks old at the start of the experiment. n = 4–6 per group.

(C) Food intake (g/24 hr).

(D) Activity in day and night.

(E) Oxygen consumption.

(F) Respiratory exchange ratio (RER).

Data in (C)–(F) are from control and Adipo-PRDM16 KO and mice after 2 weeks on HFD. The experiment was done with male mice, 8 weeks old at the start of the experiment, n = 8 per group.

Data are presented as mean ± SEM. *p < 0.05.

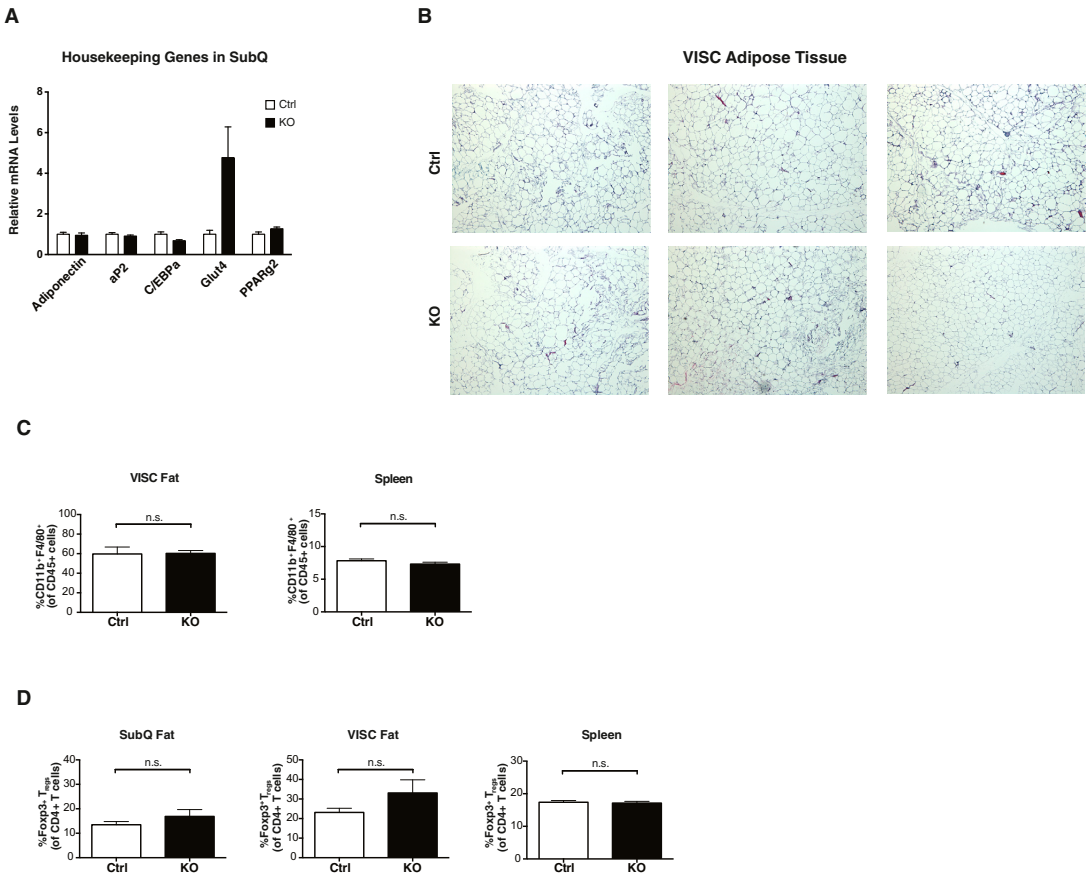

Figure S5. Altered Cell Size and Immune Cell Infiltration in Subcutaneous Adipose Tissue in Adipo-PRDM16 KO Mice, Related to Figure 5

(A) Expression levels of adipocyte differentiation genes in subcutaneous adipose tissue from male control and Adipo-PRDM16 KO mice after 18 weeks on HFD. n = 11 per group.

(B) Cell size in epididymal visceral adipose tissue from Adipo-PRDM16 KO and control mice following 18 weeks on HFD. Representative images from hematoxylin and eosin (H&E) strained sections. Images are shown at 5× magnification.

(C) $CD11b^{+}F4/80^{+}$ macrophages in visceral fat and spleen from high-fat fed control and Adipo-PRDM16 KO mice.

(D) $Foxp3^{+}$ T regulatory cells in subcutaneous and visceral fat and spleen from high-fat fed control and Adipo-PRDM16 KO mice.

For (C) and (D), experiment was done with male mice 8–10 weeks old at start of high-fat feeding, n = 5–6 per group.

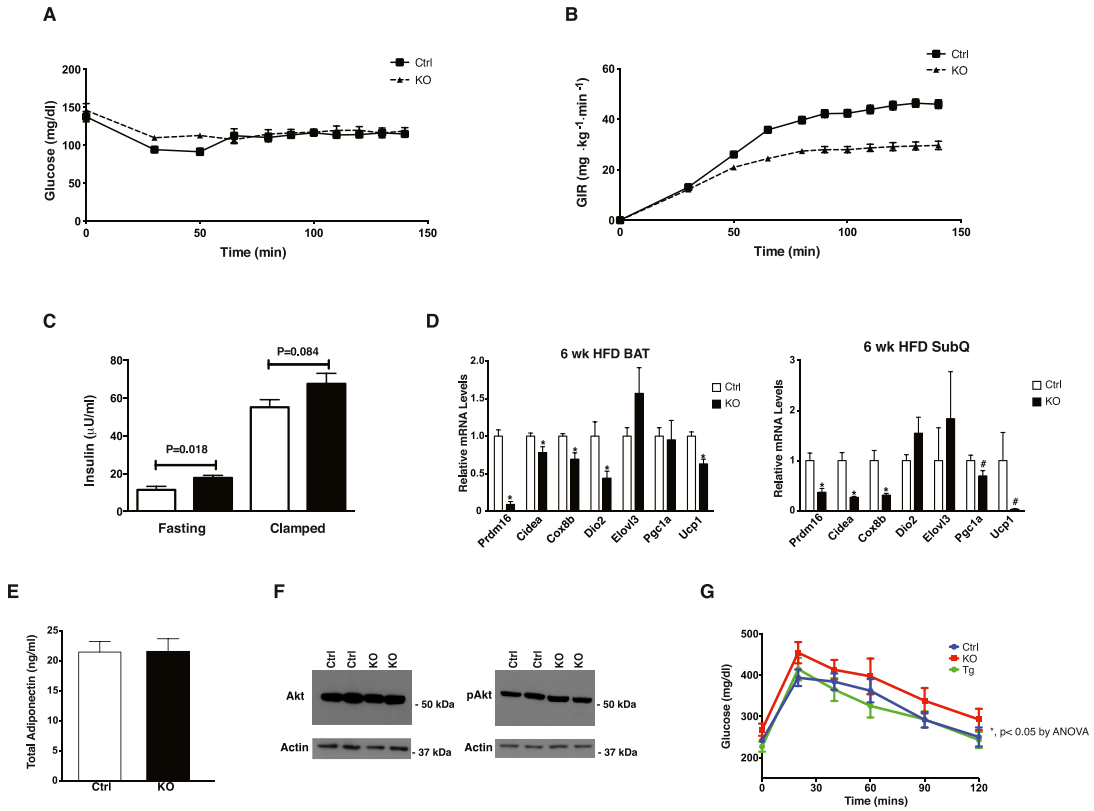

Figure S6. Hyperinsulinemic-Euglycemic Clamp Studies in Adipo-PRDM16 KO Mice, Related to Figure 6

(A) Fasting and clamped glucose values.

(B) Glucose infusion rate.

(C) Fasting and clamped insulin levels.

(D) mRNA expression levels in brown adipose tissue and subcutaneous adipose tissue.

The clamp studies were done with male mice, 8 weeks old at the start of high-fat feeding. n = 7–8 per group.

(E) Total adiponectin levels by ELISA. Levels measured in make mice after 6 weeks on HFD, n = 10 per group.

For (A)–(E), data are presented as mean ± SEM. *p < 0.05. #, 0.06 for *Pgc1a* and 0.10 for *Ucp1*.

(F) Western blot for total and phosphorylated Akt in primary subcutaneous adipocytes.

Data are from control and Adipo-PRDM16 KO primary subcutaneous adipocytes.

(G) Intraperitoneal glucose tolerance test (1.5 mg/kg) in high-fat fed recipients of Adipo-PRDM16 KO, control, or PRDM16 transgenic subcutaneous adipose tissue. The GTT was done 6 weeks following transplantation. n = 5 per group.

Data are presented as mean ± SEM. *p < 0.05 by ANOVA.

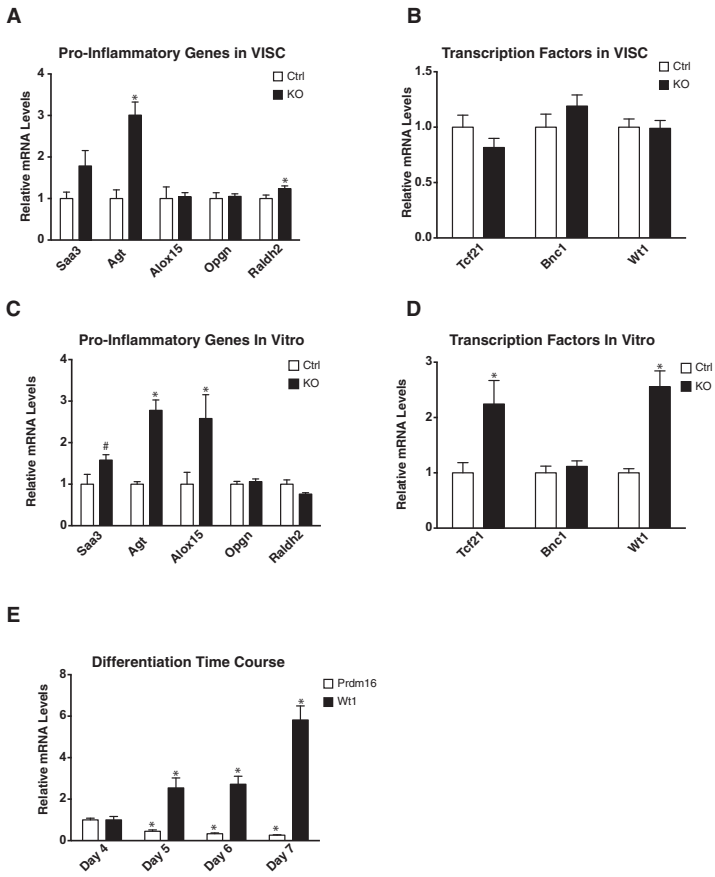

Figure S7. Cell-Autonomous Induction of a Visceral Adipose Tissue Gene Expression Profile in Adipo-PRDM16 KO Subcutaneous Adipocytes, Related to Figure 7

(A) Normalized expression of proinflammatory genes and (B) transcription factors in visceral adipose tissue from high-fat fed control and Adipo-PRDM16 KO mice. Experiments were done in male mice after 18 weeks on HFD. n = 11 per group.

(C) Normalized expression of proinflammatory genes and (D) transcription factors in primary subcutaneous adipocytes differentiated in vitro from control and Adipo-PRDM16 KO mice. n = 3 per group.

(E) Differentiation time course showing PRDM16 and Wt1 mRNA levels in primary subcutaneous adipocytes from control and Adipo-PRDM16 KO mice. *p < 0.05 versus day 4 mRNA expression level.

Data are presented as mean ± SEM. *p < 0.05. # in (C), p = 0.057.

Cell

A Special Population of Regulatory T Cells Potentiates Muscle Repair

Dalia Burzyn,[1] Wilson Kuswanto,[1] Dmitriy Kolodin,[1] Jennifer L. Shadrach,[2,3] Massimiliano Cerletti,[2] Young Jang,[2] Esen Sefik,[1] Tze Guan Tan,[1] Amy J. Wagers,[2,3] Christophe Benoist,[1] and Diane Mathis[1,*]
[1]Microbiology and Immunobiology, Harvard Medical School, Boston, MA 02115, USA
[2]Stem Cell and Regenerative Biology, Harvard University, Cambridge, MA 02138, USA
[3]Howard Hughes Medical Institute, Chevy Chase, MD 20815, USA
*Correspondence: cbdm@hms.harvard.edu
http://dx.doi.org/10.1016/j.cell.2013.10.054

SUMMARY

Long recognized to be potent suppressors of immune responses, Foxp3$^+$CD4$^+$ regulatory T (Treg) cells are being rediscovered as regulators of nonimmunological processes. We describe a phenotypically and functionally distinct population of Treg cells that rapidly accumulated in the acutely injured skeletal muscle of mice, just as invading myeloid-lineage cells switched from a proinflammatory to a proregenerative state. A Treg population of similar phenotype accumulated in muscles of genetically dystrophic mice. Punctual depletion of Treg cells during the repair process prolonged the proinflammatory infiltrate and impaired muscle repair, while treatments that increased or decreased Treg activities diminished or enhanced (respectively) muscle damage in a dystrophy model. Muscle Treg cells expressed the growth factor Amphiregulin, which acted directly on muscle satellite cells in vitro and improved muscle repair in vivo. Thus, Treg cells and their products may provide new therapeutic opportunities for wound repair and muscular dystrophies.

INTRODUCTION

Regulatory T (Treg) cells, particularly those of the Foxp3$^+$CD4$^+$ subset, are critical regulators of immune responses (Josefowicz et al., 2012). They were originally described as controlling the activities of other T cells but were later recognized to regulate B cells and several innate immune system players. There have also been recent reports of Treg cell control over nonimmunological processes. Perhaps the best-characterized example is a unique population of Treg cells residing in the visceral adipose tissue (VAT) and regulating metabolic indices (Feuerer et al., 2009; Cipolletta et al., 2011). The prevalence, transcriptome, and T cell receptor (TCR) repertoire of this population are all distinct from those of their counterparts in lymphoid organs. Surveying a variety of tissues to see whether other nonimmunological processes might be controlled by analogous Treg populations, our attention was drawn to a substantial accumulation of Foxp3$^+$CD4$^+$ T cells in skeletal muscle undergoing repair after acute injury.

Skeletal muscle regeneration follows the same orchestrated plan regardless of the cause of muscle damage. It is driven largely by satellite cells, a pool of quiescent precursors closely associated with muscle fibers (Tabebordbar et al., 2013). In response to injury, these cells become activated, proliferate, differentiate, migrate, and fuse to form new myofibers. This series of events is controlled by the sequential activation and repression of specific transcription factors (Rudnicki et al., 2008). With muscular dystrophies, in which chronic myofiber loss occurs due to genetic defects, the satellite cell pool is called on repeatedly, so it can exhaust or lose function over time, dampening the repair process (Tabebordbar et al., 2013).

Regeneration of skeletal muscle is influenced by inflammatory events that accompany repair (Tidball and Villalta, 2010). Following an early, transient recruitment of neutrophils, myeloid mononuclear cells, mainly derived from a pool of circulating monocytes, infiltrate the injured tissue. Within days, the myeloid infiltrate transitions from a pro- to an anti-inflammatory phenotype, a shift that is critical for proper muscle repair. An initial population of proinflammatory, or M1-type, macrophages is required for clearance of apoptotic or necrotic cells and derivative debris; a subsequent population of anti-inflammatory, or M2-type, macrophages has various proregenerative functions, such as matrix remodeling and promotion of angiogenesis. Ablation or impaired recruitment of macrophages severely compromises muscle repair.

Though far less markedly, lymphocytes also accumulate in skeletal muscle after acute injury, as well as in the dystrophin-deficient muscles of mice harboring the mdx mutation or humans with Duchenne muscular dystrophy (DMD) (Tidball and Villalta, 2010). Their function has not been well studied, although both CD4$^+$ and CD8$^+$ T cells seem to promote the mdx pathology. Even less is known about the composition and function of infiltrating T cell populations in models of acute muscle injury. In particular, the contribution of Treg cells is yet to be addressed.

Here, we uncover a unique population of CD4$^+$Foxp3$^+$ Treg cells that accumulates in skeletal muscle shortly after acute

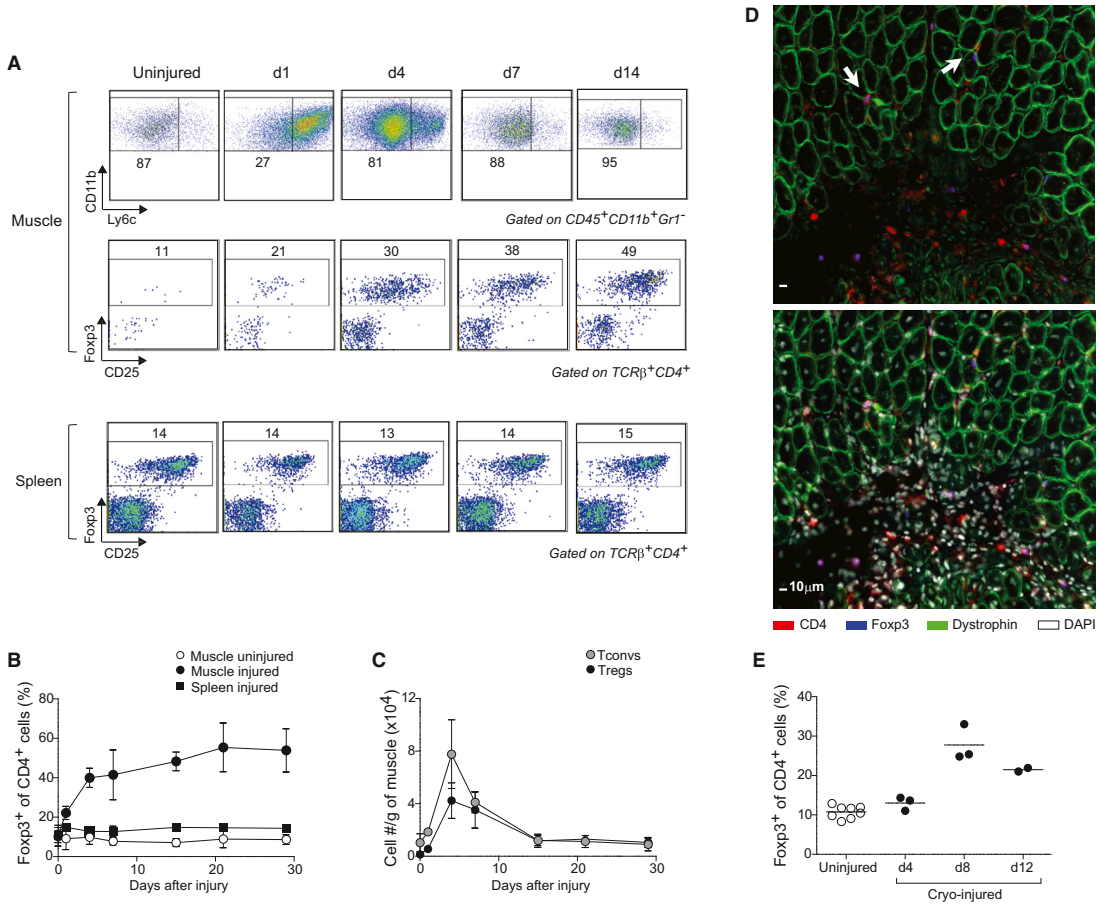

Figure 1. Treg Accumulation at the Site of Injury

(A–C) Cytofluorometric analyses of hindlimb muscle infiltrates after Ctx injury. (A) Top: Ly6c expression by $CD11b^+$ cells. Middle and bottom: Foxp3 expression by $CD4^+$ cells. Numbers depict % of gated cells. Representative of three experiments. (B and C) Summary data on fraction and number of cells. Mean ± SD ($n \geq 4$).

(D) Immunofluorescence microscopy of muscle sections 7 days after injury. The same section without (top) or with (bottom) DAPI. Arrows show Tregs in close contact with regenerating myofibers. Original magnification ×400.

(E) As in (B), but after cryoinjury.

See also Figure S1.

injury. We address the impact of this population on muscle repair, its implication in genetically determined muscle aberrancies, and the potential therapeutic effects of modulating this population and one of the proregenerative factors it produces.

RESULTS

Treg Cells Accumulate in Acutely Injured Skeletal Muscle Just as the Myeloid Cell Infiltrate Switches from a Proinflammatory to a Proregenerative Phenotype

Intramuscular (i.m.) administration of cardiotoxin (Ctx), which rapidly induces myofiber necrosis, provides a convenient and well-studied model of tissue repair after acute injury. We injected the tibialis anterior (TA), gastrocnemius, and quadriceps muscles of C57Bl/6 (B6) mice with Ctx and analyzed the resulting cellular infiltrate various times later; control cells isolated from the uninjured contralateral muscles or the spleen were evaluated in parallel. As anticipated (Arnold et al., 2007), there was a rapid increase in $CD11b^+Gr1^-$ myeloid mononuclear cells beginning before day 1, initially a proinflammatory $Ly6c^{hi}$ population but switching to an anti-inflammatory $Ly6c^{lo}$ population by day 4 (Figure 1A, top). Around this time, Treg cells began to accumulate in the injured muscle, their frequency within the $CD4^+$ T cell compartment gradually increasing to ~50% by 14 days

after Ctx injection and remaining at that level until at least day 30 (Figures 1A, middle, and 1B). Numbers of Treg and conventional $CD4^+$ T (Tconv) cells both peaked at day 4 after injury (Figure 1C), mirroring the total number of $CD45^+$ cells and T cells in the infiltrate (Figure S1 available online). However, while Tconv cell numbers had dropped to levels characteristic of uninjured muscle by 28 days after Ctx injection, the number of Treg cells remained elevated by 8-fold ($1.05 \pm 0.38 \times 10^4$ versus $0.13 \pm 0.06 \times 10^4$ cells/g muscle; $p = 0.01$; Figure 1C). Staining of frozen sections with a fluorescently tagged anti-Foxp3 monoclonal antibody (mAb) revealed $Foxp3^+$ cells both in heavily infiltrated (probably necrotic) areas and in regions between regenerating fibers (recognizable as centrally nucleated, dystrophin-positive cells) (Figure 1D). An analogous accumulation of Treg cells was observed in a cryoinjury model (Figure 1E).

The Transcriptome of Muscle Treg Cells Is Distinct from that of Other Treg Populations, Especially Those Located in Lymphoid Organs

Four or 14 days after i.m. Ctx injection, we isolated Treg and Tconv cells from muscles and lymphoid organs and performed microarray-based gene-expression profiling. (Note that inadequate numbers precluded a comparison with analogous populations from uninjured muscles.) According to both simple comparison plots (Figure 2A) and principal components analysis (PCA) (Figure 2B), the transcriptome of muscle Treg cells differed from that of their spleen or lymph node counterparts much more than the latter two did from each other. Muscle Tregs were most like Treg cells located in adipose tissue (Figure 2B) but were still readily distinguishable; a few hundred transcripts up- or downregulated >2-fold in one vis-à-vis the other. The similarity to another Treg population residing in nonlymphoid tissue, and dissimilarity to lymphoid-organ Treg cells, did not simply reflect a higher activation state in tissues, because few of the distinguishing transcripts were members of a previously determined Treg activation signature (Hill et al., 2007) (Figure 2C). Neither did it reflect a universal "inflammation signature," since the muscle Treg transcriptome was distinguishable from those of Tregs at several inflamed sites (Figure S2). While exhibiting a distinct gene-expression profile, muscle Treg cells are clearly "Treg," showing the anticipated pattern of expression of 91% of the canonical Treg signature (Hill et al., 2007); in particular, elevated levels of diagnostic transcripts such as those encoding Foxp3, CD25, and CTLA-4 (Figure 2D).

A fold-change/fold-change (FC/FC) plot afforded a more detailed look at the muscle Treg transcriptome, revealing a set of genes (highlighted in orange) that distinguish muscle Treg from spleen Treg cells and spleen or muscle Tconv cells, and another set (in gray) overexpressed by the two muscle populations vis-à-vis their two spleen counterparts (Figure 2E; Table S1). The first group includes loci encoding an anti-inflammatory cytokine (interleukin [IL]-10), chemokine receptors (e.g., CCR1), and two well-known growth factors (platelet-derived growth factor [PDGF] and Amphiregulin [Areg]) (Pastore et al., 2008). Loci upregulated in both Treg and Tconv cells from injured muscle include those encoding KLRG1, an activation marker; CCR2, important for the recruitment of various leukocyte populations to injured muscle (Warren et al., 2005); and ST2 (encoded by *Il1rl1*), which is the receptor for the "alarmin" IL-33 (Schmitz et al., 2005). A third group of genes (in pink) was repressed in muscle Treg (and to varying degrees Tconv) cells; notably, those encoding certain chemokine receptors (CXCR5 and CCR7) and several proteins implicated in the Wnt signaling pathway (TCF7, LEF1, SATB1).

We selected several of the genes upregulated in muscle Treg cells and confirmed their induced expression at the protein level by flow cytometry (Figure 2F). Such an analysis also revealed muscle Tregs to be high-level expressors of Helios and Neuropilin (Figure 2G) and were therefore likely to be Treg cells exported as such from the thymus.

Treg Cells in Injured Muscle Are Clonally Expanded and Display a Unique Repertoire of TCRs

The rapid accumulation of Treg cells at the injury site could reflect their influx, proliferation, or some combination of the two. Four days after Ctx injection, almost all muscle Treg cells stained for Ki67 (Figure 3A), which is expressed in all stages of the cell cycle except for the resting, G_0, phase. EdU (5-ethynyl-2′-deoxyuridine), incorporated by cells in S phase, was detected in 20% of muscle Tregs after 24 hr of labeling (Figure 3B). A much lower fraction of splenic Treg cells was proliferating according to both staining criteria. The muscle Tconv population also exhibited an increased frequency of $Ki67^+$ and EdU^+ cells compared with the spleen Tconv subset, although the values remained significantly lower than those observed for muscle Treg cells (Figures 3A and 3B).

To assess clonality of the Treg population expanding in acutely injured skeletal muscle, we studied TCR repertoires by sequencing the complementarity-determining region (CDR) 3 of the TCR α and TCR β chains of individually sorted cells. Already at day 2 after injury, and continuing out at least until day 8, a substantial proportion (20%–40%) of muscle Treg cells were clonally expanded (Figures 3C and 3D; Table S2). This sequence profile contrasted starkly with that of splenic Treg cells, for which there was not one repeat sequence in the 692 sampled. As expected from the Ki67 and EdU stainings, we also found clonal expansion of muscle Tconv cells (Figure 3D; Table S2). However, there was not a single example of TCR-sequence sharing between muscle Treg and Tconv cells.

In the muscle Treg data sets, there was a striking case of a repeatedly detected TCR: identical paired CDR3 α and β (and corresponding nucleotide) sequences picked up in multiple mice in completely independent experiments (Figure 3E). Interestingly, there were a few Treg cells (from multiple individuals) that had the same TCR β chain paired with an α chain whose CDR3 was modified only conservatively (AV → VL). These repeat sequences were found in mice 2 or 4, but not 8, days postinjury. They never showed up in the bulk spleen Treg or muscle Tconv cell pools.

Ablation of Treg Cells Compromises Muscle Repair According to Multiple Criteria

Having uncovered a unique population of Treg cells in the infiltrates of skeletal muscle undergoing repair in response to acute injury, we asked whether they play a role in muscle regeneration. We punctually ablated Treg cells at the time of muscle injury,

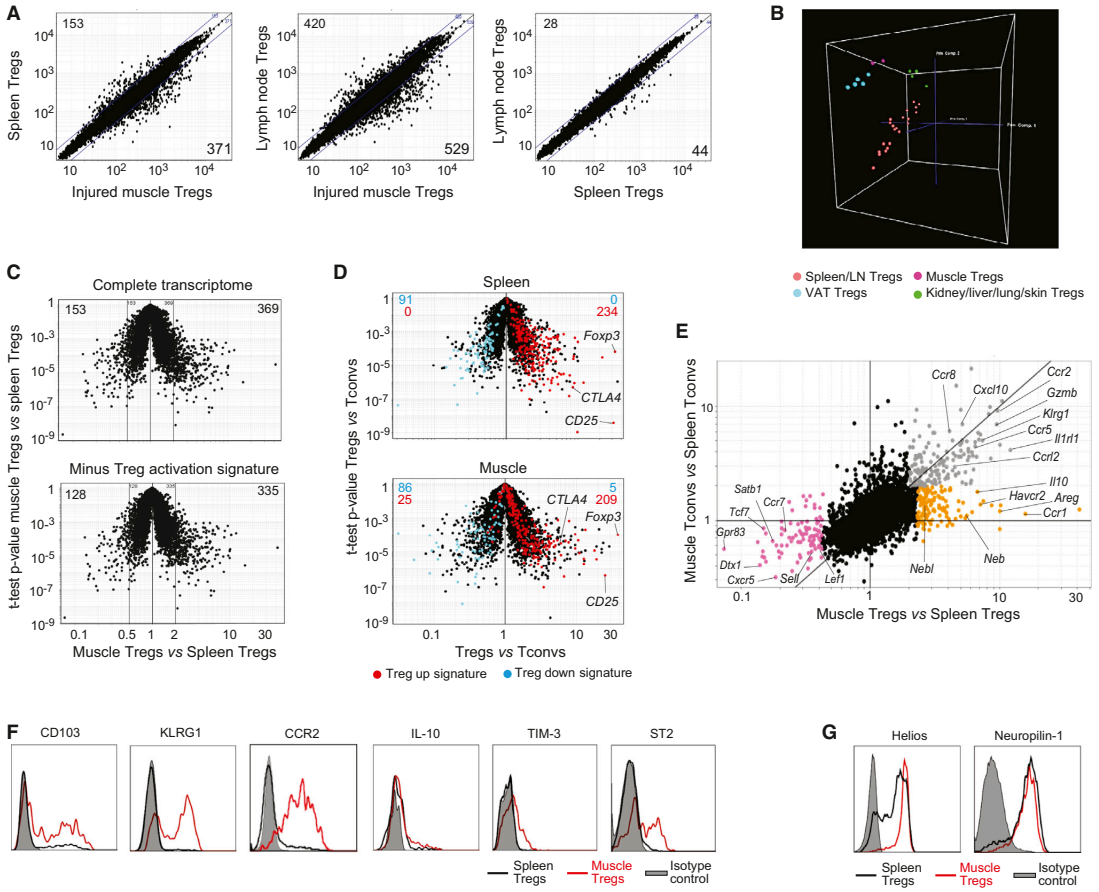

Figure 2. A Unique Population

(A–E) Gene-expression analyses on cells 14 days after Ctx injury. (A) Comparison plots of normalized expression values. Numbers indicate the number of genes whose expression differed by more than 2-fold. (B) PCA analysis comparing muscle Tregs 4 or 14 days after Ctx injury with other Treg populations. Each dot represents the mean of three independent experiments. (C) Top: volcano plot comparing gene expression of muscle versus spleen Tregs. Bottom: same plot after subtraction of the Treg activation signature (Hill et al., 2007). Numbers represent the number of differentially expressed genes (>2-fold). (D) Volcano plots comparing gene expression of Treg versus Tconv cells. Treg signature genes (Hill et al., 2007) are highlighted in red (induced) or blue (repressed). Numbers represent the number of genes from each signature expressed by each population. (E) Fold-change differences in gene expression between Treg and Tconv cells from muscle and spleen. Differentially expressed genes are highlighted in orange, gray, or pink.

(F and G) Cytofluorometric analyses of surface and intracellular markers. Histograms depict expression by Foxp3$^+$ T cells from muscle (red) or spleen (black). Gray: isotype control.

See also Figure S2 and Table S1.

exploiting a mouse line wherein the diphtheria toxin receptor (DTR) is expressed under the control of *Foxp3* regulatory elements (Kim et al., 2007). B6.Foxp3-DTR$^+$ and B6.Foxp3-DTR$^-$ littermates (hereafter referred to as DTR$^+$ and DTR$^-$, respectively) were given DT intraperitoneally (i.p.) starting from the time of im Ctx injection and were analyzed 1 week later, a time chosen to avoid the multiorgan autoimmunity provoked by long-term ablation of Treg cells (Kim et al., 2007). This protocol resulted in effective depletion of Tregs in the injured muscle of the DTR$^+$ mice (Figure 4A, top) as well as in the lymphoid organs (Figure 4A, bottom).

According to multiple criteria, the loss of Treg cells had profound effects on the muscle repair process. First, the size of the cellular infiltrate was increased in the absence of Treg cells, assessed either as numbers of total CD45$^+$ cells or as the fraction of T cells (Figure S3A). In addition, the myeloid cell compartment failed to undergo the expected switch from a primarily proinflammatory, Ly6c^{hi} to a primarily anti-inflammatory,

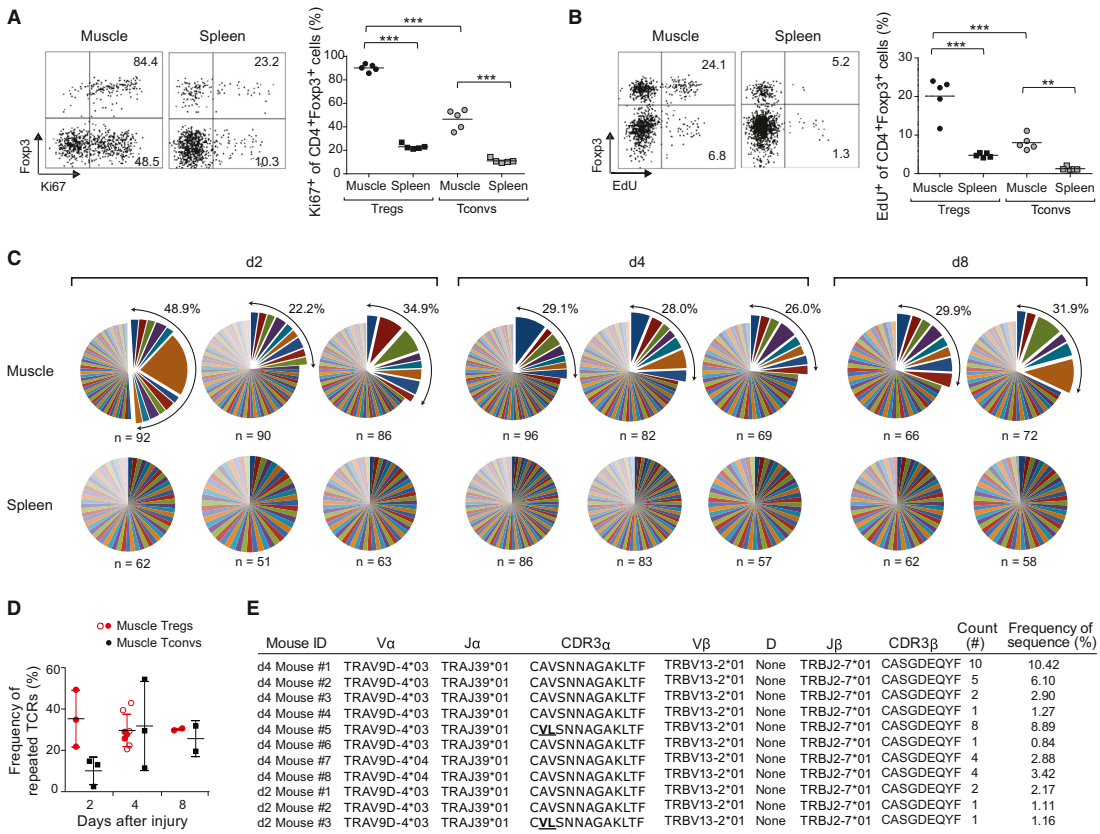

E

Mouse ID	Vα	Jα	CDR3α	Vβ	D	Jβ	CDR3β	Count (#)	Frequency of sequence (%)
d4 Mouse #1	TRAV9D-4*03	TRAJ39*01	CAVSNNAGAKLTF	TRBV13-2*01	None	TRBJ2-7*01	CASGDEQYF	10	10.42
d4 Mouse #2	TRAV9D-4*03	TRAJ39*01	CAVSNNAGAKLTF	TRBV13-2*01	None	TRBJ2-7*01	CASGDEQYF	5	6.10
d4 Mouse #3	TRAV9D-4*03	TRAJ39*01	CAVSNNAGAKLTF	TRBV13-2*01	None	TRBJ2-7*01	CASGDEQYF	2	2.90
d4 Mouse #4	TRAV9D-4*03	TRAJ39*01	CAVSNNAGAKLTF	TRBV13-2*01	None	TRBJ2-7*01	CASGDEQYF	1	1.27
d4 Mouse #5	TRAV9D-4*03	TRAJ39*01	C**VL**SNNAGAKLTF	TRBV13-2*01	None	TRBJ2-7*01	CASGDEQYF	8	8.89
d4 Mouse #6	TRAV9D-4*03	TRAJ39*01	CAVSNNAGAKLTF	TRBV13-2*01	None	TRBJ2-7*01	CASGDEQYF	1	0.84
d4 Mouse #7	TRAV9D-4*04	TRAJ39*01	CAVSNNAGAKLTF	TRBV13-2*01	None	TRBJ2-7*01	CASGDEQYF	4	2.88
d4 Mouse #8	TRAV9D-4*04	TRAJ39*01	CAVSNNAGAKLTF	TRBV13-2*01	None	TRBJ2-7*01	CASGDEQYF	4	3.42
d2 Mouse #1	TRAV9D-4*03	TRAJ39*01	CAVSNNAGAKLTF	TRBV13-2*01	None	TRBJ2-7*01	CASGDEQYF	2	2.17
d2 Mouse #2	TRAV9D-4*03	TRAJ39*01	CAVSNNAGAKLTF	TRBV13-2*01	None	TRBJ2-7*01	CASGDEQYF	1	1.11
d2 Mouse #3	TRAV9D-4*03	TRAJ39*01	C**VL**SNNAGAKLTF	TRBV13-2*01	None	TRBJ2-7*01	CASGDEQYF	1	1.16

Figure 3. Clonal Expansion of the Treg Population at the Injury Site

(A and B) Ki67 expression (A) and EdU uptake (B) 4 days after Ctx-induced injury. Left: representative dot plots of cells. Numbers refer to % marker$^+$ Treg or Tconv cells. Right: summary plots. n = 5; $^{**}p < 0.01$; $^{***}p < 0.001$.

(C) TCR CDR3 α and CDR3 β sequences for individual cells. Each pie chart represents a single mouse. n, number of analyzed sequences per mouse. Total frequency of expanded clones shown at the top right.

(D) Summary of clonal TCR frequencies over time. Open circles correspond to mice analyzed later in independent experiments for Figure 7. Mean ± SD (n ≥ 3).

(E) Identical paired CDR3-α and β sequences found in multiple individuals in independent experiments. Two CDR3 α sequences from independent mice bear two conserved substitutions.

See also Table S2.

Ly6c^{lo} phenotype (Figures 4B and S3A). Similar results were obtained when DT was administered i.m., which specifically depleted muscle Treg cells without detectably affecting their counterparts in lymphoid organs (data not shown).

DTR-mediated in vivo ablation of a designated cell population is known to be apoptotic and noninflammatory (Bennett and Clausen, 2007). Nonetheless, as detailed in Figure S3B and its legend, we performed an experiment on female heterozygous DTR-positive mice to show that the more inflammatory flavor of the infiltrate in mice lacking Treg cells was not a simple artifact related to their death, but rather a reflection of their functional absence.

Second, Treg cell ablation altered the histological features of skeletal muscle repair (Figure 4C). Although centrally nucleated fibers indicative of regeneration could be detected in muscle from both DTR$^-$ and DTR$^+$ mice, in the latter case, the tissue structure showed a disorganized pattern, with several foci of inflammation. As anticipated, no infiltrate or regenerating fibers were found in the contralateral, uninjured muscles from mice that did or did not have Treg cells (data not shown). One of the later consequences of impaired muscle repair is fibrosis: Gomori's Trichrome staining showed Treg-less mice to have a substantial accumulation of collagen in the injured muscle compared with their Treg-positive littermates (Figure 4D). To provide a more quantitative view, we returned to the cryo-injury model, wherein the area of injury is clearly delimited. Global examination confirmed the impaired reparative capacity in Treg depleted mice; a quantitative evaluation indicated that the

number of centrally nucleated fibers was significantly lower in Treg-depleted than in normal muscles, with some muscles from DTR$^+$ mice showing an almost complete absence of regenerative fibers (Figure 4E).

Third, the absence of Treg cells during muscle repair had an impact on muscle progenitor cells. Satellite cells are the predominant, if not sole, source of regenerated muscle fibers after acute injury (Tabebordbar et al., 2013). Satellite cells were isolated from uninjured or Ctx-injured muscle of DT-treated DTR$^+$ or DTR$^-$ mice by double-sorting CD45$^-$Sca-1$^-$Mac-1$^-$CXCR4$^+$ β1-integrin$^+$ myofiber-associated cells (Cerletti et al., 2008), and their functionality was evaluated in clonal myogenesis assays, as described in (Cerletti et al., 2012) (Figure 4F). Injury substantially enhanced the fraction of satellite cells from DTR$^-$ mice that formed myogenic colonies; in contrast, there was far less (not significant) injury-induced enhancement of myogenic activity in mice lacking Treg cells.

Fourth, to obtain a broad, unbiased view of the repair pathways impacted by Treg ablation, we performed microarray-based gene-expression profiling of whole, unfractionated muscle tissue. In general, for standard (DTR$^-$) mice, sets of genes were up- or downregulated early after injury (day 4), and expression values began to return to normal as the wound started to repair (day 8). The pattern of expression of many genes was altered in the absence of Treg cells (DTR$^+$) (Figures 4G, S3C, and S3D; Table S3), with three main clusters meriting discussion: One group (highlighted in blue) is composed of genes encoding proteins with important roles in muscle homeostasis and function. These loci were highly expressed in uninjured muscle and were downregulated in both DTR$^-$ and DTR$^+$ mice at day 4 after injury owing to the loss of mature muscle fibers. In muscle of DTR$^-$ mice, transcript levels began to increase by day 8, as efficient repair ensued; however, in muscle of DTR$^+$ individuals, expression of these loci remained low or in decline at day 8, confirming that the lack of Treg cells compromised the recovery of muscle homeostasis after injury. Another group (green) includes genes encoding proteins necessary for muscle repair, like MyoG (myogenin) and Mmp12 (metallopeptidase-12), but also some factors related to the immune response, in particular a number of chemokines and chemokine receptors, some cytokine receptors, and C1qa, a complement cascade trigger. In DTR$^-$ mice, expression of these loci was increased at day 4 but rapidly crashed thereafter, approaching the level in muscles of uninjured mice by day 8. However, in DTR$^+$ mice, this drop did not occur or was greatly attenuated, again suggesting an ineffective and prolonged repair process, especially given the recent report that C1qa and related molecules strongly inhibit muscle regeneration (Naito et al., 2012). Strikingly, the expression pattern of C1qa in injured muscle was mirrored by that of C1qb, C1qc, C1r, C1rb, and C1s as well (Figure S3D). A final group (highlighted in red) is composed of two types of genes: those encoding molecules characteristic of immune cells (e.g., CD8a, CD2) and those specifying matrix proteins (e.g., Col6a5). Expression of these loci was upregulated at day 4 and even more so at day 8 only in mice lacking Treg cells, reflecting their more pronounced muscle infiltrate (Figure S3A) and fibrotic collagen deposition. Microarray expression values for multiple examples of each of these groups are plotted in Figures 4G and S3D, and confirmatory quantitative PCR data for representative group members are presented in Figure S3C. Monitoring expression of these groups of genes should provide a novel and convenient means to quantitatively assess the fidelity of events underlying muscle repair.

As illustrated in Figures S3E and S3F, Rag-deficient mice, lacking all lymphoid cells, showed more pronounced fibrosis than did wild-type individuals, measured histologically or by quantifying collagen transcripts. However, fibrosis was milder and repair progressed more effectively in Rag-1-deficient mice than in Treg-depleted mice.

In summary, evaluations of myeloid cell numbers and phenotype, histology, satellite cell function, and global patterns of gene expression all argue that Treg cells are important for effective repair after acute injury of skeletal muscle. These observations raise the question of whether Treg cells impact muscle aberrancies in other contexts.

An Analogous Treg Population Is Expanded in the Damaged Muscles of Mouse Models of Muscular Dystrophy

In muscular dystrophies, chronic destruction of muscle fibers is accompanied by an inflammatory response and, in general, a permanent infiltrate. Mdx mice carry a nonsense mutation in the *Dmd* gene (encoding Dystrophin), which is analogous to those found in DMD patients. In the mouse model, as in the human disease, the most affected sites are the diaphragm and hindlimb muscles. We analyzed the muscle infiltrate in 4-week-old mdx mice, when the disease is in its acute phase, and at 12 weeks, during the chronic phase. In both muscle groups at both ages, the fraction of Treg cells was significantly elevated vis-à-vis the frequency in corresponding muscles of wild-type mice; such an increase was not observed in the spleen (Figure 5A). Likewise, the muscle infiltrates of Dysferlin-deficient mice, which model limb-girdle muscular dystrophy type 2B or Miyoshi myopathy (Tabebordbar et al., 2013), were enriched in Treg cells, while their frequency in the spleen was the same as in wild-type controls (Figure S4A).

That the Treg cells accumulating in dystrophic muscle of mdx mice were bona fide muscle Tregs was indicated by their elevated expression of phenotypic markers such as Areg, ST2, KLRG1, and TIM-3 (Figure S4B). (Unfortunately, we could not isolate adequate numbers of Treg cells from the muscles of mdx mice to perform a transcriptome analysis [<500 Tregs/mouse].) In addition, the Treg populations of mdx muscle exhibited clonal expansions, with an even greater fraction of the population derived from expanded clones and an even larger average clone size than found for Ctx-injured muscles of wild-type mice (compare Figures 5B and 3C; also see Table S2).

Next, we performed loss- and gain-of-function studies to evaluate the role(s) of muscle Treg cells in mdx mice. It was not feasible to use the B6.Foxp3-DTR system for the loss-of-function experiments because both the *Foxp3* and *Dmd* genes are located on the X chromosome. Therefore, we manipulated levels of Treg cells by treatment with an anti-CD25 mAb, an approach that has been exploited by a number of investigators to study Treg function (e.g., Suvas et al., 2004). Administration

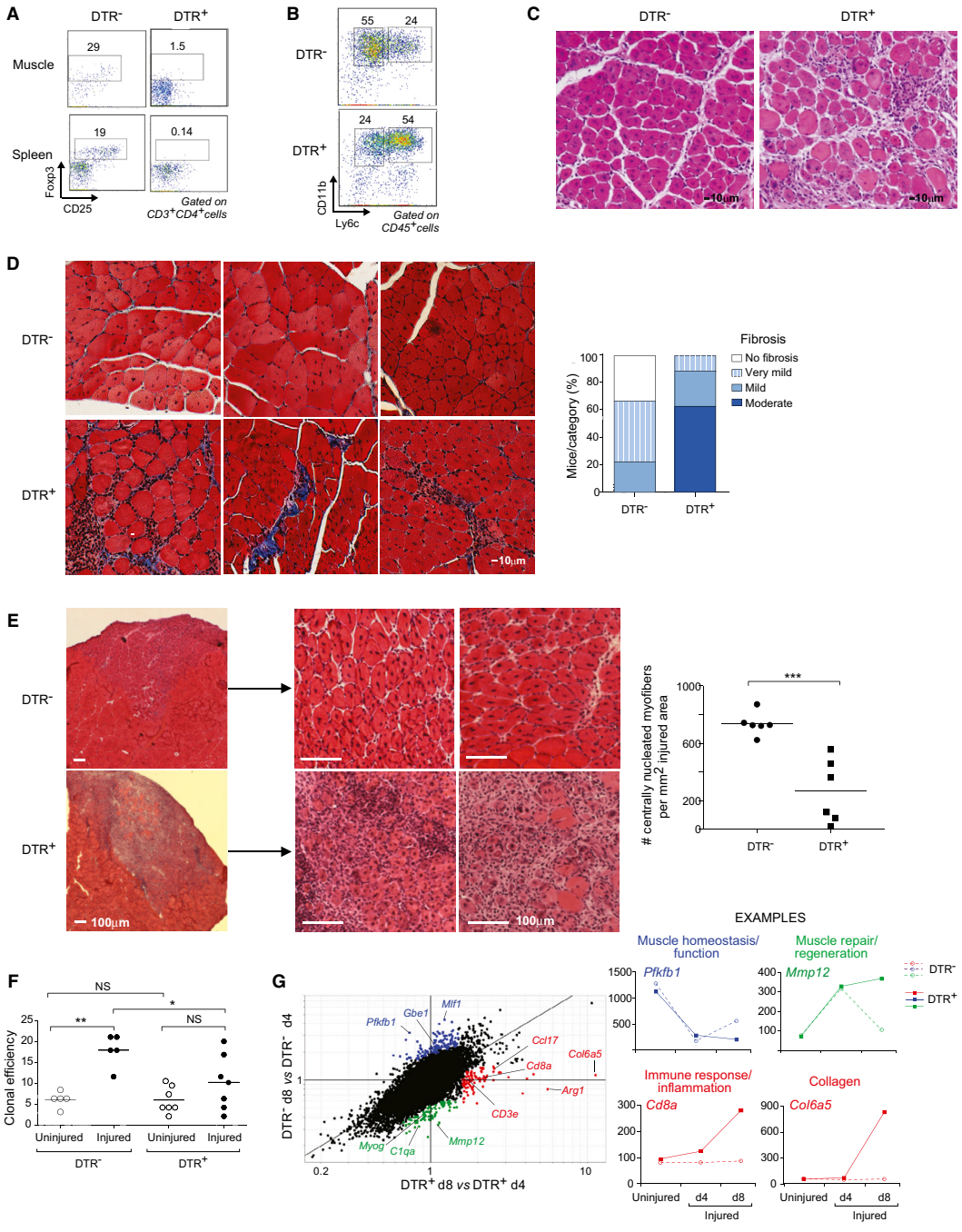

(legend on next page)

of anti-CD25 to 2.5-week-old mdx mice did not reduce overall Treg cell numbers, whether in skeletal muscle or the spleen, but did largely eliminate the fraction expressing high levels of CD25 (Figure 5C). This change was accompanied by a significant increase in serum levels of creatine kinase (CK), an enzyme released into the blood upon muscle damage and a standard indicator of muscle damage in dystrophic mouse models.

For the gain-of-function experiments, we made use of the published observation that complexes of recombinant IL-2 and a particular anti-IL-2 mAb (clone JES6-1A12) can preferentially expand Treg populations after injection into mice (Boyman et al., 2006). A few days before the peak of acute disease (3 weeks of age), we administered IL-2:JES6-1A12 complexes to mdx mice for 6 consecutive days. As anticipated, this treatment induced a significant increase in the frequency of Treg cells in the muscle, which, in addition, displayed higher levels of CD25 (Figure 5D, bottom). An elevated fraction of Treg cells was also observed in the spleen immediately after the cessation of treatment (14% and 42% of $CD4^+$ cells in control and complex-administered mice, respectively; data not shown), but this increase was not sustained (Figure 5D, top). Accompanying the boost in Treg cells was a significant reduction in serum CK levels (Figure 5D), indicative of less muscle damage.

To gain further insight into the effects of Treg depletion in dystrophic muscle, we performed whole-muscle transcriptional analyses, comparing muscles from control and Treg-depleted mdx mice (Figure S4C). The genes encoding osteopontin (*Spp1*; 2.1-fold) and connective-tissue growth factor (*Ctgf*; 1.8-fold), both of which promote skeletal muscle fibrosis and mdx pathology (Morales et al., 2011; Vetrone et al., 2009), were upregulated in the absence of Tregs. More generally, it became clear that, on the one hand, Treg cells were protecting mdx mice from muscle pathology, as their ablation downregulated most of the aforementioned gene set related to muscle homeostasis and function (highly expressed in healthy wild-type muscle), but that, on the other hand, Treg cells were promoting muscle repair because their removal upregulated expression of the set of genes whose inhibition was normally an accompaniment to healthy repair (Figure S4C). (In addition, there was a striking correspondence between the genes induced in muscle from Treg-ablated mdx mice and those repressed in muscle from amphiregulin-treated mice [discussed below].)

Amphiregulin, a Growth Factor Overexpressed by Muscle Treg Cells, Enhances Muscle Regeneration

The regulation that muscle Treg cells imposed on infiltrating myeloid cells was probably responsible, at least in part, for the impaired muscle repair observed in the absence of Tregs. However, analogous to the situation with VAT (Feuerer et al., 2009; Cipolletta et al., 2012), it is likely that other mechanisms also play a role, including a direct effect of muscle Tregs on muscle progenitors, nascent myofibers, or other nonhematopoietic cell types within muscle. Among the transcripts preferentially expressed by muscle Tregs vis-à-vis lymphoid-organ Tregs, *Areg* stood out as encoding a candidate factor capable of directly impacting muscle regeneration. Areg belongs to the epithelial growth factor (EGF) family and signals through the EGF receptor (EGFR) system (Shoyab et al., 1989). EGFR is expressed by a variety of cells, including muscle satellite cells and a myoblast cell line, in which it appears to have antiapoptotic/survival functions (Golding et al., 2007; Horikawa et al., 1999). Examination of the ImmGen database (http://www.immgen.org) indicated that most hematopoietic cell-types express no or only low levels of *Areg* transcripts (Figure 6A). Nor is *Areg* expressed at significant levels in the nonhematopoietic cell-types examined by ImmGen (Figure S5A). In addition, the base-line levels of *Areg* transcripts in injured or uninjured whole-muscle samples, wherein muscle-lineage cells were in great preponderance, argues that muscle cells do not make significant Areg in this context either (Figure S5A). However, *Areg* transcripts were readily detectable in a few Treg populations. They were found at high levels in muscle and adipose-tissue Treg cells, although hardly, if at all, in lymphoid-organ Tregs. Substantial expression of Areg protein in muscle Tregs, but only limited expression by their splenic counterparts, was confirmed by flow cytometry (Figure 6B). The fraction of muscle Treg cells expressing Areg protein began to increase at day 4 and peaked at day 7 after Ctx injury (Figure S5B).

If Areg is important for the proregenerative function of muscle Treg cells, then treatment of Treg-ablated mice with this growth factor should ameliorate their deficit in muscle repair subsequent to acute injury. To test this notion, we administered Areg to Ctx-injected, DT-treated DTR^+ mice according to the protocol illustrated in Figure 6C, and evaluated gene-expression profiles of repairing muscles at days 4 and 8 after injury. (Note that the initial Areg injection was done i.m., promoting the muscle specificity of its effects.) Transcriptome changes were evaluated in terms of the three gene clusters defined in Figure 4G and

Figure 4. Treg Ablation Impairs Muscle Regeneration after Wounding

Eight-week-old $Foxp3^-DTR^+$ or DTR^- littermates were injured with Ctx and treated with DT to induce Treg depletion.

(A and B) Flow cytometry of Treg and myeloid-lineage population, 7 days postinjury. Numbers in (A) refer to % $CD4^+$ T cells that are $Foxp3^+$, and numbers in (B) refer to % $Ly6c^{-/lo}$ or $Ly6c^{hi}$ of $CD11b^+$ cells.

(C) Hematoxylin and eosin (H&E) staining of muscle sections 7 days after Ctx injury. Representative of at least three experiments. Original magnification ×100.

(D) Left: fibrosis detection by Gomori trichrome staining of muscle sections 13 days after injury. Collagen stained in blue. Representative examples of seven DTR^+ and seven DTR^- mice. Original magnification ×200. Right: summary quantification.

(E) Left: H&E staining of muscle sections 7 days after cryoinjury. Original magnification ×25 (left) and ×100 (middle and right). Representative examples of six samples. Right: quantification of regenerative fibers per mm^2 of injured area. ***$p < 0.001$.

(F) Clonal myogenesis assays of satellite cells from uninjured or day 4 Ctx-injured muscles. Percent of wells seeded that showed a myogenic colony at day 5. Summary of six clonal assays *$p < 0.05$; **$p < 0.01$.

(G) Left: FC/FC plot of gene expression values in muscle 4 versus 8 days after Ctx-induced injury in mice without (DTR^+) or with (DTR^-) Tregs. Highlighted in different colors are sets of genes described in the text. Right, representative examples of genes in each highlighted set.

See also Figure S3 and Table S3.

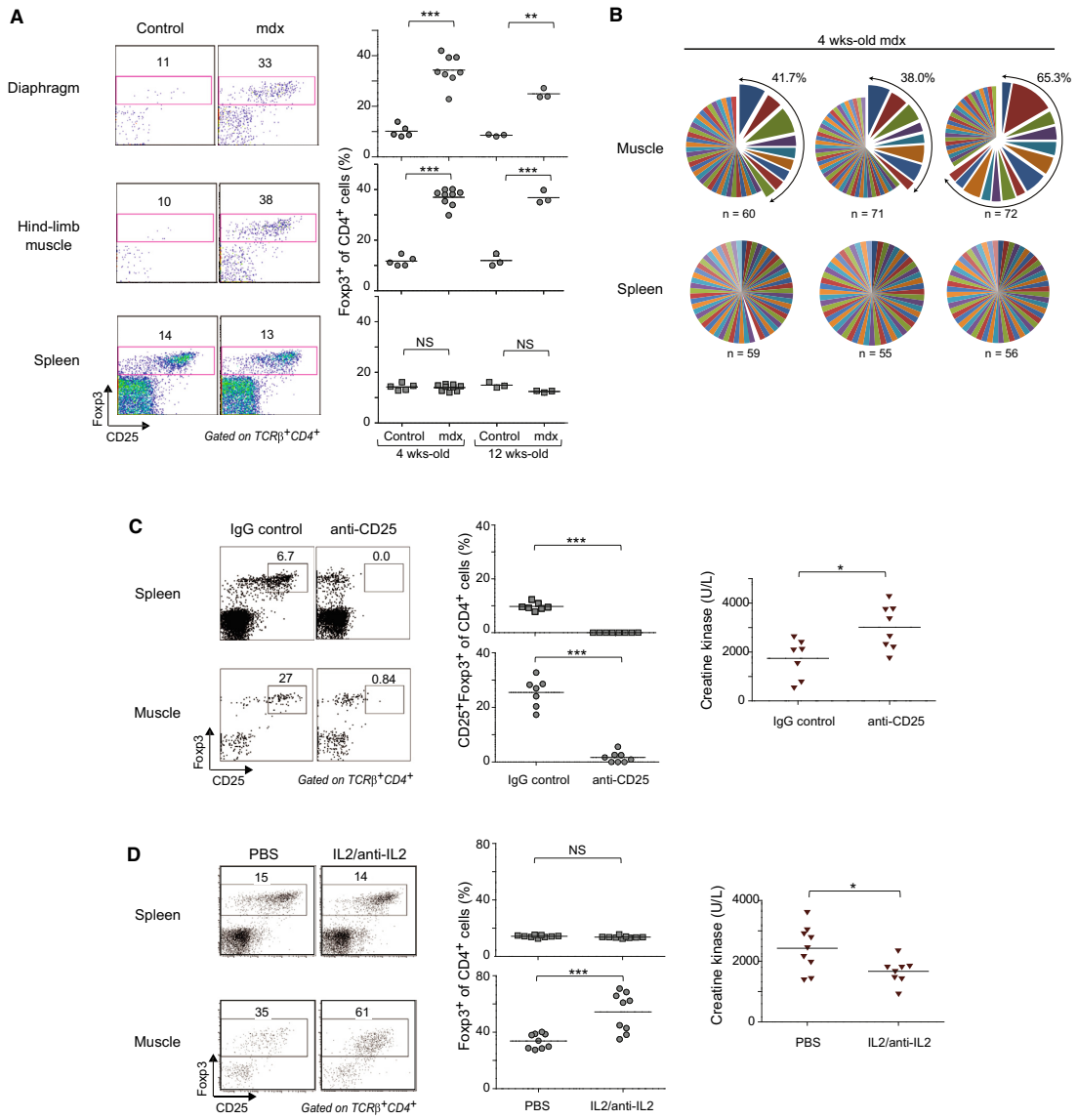

Figure 5. Treg Cells Are Enriched in Muscles of Dystrophic Mice and Impact Muscle Damage

(A) Frequency of Foxp3$^+$ cells for mdx and control C57Bl/10 mice. Left: representative dot plots. Right: summary data. n = 5; **p < 0.01; ***p < 0.001.

(B) Treg clonal expansion in mdx muscle measured as described in the legend to Figure 3C.

(C) Loss-of-function experiments. Mdx mice treated with anti-CD25 mAb (clone PC61) over 10 days.

(D) Gain-of-function experiments. Mice treated with complexes of recombinant IL-2 and anti-iL-2 mAb (clone JES6-1A12).

(C and D) Left: representative dot plot numbers refer to % of cells in the indicated gates in total CD4$^+$ cells. Middle: summary data. Right: quantification of serum CKe. *p < 0.05; ***p < 0.001.

See also Figure S4 and Table S2.

detailed above. Expression of all three gene groups was largely normalized in Areg-treated Treg-less mice: vis-à-vis buffer-only controls: ''muscle homeostasis/function'' genes were upregulated; muscle ''repair/regeneration'' loci were repressed as required for effective repair; and inflammatory transcripts and collagens were also downregulated (Figure 6C). These results were confirmed in representative RT-PCR assays (Figure S5C).

We also tested whether administration of Areg was effective in a context where Tregs were present as normal (DTR^- or B6 mice). Under these conditions, Areg had a strong and rapid impact on the ''muscle homeostasis/function'' and ''repair/regeneration'' gene groups but no significant effect on the ''immune response/inflammation'' groups, at least according to volcano-plot visualization and representative RT-PCR assays (Figures 6D and S5D). More detailed analysis showed that Areg dampened expression of several loci encoding proteins related to fibrosis (e.g., a battery of collagens, Acta2, Adam12), and enhanced expression of loci encoding molecules highly represented in healthy muscle, like Pfkfb1 and 3 and Myl2 (Figure 6E).

Because our previous results indicated that Treg cells can influence the efficacy of myogenic colony formation by muscle precursor cells (Figure 4F), and given the high-level expression of *Egfr* by the satellite cells employed in our assays (and, parenthetically, minimal expression by muscle Treg cells; Figure S5E), we investigated whether Areg might have a direct effect on satellite cells. Addition of Areg to myogenic assays significantly augmented the colony-forming efficiency of satellite cells from unmanipulated B6 mice (Figure 6F). In addition, Areg enhanced myogenic differentiation in bulk cultures of satellite cells, as indicated both by increased levels of transcripts encoding myosin heavy chain (MyHC) (Figure 6G, left) and by increased numbers of cells that stained for MyHC protein (Figure 6G, center). In contrast, there was no apparent difference in proliferation in satellite cell cultures with or without Areg (Figure 6G, right).

Since Areg was expressed by a small fraction of splenic Treg cells in addition to a considerable proportion of muscle Tregs (Figure 6B), we wondered whether the two $Areg^+$ populations might somehow be related. As opposed to the lack of clonality characteristic of bulk splenic Treg cells (Figure 3C), ~5% of the splenic $Areg^+$ subset was clonally expanded (Figure 7A). There was, indeed, some degree of overlap between the CDR3 α and CDR3 β sequences of splenic $Areg^+$ Treg cells and those of muscle Tregs (independent of their expression of Areg) (Figure 7B). The muscle $Areg^+$ and $Areg^-$ subsets showed no difference in their extent of clonal expansion (Figure 7C) or in their representation of the oft-repeated TCR sequence illustrated in Figure 3E (Table S2).

DISCUSSION

A Unique Population of Treg Cells that Accumulates in Skeletal Muscle

There is growing appreciation that the Treg compartment is heterogeneous, has multiple functions, and exerts influences exceeding the boundaries of the immune system (Josefowicz et al., 2012). Here, we have described a previously unrecognized population of Treg cells that emerges in skeletal muscle subjected to acute or chronic damage and have demonstrated that these cells are important players in the muscle-repair process.

Treg cells began to accumulate in injured muscle within days after an insult. That this enrichment represents a conversion of the Tconv to the Treg phenotype is unlikely given that essentially all of the muscle Treg cells expressed Helios and Neuropilin, considered to be markers of Treg cells exported as such from the thymus, and that none of their TCRs were shared with muscle (or lymphoid-organ) Tconv cells. Rather, the elevated levels of muscle Tregs appear to reflect population expansion: they were proliferating in the muscle, substantially more so than in the spleen, and constituted a number of clonally expanded micropopulations. There might also be preferential recruitment of muscle-type Tregs to injured muscle, perhaps driven by one or more members of the constellation of chemokine receptors up- or downregulated vis-à-vis lymphoid-organ Tregs, certain of which have been implicated in migration of diverse leukocyte subsets to skeletal muscle (Warren et al., 2005). Interestingly, a small population of $Areg^+$ splenic Treg cells appeared to include a muscle Treg constituent, evidenced by shared TCR sequences. But it is not clear at present whether the splenic population seeds or arises from the Treg population accumulating in injured muscle.

Several other elements of the muscle Treg transcriptome distinguish it from that of lymphoid-organ Treg cells. Included in the list of repressed genes is *Satb1*, which encodes a chromatin organizer that inhibits Treg suppressive activity (Beyer et al., 2011). The reduced numbers of *Satb1* transcripts, coupled with enhanced expression of transcripts encoding other molecules linked to Treg suppressive function, like IL-10, Gzmb, CTLA-4, and TIM-3 (Josefowicz et al., 2012), support the idea that muscle Treg cells might be endowed with especially strong suppressor activity. Moreover, muscle Treg cells overexpressed certain genes whose products could arm them to perform particularly effectively in the context of regenerating muscle. Areg is a prime example. Interestingly, it was recently reported that Areg might also impact Treg cells directly and enhance their ability to suppress immune responses (Zaiss et al., 2013). However, expression of *Egfr* was undetectable in Treg cells from lymphoid (spleen, lymph node) or nonlymphoid (muscle, VAT) tissues in our microarray studies.

In addition, the TCR repertoires of injured-muscle and lymphoid-organ Treg cells were clearly distinct. There were striking clonal expansions in the muscle Treg population and one TCR α and TCR β chain pair was found over and over again in different individuals despite Draconian measures to avoid contamination. Interestingly, the small subset of $Areg^+$ splenic Tregs did share TCR sequences with muscle Treg cells, whether Areg positive or negative. These findings raise the possibility that a muscle antigen might be involved in recruiting Treg cells to the site of injury and/or retaining them therein.

How Might Treg Cells Influence Muscle Repair?

Muscle repair subsequent to acute injury was impaired in the absence of Treg cells, an influence no doubt exerted at several levels. First, Tregs regulated the myeloid populations that infiltrated the damaged tissue, appearing to contain their numbers

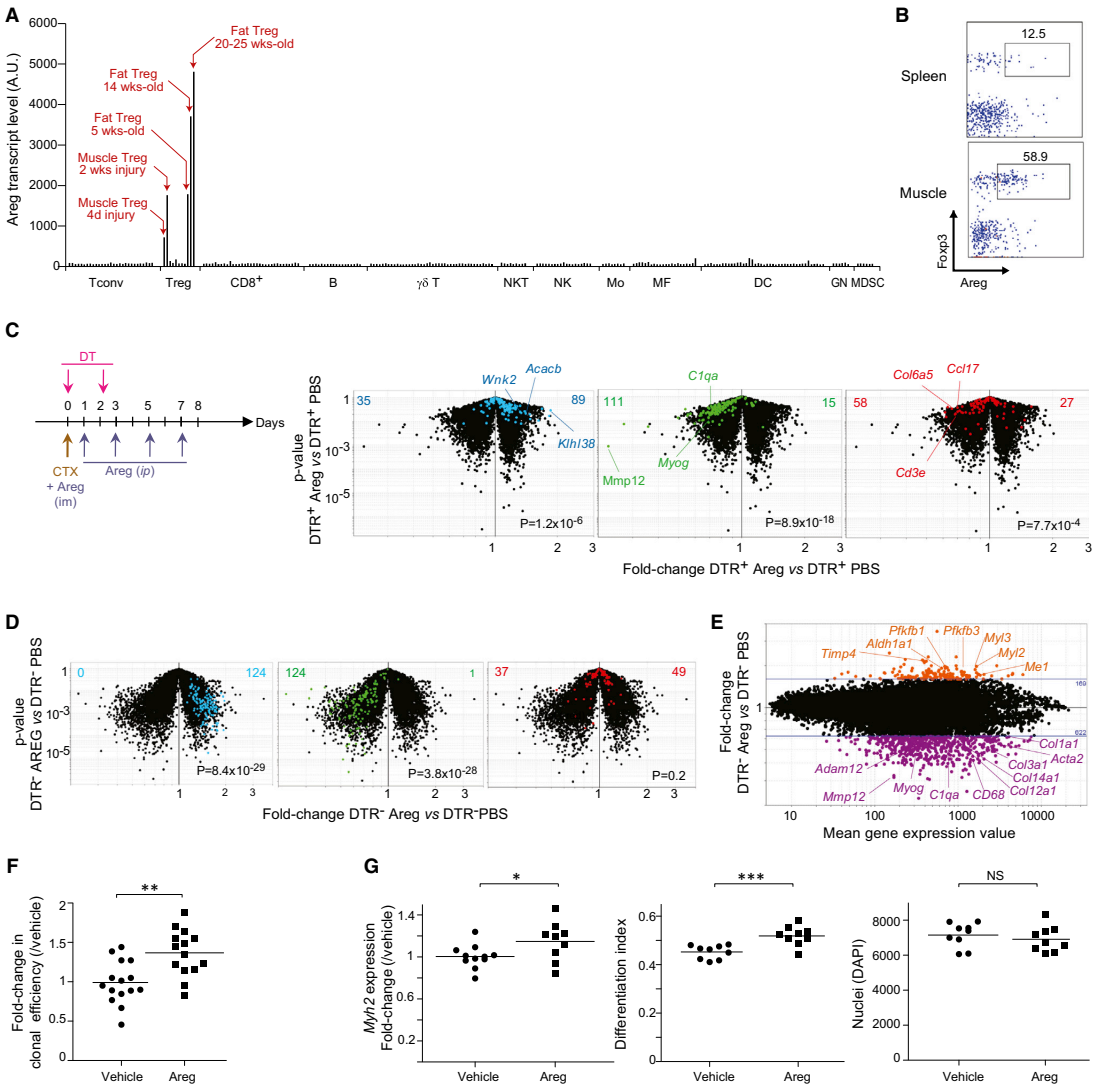

Figure 6. Areg Improves Muscle Repair after Injury

(A) Expression of *Areg* in ImmGen microarray data sets from hematopoietic-lineage cells. Mo, monocytes; MF, macrophages; DC, dendritic cells; GN, granulocytes; MDSC, myeloid-derived suppressor cells; AU, arbitrary units.

(B) Expression of Areg 2 weeks after Ctx-induced injury. Numbers represent % Foxp3$^+$ cells that are Areg$^+$.

(C) Volcano plots of transcriptomes of whole muscle from injured DTR$^+$ (Treg-less) mice treated or not treated with Areg. Left: experimental protocol. Right: superimposition of transcript sets highlighted in Figure 4G and identically color-coded. Values refer to the number of genes upregulated (right) or downregulated (left) in Areg-treated versus PBS-treated muscles. p values from a χ^2 test.

(D) As in (C), except DTR$^-$ mice were used.

(E) The same data set shown in (D) plotted as the fold-change for Areg- versus PBS-treated muscles versus the mean expression value for each transcript. Highlighted in orange and purple are genes up- or downregulated by Areg, respectively.

(F) Myogenic clonal assay in the presence of Areg. Results were plotted as the fold-change over the mean of vehicle-control treated samples per experiment. Data represent mean ± SD and five independent experiments. **p < 0.01.

(legend continued on next page)

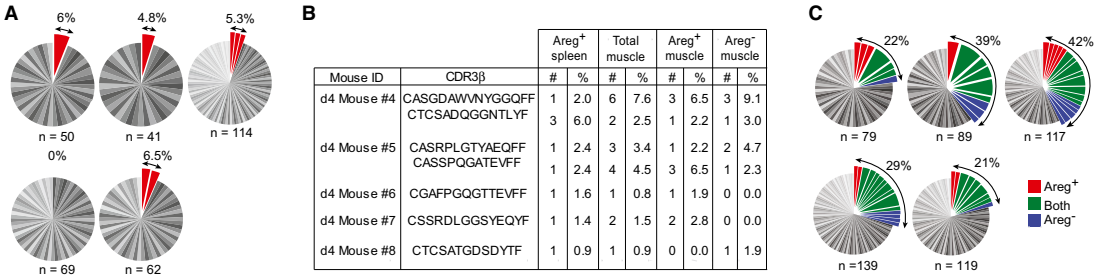

		Areg+ spleen		Total muscle		Areg+ muscle		Areg- muscle	
Mouse ID	CDR3β	#	%	#	%	#	%	#	%
d4 Mouse #4	CASGDAWVNYGGQFF	1	2.0	6	7.6	3	6.5	3	9.1
	CTCSADQGGNTLYF	3	6.0	2	2.5	1	2.2	1	3.0
d4 Mouse #5	CASRPLGTYAEQFF	1	2.4	3	3.4	1	2.2	2	4.7
	CASSPQGATEVFF	1	2.4	4	4.5	3	6.5	1	2.3
d4 Mouse #6	CGAFPGQGTTEVFF	1	1.6	1	0.8	1	1.9	0	0.0
d4 Mouse #7	CSSRDLGGSYEQYF	1	1.4	2	1.5	2	2.8	0	0.0
d4 Mouse #8	CTCSATGDSDYTF	1	0.9	1	0.9	0	0.0	1	1.9

Figure 7. Sharing of TCR Sequences between Areg$^+$ Splenic and Muscle-Infiltrating Treg Cells

(A) TCR CDR3 α and β sequences for individual Areg$^+$ splenic Treg cells. Each pie chart represents a single mouse. n, number of analyzed sequences per mouse. Total frequency of expanded clones shown at the top right.

(B) Identical paired CDR3 α (data not shown) and β sequences found in splenic Areg$^+$ and muscle Areg$^+$ and Areg$^-$ Treg cells from the same individual in independent experiments. #: number of times the sequence was found. %: frequency of Tregs expressing the same sequence.

(C) As in (A), for muscle Treg cells. Clones represented in Areg$^+$, Areg$^-$, or both subsets of muscle Tregs were labeled in red, blue, and green, respectively. See also Table S2.

and to promote their switch from a pro- to an anti-inflammatory phenotype. Both "flavors" of myeloid cell are important for proper muscle repair, and any alteration in the tightly orchestrated scenario wherein each accumulates and functions at the site of injury can be detrimental (Tidball and Villalta, 2010). A variety of intrinsic and extrinsic factors are responsible for their phenotypic polarization; we propose that Treg cells represent an additional layer of control.

Second, Treg cells also regulated coinfiltrating conventional T cell populations. Upon Treg depletion, the total number and frequency of T cells in the injured muscle was significantly increased, and many T cell-specific genes were overrepresented in whole-muscle microarrays of injured muscle from standard versus Treg-less mice. Moreover, depletion of Treg cells in Rag-deficient mice had a less severe influence on muscle regeneration after acute injury than did ablation of Tregs alone, suggesting that infiltrating Tconv cells (and/or CD8$^+$ or B cells) normally have a negative impact on muscle repair that is kept in check by Treg cells. Yet, the effect of removing Treg cells was not abrogated by eliminating the other lymphocyte classes, indicating that Tregs can impact muscle regeneration independently of either T or B cells.

Third, Treg cells impacted the activities of muscle-lineage cells, specifically satellite cells. According to clonal myogenic assays, satellite cells from Treg-deficient mice had decreased colony-forming capacity, consistent with the reduced in vivo regenerative potential of Treg-depleted muscle. Thus, Treg cells can regulate the cells that are directly responsible for the repair of injured muscle. In vitro experiments have shown that macrophages can directly influence muscle progenitors (Bosurgi et al., 2011); it is possible, then, that Treg cells act on satellite cells indirectly, by modulation of the infiltrating myeloid populations. However, two of our results suggest a more direct effect: (1) histological evidence that Treg cells were located in close proximity to regenerating fibers (in addition to being present in heavily infiltrated areas); and (2) the demonstration that muscle Tregs expressed Areg and that this molecule enhanced satellite cell differentiation in vitro and in vivo. Areg is an EGF family member known to promote healing and regeneration of multiple tissues, for example intestinal mucosa and lung epithelium (Shao and Sheng, 2010; Monticelli et al., 2011). Most relevant in the current context, previous studies have suggested that Areg might act directly on muscle cells (Golding et al., 2007; Andrechek et al., 2002). Together with these previous studies, our results suggest that Areg may directly modulate muscle repair.

Treg cells and their products are new players to consider in the orchestrated series of events underlying muscle repair in both acute and chronic contexts. Poor wound healing is a growing problem, especially given its association with diabetes and aging, both of which affect a large and increasing fraction of the population. Moreover, adequate treatments for muscular dystrophies remain elusive. Harnessing the power of Treg cells, whether in cell- or molecule-based strategies, opens novel therapeutic avenues.

EXPERIMENTAL PROCEDURES

Mice and Their Manipulation

C57BL/6, C57BL/10ScSn, RAG1-deficient, and C57BL/10ScSn-Dmd^{mdx} mice were purchased from Jackson Laboratory. Foxp3-DTR, Foxp3-IRES-gfp, and Dysferlin-deficient mice were obtained from A. Rudensky, V. Kuchroo, and R.

(G) Induction of satellite cells differentiation by Areg. Satellite cells were bulk-cultured in the presence of Areg or vehicle control for 12 days. Left: MyHC mRNA titered by quantitative PCR, represented as fold-change expression of *Myh2* relative to vehicle control. Center: MyHC protein quantified by immunofluorescence microscopy; differentiation index calculated as the mean ratio of MyHC-positive nuclei to the total nuclei per field of view. Right: sum of DAPI-positive nuclei per well. Data represent mean ± SD and four experiments. *p < 0.05; ***p < 0.0001.
See also Figure S5.

Bittner, respectively. All mice were bred in our specific-pathogen-free facilities at Harvard Medical School. Protocols were approved by Harvard Medical School's Institutional Animal Care and Use Committee.

We injected anesthetized mice i.m. with 0.03 ml/muscle of Naja mossambica mossambica cardiotoxin (0.03 mg/ml) (Sigma) in one or more hindlimb muscles. Alternatively, TA muscles were directly exposed to dry ice for 5 s.

A total of 1 mg of EdU was injected intravenously, and 24 hr later cells were processed for detection by the Click-iT EdU kit (Molecular Probes).

Foxp3-DTR$^+$ mice and Foxp3-DTR littermates were injected i.p. with DT (Sigma), at 6 ng/g body weight, every other day for 6 days, starting at the day of injury. Depletion of CD25$^+$ cells was accomplished by i.p. injection of 100 μg of anti-CD25 mAb (clone PC61) or rat IgG (Jackson ImmunoResearch) at days 17 and 20 of age. Muscle infiltrate and serum CK were analyzed 7 days after the last injection, the latter via the Creatine Kinase-SL kit (Genzyme). For expansion of Tregs, we incubated 2.5 μg of anti-mouse IL-2 mAb (JES6-1A12) and 0.25 μg of mouse IL-2 per mouse for 20 min on ice followed by i.p. injection. Then 17-day-old mdx mice were given daily injections for 6 days and were analyzed 10 days after the last injection. Control mice were administered phosphate-buffered saline (PBS).

Recombinant mouse Areg (R&D Systems) was administered i.m. (1 μg/muscle) together with Ctx at day 0. Areg was then injected i.p. (7 μg/mouse) every other day until the time of analysis.

Muscle Leukocytes and Manipulations of Them

Mice were perfused with PBS. Muscles were excised, cut up, and collagenase/DNase digested, and leukocytes were isolated by standard procedures. For RT-PCR analyses and single-cell TCR sequencing, published protocols (Wong et al., 2007; Baker et al., 2002) were followed with some modifications to the primer sets used. Raw sequencing files were filtered for sequence quality, processed in automated fashion, and parsed using IMGT/V-QUEST (Brochet et al., 2008). See detailed protocols in the Extended Experimental Procedures.

Microarray

Cells were double-sorted into TRIzol (Invitrogen). Whole-muscle tissue was flash frozen in liquid nitrogen and homogenized in TRIzol. Data sets used for comparison in the PCA were previously generated in our lab. All samples were generated in duplicate or (usually) triplicate. Sample processing and data analysis were performed as previously described (Cipolletta et al., 2012).

Clonal Myogenesis and Myogenic Differentiation Assays

For the clonal assays, myofiber-associated cells were prepared from hind-limb muscles as described (Cerletti et al., 2008). Satellite cells (CD45$^-$Sca-1$^-$Mac-1$^-$CXCR4$^+$β1-integrin$^+$) were double-sorted individually into 96-well plates and cultured for 5–7 days. Wells containing myogenic colonies were scored as described in Extended Experimental Procedures.

For differentiation assays, 3,000 satellite cells were double-sorted onto 24-well plates, cells were cultured ±1 ng/ml recombinant mouse Areg, and after 12 days the cultures were processed for RT-PCR or immunofluorescence microscopy of myosin expression as described in the Extended Experimental Procedures, which also details our method of scoring and calculation of the differentiation index.

Statistical Analyses

Data were routinely presented as means ± SD. Significance was assessed by the Student's t test or ANOVA. A p value of < 0.05 was deemed statistically significant.

ACCESSION NUMBERS

Microarray data are available from the National Center for Biotechnology Information/Gene Expression Omnibus repository under accession numbers GSE50096, GSE50094, GSE50095, and GSE50097.

SUPPLEMENTAL INFORMATION

Supplemental Information includes Extended Experimental Procedures, five figures, and four tables and can be found with this article online at http://dx.doi.org/10.1016/j.cell.2013.10.054.

ACKNOWLEDGMENTS

We thank M. Florence, K. Rothamel, N. Asinovski, A. Ortiz-Lopez, D. Jepson, K. Hattori, J. Ericson, S. Davis, H. Paik, R. Cruse, J. LaVecchio, and G. Buruzula for experimental support. Cell sorting was performed at the HSCI/DRC Flow Core (NIH P30DK036836). This work benefited from public data generated by the Immunological Genome Project (http://www.immgen.org) and was funded by NIH grants R37AI051530 and RO1DK092541 (to C.B. and D.M.) and R01AG033053 and UO1HL100402 (to A.J.W.). A.J.W. is an Early Career Scientist at the Howard Hughes Institute. D.B. was supported by a Kaneb Fellowship, D.K. by an NSF fellowship, E.S. by a Boehringer Ingelheim Fonds Fellowship, and T.G.T. by an A*STAR Graduate Scholarship (Singapore).

Received: February 6, 2013
Revised: August 5, 2013
Accepted: October 16, 2013
Published: December 5, 2013

REFERENCES

Andrechek, E.R., Hardy, W.R., Girgis-Gabardo, A.A., Perry, R.L., Butler, R., Graham, F.L., Kahn, R.C., Rudnicki, M.A., and Muller, W.J. (2002). ErbB2 is required for muscle spindle and myoblast cell survival. Mol. Cell. Biol. *22*, 4714–4722.

Arnold, L., Henry, A., Poron, F., Baba-Amer, Y., van Rooijen, N., Plonquet, A., Gherardi, R.K., and Chazaud, B. (2007). Inflammatory monocytes recruited after skeletal muscle injury switch into antiinflammatory macrophages to support myogenesis. J. Exp. Med. *204*, 1057–1069.

Baker, F.J., Lee, M., Chien, Y.H., and Davis, M.M. (2002). Restricted islet-cell reactive T cell repertoire of early pancreatic islet infiltrates in NOD mice. Proc. Natl. Acad. Sci. USA *99*, 9374–9379.

Bennett, C.L., and Clausen, B.E. (2007). DC ablation in mice: promises, pitfalls, and challenges. Trends Immunol. *28*, 525–531.

Beyer, M., Thabet, Y., Müller, R.U., Sadlon, T., Classen, S., Lahl, K., Basu, S., Zhou, X., Bailey-Bucktrout, S.L., Krebs, W., et al. (2011). Repression of the genome organizer SATB1 in regulatory T cells is required for suppressive function and inhibition of effector differentiation. Nat. Immunol. *12*, 898–907.

Bosurgi, L., Manfredi, A.A., and Rovere-Querini, P. (2011). Macrophages in injured skeletal muscle: a perpetuum mobile causing and limiting fibrosis, prompting or restricting resolution and regeneration. Front. Immunol. *2*, 62.

Boyman, O., Kovar, M., Rubinstein, M.P., Surh, C.D., and Sprent, J. (2006). Selective stimulation of T cell subsets with antibody-cytokine immune complexes. Science *311*, 1924–1927.

Brochet, X., Lefranc, M.P., and Giudicelli, V. (2008). IMGT/V-QUEST: the highly customized and integrated system for IG and TR standardized V-J and V-D-J sequence analysis. Nucleic Acids Res. *36* (Web Server issue), W503–W508.

Cerletti, M., Jurga, S., Witczak, C.A., Hirshman, M.F., Shadrach, J.L., Goodyear, L.J., and Wagers, A.J. (2008). Highly efficient, functional engraftment of skeletal muscle stem cells in dystrophic muscles. Cell *134*, 37–47.

Cerletti, M., Jang, Y.C., Finley, L.W., Haigis, M.C., and Wagers, A.J. (2012). Short-term calorie restriction enhances skeletal muscle stem cell function. Cell Stem Cell *10*, 515–519.

Cipolletta, D., Kolodin, D., Benoist, C., and Mathis, D. (2011). Tissular T(regs): a unique population of adipose-tissue-resident Foxp3+CD4+ T cells that impacts organismal metabolism. Semin. Immunol. *23*, 431–437.

Cipolletta, D., Feuerer, M., Li, A., Kamei, N., Lee, J., Shoelson, S.E., Benoist, C., and Mathis, D. (2012). PPAR-γ is a major driver of the accumulation and phenotype of adipose tissue Treg cells. Nature *486*, 549–553.

Feuerer, M., Herrero, L., Cipolletta, D., Naaz, A., Wong, J., Nayer, A., Lee, J., Goldfine, A.B., Benoist, C., Shoelson, S., and Mathis, D. (2009). Lean, but not obese, fat is enriched for a unique population of regulatory T cells that affect metabolic parameters. Nat. Med. *15*, 930–939.

Golding, J.P., Calderbank, E., Partridge, T.A., and Beauchamp, J.R. (2007). Skeletal muscle stem cells express anti-apoptotic ErbB receptors during activation from quiescence. Exp. Cell Res. *313*, 341–356.

Hill, J.A., Feuerer, M., Tash, K., Haxhinasto, S., Perez, J., Melamed, R., Mathis, D., and Benoist, C. (2007). Foxp3 transcription-factor-dependent and -independent regulation of the regulatory T cell transcriptional signature. Immunity *27*, 786–800.

Horikawa, M., Higashiyama, S., Nomura, S., Kitamura, Y., Ishikawa, M., and Taniguchi, N. (1999). Upregulation of endogenous heparin-binding EGF-like growth factor and its role as a survival factor in skeletal myotubes. FEBS Lett. *459*, 100–104.

Josefowicz, S.Z., Lu, L.F., and Rudensky, A.Y. (2012). Regulatory T cells: mechanisms of differentiation and function. Annu. Rev. Immunol. *30*, 531–564.

Kim, J.M., Rasmussen, J.P., and Rudensky, A.Y. (2007). Regulatory T cells prevent catastrophic autoimmunity throughout the lifespan of mice. Nat. Immunol. *8*, 191–197.

Monticelli, L.A., Sonnenberg, G.F., Abt, M.C., Alenghat, T., Ziegler, C.G., Doering, T.A., Angelosanto, J.M., Laidlaw, B.J., Yang, C.Y., Sathaliyawala, T., et al. (2011). Innate lymphoid cells promote lung-tissue homeostasis after infection with influenza virus. Nat. Immunol. *12*, 1045–1054.

Morales, M.G., Cabello-Verrugio, C., Santander, C., Cabrera, D., Goldschmeding, R., and Brandan, E. (2011). CTGF/CCN-2 over-expression can directly induce features of skeletal muscle dystrophy. J. Pathol. *225*, 490–501.

Naito, A.T., Sumida, T., Nomura, S., Liu, M.L., Higo, T., Nakagawa, A., Okada, K., Sakai, T., Hashimoto, A., Hara, Y., et al. (2012). Complement C1q activates canonical Wnt signaling and promotes aging-related phenotypes. Cell *149*, 1298–1313.

Pastore, S., Mascia, F., Mariani, V., and Girolomoni, G. (2008). The epidermal growth factor receptor system in skin repair and inflammation. J. Invest. Dermatol. *128*, 1365–1374.

Rudnicki, M.A., Le Grand, F., McKinnell, I., and Kuang, S. (2008). The molecular regulation of muscle stem cell function. Cold Spring Harb. Symp. Quant. Biol. *73*, 323–331.

Schmitz, J., Owyang, A., Oldham, E., Song, Y., Murphy, E., McClanahan, T.K., Zurawski, G., Moshrefi, M., Qin, J., Li, X., et al. (2005). IL-33, an interleukin-1-like cytokine that signals via the IL-1 receptor-related protein ST2 and induces T helper type 2-associated cytokines. Immunity *23*, 479–490.

Shao, J., and Sheng, H. (2010). Amphiregulin promotes intestinal epithelial regeneration: roles of intestinal subepithelial myofibroblasts. Endocrinology *151*, 3728–3737.

Shoyab, M., Plowman, G.D., McDonald, V.L., Bradley, J.G., and Todaro, G.J. (1989). Structure and function of human amphiregulin: a member of the epidermal growth factor family. Science *243*, 1074–1076.

Suvas, S., Azkur, A.K., Kim, B.S., Kumaraguru, U., and Rouse, B.T. (2004). CD4+CD25+ regulatory T cells control the severity of viral immunoinflammatory lesions. J. Immunol. *172*, 4123–4132.

Tabebordbar, M., Wang, E.T., and Wagers, A.J. (2013). Skeletal muscle degenerative diseases and strategies for therapeutic muscle repair. Annu. Rev. Pathol. *8*, 441–475.

Tidball, J.G., and Villalta, S.A. (2010). Regulatory interactions between muscle and the immune system during muscle regeneration. Am. J. Physiol. Regul. Integr. Comp. Physiol. *298*, R1173–R1187.

Vetrone, S.A., Montecino-Rodriguez, E., Kudryashova, E., Kramerova, I., Hoffman, E.P., Liu, S.D., Miceli, M.C., and Spencer, M.J. (2009). Osteopontin promotes fibrosis in dystrophic mouse muscle by modulating immune cell subsets and intramuscular TGF-beta. J. Clin. Invest. *119*, 1583–1594.

Warren, G.L., Hulderman, T., Mishra, D., Gao, X., Millecchia, L., O'Farrell, L., Kuziel, W.A., and Simeonova, P.P. (2005). Chemokine receptor CCR2 involvement in skeletal muscle regeneration. FASEB J. *19*, 413–415.

Wong, J., Obst, R., Correia-Neves, M., Losyev, G., Mathis, D., and Benoist, C. (2007). Adaptation of TCR repertoires to self-peptides in regulatory and nonregulatory CD4+ T cells. J. Immunol. *178*, 7032–7041.

Zaiss, D.M., van Loosdregt, J., Gorlani, A., Bekker, C.P., Gröne, A., Sibilia, M., van Bergen en Henegouwen, P.M., Roovers, R.C., Coffer, P.J., and Sijts, A.J. (2013). Amphiregulin enhances regulatory T cell-suppressive function via the epidermal growth factor receptor. Immunity *38*, 275–284.

EXTENDED EXPERIMENTAL PROCEDURES

Isolation of Leukocytes from Muscle

TA, gastrocnemius and quadriceps muscles were excised after perfusing the mice with PBS. Muscles were cut in small pieces and digested for 30 min with collagenase II (2 mg/ml, Invitrogen) and DNase I (150 μg/ml, Sigma). The digested product was filtered through a 70 μm mesh using a plunger to disrupt undigested tissue and washed with DMEM supplemented with serum. To separate the leukocyte fraction, the cells were resuspended in 40% Percoll, overlayed on 80% Percoll and spun for 25 min. The interphase containing leukocytes was recovered, washed and stained for analysis or sorting by flow cytometry.

Flow Cytometry

Samples were stained with the following antibodies: anti-TCRb, -CD4, -CD25, -CD11b, -CD45, -Ly6c, -Gr1, -CD103, -KLRG1, -IL-10, -TIM3, -Helios (all Biolegend); anti-CCR2, -amphiregulin, -neuropilin and -ST2 (all R&D); anti-Foxp3 (eBioscience) and anti-Ki67 (BD Pharmingen). Intracellular expression of Foxp3 and Ki67 was determined using the Intracellular Fixation & Permeabilization buffer set (eBioscience) according to the manufacturer's protocol. EdU detection was done after the last wash with permeabilization buffer following the Click-iT EdU kit (Molecular Probes) instructions. Samples were acquired with an LSR II (BD Bioscience) and data were analyzed with FlowJo (Tree Star).

Single-Cell Sorting, RT-PCR, and TCR Sequence Analysis

$CD4^+Foxp3^+$ and $CD4^+Foxp3^-$ from injured Foxp3-IRES-gfp mice and $CD4^+CD25^+$ cells from mdx mice were first sorted in bulk before resorting as individual cells into wells of 96-well PCR plates containing the reverse transcriptase reaction mix and cDNA was prepared as described by (Wong et al., 2007). Extreme caution was taken to minimize PCR and cross-contamination between wells. Preparation of reverse transcriptase reaction mix, cDNA synthesis, and first round of PCR was performed in a different building from second round PCR and final PCR product isolation. At least 2 columns of every plate were left blank for negative controls to monitor for contamination. Experiments showing evidence of PCR contamination were discarded. Resulting cDNA (1.5 μl) from each cell was split to perform multiplex nested PCR reactions to amplify the corresponding CDR3 α and β transcripts using the protocol and CDR3β primers published in (Baker et al., 2002). Primers used to amplify CDR3 α were designed based on nucleotide sequences of the TCRα families from the IMGT database (http://www.imgt.org; Brochet et al., 2008) (Table S4). Aliquots of the PCR products were visualized on a 1.5% agarose gel. Samples containing PCR product for both TCRα and TCRβ chains were cleaned up using ExoSAP-IT For PCR Clean-Up (Affymetrix) per manufacturers protocol and were subjected to automated sequencing (Dana-Farber/Harvard Cancer Center High-Throughput Sequencing Core). Raw sequencing files were filtered for sequence quality, processed in automated fashion, and parsed using IMGT/V-QUEST (Brochet et al., 2008). Only sequences that produced functional in-frame rearrangements of both TCRα and TCRβ chains were used for analysis.

Quantitative PCR Analysis

Muscle tissue was frozen in liquid N_2 and homogenized in Trizol (Invitrogen) before RNA extraction following Trizol manufacturer's instructions. RNA was reverse transcribed with oligo(dT) primers and SuperScript Polymerase 2 (Invitrogen). Real-time quantitative PCR was performed using gene-specific fluorogenic assays (TaqMan; Applied Biosystems). Transcript levels were normalized to those from the mouse *Gapdh* gene. Primers and probe sequences are listed in Table S4.

Histology

TA muscles were excised and fixed in 4% paraformaldehyde. Paraffin sections were stained with H&E or Gomori's Trichrome staining (to detect collagen deposition). Fibrosis scoring was performed in a blinded fashion by two independent investigators.

For immunofluorescence microscopy, harvested muscle was snap-frozen in liquid nitrogen cooled isopentane and sectioned using Microm HM550 cryostat (Thermo Scientific). After fixation with 4% paraformaldehyde, sections were treated with 0.2% Triton X-100 (2 min.), blocked and stained with polyclonal rabbit anti-mouse anti-dystrophin (1:200) (Abcam, Cambridge, MA), anti-mouse Foxp3 (1:50) (clone FJK-16, eBioscience) and anti-mouse CD4 (1:100) (clone RM4-5, Biolegend). Images were acquired with a Zeiss Axio Imager.M1 microscope. For analysis of cryo-injury, harvested muscle was snap-frozen in liquid nitrogen-cooled isopentane and sectioned using Microm HM550 cryostat (Thermo Scientific). H&E staining was performed on 8-10 μm tissue cryo-sections for quantification of newly-formed (centrally nucleated) regenerative myofibers.

Clonal Myogenesis Assay

Satellite cells ($CD45^-Sca\text{-}1^-Mac\text{-}1^-CXCR4^+\beta1\text{-}integrin^+$) were first sorted in bulk and then individually into 96-well plates coated with collagen (1 μg/ml, Sigma) and laminin (10 μg/ml, Invitrogen). Cells were cultured in F10 medium with 20% horse serum and 5 ng/ml bFGF (Sigma) for 5-7 days, with fresh bFGF added daily, and wells containing myogenic colonies were scored by brightfield microscopy at day 5 or 7.

Myogenic Differentiation Assay

3000 satellite cells were double sorted onto collagen/laminin coated 24-well plates as described above. Cells were fed 5 ng of bFGF (Sigma) per well for 2 days. 1 ng/ml of recombinant mouse Areg (R&D systems) or vehicle control was added daily. Following 12 days in culture, cells were either fixed in 4% paraformaldehyde or mixed extensively with TRIzol (Invitrogen) for quantitative PCR. For immunofluorescence microscopy, fixed cells were permeabilized and blocked with 1% bovine serum albumin/0.5% triton-X/0.5% goat serum. Cells were then labeled with anti-skeletal myosin (FAST) antibody (Sigma), goat anti-mouse IgG (H^+L)-Cy3 (Jackson ImmunoResearch), and DAPI (Invitrogen). The same 20 representative field-of-views in a well were captured on an ImageXpress *Micro* plate reader and analyzed using MetaXpress and ImageJ. The nuclei in a given field-of-view were counted using the NucleiCount algorithm on MetaXpress. Samples were blinded and myosin-heavy-chain associated nuclei were manually counted using ImageJ. The differentiation index was calculated as the average ratio of myosin-heavy-chain positive nuclei to total nuclei per field of view.

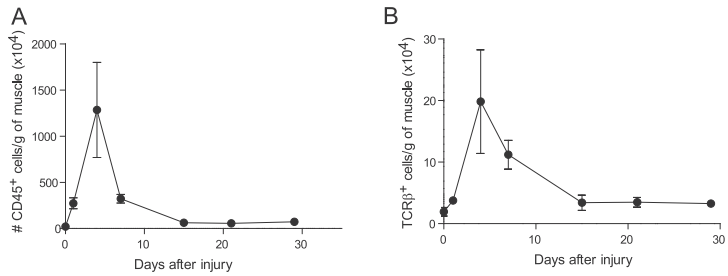

Figure S1. Treg Accumulation at the Site of Injury, Related to Figure 1

Cytofluorometric analysis of the muscle immune infiltrate after injury with cardiotoxin.
(A) Number of $CD45^+$ cells per g of muscle.
(B) Number of $TCR\beta^+$ cells per g of muscle.
Data represent means ± SD ($n \geq 4$).

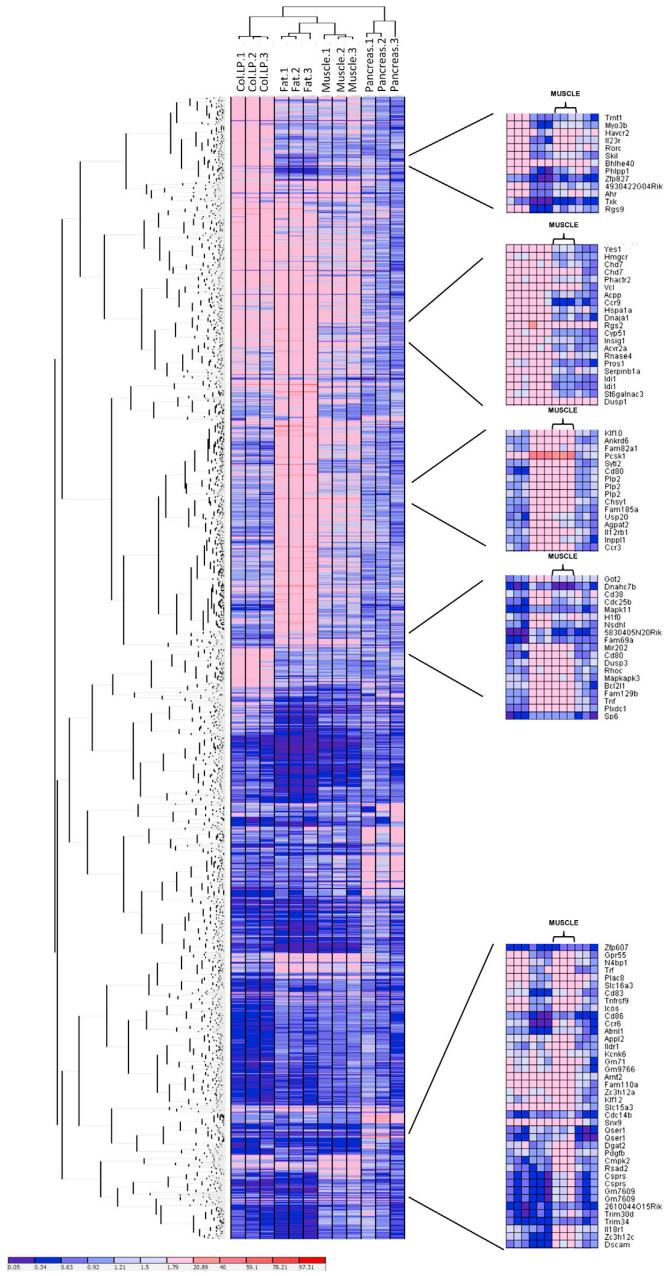

Figure S2. Muscle Treg Cells Have a Unique Transcriptome Compared with Other Inflamed-Tissue Treg Cells, Related to Figure 2

Transcriptome comparison of VAT, muscle, colonic lamina propria and pre-diabetic NOD pancreas Treg cells (triplicates per group). Hierarchical clustering based on a list of 1,853 up- and downregulated genes in nonlymphoid tissue-Treg cells versus lymphoid-Treg cells (pool of all genes with a > 2-fold change in each tissue versus spleen/LN). Values (each square) represent the fold change of non-lymphoid tissue Treg versus lymphoid tissue Treg. Highlighted on the right, a few examples of similarities and dissimilarities between muscle Treg cells and the other populations.

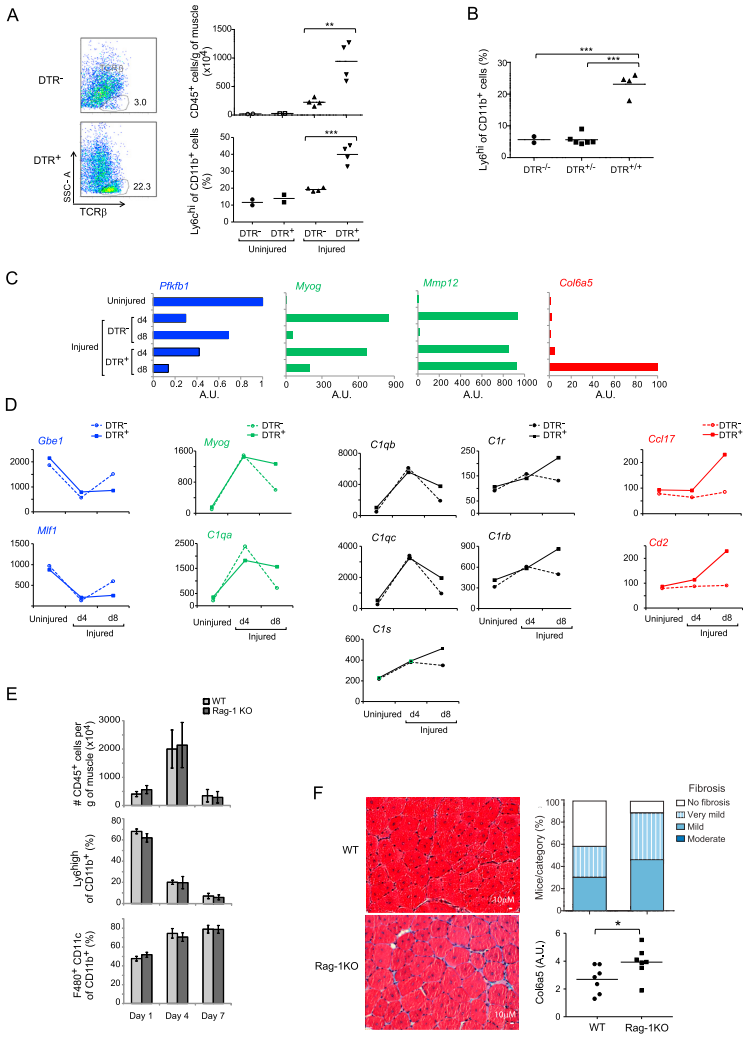

Figure S3. Treg Ablation Impairs Muscle Regeneration after Wounding, Related to Figure 4

DTR$^+$ and DTR$^-$ mice were injured by im injection of Ctx at day 0 and treated with diphtheria toxin from day 0 to induce Treg depletion.

(A) The muscle infiltrate was analyzed by flow cytometry 7 days after injury. Left: the frequency of T cells (CD45$^+$TCR$^+$) in the muscle infiltrate was assessed. Right: total number of CD45$^+$ cells and frequency of Ly6c^{high}/CD11b$^+$ cells. Results are representative of 3 experiments, each with 2-4 animals per group. **p < 0.01; ***p < 0.001.

(B) To assess the possibility that the death, rather than the absence of, Treg cells in repairing muscle explained the persistent inflammation observed, we analyzed the frequency of Ly6c^{high} cells in the infiltrate of Ctx-injured DTR$^{-/-}$, DTR$^{+/-}$ and DTR$^{+/+}$ females. In the heterozygous female setting, DTR is expressed on only half of the Treg cells owing to X chromosome inactivation, so there is substantial cell demise in response to DT treatment – but this death occurs in the continued presence of Tregs. ***p < 0.001.

(C) Expression of representative genes of the 3 gene clusters highlighted in Figure 4C, as measured by quantitative PCR. A representative experiment of three is shown.

(D) Additional representative examples of genes belonging to each gene cluster from Figure 4C. Normalized expression values from the microarray are shown.

(E) Analysis of muscle infiltrate in Ctx-injured RAG1-KO mice by flow cytometry. Data represent mean ± SD (n = 7).

(F) Analysis of fibrosis in Ctx-injured RAG1-KO muscles. Left: Fibrosis detection by Gomori's Trichrome staining of muscle sections 13 days after injury. Collagen is stained in blue. Representative examples of 6 WT and 6 RAG1-KO mice. Magnification: 200X. Top right: summary quantification. Bottom right: expression of collagen, type VI, alpha 5 in muscle by quantitative RT-PCR. *p < 0.05. Data represent means ± SD.

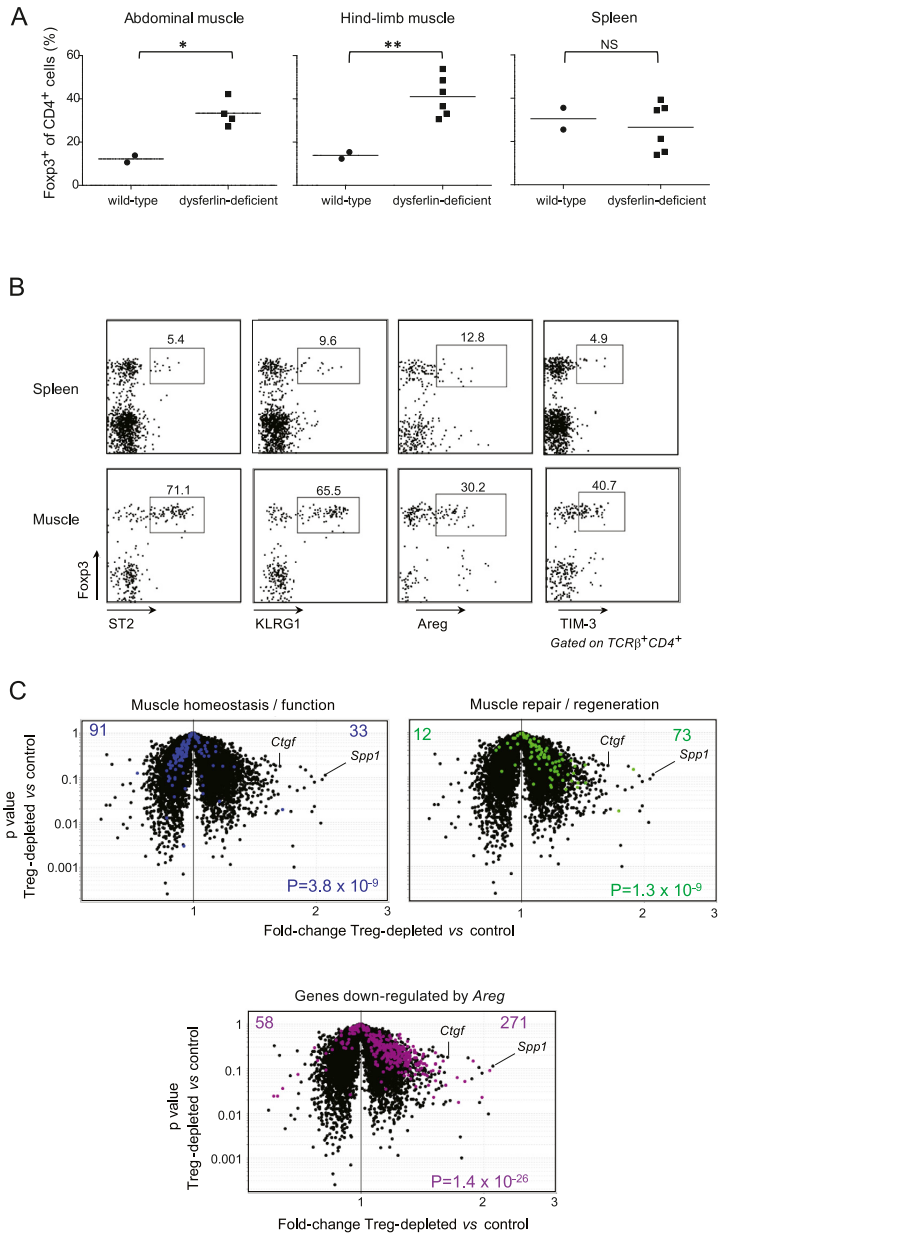

Figure S4. Treg Cells Are Enriched in Muscles of Dystrophic Mice and Impact Muscle Damage, Related to Figure 5

(A) Frequency of Foxp3$^+$ T cells in abdominal muscle, hind limb muscles and spleen of 8 months-old dysferlin-deficient or C57BL/10 mice. **$p < 0.01$; *$p < 0.05$.

(B) Cytofluorometric analysis of surface markers expressed by muscle Treg cells from mdx mice. Dot plots depict the expression of selected markers in TCR$^+$CD4$^+$ cells from spleen (top) or muscle (bottom). Numbers refer to % marker$^+$ Treg cells. Representative plots of n = 4 are shown.

(C) Microarray analysis of whole-muscle tissue from mdx mice treated with anti-CD25. Highlighted in blue and green (top left and top right), gene sets described in Figure 4G. Highlighted in purple (bottom): gene set described in Figure 6E.

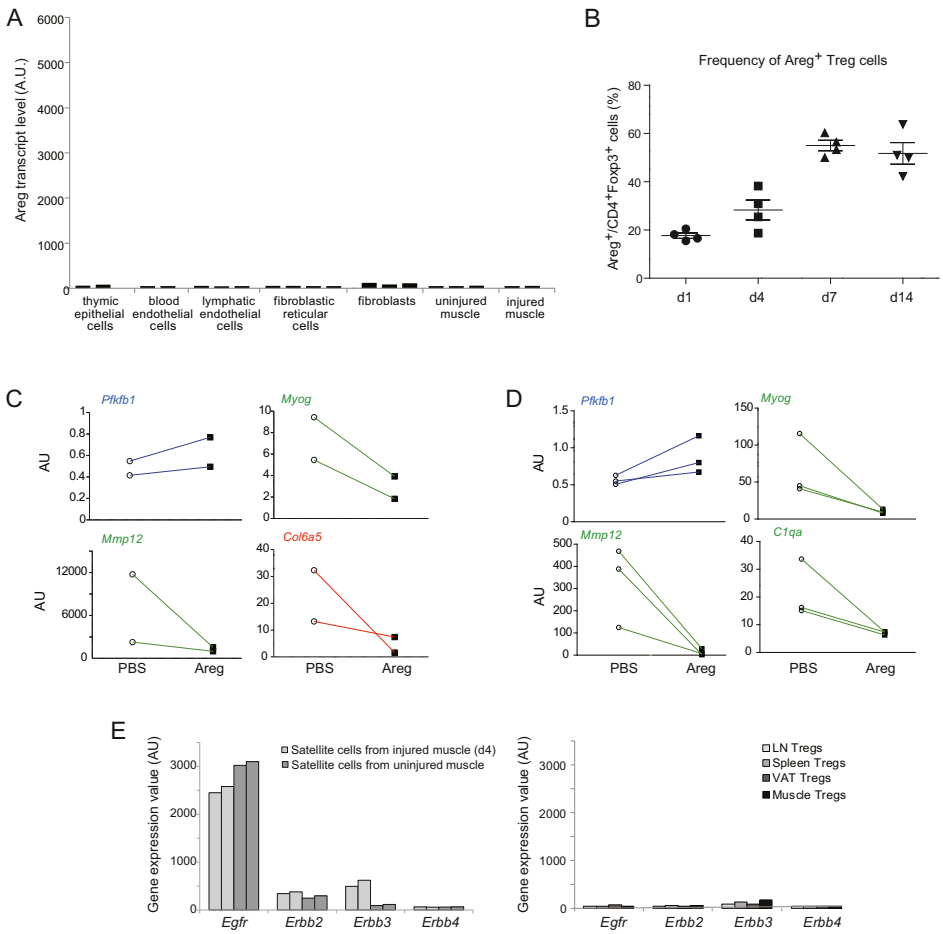

Figure S5. Areg Improves Muscle Repair after Injury, Related to Figure 6

(A) Expression of *Areg* in ImmGen microarray data sets from nonhematopoietic-lineage cells and in whole-muscle samples. AU, arbitrary units.

(B) Frequency of Areg$^+$ muscle Tregs at different time points after Ctx injury, measured by flow cytometry. Data represent mean ± SD (n = 4).

(C and D) Expression of representative genes of the 3 gene clusters highlighted in Figure 4G, as measured by quantitative RT-PCR in muscles from injured DTR$^+$ (C) or DTR$^-$ (D) mice treated or not treated with Areg, normalized to the expression of that transcript in uninjured muscle. AU: arbitrary units. Two to three independent experiments.

(E) Gene expression levels of members of the EFGR family in satellite cells sorted from uninjured or injured muscle (left) or in Treg cells from different tissues (right). Normalized expression values from microarray analyses are shown (each bar represents one experimental replicate). AU, arbitrary units. Data represent means ± SD.

Seminars in Immunology 23 (2011) 431–437

Contents lists available at ScienceDirect

Seminars in Immunology

journal homepage: www.elsevier.com/locate/ysmim

Review

Tissular T_{regs}: A unique population of adipose-tissue-resident Foxp3+CD4+ T cells that impacts organismal metabolism

Daniela Cipolletta [1], Dmitriy Kolodin [1], Christophe Benoist*, Diane Mathis*

Department of Pathology, Harvard Medical School, Boston, MA 02115, United States

ARTICLE INFO

Keywords:
Regulatory T cells
Obesity
Type 2 diabetes
Inflammation
Adipose tissue

ABSTRACT

Foxp3+CD4+ regulatory T (T_{reg}) cells are a key population in controlling the immune response. Recently, their roles have been expanded to broader, non-immune, contexts, in particular the metabolic consequences downstream of obesity-induced inflammation, e.g. type-2 diabetes and cardiovascular disease. This review highlights the major innate and adaptive immune cell subsets contributing to adipose-tissue inflammation, the key role played by fat-resident T_{regs}, and the potential of T_{reg}-based therapies for treatment of the metabolic syndrome.

1. Introduction

In recent years, regulatory T (T_{reg}) cells have emerged as one of the most important guardians of the immune response. Usually making up approximately 5–20% of the CD4+ T cell compartment, T_{regs} play a key role in controlling autoimmunity, allergic responses, inflammation, and responses to infection [1]. Traditionally, they were thought to regulate the activities of other T cells, but there has been growing appreciation of their impact on innate immune system cells, e.g. macrophages and neutrophils. Recent data argue for an even broader role, in non-immune contexts such as cardiovascular disease [2–4] and, obesity-induced insulin resistance [5,6], the focus of this review.

Over the past several decades, there has been a world-wide increase in obesity, in parallel with an impressive rise in a cluster of abnormalities termed the "metabolic syndrome", in particular type-2 diabetes (TD2). According to the latest estimates from the Centers for Disease Control, over 25 million people in the United States suffer from diabetes, which is associated with tremendous societal and economic burdens [7]. There is by now a large body of evidence that implicates obesity in provoking chronic, low-grade inflammation which, in turn, promotes metabolic dysregulation and systemic insulin resistance [8,9]. It turns out that the function of adipose tissue is not limited to the storage of excess triglycerides, but that it is also an active endocrine organ playing multiple roles in orchestrating system-wide metabolism. A seminal insight into the pro-inflammatory potential of adipose tissue in response to obesity came from Hotamisligil et al., who demonstrated increased levels of tumor necrosis factor-α (TNF-α) mRNA in adipocytes in visceral adipose tissue (epididymal, omental, etc.), but not subcutaneous fat, of obese versus lean mice [10]. Since then, an increasing number of adipocyte-derived mediators, collectively called adipokines, have been described. These molecules, which can increase or decrease in response to extended caloric excess, have multiple effects on a variety of cell populations, both locally in adipose tissue and systemically (reviewed in [11]). They include, but are not limited to, interleukin-1β (IL-1β) [12], IL-6 [13], serum amyloid A3 (SAA3) [14], and macrophage chemoattractant protein-1 (MCP-1) [15]. Obesity, by triggering endoplasmic reticulum (ER) stress [16], hypoxia [17], and oxidative stress [18], results in adipocyte dysfunction, dysregulated expression of adipokines, and inappropriate inflammatory responses [8,9]. There are changes in the cellular composition of adipose tissue, including adjustments in the numbers, phenotypes, and localization of multiple immune cell subsets. There are also systemic metabolic alterations through a complex signaling network that affects insulin signaling in the liver, kidney, and skeletal muscle. Activation of NF-κB [19] and the JUN N-terminal kinase family of serine/threonine protein kinases [20] leads to phosphorylation and inactivation of the insulin receptor substrate (IRS) family, which collectively results in tissues becoming unresponsive to insulin signaling [16,21,22].

Here, we will outline contributions of both the innate and the adaptive immune systems to obesity-associated pathologies, highlight the protective role of fat-resident T_{reg} cells, and discuss the possible clinical implications of these findings for treatment of T2D.

* Corresponding authors at: Department of Pathology, Harvard Medical School, 77 Avenue Louis Pasteur, Boston, MA 02115, United States.
Tel.: +1 617 432 7741; fax: +1 617 432 7744.
E-mail addresses: cb@hms.harvard.edu (C. Benoist), dm@hms.harvard.edu (D. Mathis).
[1] These authors contributed equally to this work.

1044-5323/$ – see front matter © 2011 Elsevier Ltd. All rights reserved.
doi:10.1016/j.smim.2011.06.002

2. Immune effector cells in obesity-induced T2D

2.1. Innate immune system

A number of studies have implicated innate immune system cell types, such as neutrophils, mast cells, and macrophages in obesity-induced pathology. In a mouse model of obesity triggered by a high-fat diet (HFD), neutrophils were early infiltrators of the adipose tissue, detectable already at 3 weeks of HFD, suggesting a possible role in early phases of adipose tissue inflammation. However, the importance of neutrophils in downstream metabolic consequences remains to be established [23].

Recently, Liu et al. argued for a role for mast cells in obesity and its sequelae [24]. They found that mast cell numbers were increased in the adipose tissue of obese mice and humans compared with those of lean controls. Mice carrying a genetic deficiency in mast cells or treated with mast-cell-stabilizing drugs displayed a significantly reduced body weight and visceral fat pad mass when on HFD through a proposed mechanism of decreased angiogenesis and increased apoptosis of muscle and adipose tissue. It is important to note that the primary effect of mast cell deficiency/stabilization was on obesity-induced weight gain, which would have secondarily altered insulin sensitivity. Finally, using genetic knockout mice, the authors showed that IL-6 and interferon-γ (IFN-γ) produced by mast cells were key cytokines for attenuating weight gain. These findings suggest a role for mast cells in obesity-associated abnormalities through promoting adipose tissue growth.

To date, the largest body of evidence implicates subsets of macrophages/monocytes as major effectors in obesity-induced pathology. Accumulations of large numbers of macrophages around dead adipocytes, forming "crown-like structures," have been observed in visceral fat tissue of obese mice and humans [25,26]. Under normal chow conditions, adipose tissue presents an anti-inflammatory environment, where resident macrophages display a phenotype similar to the anti-inflammatory or alternatively-activated "M2" state, producing factors such as interleukin-10 (IL-10) and transforming growth factor-β (TGF-β) [15,27–31]. In contrast, in obese adipose tissue, resident and infiltrating macrophages appear to be in the pro-inflammatory or classically activated "M1" state, synthesizing numerous inflammatory factors, including TNF-α, IL-6, matrix metalloproteinases, and peroxisome proliferator activated receptor-γ (Pparg) [15,26,29–31].

It is important to note, however, that, while adipose tissue macrophages have been historically subdivided into M1 and M2 subsets [30,31], and this is an attractively simple dichotomy, recent studies have challenged this binary classification, instead arguing in favor of a spectral classification [27,32,33]. A recent study demonstrated the importance of the NLRP3 (nucleotide-binding domain leucine-rich repeat containing family, pyrin domain containing 3) inflammasome in activation of adipose-tissue macrophages and subsequent development of insulin resistance [34]. The inflammasome is a key player in sensing various "danger" stimuli, leading to secretion of IL-1β and initiation of a pro-inflammatory immune response (reviewed in [35]). Previous studies have demonstrated that cholesterol or similar crystals cause Nlrp3 inflammasome activation in macrophages found in atherosclerotic lesions [36,37]. By analogy, one might speculate that HFD leads to formation of cholesterol crystals activate the Nlrp3 inflammasome, in particular in adipose tissue macrophages, resulting in a pro-inflammatory activation state and ultimately resulting in systemic inflammation and insulin resistance. Additionally, activation of adipose tissue macrophages has been shown to result from recognition of free fatty acids by Toll-like receptors (TLR) 2 and 4 in mice on HFD (Fig. 1) [38].

2.2. Adaptive immune system

The contributions of the innate immune system, in particular of macrophages, to obesity-induced inflammation have been the central focus of by far most of the relevant studies, but of late there has been a growing interest in the role of the adaptive immune system as well. A T cell implication in T2D would not be so surprising given their crucial roles in various other inflammatory contexts. Early studies noted an increased frequency of CD3+ cells in the adipose tissue of obese humans and mice [39]. Since then, accumulations of both CD4+ and CD8+ T cells have been reported, and evidence of a significant role presented, but there remains substantial controversy over the extent to which the two compartments contribute to disease progression.

Several recent studies have evaluated the role of CD8+ T cells in adipose tissue inflammation. They were found infiltrate visceral adipose tissue in response to HFD, reportedly prior to the characteristic increase in macrophages [40]. Depletion of CD8+ T cells via either antibody treatment or genetic ablation resulted in reduced macrophage infiltration into visceral fat depots, decreased production of key pro-inflammatory mediators such as TNF-α, IL-1, IL-6, and MCP-1, and improved insulin sensitivity. *In vitro* experiments demonstrated that CD8+ T cells isolated from obese adipose tissue had a highly activated phenotype and produced large quantities of pro-inflammatory mediators known to function in macrophage recruitment and activation [40,41]. The frequency of CD44+CD62L− effector-memory cells was significantly higher, while naïve CD44−CD62L+CD8+ T cells was decreased, in obese compared with lean adipose tissue, consistent with the notion of an activated CD8+ T cell phenotype in obese fat [41]. Together, these findings suggest that obesity promotes activation of CD8+ T cells in fat, which, in turn, leads to the recruitment, differentiation and activation of activated macrophages via pro-inflammatory mediators.

Other studies have characterized the pro-inflammatory properties of adipose-resident effector CD4+ T cells, especially given their well-established ability to promote inflammation and recruit macrophages. A significant increase in CD4+ T cells residing in adipose tissue of obese humans and mice was reported [41,42]. The fat-resident CD4+ T cell compartment of obese mice was enriched for CD44+CD62L− effector-memory cells [41], phenotype characterized by production of IFN-γ [5,42,43]. T cell receptor (TCR) sequence analysis revealed a repertoire bias among T cells isolated from obese compared with lean adipose tissue, suggestive of antigen-driven T cell activation, expansion, and/or infiltration [41,42]. An increase in IFN-γ expression can enhance the accumulation of M1 macrophages in obese fat, accompanied by elevated expression of TNFα, and MCP-1 [44]. Finally, enflamed adipose tissue may further propagate Th1 cell polarization through the production of leptin, which can act on T cells directly and indirectly to promote increased proliferation and cytokine production, specifically of IL-2 and IFNγ [45]. The proposal that Th1 polarization is at the expense of Th2 cells [42] is poorly substantiated as Gata3+CD4+ and Th2 cells cannot be equated [46].

One report has proposed a protective role for effector CD4+ T cells in obesity-induced insulin resistance [42]. CD4+ T cells were adoptively transferred into recombination-activating genes (RAG)-null mice, which have no T or B cells [47], and a decreased body weight and fat pad mass, and an improved insulin sensitivity were observed 2–4 weeks later. The authors proposed that the improved metabolic parameters reflected protection by Th2 cells. However, an alternative interpretation is that the improvement is due to a lower body weight in the recipient mice coupled with the insulin-sensitizing effect of T_{reg} cells. Transfer of CD4+ T cell populations depleted of Foxp3+ T_{regs} or CD4+ T cells from IL-10-deficient mice into immunodeficient recipients are both well-established animal

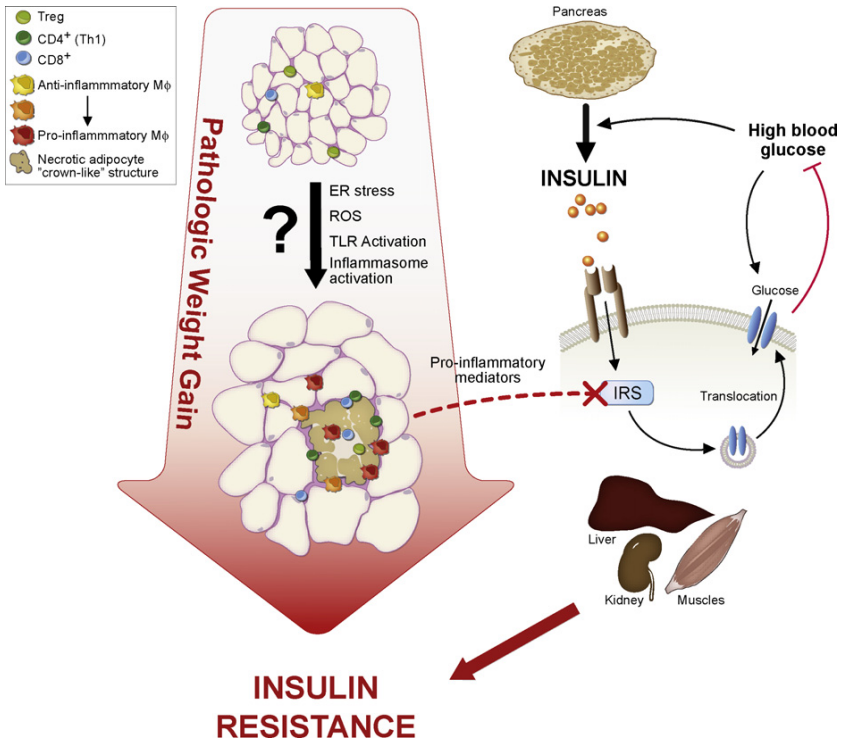

Fig. 1. Obesity results in systemic, chronic, low-grade inflammation and insulin resistance. Excess weight gain leads to necrotic and apoptotic death of adipocytes, thereby activating various inflammatory responses such as TLR and inflammasome activation, release of reactive oxygen species (ROS), and endoplasmic reticulum (ER) stress. In response to these inflammatory stimuli, adipocytes and infiltrating leukocytes release a variety of pro-inflammatory mediators that act locally in adipose tissue and distally in liver, muscle, and kidneys to inactivate insulin receptor substrates (IRS), leading to insulin resistance and persistent high blood glucose.

models of colitis [48,49]. Therefore, the decreased weight gain of the recipient RAG-null mice following CD4+ T cell transfer was likely due to the initiation of colitis, and the improved metabolic parameters were merely a reflection of decreased body weight. The presence of colitis is further substantiated by the fact that there was no attenuated weight gain or improvement in metabolic parameters following the transfer of CD8+ T cells [49] or OT2 TCR-transgenic CD4+ T cells [50], because neither of these cell types is able to transfer colitis. In addition, the authors proposed that the protective effect of CD4+ T cells was a result of their Th2 polarization by showing that transferred CD4+ T cells produced IL-4 and IL-13 following restimulation and that there was a lower frequency of Gata3+ T cells in visceral adipose tissue of obese compared with lean animals. Under lymphopenic conditions, CD4+ T cells become activated and differentiate into Th2 cells, as suggested by the authors, but they also differentiate into Th1 cells; therefore, upon restimulation, CD4+ T cells from a lymphopenic host may produce IL-4 and IL-13, as seen in the paper, but they would also produce IFNγ, which was not measured. Furthermore, it was recently shown that T_{regs} can express high levels of Gata-3 [46]. Therefore, it is possible that the loss of Gata3+CD4+ T cells from abdominal adipose tissue following HFD is actually due to loss of T_{reg} cells. Thus, the root of the observed protection bears re-examination.

There are substantial contradictions among the aforementioned studies on the contributions of CD4+ and CD8+ T cells to obesity-associated inflammation and insulin resistance. Several groups reported an increase in the fraction of CD8+ T cells in response to HFD [40,41,51]; however, a more recent study found no such difference [43]. Similarly, some groups described significant CD4+ T cell accumulation in adipose tissue of obese humans and HFD-fed mouse models [42,51], while another study did not see this increase [43], and still another saw a decrease [40]. In interpreting and comparing these seemingly contradictory results, it needs to be kept in mind that methods used to quantify T cells by flow cytometry differed in various studies. In addition, there were multiple divergences in the HFD protocols used, including the age of the mice at introduction of the enriched diet, length of time on the diet, and the composition, in particular the fat content, of the HFD and normal chow comparator.

With the recognition of an important role for T cells in obesity-associated pathologies, there is an increased interest in the function of B cells in these abnormalities. Recent studies on HFD-fed mice revealed that B cells infiltrated adipose tissue within the first 3 weeks of diet changes [52,53], and that there was a rise in serum immunoglobulin (Ig) levels. Analysis of B-cell-deficient mice on HFD revealed that the absence of B cells led to increased insulin sensitivity compared with wild-type controls. Additionally, transfer of B cells or serum IgG isolated from HFD-fed mice into B-cell-deficient recipients resulted in transfer of insulin resistance; however, there was no change in insulin resistance when transferred B cells or IgG were isolated from lean normal-chow-fed mice. Finally, the authors showed that insulin resistant human patients had a distinct IgG profile compared with age- and weight-matched insulin sensitive subjects. While it is clear from this study that Igs can have an effector function in promoting insulin resistance, perhaps through adipocyte death and the generation of antibodies that inhibit insulin signaling molecules, their role in more upstream events is more cloudy, given the well-known T cell aberrancies in B-cell deficient mice [54–56].

3. Role of fat-resident T_{reg} cells in obesity-induced T2D

Foxp3+ T_{reg} cells are important regulators of essentially every category of immune response. While Foxp3 is a critical orchestrator of the T_{reg} phenotype, it, alone, is not sufficient to drive the full phenotype program [57,58]. For example, the induction of Foxp3 expression through "conversion" of conventional T (T_{conv}) cells (by *in vitro* culture with TGF-β, *in vivo* exposure to agonist peptide, or *in vivo* homeostatic proliferation) or by retroviral transduction of T_{conv} cells with *Foxp3* can only partially recapitulate the canonical "T_{reg} signature" [57,58]. Furthermore, Foxp3 is not necessary for expression of all of the suppressive activities characteristic of T_{reg} cells. Disruption of the *Foxp3* gene in mice by insertion of the green fluorescent protein (GFP) results in the generation of so-called T_{reg} "wannabes," cells expressing a number of the canonical T_{reg} markers (such as CTLA4, ICOS, IL-2ra), but lacking any suppressive function [59,60]. These findings suggest that the regulatory activities of T_{regs} are subject to a level of regulation upstream of Foxp3. Finally, the gene-expression profiles of different subtypes of Foxp3+ cells (thymus-derived T_{regs}, splenic, converted, etc.) [57,58,61] coupled with findings on transcription factor knockout mice [62–64], have revealed that T_{reg} cells come in "different flavors", determined by distinct origins and anatomic locations.

So far, the most striking example of a distinct subset of T_{reg} cells came from the identification of an adipose-tissue-resident population that seems to impact metabolic parameters, in particular of insulin resistance secondary to obesity [5]. Such cells accumulated with age in lean mice to eventually represent more than half of the CD4+ T lymphocytes residing in the visceral fat. This is a much greater fraction than the 15% or so normally found in lymphoid tissues. Interestingly, T_{regs} were not enriched in subcutaneous adipose depots – interesting because changes in visceral, but not a subcutaneous, fat have been associated with insulin resistance [65].

Characterization of fat T_{reg} cells via gene-expression profiling and TCR repertoire analysis revealed a population distinct from counterparts in lymphoid organs. Fat-resident Foxp3+CD4+ cells retained about 60% of the canonical T_{reg} signature; however, they specifically over- or under-expressed many genes, especially those coding for molecules involved in leukocyte migration and extravasation, such as CCR1, CCR2, CCR9, CXCL10 (over-represented in fat T_{regs}); and CCL5 and CXCR3 (under-represented in fat T_{regs}). In addition, the repertoire of TCRs displayed by adipose T_{regs} was distinct from that of fat T_{convs} as well as T_{reg} and T_{convs} from lymphoid tissues. Intriguingly, there were multiple examples, in the same or in different mice, of a particular CDR3 amino-acid sequence encoded by different nucleotide sequences. This finding suggests that in adipose tissue, T_{regs} may undergo a selective pressure favoring the display of a TCR with a particular antigenic specificity. Moreover, the fact that fat T_{regs} shared almost no TCR sequences with the T_{conv} cells in fat or LN, suggested that the accumulation of Foxp3+ T_{regs} in the abdominal adipose tissue is unlikely to be due to a local conversion of T_{conv} cells [5].

Interestingly, fat T_{regs} expressed a very high level of the anti-inflammatory cytokine, IL-10 [5]. In an *in vitro* experimental model that reproduces the main mechanism of induction of cellular insulin resistance (treatment of a cultured pre-adipocyte line with TNF-α), IL-10 could suppress markers of inflammation and restore the expression of the transporter for glucose, GLUT4 [5]. However, other mechanisms of suppression are also possible, even likely, given that they express other molecules like Granzyme-b and CTLA-4 that could be responsible for their regulatory activity [66].

The potential role of fat T_{reg} cells in modulating adipose tissue inflammation was also demonstrated via gain- and loss-of-function experiments. It is possible to expand T_{regs} *in vivo* using IL-2/anti-IL-2 complexes or, conversely, deplete them by injecting diphtheria toxin (DT) in a mouse model where *Foxp3* promoter/enhance elements drive the expression of the diphtheria toxin receptor (*Foxp3*-DTR mice) [67,68]. Both *in vivo* manipulations impacted metabolic parameters, improving (by IL-2/anti-IL-2 complexes) or compromising (by DT) their insulin sensitivity [5]. Moreover, an interesting, but indirect, indication of the involvement of T_{regs} in the control of metabolic functions came from studies performed using several animal models of obesity and insulin resistance, such as leptin-deficient mice ($Lep^{ob/ob}$), mice heterozygous for the yellow spontaneous mutation (A^y/a) and mice chronically fed a high-fat diet (HFD). In all of these models, the percentage and number of fat T_{regs} was substantially reduced compared with that of lean controls [5,69–71]. Similar to the mouse data, a reduction in *Foxp3* transcripts was also observed in the omental vis-à-vis subcutaneous fat of obese humans [5].

However, Winer et al. did not see a dramatic decrease in fat T_{reg} numbers in mice fed an HFD [42]. We attribute this difference to their use of the "Foxp3-GFP" mouse line, in which the GFP reporter is fused near the N terminus of the Foxp3 protein. Our group, as well as other laboratories, has found abnormal T_{reg} activity in these mice in the context of autoimmune and inflammatory diseases, including in the fat (unpublished data).

Why the T_{reg} fraction in abdominal adipose tissue decreases during obesity is still not clear. Even though only a few years have passed since the first report on fat T_{regs} and their role in guarding against insulin resistance, several groups have already contributed to this discussion. An interesting model to explain such a dramatic reduction in fat T_{regs} with obesity has been proposed by Matarese et al. [71]. Leptin is an adipokine that controls food intake and promotes the activation of T lymphocytes, enhancing the proliferation of Th1 cells and their production of pro-inflammatory cytokines [72]. Conversely, leptin inhibits the proliferation of T_{reg} cells [73,74]. The elevated levels of leptin accompanying obesity could dampen T_{reg} proliferation, perhaps explaining why their numbers decrease. But, this speculation is difficult to reconcile with the striking loss of fat T_{regs} in the leptin-deficient mouse model [5]. Alternatively, Deiuliis et al. have argued that the reduced accumulation of fat T_{regs} in obese individuals is a direct consequence of inflammatory signals produced by macrophages [6]. However, their arguments assumed that fat T_{regs} result from peripheral conversion of T_{conv} cells, for which there are few supporting data but several lines of evidence in contradiction [5]. Further, while this group suggested that peripheral T_{regs} may home to the adipose tissue through the expression of CXCR3 and CCR7, it has been reported that these chemokine receptors are down-regulated in fat T_{reg} cells [5,6].

Lastly, there seems to be an interesting parallelism in the cellular mechanisms underlying insulin resistance and atherosclerosis. T_{regs} were prominent in the atherosclerotic lesion of Apolipoprotein-E-deficient mice, a standard model, and they decreased with age [2,75]. Moreover, depletion of T_{regs} through genetic ablation of CD80/86, CD28 or ICOS, or via anti-CD25 mAb treatment, enhanced atherogenesis and lesion inflammation. Conversely, adoptive transfer of T_{regs} prevented the development of atherosclerotic plaques [3,76]. In humans, impairment in the number and function of circulating T_{regs} was observed in patients with acute coronary syndrome [77]. Interestingly, no T cells were found in normal vessel fragments while a few T_{regs} (0.5–5%) were detected in the intima during all stages of plaque development [77]. It has not been clear whether the loss/lack of T_{regs} is the cause or the effect of the atherosclerotic lesions.

4. Regulatory T cells as potential immunotherapy

As illustrated using many rodent disease models, the therapeutic potential of manipulating T_{reg} cells is enormous. T_{reg} activity

can be attenuated to improve anti-tumor or anti-microbe responses [78,79], or enhanced to treat allergic, inflammatory or autoimmune diseases [80–87]. Treatment with anti-CD3 mAb is a promising approach, already in the clinic: this agent seems to evacuate T effectors cells while concomitantly enhancing the representation of T_{reg} cells [88].

Potential application of T_{regs} to therapy of T2D has only recently been explored. Winer et al., using the non-mitogenic $F(ab^1)_2$ fragment of anti-CD3 mAb, described a long-term normalizing effect on insulin resistance and glucose tolerance in mice treated with a short regime of 5 days [42]. They highlighted a correlation between the improved metabolic profile and the increase in numbers of adipose-tissue T_{regs} and anti-inflammatory macrophages.

Ilan et al., on the other hand, employed oral administration of anti-CD3-mAb in combination with β-glucosylceramide (GC) [89]. GC, an intermediate of glycosphingolipid metabolism, interacts with CD1d, a molecule recognized by NK-T cells. Oral administration of GC led to decreased intra-hepatic NK-T cell numbers and amelioration of the metabolic syndrome in *Lep*$^{ob/ob}$ mice [90]. This protocol results in anti-CD3s uptake by the gut-associated lymphoid tissue, and the induction of CD4+CD25− T_{reg} cells expressing TGF-β1 latency-associated peptide (LAP) [91]. The suppressive capacity of such cells has been studied in several diseases, like autoimmune diabetes, experimental encephalomyelitis and systemic erythematosus lupus [91–93]. Body weight did not change after oral treatment of *Lep*$^{ob/ob}$ mice with anti-CD3 mAb. There was an induction of CD4+ LAP+ T cells, and a concomitant reduction of NK-T cells, in the mesenteric lymph nodes, blood and spleen, but, surprisingly, there was an increase of T_{regs}, but not of CD4+LAP+ T cells, in the adipose tissue. The authors suggested that the increase in fat T_{regs} may have resulted from increased production of TGF-β by LAP-positive T cells, which correlates with a decrease in adipose tissue inflammation. Metabolic parameters were impaired by oral anti-CD3 mAb treatment: a reduction in blood-glucose, cholesterol and aspartate amino transferase levels.

Interestingly, none of effects on the metabolic and pathologic abnormalities could be recapitulated when *Lep*$^{ob/ob}$ mice were treated singly with either anti-CD3 or GC. The authors hypothesized that T_{regs} activation was induced through engagement of the TCR by anti-CD3, and that tolerogenic DCs were promoted by NK-T cells, further inducing T_{reg}. In conclusion, this report made the novel suggestion that a previously described interaction between T_{regs} and NK-T cells may play an important role in controlling the inflammation associated with T2D [94]. However, transfer of the induced CD4+LAP+ (but not CD4+LAP−) T cells to *Lep*$^{ob/ob}$ mice ameliorated blood glucose and aspartate amino transferase levels and reduced levels of inflammatory mediators like IL-6, IFN-γ and IL-17 produced by stimulated splenocytes, suggesting that the main factor in controlling insulin resistance may rather be the expansion of CD4+LAP+ T cells in the periphery rather than the induction of T_{reg} cells. Finally, it would be useful to supplement these results with data on the commonly accepted measures of insulin resistance, including levels of blood insulin, the glucose tolerance test and HOMA-IR (Homeostatic Model Insulin Resistance) to better situate them in the context of T2D in humans and animal models.

To date, approaches to T2D therapy have been focused on sulfonylureas, biguanides, and thiazolidinediones. However, the aforementioned studies all support the idea that T_{regs} and their products may represent novel targets. Similarly, the use of anti-CD3 mAb has been proposed to explore the potential beneficial effect of *in vivo* T_{reg} induction in the context of atherosclerosis. Preventive therapy with anti-CD3 reduced plaque development and its therapeutic use decreased lesion progression in mice with established atherosclerosis [95].

Cellular therapy based on the administration of *ex vivo* expanded T_{regs} is currently the object of extensive research for the treatment of autoimmune and graft-versus-host disease. However, several issues must be addressed before their clinical use. First of all, large numbers of customized T_{regs} will be needed for transfer into humans. Presently, much effort is directed at developing protocols to achieve their *ex vivo* expansion and to ensure the maintenance of their phenotypic and functional purity. Moreover, the possibility for contamination of T_{reg} preparations by effector T cells must be carefully addressed because this could result in exacerbation of inflammatory responses on adoptive transfer. Achieving the goal of a pure preparation of patient-derived T_{reg} cells will require the identification of a more specific surface marker of natural T_{regs} or, as proposed by Battaglia et al., the use of drugs like rapamycin which appear to induce T_{regs} while blocking the proliferation of effector T cells [96].

In conclusion, T_{reg} numbers, purity, diversity, allo-reactivity and antigen specificity are all factors that render their translation from the bench to the bedside very difficult. The identification/design of compounds that can selectively expand T_{reg} cells *in vivo* would be an elegant solution to the aforementioned concerns. Given our recent appreciation of T_{reg} heterogeneity based on anatomic location and physiologic functions, this goal is simultaneously made more complex and more attractive with regard to the specificity of targets.

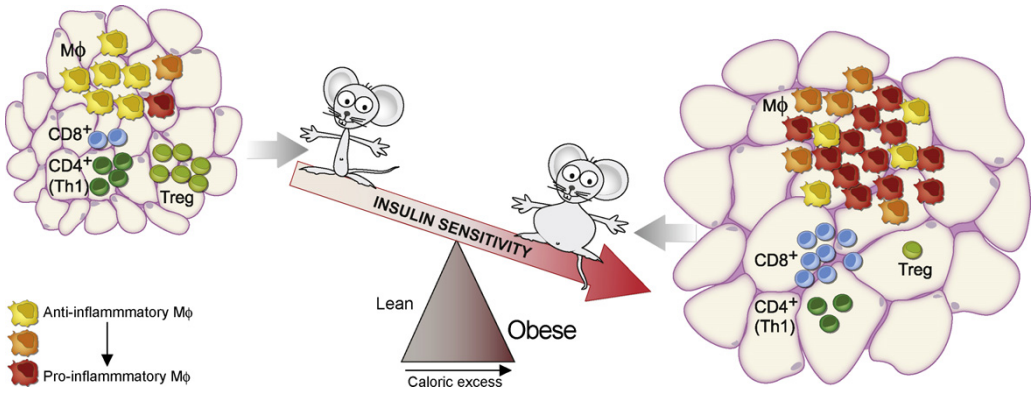

Fig. 2. Cellular and metabolic alterations in adipose tissue during obesity. In lean mice, the abdominal adipose tissue hosts anti-inflammatory macrophages, as well as an elevated fraction of T_{regs}. In obese mice, by contrast, there is a switch in cellular equilibrium: more CD8+ than Th1 CD4+ T cells, fewer regulatory T cells and a preponderance of pro-inflammatory macrophages. These effector cells promote inflammation and exacerbate adipose tissue dysfunction through the production of inflammatory cytokines.

5. Concluding remarks and future prospects

Inflammation is a critical link between obesity and T2D. Recent studies have painted a picture in which the inflammation of adipose tissue is correlated with alterations in the balance between different T cell populations. In lean mice, production of IL-10 by regulatory T cells and anti-inflammatory macrophages ensures the maintenance of adipocyte insulin sensitivity. Conversely, in obese mice, the equilibrium is shifted in the direction of CD8+ T cells and pro-inflammatory macrophages (Fig. 2).

Finding a unique population of regulatory T lymphocytes in the abdominal adipose tissue of lean, but not obese, mice gives rise to many interesting questions. First, where do fat T_{regs} come from? When and where do they acquire their unique phenotype? Why and how do they accumulate in the visceral fat with age? Do they respond to an antigen or antigens and, if so, what is it? What chemokine/chemokine receptors are necessary for their homing to/retention in the fat? What precise functions do they perform in the adipose tissue? By what mechanisms? Do they operate directly on adipocytes, on macrophages or both? Why do T_{regs} evacuate obese adipose tissue?

Studies aimed to address these questions ultimately may result in treatments to modulate fat T_{reg} cell numbers and function in order to address the inflammation of the adipose tissue that promotes the metabolic syndrome.

Conflict of interest statement

The authors declare no conflict of interest.

Acknowledgement

We would like to thank the National Science Foundation for providing DK with a Graduate Research Fellowship.

References

[1] Sakaguchi S, Yamaguchi T, Nomura T, Ono M. Regulatory T cells and immune tolerance. Cell 2008;133:775–87.
[2] Mor A, Planer D, Luboshits G, Afek A, Metzger S, Chajek-Shaul T, et al. Role of naturally occurring CD4+ CD25+ regulatory T cells in experimental atherosclerosis. Arterioscler Thromb Vasc Biol 2007;27:893–900.
[3] Ait-Oufella H, Salomon BL, Potteaux S, Robertson AK, Gourdy P, Zoll J, et al. Natural regulatory T cells control the development of atherosclerosis in mice. Nat Med 2006;12:178–80.
[4] Xie JJ, Wang J, Tang TT, Chen J, Gao XL, Yuan J, et al. The Th17/Treg functional imbalance during atherogenesis in ApoE(−/−) mice. Cytokine 2010;49:185–93.
[5] Feuerer M, Herrero L, Cipolletta D, Naaz A, Wong J, Nayer A, et al. Lean, but not obese, fat is enriched for a unique population of regulatory T cells that affect metabolic parameters. Nat Med 2009;15:930–9.
[6] Deiuliis J, Shah Z, Shah N, Needleman B, Mikami D, Narula V, et al. Visceral adipose inflammation in obesity is associated with critical alterations in tregulatory cell numbers. PLoS One 2011;6:e16376.
[7] Center for Disease Control and Prevention. 2011 National diabetes fact sheet; 2011.
[8] Shoelson SE, Lee J, Goldfine AB. Inflammation and insulin resistance. J Clin Invest 2006;116:1793–801.
[9] Hotamisligil GS. Inflammation and metabolic disorders. Nature 2006;444:860–7.
[10] Hotamisligil GS, Shargill NS, Spiegelman BM. Adipose expression of tumor necrosis factor-alpha: direct role in obesity-linked insulin resistance. Science 1993;259:87–91.
[11] Ouchi N, Parker JL, Lugus JJ, Walsh K. Adipokines in inflammation and metabolic disease. Nat Rev Immunol 2011;11:85–97.
[12] Jager J, Gremeaux T, Cormont M, Le Marchand-Brustel Y, Tanti JF. Interleukin-1beta-induced insulin resistance in adipocytes through down-regulation of insulin receptor substrate-1 expression. Endocrinology 2007;148:241–51.
[13] Rotter V, Nagaev I, Smith U. Interleukin-6 (IL-6) induces insulin resistance in 3T3-L1 adipocytes and is, like IL-8 and tumor necrosis factor-alpha, overexpressed in human fat cells from insulin-resistant subjects. J Biol Chem 2003;278:45777–84.
[14] Han CY, Subramanian S, Chan CK, Omer M, Chiba T, Wight TN, et al. Adipocyte-derived serum amyloid A3 and hyaluronan play a role in monocyte recruitment and adhesion. Diabetes 2007;56:2260–73.
[15] Kamei N, Tobe K, Suzuki R, Ohsugi M, Watanabe T, Kubota N, et al. Overexpression of monocyte chemoattractant protein-1 in adipose tissues causes macrophage recruitment and insulin resistance. J Biol Chem 2006;281:26602–14.
[16] Ozcan U, Cao Q, Yilmaz E, Lee AH, Iwakoshi NN, Ozdelen E, et al. Endoplasmic reticulum stress links obesity, insulin action, and type 2 diabetes. Science 2004;306:457–61.
[17] Halberg N, Khan T, Trujillo ME, Wernstedt-Asterholm I, Attie AD, Sherwani S, et al. Hypoxia-inducible factor 1alpha induces fibrosis and insulin resistance in white adipose tissue. Mol Cell Biol 2009;29:4467–83.
[18] Minamino T, Orimo M, Shimizu I, Kunieda T, Yokoyama M, Ito T, et al. A crucial role for adipose tissue p53 in the regulation of insulin resistance. Nat Med 2009;15:1082–7.
[19] Yuan M, Konstantopoulos N, Lee J, Hansen L, Li ZW, Karin M, et al. Reversal of obesity- and diet-induced insulin resistance with salicylates or targeted disruption of Ikkbeta. Science 2001;293:1673–7.
[20] Hirosumi J, Tuncman G, Chang L, Gorgun CZ, Uysal KT, Maeda K, et al. A central role for JNK in obesity and insulin resistance. Nature 2002;420:333–6.
[21] Elchebly M, Payette P, Michaliszyn E, Cromlish W, Collins S, Loy AL, et al. Increased insulin sensitivity and obesity resistance in mice lacking the protein tyrosine phosphatase-1B gene. Science 1999;283:1544–8.
[22] Feinstein R, Kanety H, Papa MZ, Lunenfeld B, Karasik A. Tumor necrosis factor-alpha suppresses insulin-induced tyrosine phosphorylation of insulin receptor and its substrates. J Biol Chem 1993;268:26055–8.
[23] Elgazar-Carmon V, Rudich A, Hadad N, Levy R. Neutrophils transiently infiltrate intra-abdominal fat early in the course of high-fat feeding. J Lipid Res 2008;49:1894–903.
[24] Liu J, Divoux A, Sun J, Zhang J, Clement K, Glickman JN, et al. Genetic deficiency and pharmacological stabilization of mast cells reduce diet-induced obesity and diabetes in mice. Nat Med 2009;15:940–5.
[25] Cinti S, Mitchell G, Barbatelli G, Murano I, Ceresi E, Faloia E, et al. Adipocyte death defines macrophage localization and function in adipose tissue of obese mice and humans. J Lipid Res 2005;46:2347–55.
[26] Weisberg SP, McCann D, Desai M, Rosenbaum M, Leibel RL, Ferrante Jr AW. Obesity is associated with macrophage accumulation in adipose tissue. J Clin Invest 2003;112:1796–808.
[27] Mosser DM, Edwards JP. Exploring the full spectrum of macrophage activation. Nat Rev Immunol 2008;8:958–69.
[28] Odegaard JI, Ricardo-Gonzalez RR, Goforth MH, Morel CR, Subramanian V, Mukundan L, et al. Macrophage-specific PPARgamma controls alternative activation and improves insulin resistance. Nature 2007;447:1116–20.
[29] Fujisaka S, Usui I, Bukhari A, Ikutani M, Oya T, Kanatani Y, et al. Regulatory mechanisms for adipose tissue M1 and M2 macrophages in diet-induced obese mice. Diabetes 2009;58:2574–82.
[30] Lumeng CN, Bodzin JL, Saltiel AR. Obesity induces a phenotypic switch in adipose tissue macrophage polarization. J Clin Invest 2007;117:175–84.
[31] Lumeng CN, Deyoung SM, Bodzin JL, Saltiel AR. Increased inflammatory properties of adipose tissue macrophages recruited during diet-induced obesity. Diabetes 2007;56:16–23.
[32] Shaul ME, Bennett G, Strissel KJ, Greenberg AS, Obin MS. Dynamic, M2-like remodeling phenotypes of CD11c+ adipose tissue macrophages during high-fat diet-induced obesity in mice. Diabetes 2010;59:1171–81.
[33] Herrero L, Shapiro H, Nayer A, Lee J, Shoelson SE. Inflammation and adipose tissue macrophages in lipodystrophic mice. Proc Natl Acad Sci U S A 2010;107:240–5.
[34] Vandanmagsar B, Youm YH, Ravussin A, Galgani JE, Stadler K, Mynatt RL, et al. The NLRP3 inflammasome instigates obesity-induced inflammation and insulin resistance. Nat Med 2011;17:179–88.
[35] Schroder K, Tschopp J. The inflammasomes. Cell 2010;140:821–32.
[36] Duewell P, Kono H, Rayner KJ, Sirois CM, Vladimer G, Bauernfeind FG, et al. NLRP3 inflammasomes are required for atherogenesis and activated by cholesterol crystals. Nature 2010;464:1357–61.
[37] Rajamaki K, Lappalainen J, Oorni K, Valimaki E, Matikainen S, Kovanen PT, et al. Cholesterol crystals activate the NLRP3 inflammasome in human macrophages: a novel link between cholesterol metabolism and inflammation. PLoS One 2010;5:e11765.
[38] Nguyen MT, Favelyukis S, Nguyen AK, Reichart D, Scott PA, Jenn A, et al. A subpopulation of macrophages infiltrates hypertrophic adipose tissue and is activated by free fatty acids via Toll-like receptors 2 and 4 and JNK-dependent pathways. J Biol Chem 2007;282:35279–92.
[39] Kintscher U, Hartge M, Hess K, Foryst-Ludwig A, Clemenz M, Wabitsch M, et al. T-lymphocyte infiltration in visceral adipose tissue: a primary event in adipose tissue inflammation and the development of obesity-mediated insulin resistance. Arterioscler Thromb Vasc Biol 2008;28:1304–10.
[40] Nishimura S, Manabe I, Nagasaki M, Eto K, Yamashita H, Ohsugi M, et al. CD8+ effector T cells contribute to macrophage recruitment and adipose tissue inflammation in obesity. Nat Med 2009;15:914–20.
[41] Yang H, Youm YH, Vandanmagsar B, Ravussin A, Gimble JM, Greenway F, et al. Obesity increases the production of proinflammatory mediators from adipose tissue T cells and compromises TCR repertoire diversity: implications for systemic inflammation and insulin resistance. J Immunol 2010;185:1836–45.
[42] Winer S, Chan Y, Paltser G, Truong D, Tsui H, Bahrami J, et al. Normalization of obesity-associated insulin resistance through immunotherapy. Nat Med 2009;15:921–9.

[43] Strissel KJ, DeFuria J, Shaul ME, Bennett G, Greenberg AS, Obin MS. T-cell recruitment and Th1 polarization in adipose tissue during diet-induced obesity in C57BL/6 mice. Obesity (Silver Spring) 2010;18:1918–25.
[44] Rocha VZ, Folco EJ, Sukhova G, Shimizu K, Gotsman I, Vernon AH, et al. Interferon-gamma, a Th1 cytokine, regulates fat inflammation: a role for adaptive immunity in obesity. Circ Res 2008;103:467–76.
[45] Lord GM, Matarese G, Howard JK, Baker RJ, Bloom SR, Lechler RI. Leptin modulates the T-cell immune response and reverses starvation-induced immunosuppression. Nature 1998;394:897–901.
[46] Wang Y, Souabni A, Flavell RA, Wan YY. An intrinsic mechanism predisposes Foxp3-expressing regulatory T cells to Th2 conversion in vivo. J Immunol 2010;185:5983–92.
[47] Mombaerts P, Iacomini J, Johnson RS, Herrup K, Tonegawa S, Papaioannou VE. RAG-1-deficient mice have no mature B and T lymphocytes. Cell 1992;68:869–77.
[48] Powrie F, Leach MW, Mauze S, Menon S, Caddle LB, Coffman RL. Inhibition of Th1 responses prevents inflammatory bowel disease in scid mice reconstituted with CD45RBhi CD4+ T cells. Immunity 1994;1:553–62.
[49] Davidson NJ, Leach MW, Fort MM, Thompson-Snipes L, Kuhn R, Muller W, et al. T helper cell 1-type CD4+ T cells, but not B cells, mediate colitis in interleukin 10-deficient mice. J Exp Med 1996;184:241–51.
[50] Feng T, Wang L, Schoeb TR, Elson CO, Cong Y. Microbiota innate stimulation is a prerequisite for T cell spontaneous proliferation and induction of experimental colitis. J Exp Med 2010;207:1321–32.
[51] Rausch ME, Weisberg S, Vardhana P, Tortoriello DV. Obesity in C57BL/6J mice is characterized by adipose tissue hypoxia and cytotoxic T-cell infiltration. Int J Obes (Lond) 2008;32:451–63.
[52] Duffaut C, Galitzky J, Lafontan M, Bouloumie A. Unexpected trafficking of immune cells within the adipose tissue during the onset of obesity. Biochem Biophys Res Commun 2009;384:482–5.
[53] Winer DA, Winer S, Shen L, Wadia PP, Yantha J, Paltser G, et al. B cells promote insulin resistance through modulation of T cells and production of pathogenic IgG antibodies. Nat Med 2011;17:610–7.
[54] Ngo VN, Cornall RJ, Cyster JG. Splenic T zone development is B cell dependent. J Exp Med 2001;194:1649–60.
[55] Baumgarth N, Jager GC, Herman OC, Herzenberg LA. CD4+ T cells derived from B cell-deficient mice inhibit the establishment of peripheral B cell pools. Proc Natl Acad Sci U S A 2000;97:4766–71.
[56] Linton PJ, Harbertson J, Bradley LM. A critical role for B cells in the development of memory CD4 cells. J Immunol 2000;165:5558–65.
[57] Hill JA, Feuerer M, Tash K, Haxhinasto S, Perez J, Melamed R, et al. Foxp3 transcription-factor-dependent and -independent regulation of the regulatory T cell transcriptional signature. Immunity 2007;27:786–800.
[58] Feuerer M, Hill JA, Kretschmer K, von Boehmer H, Mathis D, Benoist C. Genomic definition of multiple ex vivo regulatory T cell subphenotypes. Proc Natl Acad Sci U S A 2010;107:5919–24.
[59] Lin W, Haribhai D, Relland LM, Truong N, Carlson MR, Williams CB, et al. Regulatory T cell development in the absence of functional Foxp3. Nat Immunol 2007;8:359–68.
[60] Gavin MA, Rasmussen JP, Fontenot JD, Vasta V, Manganiello VC, Beavo JA, et al. Foxp3-dependent programme of regulatory T-cell differentiation. Nature 2007;445:771–5.
[61] Feuerer M, Hill JA, Mathis D, Benoist C. Foxp3+ regulatory T cells: differentiation, specification, subphenotypes. Nat Immunol 2009;10:689–95.
[62] Zheng Y, Chaudhry A, Kas A, Deroos P, Kim JM, Chu TT, et al. Regulatory T-cell suppressor program co-opts transcription factor IRF4 to control T(H)2 responses. Nature 2009;458:351–6.
[63] Chaudhry A, Rudra D, Treuting P, Samstein RM, Liang Y, Kas A, et al. CD4+ regulatory T cells control TH17 responses in a Stat3-dependent manner. Science 2009;326:986–91.
[64] Koch MA, Tucker-Heard G, Perdue NR, Killebrew JR, Urdahl KB, Campbell DJ. The transcription factor T-bet controls regulatory T cell homeostasis and function during type 1 inflammation. Nat Immunol 2009;10:595–602.
[65] Tran TT, Yamamoto Y, Gesta S, Kahn CR. Beneficial effects of subcutaneous fat transplantation on metabolism. Cell Metab 2008;7:410–20.
[66] Vignali DA, Collison LW, Workman CJ. How regulatory T cells work. Nat Rev Immunol 2008;8:523–32.
[67] Thorburn J, Frankel AE, Thorburn A. Apoptosis by leukemia cell-targeted diphtheria toxin occurs via receptor-independent activation of Fas-associated death domain protein. Clin Cancer Res 2003;9:861–5.
[68] Boyman O, Kovar M, Rubinstein MP, Surh CD, Sprent J. Selective stimulation of T cell subsets with antibody–cytokine immune complexes. Science 2006;311:1924–7.
[69] Pelleymounter MA, Cullen MJ, Baker MB, Hecht R, Winters D, Boone T, et al. Effects of the obese gene product on body weight regulation in ob/ob mice. Science 1995;269:540–3.
[70] Klebig ML, Wilkinson JE, Geisler JG, Woychik RP. Ectopic expression of the agouti gene in transgenic mice causes obesity, features of type II diabetes, and yellow fur. Proc Natl Acad Sci U S A 1995;92:4728–32.
[71] Matarese G, Procaccini C, De RV, Horvath TL, La CA. Regulatory T cells in obesity: the leptin connection. Trends Mol Med 2010;16:247–56.
[72] Schwartz MW, Woods SC, Porte Jr D, Seeley RJ, Baskin DG. Central nervous system control of food intake. Nature 2000;404:661–71.
[73] Matarese G, Di GA, Sanna V, Lord GM, Howard JK, Di TA, et al. Requirement for leptin in the induction and progression of autoimmune encephalomyelitis. J Immunol 2001;166:5909–16.
[74] De RV, Procaccini C, Cali G, Pirozzi G, Fontana S, Zappacosta S, et al. A key role of leptin in the control of regulatory T cell proliferation. Immunity 2007;26:241–55.
[75] Wigren M, Bengtsson D, Duner P, Olofsson K, Bjorkbacka H, Bengtsson E, et al. Atheroprotective effects of alum are associated with capture of oxidized LDL antigens and activation of regulatory T cells. Circ Res 2009;104:e62–70.
[76] Gotsman I, Grabie N, Gupta R, Dacosta R, MacConmara M, Lederer J, et al. Impaired regulatory T-cell response and enhanced atherosclerosis in the absence of inducible costimulatory molecule. Circulation 2006;114:2047–55.
[77] de Boer OJ, van der Meer JJ, Teeling P, van der Loos CM, van der Wal AC. Low numbers of FOXP3 positive regulatory T cells are present in all developmental stages of human atherosclerotic lesions. PLoS One 2007;2:e779.
[78] Baecher-Allan C, Anderson DE. Regulatory cells and human cancer. Semin Cancer Biol 2006;16:98–105.
[79] Belkaid Y, Rouse BT. Natural regulatory T cells in infectious disease. Nat Immunol 2005;6:353–60.
[80] Miyara M, Amoura Z, Parizot C, Badoual C, Dorgham K, Trad S, et al. Global natural regulatory T cell depletion in active systemic lupus erythematosus. J Immunol 2005;175:8392–400.
[81] Baecher-Allan C, Viglietta V, Hafler DA. Human CD4+CD25+ regulatory T cells. Semin Immunol 2004;16:89–98.
[82] Taylor PA, Noelle RJ, Blazar BR. CD4(+)CD25(+) immune regulatory cells are required for induction of tolerance to alloantigen via costimulatory blockade. J Exp Med 2001;193:1311–8.
[83] Borish L, Aarons A, Rumbyrt J, Cvietusa P, Negri J, Wenzel S. Interleukin-10 regulation in normal subjects and patients with asthma. J Allergy Clin Immunol 1996;97:1288–96.
[84] Viglietta V, Baecher-Allan C, Weiner HL, Hafler DA. Loss of functional suppression by CD4+CD25+ regulatory T cells in patients with multiple sclerosis. J Exp Med 2004;199:971–9.
[85] Ehrenstein MR, Evans JG, Singh A, Moore S, Warnes G, Isenberg DA, et al. Compromised function of regulatory T cells in rheumatoid arthritis and reversal by anti-TNFalpha therapy. J Exp Med 2004;200:277–85.
[86] Tang Q, Henriksen KJ, Bi M, Finger EB, Szot G, Ye J, et al. In vitro-expanded antigen-specific regulatory T cells suppress autoimmune diabetes. J Exp Med 2004;199:1455–65.
[87] Tarbell KV, Yamazaki S, Olson K, Toy P, Steinman RM. CD25+ CD4+ T cells, expanded with dendritic cells presenting a single autoantigenic peptide suppress autoimmune diabetes. J Exp Med 2004;199:1467–77.
[88] Chatenoud L, Bluestone JA. CD3-specific antibodies: a portal to the treatment of autoimmunity. Nat Rev Immunol 2007;7:622–32.
[89] Ilan Y, Maron R, Tukpah AM, Maioli TU, Murugaiyan G, Yang K, et al. Induction of regulatory T cells decreases adipose inflammation and alleviates insulin resistance in ob/ob mice. Proc Natl Acad Sci U S A 2010;107:9765–70.
[90] Margalit M, Shalev Z, Pappo O, Sklair-Levy M, Alper R, Gomori M, et al. Glucocerebroside ameliorates the metabolic syndrome in OB/OB mice. J Pharmacol Exp Ther 2006;319:105–10.
[91] Ochi H, Abraham M, Ishikawa H, Frenkel D, Yang K, Basso AS, et al. Oral CD3-specific antibody suppresses autoimmune encephalomyelitis by inducing CD4+. Nat Med 2006;12:627–35.
[92] Ishikawa H, Ochi H, Chen ML, Frenkel D, Maron R, Weiner HL. Inhibition of autoimmune diabetes by oral administration of anti-CD3 monoclonal antibody. Diabetes 2007;56:2103–9.
[93] Wu HY, Center EM, Tsokos GC, Weiner HL. Suppression of murine SLE by oral anti-CD3: inducible CD4+CD25-LAP+ regulatory T cells control the expansion of IL-17+ follicular helper T cells. Lupus 2009;18:586–96.
[94] La CA, Van KL, Fu DS. CD4+CD25+ Tregs and NKT cells: regulators regulating regulators. Trends Immunol 2006;27:322–7.
[95] Steffens S, Burger F, Pelli G, Dean Y, Elson G, Kosco-Vilbois M, et al. Short-term treatment with anti-CD3 antibody reduces the development and progression of atherosclerosis in mice. Circulation 2006;114:1977–84.
[96] Battaglia M, Stabilini A, Roncarolo MG. Rapamycin selectively expands CD4+CD25+FoxP3+ regulatory T cells. Blood 2005;105:4743–8.